

**Development of Robust Three-Phase Equilibrium Calculation Algorithms for
Complex Reservoir Fluids**

by

Ruixue Li

A thesis submitted in partial fulfillment of the requirements for the degree of

Doctor of Philosophy

in

Petroleum Engineering

Department of Civil and Environmental Engineering
University of Alberta

© Ruixue Li, 2019

ABSTRACT

Three-phase equilibria, such as three-phase vapor-liquid-aqueous (VLA) equilibria and three-phase vapor-liquid-asphaltene (VLS) equilibria, can frequently appear in hydrocarbon reservoirs. In three-phase equilibrium calculations, one of the most prominent problems is caused by the lack of a prior knowledge of the phases that are actually present. Trivial computing results can frequently appear if the equilibrium calculations are improperly initialized. The presence of the aqueous phase or the asphaltene phase (which is nearly a pure phase in most cases) skews the topography of the free-energy surface, leading to that one of the stationary points may appear near the boundary of the Gibbs free-energy surface. This substantially increases the probability of encountering convergence problem in the three-phase equilibrium calculations. In this research, we aim to develop a suite of techniques to improve the robustness of the three-phase equilibrium calculation algorithms for the VLA and VLS equilibria.

In most cases, the aqueous phase can be considered as a pure water phase (the so-called “free-water assumption”). With this assumption, we first develop a robust and efficient algorithm used for conducting isothermal three-phase equilibrium calculations which can consider single-phase, two-phase, and three-phase VLA equilibria. Subsequently, we develop a three-phase free-water isenthalpic equilibrium calculation algorithm by combining the newly developed VLA algorithm with the energy conservation equation which is used to convert enthalpy to temperature. This three-phase free-water isenthalpic equilibrium calculation algorithm can be applied to reservoirs undergoing thermal enhanced oil recovery treatments (in which temperature dramatically changes and is difficult to be known beforehand). A number of example calculations are carried out to

demonstrate the performance of these two algorithms. Testing results prove that the newly developed algorithms are robust and effective. For some reservoir mixtures (e.g., a mixture containing CO₂ or H₂S), the free-water assumption may not be valid since the aqueous phase can contain a significant amount of other species; to accurately capture the three-phase equilibria for such mixtures, we develop a new initialization scheme as well as a new procedure to improve the robustness of the three-phase isothermal equilibrium calculation algorithm. To test the robustness of this algorithm, it is applied to several fluid mixtures to generate pressure-temperature (P-T) phase diagrams, showing that the newly developed algorithm is both robust and efficient.

Moreover, we further develop a three-phase VLS isothermal equilibrium calculation algorithm by applying the asphaltene-precipitation model proposed by Nghiem *et al.* (1993). In their model, they assume that the asphaltenes form a pure phase; this assumption is similar to the free-water assumption. This three-phase VLS isothermal equilibrium calculation algorithm aims to model the CO₂ flooding in light oil reservoirs. New initialization methods of equilibrium ratios are provided in this algorithm for both stability test and flash calculation. To test the performance of this algorithm, it is run to generate pressure-composition (P-X) phase diagrams for several reservoir fluids. The new algorithm is shown to be robust as it can always converge to the correct phase equilibrium for all the tested cases. Afterwards, by applying the three-phase VLS equilibrium calculation algorithm, we develop a multiple-mixing-cell (MMC) method to predict the minimum miscibility pressure (MMP) with the consideration of asphaltene-precipitation effect. Example calculations are carried out to predict MMPs between reservoir fluid and pure or impure CO₂. The MMPs predicted by our algorithm

and those predicted by the MMC algorithm without considering asphaltene-precipitation effect are both compared with the MMPs measured by slim tube experiments. The comparison results show that the MMPs predicted by our algorithm agree reasonably well with the measured MMPs.

PREFACE

A version of Chapter 2 has been published as Li, R. and Li, H.A. (2018), New two-phase and three-phase Rachford-Rice algorithms based on free-water assumption, *The Canadian Journal of Chemical Engineering*, 96(1): 390-403. Li, R. is responsible for the theoretical development, simulation results, analysis, and manuscript composition. Li, H.A. is the supervisory author and gets involved in the concept formation, theoretical development, analysis and manuscript composition.

A version of Chapter 3 has been published as Li, R. and Li, H.A. (2018), A robust three-phase isenthalpic flash algorithm based on free-water assumption, *Journal of Energy Resources Technology*, 140(3): 032902. Li, R. is responsible for the theoretical development, simulation results, analysis, and manuscript composition. Li, H.A. is the supervisory author and gets involved in the concept formation, theoretical development, analysis, and manuscript composition.

A version of Chapter 4 has been published as Li, R. and Li, H.A. (2019), Improved three-phase equilibrium calculation algorithm for water/hydrocarbon mixtures, *Fuel*, 244: 517-527. Li, R. is responsible for the theoretical development, simulation results, analysis, and manuscript composition. Li, H.A. is the supervisory author and gets involved in the concept formation, theoretical development, analysis, and manuscript composition.

A version of Chapter 5 is submitted to *Industrial & Engineering Chemistry Research* for publication as Li, R. and Li, H.A., Robust three-phase vapor-liquid-asphaltene equilibrium calculation algorithm for isothermal CO₂ flooding application. Li, R. is

responsible for the theoretical development, simulation results, analysis, and manuscript composition. Li, H.A. is the supervisory author and gets involved in the concept formation, theoretical development, analysis, and manuscript composition.

A version of Chapter 6 is submitted to *Industrial & Engineering Chemistry Research* for publication as Li, R. and Li, H.A. (2018), A modified multiple-mixing-cell algorithm for minimum miscibility pressure prediction with the consideration of asphaltene-precipitation effect. Li, R. is responsible for the theoretical development, simulation results, analysis, and manuscript composition. Li, H.A. is the supervisory author and gets involved in the concept formation, theoretical development, analysis, and manuscript composition.

Chapter 1 summarizes the research background, problem statement, research objectives, and thesis structure. Chapter 7 summarizes the conclusions reached in this thesis as well as the recommendations for future research. Chapters 1 and 7 are originally written by Li, R. and have never been published elsewhere.

ACKNOWLEDGMENTS

I would like to express my sincere appreciations to my supervisor Dr. Huazhou Andy Li for providing me a precious opportunity working with him as well as his technical and financial support during my PhD study. I also thank my committee members Dr. Mingzhe Dong, Dr. Zhehui Jin, Dr. Nobuo Maeda, and Dr. Yang Liu for their excellent comments and suggestions on my PhD thesis, and Dr. Alireza Nouri for serving as the chair of my PhD defense.

I also wish to acknowledge the following individuals or organizations during my PhD study at the University of Alberta:

- Natural Sciences and Engineering Research Council (NSERC) of Canada for a Discovery Grant to Dr. H.A. Li;
- The University of Alberta International for a China Opportunity Fund to Dr. H.A. Li;
- Dr. Ergun Kuru and Dr. Zukui Li for serving as my candidacy exam committee members;
- Past and present group members in Dr. H.A. Li's research group; and
- My friend Miss Yanan Hou.

DEDICATION

This dissertation is dedicated to my dearest parents: my mother Mrs. Cuiyan Diao and
my father Mr. Quansheng Li.

TABLE OF CONTENTS

ABSTRACT.....	ii
PREFACE.....	v
ACKNOWLEDGMENTS	vii
DEDICATION	viii
TABLE OF CONTENTS.....	ix
LIST OF TABLES	xiv
LIST OF FIGURES.....	xvi
CHAPTER 1 INTRODUCTION	1
1.1 Research Background	1
1.2 Problem Statement.....	5
1.3 Research Objectives	7
1.4 Thesis Structure.....	8
1.5 References.....	9
CHAPTER 2 NEW TWO-PHASE AND THREE-PHASE RACHFORD-RICE ALGORITHMS BASED ON FREE-WATER ASSUMPTION.....	11
Abstract.....	12
2.1 Introduction.....	13
2.2 Mathematical Formulations	16
2.3 Two-Phase and Three-Phase Free-Water Flash Algorithm	22
2.3.1 Procedure of the Two-Phase and Three-Phase Free-Water Flash Algorithm...22	
2.3.2 Criteria for Switching from a Three-Phase Free-Water Flash to a Two-Phase Flash	26

2.4 Example Applications.....	29
2.4.1 Water/C4/C20 Mixture	29
2.4.2 Water/N ₂ /C10/C20 Mixture	35
2.4.3 Water/Reservoir Fluid Mixture	37
2.5 Conclusions.....	44
2.6 References.....	48
Appendix 2-A: Algorithm for the Two-Phase Free-Water Flash	50
Appendix 2-B: Algorithm for the Three-Phase Free-Water Flash.....	52
Appendix 2-C: Component Properties and BIPs	56
 CHAPTER 3 A ROBUST THREE-PHASE ISENTHALPIC FLASH ALGORITHM BASED ON FREE-WATER ASSUMPTION.....	
Abstract.....	59
3.1 Introduction.....	60
3.2 Mathematical Formulation.....	64
3.3 Algorithm.....	66
3.4 Example Applications.....	73
3.4.1 Case 1 (Water/C3/C16 Mixture)	73
3.4.2 Case 2 (Water/Pseudo-Components Mixture)	78
3.4.3 Case 3 (Water/C1/C7/C _D Mixture).....	83
3.5 Conclusions.....	87
3.6 References.....	91
Appendix 3-A: Component Properties and BIPs	97
 CHAPTER 4 IMPROVED THREE-PHASE EQUILIBRIUM CALCULATION	

ALGORITHM FOR WATER/HYDROCARBON MIXTURES WITH A NEW	
INITIALIZATION SCHEME	100
Abstract.....	101
4.1 Introduction.....	102
4.2 Theoretical Background.....	106
4.2.1 Phase Stability Test	106
4.2.2 Flash Calculation	108
4.2.3 Conventional Three-Phase Equilibrium Calculation Algorithm.....	109
4.3 Improved Three-Phase VLA equilibrium Calculation Algorithm with a New	
Initialization Scheme	110
4.4 Example Calculations	116
4.4.1 Case 1 (Water/C3/C16 Mixture)	117
4.4.2 Case 2 (Water/C4/C20 Mixture)	124
4.4.3 Case 3 (Water/Pseudo-Components Mixture)	127
4.4.4 Case 4 (Water/C1/C7/C _D Mixture).....	131
4.5 Conclusions	132
4.6 References	134
Appendix 4-A: Component Properties and BIPs	138
CHAPTER 5 ROBUST THREE-PHASE VAPOR-LIQUID-ASPHALTENE	
EQUILIBRIUM CALCULATION ALGORITHM FOR ISOTHERMAL CO ₂	
FLOODING APPLICATIONS.....	140
Abstract.....	141
5.1 Introduction.....	142

5.2 Mathematical Formulations	147
5.2.1 Thermodynamic Model.....	147
5.2.2 Phase Stability Test	148
5.2.3 Flash Calculation	149
5.3 Three-Phase VLS Equilibrium Calculation Algorithm	155
5.4 Results and Discussion	160
5.4.1 Oil Sample 1	161
5.4.2 Oil Sample 2.....	177
5.5 Conclusions.....	185
5.6 References.....	188
Appendix 5-A: Two-Phase V/L-S Flash Calculation Algorithm.....	193
Appendix 5-B: Three-Phase VLS Flash Calculation Algorithm #2.....	195
CHAPTER 6 A MODIFIED MULTIPLE-MIXING-CELL ALGORITHM FOR	
MINIMUM MISCIBILITY PRESSURE PREDICTION WITH THE CONSIDERATION	
OF ASPHALTENE-PRECIPIATION EFFECT	
Abstract.....	198
6.1 Introduction.....	200
6.2 Thermodynamic Model.....	203
6.3 MMC Algorithm Considering Asphaltene-Precipitation Effect	206
6.4 Results and Discussion	211
6.4.1 Case Study 1: Fluid W1 Displaced by Gas 1 (Pure CO ₂).....	216
6.4.2 Case Study 2: Fluid W1 Displaced by Gas 2 (Impure CO ₂).....	220
6.4.3 Case Study 3: Fluid W1 Displaced by Gas 3 (Impure CO ₂).....	226

6.4.4 Comparison of Measured and Predicted MMPs	233
6.5 Conclusions	235
6.6 References	238
CHAPTER 7 CONCLUSIONS, CONTRIBUTIONS AND RECOMMENDATIONS .	243
7.1 Conclusions and Scientific Contributions to the Literature	243
7.2 Suggested Future Work	248
7.3 References	250
BIBLIOGRAPHY	252

LIST OF TABLES

Table 2-1 Comparison of the numbers of stability tests and flashes needed by the conventional full three-phase flash package and the three-phase free-water flash package	25
Table 2-2 Comparison between the mole fractions obtained by applying the two-phase free-water flash and those obtained by applying the conventional two-phase flash for the water/reservoir fluid mixture at 450 K and 400 bar	41
Table 2-3 Comparison between the mole fractions obtained by applying the three-phase free-water flash and those obtained by applying the conventional three-phase flash for the water/reservoir fluid mixture at 450 K and 200 bar	42
Table 2-C.1 Component properties and feed composition for the water/C4/C20 mixture	56
Table 2-C.2 Component properties and feed composition for the water/N ₂ /C10/C20 mixture by Lapene <i>et al.</i> ^[14]	56
Table 2-C.3 BIPs between the components in the water/N ₂ /C10/C20 mixture by Lapene <i>et al.</i> ^[14]	56
Table 2-C.4 Component properties and feed composition for the water/reservoir fluid mixture by Lapene <i>et al.</i> ^[14]	57
Table 2-C.5 BIPs between the components in the water/reservoir fluid mixture by Lapene <i>et al.</i> ^[14]	57
Table 3-A.1 Component properties for the water/C3/C16 mixture [28]	97
Table 3-A.2 BIPs between the components in the water/C3/C16 mixture [28]	97
Table 3-A.3 Component properties for the water/pseudo-components mixture [28]	98
Table 3-A.4 BIPs between the components in the water/pseudo-components mixture [28]	98
Table 3-A.5 Component properties for the water/C1/C7/C _D mixture [37]	98
Table 3-A.6 BIPs between the components in the water/C1/C7/C _D mixture [37]	99
Table 4-1 Comparison between the number of initial estimates of equilibrium ratios used in the newly developed algorithm and the conventional three-phase equilibrium calculation algorithm	116
Table 4-A.1 Component properties and feed composition for the water/C3/C16 mixture [28]	138
Table 4-A.2 BIPs between the components in the water/C3/C16 mixture [28]	138
Table 4-A.3 Component properties and feed composition for the water/C4/C20 mixture [30]	138
Table 4-A.4 BIPs between the components in the water/C4/C20 mixture [30]	139
Table 4-A.5 Component properties and feed composition for the water/pseudo-components mixture [28]	139
Table 4-A.6 BIPs between the components in the water/pseudo-components mixture [28]	139
Table 4-A.7 Component properties and feed composition for the water/C1/C7/C _D mixture	139

[29]	139
Table 4-A.8 BIPs between the components in the water/C1/C7/C _D mixture [29]	139
Table 5-1 Compositions of oil sample 1 and injection gas [4]	161
Table 5-2 Composition and component properties of oil sample 1 [32, 33]	163
Table 5-3 Adjustable parameters and their values used in our algorithm for oil sample 1 mixed with impure CO ₂	165
Table 5-4 BIPs used for oil sample 1 calculations [33]	165
Table 5-5 Compositions of oil sample 2 and three injection gases [4, 35]	177
Table 5-6 Composition and component properties of oil sample 2 [32, 33]	178
Table 5-7 Adjustable parameters and their values used in our algorithm for oil sample 2 mixed with pure CO ₂	179
Table 5-8 BIPs used for oil sample 2 calculations [33]	179
Table 6-1 Compositions of Fluid W1 and three injection gases [3, 26]	212
Table 6-2 Composition and component properties of Fluid W1 [16, 20, 27]	213
Table 6-3 Adjustable parameters and their adjusted values used in three-phase VLS equilibrium calculation algorithm for Fluid W1 mixed with pure CO ₂ [20]	214
Table 6-4 BIPs used for Fluid W1 [20, 27]	215
Table 6-5 Comparison of measured and predicted MMPs for Fluid W1 displaced by three gases at 59°C	235

LIST OF FIGURES

Figure 1-1 Schematic of the possible phase equilibria in a three-phase VLA or VLS equilibrium calculations.	2
Figure 2-1 Flow chart of a new three-phase free-water flash package.....	24
Figure 2-2 Phase fractions obtained by applying the standalone three-phase free-water flash algorithm for the water/C4/C20 mixture at 50 bar	27
Figure 2-3 Three-phase triangles for the water/C4/C20 mixtures at 50 bar	28
Figure 2-4 Calculated three-phase envelopes for the water/C4/C20 mixture and calculated two-phase envelopes for the C4/C20 mixture. Both the conventional three-phase flash and the three-phase free-water flash packages have been used to calculate the three-phase envelopes	30
Figure 2-5 Comparison between the mole fractions of individual components in the hydrocarbon-rich phase obtained by applying the three-phase free-water flash package and those obtained by applying the conventional three-phase flash package for the water/C4/C20 mixture at 50 bar: (a) variation of the mole fractions of individual components in the hydrocarbon-rich phase as a function of temperature; (b) absolute deviations in the mole fractions of individual components that are calculated with the two three-phase flash packages	31
Figure 2-6 Comparison between the phase fractions obtained by applying the three-phase free-water flash package and those obtained by applying the conventional three-phase flash package for the water/C4/C20 mixture at 50 bar: (a) variation of the phase fractions as a function of temperature; (b) absolute deviations in the phase fractions that are calculated with the two three-phase flash packages	33
Figure 2-7 Comparison between the number of iterations in the outer loop required by the three-phase free-water flash algorithm and those required by the conventional three-phase flash algorithm for the water/C4/C20 mixture at 50 bar	34
Figure 2-8 Comparison between the total computational time of one run of the three-phase free-water flash package and one run of the conventional three-phase flash package for the water/C4/C20 mixture at 50 bar.....	35
Figure 2-9 Comparison between the phase fractions obtained by applying the three-phase free-water flash package and those obtained by applying the conventional three-phase flash package for the water/N ₂ /C10/C20 mixture at 450 K: (a) variation of the phase fractions as a function of pressure; (b) deviations in the phase fractions that are calculated with the two three-phase flash packages	36
Figure 2-10 Comparison between the phase fractions obtained by applying the standalone three-phase free-water flash algorithm and those obtained by applying the conventional three-phase flash package for the water/N ₂ /C10/C20 mixture at 450 K.....	37
Figure 2-11 Comparison between the phase fractions obtained by applying the three-phase free-water flash package and those obtained by applying the conventional three-phase flash package for the water/reservoir fluid mixture at 50 bar: (a) variation of the phase fractions as a function of temperature; (b) deviations in the phase fractions that are calculated with the two three-phase flash packages	39
Figure 2-12 Comparison between the phase fractions obtained by applying the three-phase	

free-water flash package and those obtained by applying the conventional three-phase flash package for the water/reservoir fluid mixture at 450 K: (a) variation of the phase fractions as a function of pressure; (b) absolute deviations in the phase fractions that are calculated with the two three-phase flash packages	40
Figure 2-13 Comparison between the mole fractions of water in the hydrocarbon-rich phase obtained by applying the three-phase free-water flash package and those obtained by applying the conventional three-phase flash package for the water/reservoir fluid mixture at 50 bar	43
Figure 2-14 Comparison between the phase fractions obtained by applying the standalone three-phase free-water flash algorithm and those obtained by applying the conventional three-phase flash package for the water/reservoir fluid mixture: (a) at 50 bar; (b) at 450 K	44
Figure 2-A.1 Flow chart of the two-phase free-water flash algorithm.....	51
Figure 2-B.1 Flow chart of the three-phase free-water flash algorithm	55
Figure 3-1 Flow chart of the multiphase isenthalpic flash algorithm based on the free-water assumption	72
Figure 3-2 Case study 1 (water/C3/C16 mixture): comparison between temperatures obtained by the new isenthalpic flash algorithm and those obtained by the Zhu and Okuno [28] at 80 bar.....	74
Figure 3-3 Case study 1 (water/C3/C16 mixture): (a) absolute deviations between the calculated total molar enthalpies obtained by the conventional three-phase isothermal flash and those obtained by the three-phase free-water isothermal flash at 80 bar and different temperatures; (b) mole fraction of C3 in the water-rich phase as calculated by the conventional three-phase isothermal flash at 80 bar and different temperatures.....	75
Figure 3-4 Case study 1 (water/C3/C16 mixture): evolution of the number of phases and temperatures as a function of the iteration number of the outer loop at 80 bar and four different values of the specified enthalpy: (a) $H_{spec} = -15000$ J/mol; (b) $H_{spec} = -8000$ J/mol; (c) $H_{spec} = 0$ J/mol; (d) $H_{spec} = 8000$ J/mol.....	78
Figure 3-5 Case study 2 (water/pseudo-components mixture): comparison between temperatures obtained by the new isenthalpic flash algorithm and those obtained by the Zhu and Okuno [28] at 30 bar.....	79
Figure 3-6 Case study 2 (water/pseudo-components mixture): variation in the number of iterations as a function of the calculated temperatures experienced by the new isenthalpic flash algorithm at 30 bar.....	80
Figure 3-7 Case study 2 (water/pseudo-components mixture): evolution of the number of phases and temperatures as a function of the iteration number of the outer loop at 30 bar and four different values of the specified enthalpy: (a) $H_{spec} = -49000$ J/mol; (b) $H_{spec} = -45000$ J/mol; (c) $H_{spec} = -28000$ J/mol; (d) $H_{spec} = -24000$ J/mol.....	82
Figure 3-8 Case study 3 (Water/C1/C7/C _D mixture): comparison between temperatures obtained by the multiphase isenthalpic flash algorithm provided in this work and those obtained by the Zhu and Okuno [37], (a) at 20 bar and (b) at 210 bar.....	84
Figure 3-9 Case study 3 (Water/C1/C7/C _D mixture): (a) mole fraction of C1 in the water-rich phase calculated by the conventional three-phase isothermal flash at 210 bar and	

different temperatures; (b) comparison between the phase fractions obtained by the three-phase free-water isothermal flash and those obtained by the conventional three-phase isothermal flash at 210 bar and different temperatures. 86

Figure 3-10 Case study 3 (Water/C1/C7/C_D mixture): evolution of the number of iterations as a function of the calculated temperatures at 210 bar as experienced by the new isenthalpic flash algorithm..... 87

Figure 4-1 Flow chart of the improved three-phase VLA equilibrium calculation algorithm developed in this work..... 115

Figure 4-2 Number of equilibrium phases in a PT phase diagram for the water/C3/C16 mixture..... 118

Figure 4-3 Number of equilibrium phases in a PT phase diagram for the water/C3/C16 mixture at the near critical region 119

Figure 4-4 Distribution of the initial estimates of the equilibrium ratios used in two-phase flash calculations for the water/C3/C16 mixture by applying: (a) approach proposed by Gorucu and Johns [11]; (b) approach developed in this paper; and (c) comparison between the boundary lines of different kinds of initial equilibrium-ratio estimates selected by the approach proposed by Gorucu and Johns [11] and those selected by our approach..... 122

Figure 4-5 Value of the TPD function for the water/C3/C16 mixture at 500 K and 80 bar: (a) top view; and (b) 3D diagram. 123

Figure 4-6 Number of equilibrium phases in a PT phase diagram for the water/C4/C20 mixture..... 125

Figure 4-7 Value of the TPD function for the water/C4/C20 mixture at 490 K and 100 bar: (a) a top view; and (b) a 3D view..... 126

Figure 4-8 Number of equilibrium phases in a PT phase diagram for the water/pseudo-components mixture 127

Figure 4-9 Comparison between the phase boundaries calculated by this study and those calculated by Zhu and Okuno [28] for the water/pseudo-components mixture..... 128

Figure 4-10 Distribution of the initial estimates of equilibrium ratios used in two-phase flash calculations for the water/pseudo-components mixture by applying: (a) approach proposed by Gorucu and Johns [11]; (b) approach developed in this paper; and (c) comparison between the boundary lines of different kinds of initial equilibrium-ratio estimates selected by the approach proposed by Gorucu and Johns [11] and those selected by our approach..... 130

Figure 4-11 Number of equilibrium phases in a PT phase diagram for the water/C1/C7/C_D mixture..... 131

Figure 5-1 Flow chart of three-phase VLS equilibrium calculation algorithm. V: vapor phase; L: liquid phase; and S: solid asphaltene phase..... 160

Figure 5-2 Comparison between the weight fractions of the precipitated asphaltenes as a function of gas concentration calculated by our algorithm with the adjusted parameters and those measured by Srivastava *et al.* [4] for oil sample 1 at 61°C and 160 bar 166

Figure 5-3 Effect of asphaltene content in oil sample 1 on asphaltene precipitation under different gas concentrations 167

Figure 5-4 Effect of the critical gas concentration (above which asphaltenes start to precipitate) on asphaltene precipitation under different gas concentrations 168

Figure 5-5 Effect of the exponential parameter (θ) on asphaltene precipitation under different gas concentrations	170
Figure 5-6 Effect of the BIP between CO ₂ and HCs on the asphaltene precipitation under different gas concentrations	171
Figure 5-7 P-X phase diagram calculated by the three-phase VLS equilibrium calculation algorithm with the adjusted parameters for oil sample 1 mixed with impure CO ₂ at 61°C. V: vapor phase; L: liquid phase; and S: solid asphaltene phase.	172
Figure 5-8 P-X phase diagrams for oil sample 1 mixed with impure CO ₂ at 61°C yielded by our three-phase VLS equilibrium calculation algorithm with different V_s : (a) V_s is set to be 0.5000 m ³ /kmol; (b) V_s is set to be 0.5500 m ³ /kmol; and (c) comparison of the different P-X phase boundaries yielded by our algorithm with different V_s . V: vapor phase; L: liquid phase; and S: solid asphaltene phase.	174
Figure 5-9 Weight fractions (in wt%) of the precipitated asphaltenes calculated by our algorithm with different V_s as a function of pressure and gas concentration at 61°C: (a) V_s is set to be 0.4323 m ³ /kmol; (b) V_s is set to be 0.5000 m ³ /kmol; and (c) V_s is set to be 0.5500 m ³ /kmol.	176
Figure 5-10 Comparison between the weight fractions of the precipitated asphaltenes as a function of gas concentration calculated by our algorithm with the adjusted parameters and those obtained by experiments conducted by Srivastava <i>et al.</i> [4] for oil sample 2 at 59°C and 160 bar.....	180
Figure 5-11 P-X phase diagram calculated by the three-phase VLS equilibrium calculation algorithm with the adjusted parameters for Oil sample 2 mixed with Gas 1 (pure CO ₂) at 59°C. V: vapor phase; L: liquid phase; and S: solid asphaltene phase.....	182
Figure 5-12 P-X phase diagrams calculated by the three-phase VLS equilibrium calculation algorithm with the adjusted parameters for Oil sample 2 mixed with impure CO ₂ at 59°C: (a) Gas 2 and (b) Gas 3. V: vapor phase; L: liquid phase; and S: solid asphaltene phase.....	184
Figure 5-A.1 Flow chart of the two-phase V/L-S flash calculation algorithm	194
Figure 5-B.1 Flow chart of the three-phase VLS flash calculation Algorithm #2.....	196
Figure 6-1 Schematic of the contact method adopted by the MMC method considering asphaltene-precipitation effect. G: injection gas; O: oil; X: equilibrium liquid phase; Y: equilibrium vapor phase; S: solid asphaltene phase; and 1 st contact, 2 nd contact, 3 rd contact, ..., and N th contact: contact times.	210
Figure 6-2 P-X phase diagram generated by Li and Li [20] for Fluid W1 mixed with Gas 1 (pure CO ₂) at 59°C. V: vapor phase; L: liquid phase; S: solid asphaltene phase; and Region 1: three-phase VLS equilibrium region where the liquid phase is very dense and more like an asphaltene phase.	216
Figure 6-3 Variation of the minimum tie lie lengths as a function of pressure for Fluid W1 displaced by Gas 1 at 59°C: (a) comparison of the minimum tie lie lengths yielded by the MMC method proposed by Ahmadi and Johns [17] and those yielded by the MMC method proposed by this work; (b) extrapolation of the minimum tie lie lengths yielded by the MMC method proposed by Ahmadi and Johns [17]; and (c) extrapolation of the minimum tie lie lengths yielded by the MMC method proposed by this work.	219

Figure 6-4 Variation of the tie line length calculated by our MMC algorithm as a function of contact number for Fluid W1 displaced by Gas 1 at 59°C and 110 bar 220

Figure 6-5 Variation of the minimum tie lie lengths as a function of pressure for Fluid W1 displaced by Gas 2 at 59°C: (a) comparison of the minimum tie lie lengths yielded by the MMC method proposed by Ahmadi and Johns [17] and those yielded by the MMC method proposed by this work; (b) extrapolation of the minimum tie lie lengths yielded by the MMC method proposed by Ahmadi and Johns [17]; and (c) extrapolation of the minimum tie lie lengths yielded by the MMC method proposed by this work. 222

Figure 6-6 Variation of the tie line length calculated by our MMC algorithm as a function of contact number for Fluid W1 displaced by Gas 2 at 59°C and 110 bar 223

Figure 6-7 Fluid W1 displaced by Gas 2 at 59°C and 110 bar: (a) Variation of the weight fractions of precipitated asphaltene calculated by our MMC algorithm as a function of contact number in different contact times. (b) Weight fractions of precipitated asphaltene and tie line lengths calculated by our MMC algorithm as a function of contact number when the total contact number is 100. 225

Figure 6-8 Variation of minimum tie lie lengths as a function of pressure for Fluid W1 displaced by Gas 3 at 59°C: (a) comparison of the minimum tie lie lengths yielded by the MMC method proposed by Ahmadi and Johns [17] and those yielded by the MMC method proposed by this work; (b) extrapolation of the minimum tie lie lengths yielded by the MMC method proposed by Ahmadi and Johns [17]; and (c) extrapolation of the minimum tie lie lengths yielded by the MMC method proposed by this work. 228

Figure 6-9 Variation of the tie line length calculated by our MMC algorithm as a function of contact number for Fluid W1 displaced by Gas 3 at 59°C and 110 bar 229

Figure 6-10 Variation of the vapor-liquid equilibrium ratios calculated by the two-phase flash calculation in our MMC algorithm as a function of contact number for Fluid W1 displaced by Gas 3 at 59°C: (a) 90 bar; (b) 110 bar; (c) 170 bar; and (d) 193 bar..... 233

CHAPTER 1 INTRODUCTION

1.1 Research Background

Most of compositional simulators only conduct two-phase vapor-liquid (VL) equilibrium calculations since this type of equilibria is most common in hydrocarbon reservoirs. However, three-phase equilibria can frequently appear as well. The most possible third phase is an aqueous phase which comes from either the aquifer or the water injected for oil recovery purposes. Moreover, the appearance of the asphaltene is also common during gas injection process in light oil reservoirs. When the third phase appears, a compositional simulator which can consider the three-phase equilibria is required in order to have a precise capture of the actual multiphase flow in such reservoirs (Lapene *et al.* 2010; Mortezaazadeh and Rasaeiuse 2017). However, there is still a lack of robust three-phase equilibrium calculation algorithms. Many technical problems need to be resolved in order to develop robust three-phase equilibrium calculation algorithms.

The primary problem in three-phase equilibrium calculations is the lack of a prior knowledge of the number of the present phases. Three-phase equilibrium calculations are much more complex than two-phase equilibrium calculations. **Figure 1-1** illustrates the schematic of the possible phase equilibria in a three-phase vapor-liquid-aqueous (VLA) or vapor-liquid-solid (VLS) equilibrium calculation. Five kinds of possible phase equilibria should be considered in three-phase equilibrium calculations, while only single-phase and two-phase equilibria need to be considered in two-phase equilibrium calculations. Since we do not know the phases which will be actually present prior to conducting a phase equilibrium calculation, more possible types of phase equilibria which can appear will

substantially increase the difficulty of conducting three-phase equilibrium calculations.

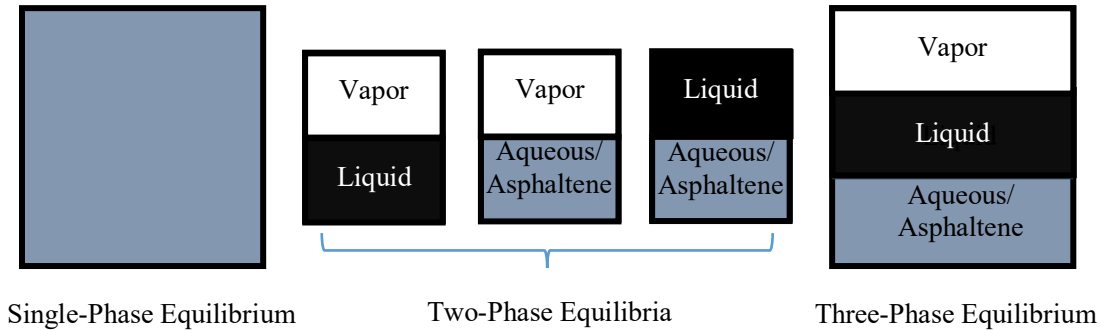


Figure 1-1 Schematic of the possible phase equilibria in a three-phase VLA or VLS equilibrium calculations.

Due to the unknown number of the present phases, three-phase equilibrium calculations are suggested to be conducted with a stage-wise manner (Michelsen 1982b). Phase stability tests are adopted to determine whether the tested mixture is stable or will split into two or more phases by detecting the negative stationary point(s) on the tangent plane distance (TPD) function (Michelsen 1982a), while flash calculations are performed at the given number of phases to calculate the phase fractions and phase compositions (Michelsen 1982b). Two stage-wise approaches are extensively applied. One is first to perform the stability test. If the tested phase is unstable, the phase number needs to be increased and flash calculation is required (Michelsen 1982b). In this approach, multiple initial estimates are applied in both the stability test and flash calculation to ensure the robustness of the algorithm (Li and Firoozabadi 2012; Gorucu and Johns 2016), which, however, increases the computational load. Another approach to conducting multiphase equilibrium calculations is first to conduct the flash calculation with a pre-set number of the present phases. If any of the phases has a negative phase fraction, the flash calculation needs to be conducted with a decreased number of phases (Whitson and Michelsen 1989;

Leibovici and Neoschil 1995). This approach is more efficient since it does not require a stability test. However, it is difficult for one to provide good initial estimates of equilibrium ratios when the number of the present phases is three or more (Li and Firoozabadi 2012).

Another problem in three-phase equilibrium calculation is the frequent appearance of convergence problems, even when the aforementioned stage-wise procedure is rigorously applied. One reason is that several stationary points may exist on the TPD surface in three-phase equilibrium calculations. Thus, in three-phase equilibrium calculations, there is a high possibility that the stability test fails to detect the negative stationary point(s), since the negative stationary point(s) may be hidden by the positive one(s). To increase the chance of finding the negative stationary point(s), stability test is required to be conducted with multiple sets of initial equilibrium ratios (Michelsen 1982a and Li and Firoozabadi 2012). Different initialization methods of equilibrium ratios should be adopted for different types of fluids. For hydrocarbon fluids mixed with CO₂, Li and Firoozabadi (2012) suggested that $(c+4)$ initial estimates of equilibrium ratios should be applied for stability tests (where c represents the number of components). Connolly (2018) provided an approach to identify the aqueous-like stationary point. In this approach, the mole fraction of water in the trail phase is set as 99.9 mol%, while others equally share 0.1 mol%. However, this approach still does not perform well in identifying an aqueous-like stationary point in some cases.

Moreover, when the third phase is nearly a pure substance, e.g., aqueous phase or asphaltene phase, additional difficulties will be brought to both the stability test and flash calculation. For stability tests, the conventional methods of initializing the equilibrium

ratios may fail to identify an aqueous-like or asphaltene-like stationary point on the TPD surface. For flash calculations, an aqueous-like or asphaltene-like composition should be applied to initialize a two-phase flash calculation in order to obtain a two-phase equilibrium containing an aqueous or asphaltene phase. Otherwise, if the aqueous or asphaltene phase appears in the actual phase equilibrium, the flash calculation may easily converge to a trivial phase equilibrium.

In order to simplify multiphase flash calculations, Michelsen (1994) suggested that some phases can be considered as a pure substance. For aqueous phase, Tang and Saha (2003) proposed that it can be regarded as pure water phase, which is called the free-water assumption. Based on this assumption, Lapene *et al.* (2010) proposed a three-phase free-water flash algorithm using a modified Rachford-Rice (RR) equation they have developed. This algorithm replaces the three-phase flash calculation by a pseudo-two-phase flash calculation, which enhances the computational efficiency of the algorithm. For asphaltene phase, Nghiem *et al.* (1993) developed an efficient asphaltene-precipitation model. In their model, vapor and liquid phases are modeled using a cubic EOS, while the asphaltene precipitated are regarded as a pure dense phase. Moreover, they assumed that the heaviest component in crude oil can be divided into a precipitating component and a non-precipitating component. These two components had identical critical properties and acentric factors, but different binary interaction parameters (BIPs) with the lighter components. A good agreement can be seen between the experimental results and the results yielded by this model with some parameters adjusted by the experimental data.

1.2 Problem Statement

Some technical problems still exist in three-phase equilibrium calculations. When conducting three-phase equilibrium calculations without a prior knowledge of the present phases, we may easily end up with a trivial solution (corresponding to a phase equilibrium). This issue is more severe when one of the possible phases in a three-phase equilibrium calculation is nearly a pure substance. There is still a lack of robust and efficient three-phase VLA and VLS equilibrium calculation algorithms which can be reliably applied in compositional simulators. The main research problems to be addressed in this dissertation include the following:

- Multiple stationary points may appear on the Gibbs free energy surface in a three-phase equilibrium calculation. When the possible three phases contain an aqueous phase or an asphaltene phase, one of the stationary points may appear near the boundary of the Gibbs free energy surface. This will lead to a high chance that the existing initialization methods of equilibrium ratios for stability tests fail to identify this kind of stationary points. This requires us to develop a new initialization approach which has a relatively high possibility of identifying all the stationary points on the Gibbs free-energy surface without obviously increasing the computational loads of stability tests in both three-phase VLA and VLS equilibrium calculations.
- In three-phase equilibrium calculations, two-phase flash calculations may frequently converge to a trivial phase equilibrium when multiple stationary points appear on the Gibbs free energy surface. This is because the flash calculation may converge to a local minimum Gibbs free energy instead of the global minimum

Gibbs free energy. The results of a flash calculation heavily depend on how the equilibrium ratios are initialized. If one of the present phases is an aqueous phase or an asphaltene phase, improved initialization scheme of the equilibrium ratios used in flash calculations should be developed to ensure the robustness of the three-phase equilibrium calculation algorithm. We are still lacking a comprehensive and robust initialization scheme for the flash calculations in the three-phase VLA or VLS equilibrium calculations.

- How to develop robust and efficient three-phase isothermal equilibrium calculation algorithms for the three-phase VLA and VLS equilibria by assuming that the aqueous phase or the asphaltene phase is a pure substance? New robust and efficient procedures for conducting the three-phase VLA and VLS equilibrium calculations need to be developed.
- How to incorporate the three-phase free-water isothermal equilibrium calculation algorithm into an isenthalpic equilibrium calculation algorithm? In thermal oil recovery processes, an isenthalpic three-phase VLA equilibrium calculation algorithm, instead of an isothermal VLA equilibrium calculation algorithm, is preferred.
- How to model the effect of asphaltene precipitation on the MMP of gas injection process by incorporating the three-phase VLS equilibrium calculation algorithm into the multiple-mixing-cell (MMC) method proposed by Ahmadi and Johns (2011)? Three VLS equilibrium calculation algorithm can be incorporated into the MMC method proposed by Ahmadi and Johns (2011) to study the effect of

asphaltene precipitation on the MMP of gas injection process as well as reveal the oil recovery mechanisms associated with such a process.

1.3 Research Objectives

The objective of this research is to develop more efficient and robust algorithms to simulate the three-phase VLA and VLS equilibria for reservoir fluids using the Peng-Robinson equation of state (PR EOS) (Peng and Robinson 1976). Short-term and long-term objectives are listed as follows:

Short-term objectives:

- Develop a three-phase isothermal equilibrium calculation algorithm where single-phase, two-phase, and three-phase VLA equilibria can be considered based on the free-water assumption for water/hydrocarbon mixtures;
- Develop a three-phase isenthalpic equilibrium calculation algorithm which can handle single-phase, two-phase, and three-phase VLA equilibria based on the free-water assumption for water/hydrocarbon mixtures;
- In cases where the free-water assumption does not hold, modify the conventional isothermal three-phase equilibrium calculation algorithm for water/hydrocarbon mixtures by applying a new initialization scheme to simultaneously ensure its robustness and enhance its computational efficiency;
- Develop a three-phase VLS isothermal equilibrium calculation algorithm where single-phase, two-phase, and three-phase VLS equilibria can be considered by applying the asphaltene-precipitation model proposed by Nghiem *et al.* (1993) for the hydrocarbon/asphaltene mixtures;

- Develop a modified MMC method, which can be used to predict MMP under the influence of asphaltene-precipitation phenomenon, by implementing the newly developed three-phase VLS isothermal equilibrium calculation algorithm.

Long-term objectives:

- Apply the newly developed algorithms to reservoir and wellbore simulators to more accurately simulate multiphase flow inside reservoir and wellbore and gain a better understanding of the effect of the aqueous phase's or asphaltene phase's appearance on the multiphase flow.

1.4 Thesis Structure

There are seven chapters in this dissertation. In **Chapter 1**, we introduce the research background, problem statement, and major research objectives. **Chapter 2** presents the development of the three-phase isothermal equilibrium calculation algorithm based on the free-water assumption for water/hydrocarbon mixtures. **Chapter 3** depicts the algorithm developed to conduct the three-phase isenthalpic equilibrium calculation with the free-water assumption for water/hydrocarbon mixtures. In **Chapter 4**, we modify the conventional isothermal three-phase VLA equilibrium calculation algorithm with the adoption of a new initialization scheme for cases where the free-water assumption does not hold. **Chapter 5** shows the development of the three-phase VLS isothermal equilibrium calculation algorithm by applying the asphaltene-precipitation model proposed by Nghiem *et al.* (1993). **Chapter 6** presents the revised MMC method developed to predict MMP considering asphaltene-precipitation effect by implementing the newly developed three-phase VLS isothermal equilibrium calculation algorithm. Finally, **Chapter 7**

summarizes the conclusions of the present research and the recommendations for future work.

1.5 References

Ahmadi, K., and Johns, R.T., 2011, Multiple-mixing-cell method for MMP calculations, *SPE J.* **16** (04): 733-742.

Connolly, M., 2018, An isenthalpic-based compositional framework for nonlinear thermal simulation, PhD thesis, Stanford University.

Gorucu, S.E., and Johns, R.T., 2016, Robustness of three-phase equilibrium calculations, *J. Petrol. Sci. Eng.* **143**: 72-85.

Lapene, A., Nichita, D.V., Debenest, G., and Quintard, M., 2010, Three-phase free-water flash calculations using a new Modified Rachford-Rice equation, *Fluid Phase Equilibr.* **297** (1):121-128.

Leibovici, C.F., and Neoschil, J., 1995, A solution of Rachford-Rice equations for multiphase systems, *Fluid Phase Equilibr.* **112**: 217-221.

Li, Z., and Firoozabadi, A., 2009, Cubic-plus-association equation of state for water-containing mixtures: Is “cross association” necessary? *AIChE J.* **55** (7): 1803-1813.

Michelsen, M.L., 1982a, The isothermal flash problem. Part I. Stability, *Fluid Phase Equilibr.* **9** (1): 1-19.

Michelsen, M.L., 1982b, The isothermal flash problem. Part II. Phase-split calculation, *Fluid Phase Equilibr.* **9** (1): 21-40.

Michelsen, M.L., 1994, Calculation of multiphase equilibrium, *Comput. Chem. Eng.* **18** (7): 545-550.

- Mortezazadeh, E., and Rasaei, M.R., 2017, A robust procedure for three-phase equilibrium calculations of water-hydrocarbon systems using cubic equations of state, *Fluid Phase Equilib.* **450**: 150-174.
- Nghiem, L.X., Hassam, M.S., Nutakki, R., and George, A.E.D., 1993, Efficient modelling of asphaltene precipitation, presented at SPE Annual Technical Conference and Exhibition, Houston, Texas.
- Peng, D.Y., and Robinson, D.B., 1976, A new two-constant equation of state, *Ind. Eng. Chem. Fundam.* **15** (1): 59-64.
- Tang, Y., and Saha, S., 2003, An efficient method to calculate three-phase free-water Flash for water-hydrocarbon systems, *Ind. Eng. Chem. Res.* **42** (1): 189-197.
- Whitson, C.H., and Michelsen, M.L., 1989, The negative flash, *Fluid Phase Equilib.* **53**: 51-71.

**CHAPTER 2 NEW TWO-PHASE AND THREE-PHASE
RACHFORD-RICE ALGORITHMS BASED ON FREE-WATER
ASSUMPTION**

A version of this chapter has been accepted for publication in *The Canadian Journal of Chemical Engineering*.

Abstract

Based on the free-water assumption that the water-rich liquid phase contains only pure water, we develop two simple free-water Rachford-Rice methods: 1) a two-phase free-water Rachford-Rice method where the phase fractions can be analytically solved; and 2) a three-phase free-water Rachford-Rice method where there is only one unknown in the objective function (i.e., the vapour-phase fraction) that is used for solving the phase fractions. Combining with these two Rachford-Rice methods, a new free-water flash algorithm is developed to perform multiphase flash calculations where single-phase equilibria, two-phase equilibria, and three-phase vapour-liquid-aqueous equilibria can be considered. In this free-water flash algorithm, we first test if the mixture is stable; if the mixture is found to be unstable, we directly initiate the three-phase free-water flash. A set of criteria is developed for one to properly switch from a three-phase free-water flash to either a two-phase free-water flash or a conventional two-phase flash, depending on whether a water-rich phase is present in the two-phase equilibrium. We also develop efficient and robust methods for initializing the equilibrium ratios for the two-phase flashes. The negative flash is allowed in the flash calculation algorithms. A number of example calculations are carried out to demonstrate the robustness of the newly developed algorithm. A good agreement can be achieved between the flash results obtained by the new flash algorithm and those obtained by the conventional full three-phase flash algorithm.

Keywords

Free-water flash, Two-phase equilibrium, Three-phase equilibrium, Negative flash, Optimization algorithm

2.1 Introduction

Multiphase equilibria are frequently encountered in oil/gas reservoirs where various hydrocarbon recovery processes take place. As a type of multiphase equilibria, a three-phase vapour-liquid-aqueous equilibrium can readily occur when the reservoir fluid contains water. To show the importance of the three-phase equilibrium, steam assisted gravity drainage (SAGD) process and solvent-assisted SAGD (SA-SAGD) process can be taken as examples. SAGD is one of the most successful methods for in-situ bitumen recovery.^[1] SA-SAGD is recently proposed to further enhance the bitumen drainage rate by taking advantage of the mass transfer from solvent into bitumen.^[2] Steam is continuously injected into the reservoir from the injector and forms a steam chamber in the SAGD process, while steam and a small amount of solvent are injected in the SA-SAGD process. Steam reduces the viscosity of bitumen by heating, while solvent reduces the viscosity of heavy oil through dilution.^[2] Multiphase equilibria, for example three-phase vapour-liquid-aqueous equilibrium, can form at the steam chamber boundary, exerting a remarkable influence on the drainage behaviour of bitumen.^[3, 4] In order to analyze the detailed hydrocarbon recovery mechanisms near the steam chamber boundary in SAGD or SA-SAGD processes, phase behaviour near the steam chamber boundary should be accurately captured. Due to the existence of water in the SAGD and SA-SAGD processes, it is necessary to consider multiphase equilibria consisting of single-phase equilibrium, two-phase equilibrium, and three-phase vapour-liquid-aqueous equilibrium, albeit the type of equilibrium depends on the feed composition that is present in the pore space as well as reservoir temperature/pressure.

For multiphase flash, the primary problem is the determination of the number of existing

phases. Two stage-wise approaches are implemented to solve this problem. One approach is performing the flash calculations with a pre-set number of existing phases. If any of the phases has a negative phase fraction, the flash calculations need to be conducted with a decreased number of phases.^[5, 6] As for this approach, it is difficult for one to obtain good initial values of the equilibrium ratios.^[7] Given a pre-set number of existing phases, a flash calculation normally requires the use of two iteration loops in order to solve the phase fractions and phase compositions. The outer loop is used to update the equilibrium ratios based on the fugacity equations, while the inner loop is used to calculate the phase fractions. Rachford-Rice equations^[8] are commonly used to solve phase fractions in the inner loop. The other widely used method is conducting the stability test prior to a flash calculation to determine if the number of phases needs to be increased.^[9-11] As for this method, the computational cost becomes escalated for multiphase flashes. For example, a three-phase flash involves two runs of stability tests, each of which may require multiple initial guesses of equilibrium ratios to enhance the accuracy of the stability test.^[7]

Considering the computational efficiency, only a vapour phase and a hydrocarbon-rich liquid phase are included in the phase equilibrium calculations in most of the equation-of-state-based compositional models.^[12, 13] These compositional models can be applied to approximately simulate the three-phase vapour-liquid-aqueous equilibria based on the fact that little hydrocarbons can be dissolved in the aqueous phase.^[12, 13] However, as pointed by Lapene *et al.*,^[14] adding water breaks the two-phase vapour-liquid equilibrium and moves the evaporation or condensation curve. Therefore, only conducting a two-phase vapour-liquid phase equilibrium calculation cannot yield an accurate description of the real phase behaviour where a three-phase

vapour-liquid-aqueous equilibrium exists. Hence, in order to simultaneously consider the effect of water and enhance the calculation speed, Lapene *et al.*^[14] proposed a three-phase free-water flash method using a newly modified Rachford-Rice equation^[8] based on the free-water assumption which considers the water-rich phase as pure phase.^[15] The fraction of the water-rich phase can be calculated based on the vapour-phase fraction in the modified Rachford-Rice equation. This algorithm replaces the three-phase flash by a pseudo-two-phase flash, leading to a significant improvement in the calculation speed. In this algorithm, they proposed an approach to determine whether a two-phase equilibrium or a three-phase equilibrium appears by analyzing the modified Rachford-Rice equation. The constraints proposed by Leibovici and Neoschil^[16] were applied in this algorithm. It is more accurate than the conventional approach mentioned above since water is considered as a feed component. However, if the water-rich liquid phase appears in the two-phase equilibrium, this algorithm may fail sometimes due to the absence of a good initialization method for the equilibrium ratios.

In this work, we provide new algorithms for conducting the two-phase/three-phase free-water flash based on a simplified version of the objective function proposed for multiphase flash computations^[17, 18] within the constraints proposed by Okuno *et al.*^[18] The so-called two-phase free-water flash refers to the case where an aqueous phase equilibrates with another phase, while the so-called three-phase free-water flash refers to the case where an aqueous phase equilibrates with one vapour phase and one hydrocarbon-rich liquid phase. As for the two-phase free-water flash, the phase fraction of the aqueous phase can be analytically solved; as for the three-phase free-water flash, the phase fractions of different phases can be iteratively solved, but only one unknown

variable in the objective function needs to be solved.^[14] The negative flash is permitted in the flash calculations.^[7, 19] Efficient and robust initialization methods for the equilibrium ratios are provided in the new flash algorithms. By combining these two free-water flash algorithms, a new flash package is then developed to compute multiphase equilibria that are comprised of single-phase equilibria, two-phase equilibria, and three-phase vapour-liquid-aqueous equilibria. A set of criteria are developed to replace the stability test^[10] required for properly switching between a two-phase flash and a three-phase flash. We demonstrate the performance of the new flash package through several example calculations.

2.2 Mathematical Formulations

The number of components in the mixture is assumed to be c , while the mixture is assumed to be able to split into N_p phases containing a water-rich liquid phase. The multiphase equilibrium can be described in terms of chemical potential as follows:

$$f_{ix} = f_{i1} = \dots = f_{ij}, i = 1, \dots, c, j = 1, \dots, N_p - 1 \quad (2-1)$$

where f represents fugacity. The first subscript i is the component index, while the second subscripts x and j are the phase index. In our case, we assume $i = 1$ represents the water component, and $j = 1$ represents the water-rich liquid phase. The x phase is chosen as the reference phase. Therefore, the equilibrium ratios can be defined as follows:

$$K_{ij} = \frac{y_{ij}}{x_i} = \frac{\phi_{ix}}{\phi_{ij}}, i = 1, \dots, c, j = 1, \dots, N_p - 1 \quad (2-2)$$

where K represents the equilibrium ratio; ϕ represents the fugacity coefficient; x and y are the mole fractions in the reference phase and the non-reference phase, respectively.

In the free-water assumption,^[15] we assume that water component can be present in all

phases, while the non-water components can be only dissolved in the non-water-rich phases. In other words, the water-rich phase is assumed as pure water. Then the following expressions are valid for the mole fractions of each component in the water-rich phase:

$$y_{i1} = \begin{cases} 1, i=1 \\ 0, i \neq 1 \end{cases} \quad (2-3)$$

For the equilibrium ratios of the water-rich phase with respect to the reference phase, only the one for the water component, i.e. K_{11} , is valid, while all the other equilibrium ratios for non-water components are zero. The mole fractions of water component in the reference phase and the non-reference phases (except the water-rich phase) can be inferred as follows:

$$x_1 = \frac{1}{K_{11}} \quad (2-4)$$

and

$$y_{1j} = \frac{K_{1j}}{K_{11}}, j = 2, \dots, N_p - 1 \quad (2-5)$$

Material balance requires the following equations:

$$z_i = \beta_x x_i + \sum_{j=2}^{N_p-1} \beta_j y_{ij} + \beta_1 y_{i1}, i = 1, \dots, c \quad (2-6)$$

$$\beta_x + \sum_{j=2}^{N_p-1} \beta_j + \beta_1 = 1 \quad (2-7)$$

where z represents the mole fraction in the feed; and β represents the phase mole fraction. Subsequently, the phase fraction of the water-rich phase can be obtained by substituting Equation (2-7) into Equation (2-6) for the water component:

$$\beta_1 = \frac{z_1 + \sum_{j=2}^{N_p-1} [(x_1 - y_{1j}) \beta_j] - x_1}{1 - x_1} \quad (2-8)$$

In particular, for a two-phase flash involving an aqueous phase, the Equation (8) can be simplified as follows:

$$\beta_1 = \frac{z_1 - x_1}{1 - x_1} \quad (2-9)$$

which indicates that the phase fractions can be analytically solved.

For the non-water components, Equation (2-6) can be simplified as follows:

$$z_i = x_i \left(1 - \sum_{j=2}^{N_p-1} \beta_j - \beta_1 \right) + \sum_{j=2}^{N_p-1} K_{ij} \beta_j x_i, \quad i \neq 1 \quad (2-10)$$

We thereby obtain the expression for the mole fractions of non-water components in the reference phase by substituting Equation (2-8) into Equation (2-10):

$$x_i = \frac{z_i}{1 + \sum_{j=2}^{N_p-1} \left(K_{ij} - 1 + \frac{y_{1j} - x_1}{1 - x_1} \right) \beta_j + \frac{x_1 - z_1}{1 - x_1}} = \frac{z_i}{\sum_{j=2}^{N_p-1} (K_{ij} - K_{wj}^*) \beta_j + K_{wz}^*}, \quad i \neq 1 \quad (2-11)$$

where,

$$\begin{cases} K_{wj}^* = \frac{1 - y_{1j}}{1 - x_1}, \quad j \neq 1 \\ K_{wz}^* = \frac{1 - z_1}{1 - x_1} \end{cases} \quad (2-12)$$

Equation (2-12) refers to the “effective” equilibrium constants as defined by Tang and Saha.^[15] Combining Equations (2-2) and (2-11) gives the mole fractions of non-water components in the non-reference phases except the water-rich phase:

$$y_{ij} = \frac{K_{ij}z_i}{1 + \sum_{j=2}^{N_p-1} \left(K_{ij} - 1 + \frac{y_{1j} - x_1}{1 - x_1} \right) \beta_j + \frac{x_1 - z_1}{1 - x_1}} = \frac{K_{ij}z_i}{\sum_{j=2}^{N_p-1} (K_{ij} - K_{wj}^*) \beta_j + K_{wz}^*}, \quad i \neq 1, j \neq 1 \quad (2-13)$$

The following gives the expression of the objective function and constraints for a multiphase flash which were developed by Okuno *et al.*:^[18]

$$\begin{cases} \min : f(\boldsymbol{\beta}) = \sum_{i=1}^c -z_i \ln \left| 1 - \sum_{j=1}^{N_p-1} (1 - K_{ij}) \beta_j \right|, \quad i = 1, \dots, c \\ \text{Subject to : } \mathbf{a}_i^T \boldsymbol{\beta} \leq \mathbf{b}_i, \quad i = 1, \dots, c \end{cases} \quad (2-14)$$

where $\mathbf{a}_i = \{1 - K_{ij}\}$, $\boldsymbol{\beta} = \{\beta_j\}$, and $\mathbf{b}_i = \min\{1 - z_i, \min_j \{1 - K_{ij}z_i\}\}$. By combining the above objective function with Equation (2-8), the reduced objective function for the multiphase free-water flash can be obtained as follows:

$$f(\beta_j) = \sum_{i=2}^c -z_i \ln \left| \sum_{j=2}^{N_p-1} (K_{ij} - K_{wj}^*) \beta_j + K_{wz}^* \right| + \left(-z_1 \ln \left| \frac{z_1}{x_1} \right| \right), \quad j = 2, \dots, N_p - 1 \quad (2-15)$$

It is noted that z_1 is known as the mole fraction of water component in the feed. When conducting flash calculations, equilibrium ratios and phase compositions are updated in the outer loop, while the phase fractions are solved by minimizing the objective function in the inner loop. When the objective function is minimized in each inner loop, x_1 is a constant that is fed from the outer loop. Hence, $-z_1 \ln \left| \frac{z_1}{x_1} \right|$ should be a constant in every inner loop.

This term will only translate the objective function upward or downward and will not affect the result of β_j to be solved. Therefore, the constant term, $-z_1 \ln \left| \frac{z_1}{x_1} \right|$, can be removed from the objective function. The objective function for the multiphase free-water flash is hence shown as follows:

$$f(\beta_j) = \sum_{i=2}^c -z_i \ln \left| \sum_{j=2}^{N_p-1} (K_{ij} - K_{wj}^*) \beta_j + K_{wz}^* \right|, j = 2, \dots, N_p - 1 \quad (2-16)$$

The constraints for non-water components can be simplified as follows on the basis of the free-water assumption:

$$\sum_{j=2}^{N_p-1} (1 - K_{ij}) \beta_j + \beta_1 \leq \min \left\{ 1 - z_i, \min_{j \neq 1} \{1 - K_{ij} z_i\} \right\}, i \neq 1 \quad (2-17)$$

By substituting Equation (2-8) into Inequality (2-17), the constraints for non-water components can be rewritten as follows:

$$\sum_{j=2}^{N_p-1} (K_{wj}^* - K_{ij}) \beta_j \leq \min \left\{ K_{wz}^* - z_i, \min_{j \neq 1} \{K_{wj}^* - K_{ij} z_i\} \right\}, i \neq 1 \quad (2-18)$$

For the water component, substituting Equation (2-2) and (2-8) into the left-hand side (LHS) of the constraints yields the following term:

$$LHS = \sum_{j=2}^{N_p-1} \left(1 - \frac{y_{1j}}{x_1} \right) \beta_j + \left(\frac{x_1 - 1}{x_1} \right) \frac{z_1 + \sum_{j=2}^{N_p-1} [(x_1 - y_{1j}) \beta_j] - x_1}{1 - x_1} = 1 - \frac{z_1}{x_1} \quad (2-19)$$

For any x_1 belonging to $[0, 1]$, we can obtain $\frac{1}{x_1} \geq 1$, which can be used to prove that

$1 - \frac{z_1}{x_1} \leq 1 - z_1$. Since $y_{1j} \leq 1$, we can also prove that $1 - \frac{z_1}{x_1} \leq 1 - y_{1j} \frac{z_1}{x_1} = 1 - K_{1j} z_1, j \neq 1$. In

addition, $1 - \frac{z_1}{x_1} = 1 - K_{11} z_1$. Hence, it can be verified that, for the water component, the

constraints always hold. Therefore, only the constraints as given by Inequality (2-18) are necessary to be included in this minimization problem. In summary, the objective function and constraints for the multiphase free-water flash using an optimization method can be expressed by the following:

$$\left\{ \begin{array}{l} \min : f(\beta_j) = \sum_{i=2}^c -z_i \ln \left| \sum_{j=2}^{N_p-1} (K_{ij} - K_{wj}^*) \beta_j + K_{wz}^* \right| \\ \text{Subject to : } \sum_{j=2}^{N_p-1} (K_{wj}^* - K_{ij}) \beta_j \leq \min \left\{ K_{wz}^* - z_i, \min_{j \neq 1} \{ K_{wz}^* - K_{ij} z_i \} \right\}, i \neq 1 \end{array} \right. \quad (2-20)$$

Since the modified objective function has the similar form to the original objective function^[17, 18], convexity of this modified objective function can be similarly proved. For a three-phase vapour-liquid-aqueous equilibrium, the objective function and constraints can be expressed as follows:

$$\left\{ \begin{array}{l} \min : f(\beta_y) = \sum_{i=2}^c -z_i \ln \left| (K_{iy} - K_{wy}^*) \beta_y + K_{wz}^* \right| \\ \text{Subject to : } (K_{wy}^* - K_{iy}) \beta_y \leq \min \left\{ K_{wz}^* - z_i, K_{wz}^* - K_{iy} z_i \right\}, i \neq 1 \end{array} \right. \quad (2-21)$$

where,

$$\left\{ \begin{array}{l} K_{wy}^* = \frac{1 - y_{1y}}{1 - x_1} \\ K_{wz}^* = \frac{1 - z_1}{1 - x_1} \end{array} \right. \quad (2-22)$$

where the subscript y represents the vapour phase. Note that the only one unknown in the above objective function is the fraction of the vapour phase. The hydrocarbon-rich phase is chosen as the reference phase. By integrating the modified Rachford-Rice equation derived by Lapene *et al.*,^[14] the same objective function can be obtained as well. To prove that the new constraints given by formula (2-21) maintain or shrink the feasible region as constructed by Lapene *et al.*,^[14] we express an alternative version of the new constraints given by formula (2-21) as below:

$$\max_{K_y > K_{wy}^*} \left\{ \frac{K_{wz}^* - z_i}{K_{wy}^* - K_{iy}}, \frac{K_{wz}^* - K_{iy} z_i}{K_{wy}^* - K_{iy}} \right\} \leq \beta_y \leq \min_{K_y < K_{wy}^*} \left\{ \frac{K_{wz}^* - z_i}{K_{wy}^* - K_{iy}}, \frac{K_{wz}^* - K_{iy} z_i}{K_{wy}^* - K_{iy}} \right\}, i \neq 1 \quad (2-23)$$

while the following shows the constraints given by Lapene *et al.*:^[14]

$$\max_{K_{iy} > K_{iy}^*} \left\{ \frac{K_{wz}^* - K_{iy} z_i}{K_{wy}^* - K_{iy}} \right\} \leq \beta_y \leq \min_{K_{iy} < K_{iy}^*} \left\{ \frac{K_{wz}^* - z_i}{K_{wy}^* - K_{iy}} \right\}, i \neq 1 \quad (2-24)$$

By comparing these two Inequalities (2-23) and (2-24), it is obvious that the feasible region defined by the constraints in the formula (2-21) is indeed smaller than, or at least, the same as the one given by Lapene *et al.*:^[14]

2.3 Two-Phase and Three-Phase Free-Water Flash Algorithm

2.3.1 Procedure of the Two-Phase and Three-Phase Free-Water Flash Algorithm

Simpler free-water flashes can be implemented by applying the simplified objective functions discussed above. We provide the detailed procedures for performing the two-phase and three-phase free-water flashes in the Appendix 2-A and 2-B, respectively. Combing with the flash algorithms simplified by the free-water assumption,^[15] we aim to develop an efficient flash package that can handle multiphase equilibrium calculations involving single-phase equilibria, two-phase equilibria, and three-phase vapour-liquid-aqueous equilibria. Later on, the term three-phase free-water flash means the standalone algorithm where only the three-phase vapour-liquid-aqueous equilibrium is considered, while the three-phase free-water flash package means the complete algorithm which considers all the one-phase equilibria, two-phase equilibria, and three-phase vapour-liquid-aqueous equilibria.

An essential task associated with the multiphase flash calculations is the determination of the number of existing phases. In this study, we first test the stability of the feed using the conventional stability test.^[10] Then, we initiate three-phase free-water flash calculations. Based on the criteria to be discussed below, we can determine if two-phase flashes are

required. The number of phase-fraction variables to be solved in the three-phase free-water flash is reduced to one as mentioned previously. It will not be computationally expensive to initiate calculations from a pre-set three phases, since it is easy to find the minimum value of the objective function with only one unknown. Figure 2-1 shows the calculation procedure adopted by the new flash package. Its procedure is outlined as follows:

- 1) Check the stability of the feed by stability analysis. In the stability analysis, the tangent plane distance (TPD) function is assessed.^[9, 10] If the TPD is found to be nonnegative, the feed is stable; otherwise, the feed is unstable;
- 2) If the feed is stable, a single-phase equilibrium can be concluded. If the feed is unstable, a three-phase free-water flash is directly initiated;
- 3) If an open feasible region, corresponding to a region where at least one of the endpoints is a pole, appears in any iteration or any of the ultimately calculated phase fractions do not fall into $[0, 1]$, a two-phase flash needs to be conducted;
- 4) The phase disappears when the corresponding phase fraction becomes negative. An aqueous phase is considered not to appear in a two-phase equilibrium if either of the following three scenarios appears: 1) The open feasible region does not appear in any iteration and the ultimately solved aqueous-phase fraction is the smallest and negative; 2) The open feasible region appears in the first iteration and the feasible region does not have an upper bound; and 3) The open feasible region appears after the first iteration and the aqueous-phase fraction that is solved in the last iteration before the open feasible region appears is the smallest and negative; and
- 5) A conventional two-phase flash will be conducted if the aqueous phase does not appear. Otherwise, a two-phase free-water flash needs to be conducted.

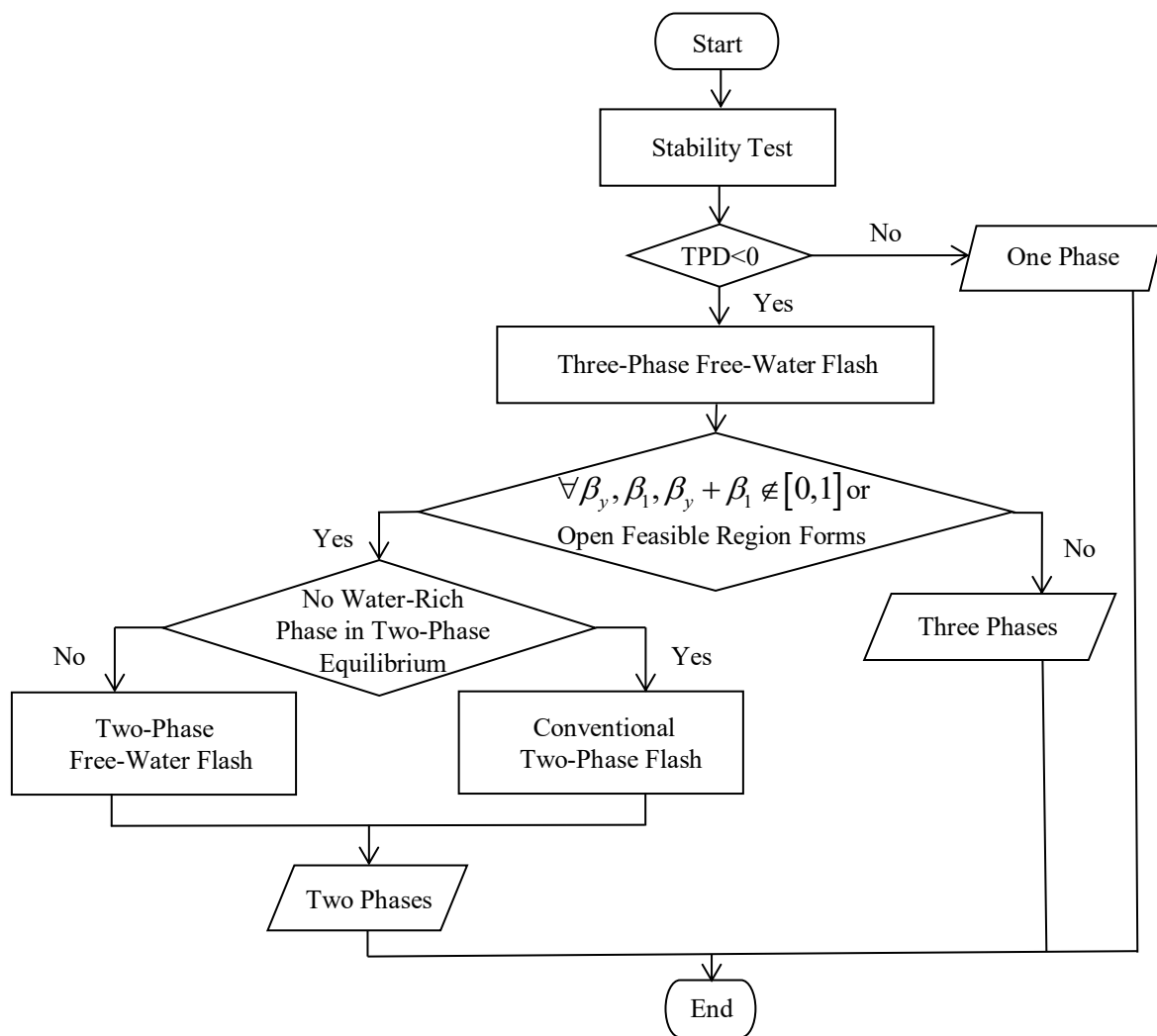


Figure 2-1 Flow chart of a new three-phase free-water flash package

Table 2-1 shows the comparison of the numbers of stability tests and flashes that need to be conducted in the conventional full three-phase flash package and in the new three-phase free-water flash package, respectively. In this table, *FWF* represents the new free-water flash package. As seen from Table 2-1, overall, our flash algorithm requires a reduced number of stability tests than the conventional flash algorithm. In the case of a three-phase equilibrium, our flash package eliminates one run of stability test and one run of two-phase flash. In the case of a two-phase equilibrium, our flash package replaces one run of stability

test with a three-phase free-water flash.

Table 2-1 Comparison of the numbers of stability tests and flashes needed by the conventional full three-phase flash package and the three-phase free-water flash package

Type of Calculation	One-Phase Equilibrium		Two-Phase Equilibrium		Three-Phase Equilibrium	
	FWF*	Conventional	FWF*	Conventional	FWF*	Conventional
Stability Test	1	1	1	2	1	2
Two-Phase Flash	0	0	1	1	0	1
Three-Phase Flash	0	0	1	0	1	1

Note: *stands for the free-water flash.

Appropriate initialization of equilibrium ratios plays an important role in enhancing the efficiency and robustness of multiphase flash algorithms. In this study, the method for initializing the equilibrium ratios given by Lapene *et al.*^[14] is applied for the three-phase free-water flash as well as the conventional two-phase vapour-liquid flash. For the two-phase free-water flash, we first initialize the compositions of the two phases as follows:

- For the water-rich liquid phase: Based on the fact that little hydrocarbons can be dissolved in the water-rich phase, the initial molar fractions of the non-water components are set to 10^{-10} , while water's initial molar fraction is set to be $1-(c-1)\times 10^{-10}$; and
- For the other phase: The compositions are set equally as $1/c$.

Then the equilibrium ratios can be calculated by the initialized compositions. Appendix 2-A shows the details of this initialization method.

2.3.2 Criteria for Switching from a Three-Phase Free-Water Flash to a Two-Phase Flash

One needs to make sure that the switching from a three-phase equilibrium to a two-phase equilibrium is always correct if a three-phase equilibrium is false. When the three-phase free-water flash is immediately initiated after the stability test dictates that the mixture is unstable, two kinds of unphysical results obtained by the three-phase flash will tell that a two-phase equilibrium will appear.

The first case refers to the case that the phase fractions can be solved by the three-phase free-water flash, but some of the solved phase fractions do not belong to $[0, 1]$. Whitson and Michelsen^[5] described this as negative flash and discussed the reason and meaning of this phenomenon. In this case, the feasible region is always closed and solutions exist within the feasible region. The other case is that the open feasible region appears during the running of the three-phase free-water flash algorithm, leading to the fact that the phase fractions cannot be solved. Under such circumstance, no feed composition can satisfy the material balance relations in a three-phase equilibrium including a water-rich liquid phase. Herein, we use an example calculation for the water/C4/C20 mixture to illustrate the second case, i.e., the appearance of an open feasible region. Appendix 2-C shows the feed compositions, component properties, and binary interaction parameters (BIPs) used in the calculation. Figure 2-2 shows the phase fractions obtained by applying the standalone three-phase free-water flash algorithm for the water/C4/C20 mixture at 50 bar. In this figure, V represents the vapour phase, HC represents the hydrocarbon-rich phase, and W represents the water-rich liquid phase. As shown in Figure 2-2, three-phase equilibria occur from 450.9 K to 523.1 K. The two-phase and three-phase boundary temperature (i.e.,

450.9 K and 523.1 K in this case) is determined to be the temperature where any of the phase fractions of the three phases becomes zero.

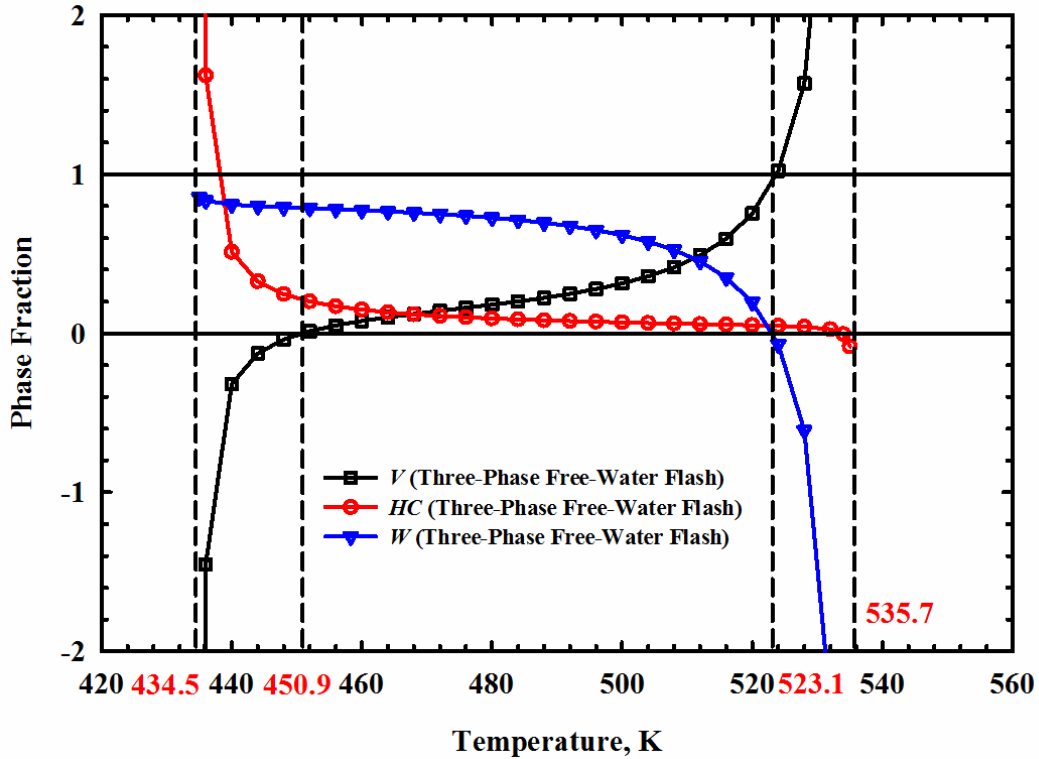


Figure 2-2 Phase fractions obtained by applying the standalone three-phase free-water flash algorithm for the water/C4/C20 mixture at 50 bar

Figure 2-3 shows the ternary diagram for the water/C4/C20 mixture at 50 bar and several different temperatures. The triangles shown in Figure 2-3 correspond to the three-phase tie triangles. Over this temperature range, the feed composition is inside the triangles shown in Figure 2-3, such that we can obtain three physical phase fractions. At a temperature beyond 450.9 K-523.1 K, unphysical phase fractions will be obtained and the feed composition is outside the triangles.^[5] As shown in Figure 2-3, when the temperature is 434.5 K or 535.7 K, the triangle is nearly collapsing into a straight line. When the triangle becomes a line, no feed composition can form a three-phase equilibrium. The disappearance of the triangle in

the ternary diagram is caused by the narrowing of the difference between the compositions of any arbitrary two phases: 1) If the two phases contain a water-rich phase, equilibrium ratios in the vapour phase with respect to the reference phase, so-called K_{iy} , may become zero or infinity for the non-water components; and 2) If the two phases do not contain a water-rich phase, K_{iy} may become one for the non-water components. As a result, the coefficient of β_y in the constraints will be the same for every non-water component. Therefore, an open feasible region will form and the objective function cannot be solved.

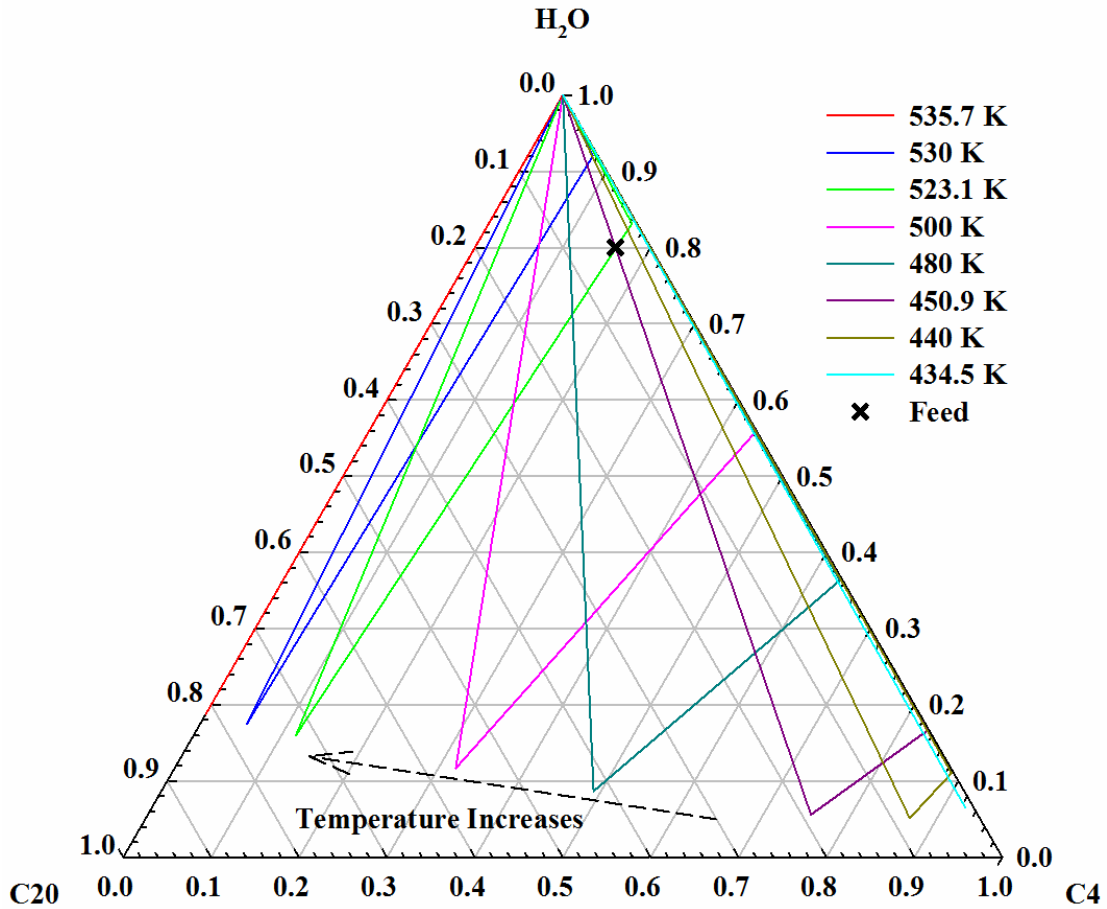


Figure 2-3 Three-phase triangles for the water/C4/C20 mixtures at 50 bar

2.4 Example Applications

To test the robustness of the new flash package, we apply it to both synthetic and real fluid mixtures containing water. We then compare the calculation results obtained from our method to those obtained from the conventional multiphase flash method. Peng-Robinson equation of state (PR EOS) is used in all the calculations.^[20] Appendix 2-C shows the feed compositions, component properties, and BIPs used for these examples. In the upcoming figures, V represents the vapour phase, HC represents the hydrocarbon-rich phase, and W represents the water-rich liquid phase.

2.4.1 Water/C4/C20 Mixture

The water/C4/C20 mixture is a simple synthetic fluid mixture which contains water, a solvent, and a heavy hydrocarbon. This mixture is proposed for emulating the water/solvent/bitumen mixture associated with the SA-SAGD process. Figure 2-4 shows the three-phase envelope calculated for the water/C4/C20 mixture (See Table C.1). Figure 2-4 also shows the two-phase envelope calculated for the C4/C20 mixture (80 mol% C4, 20 mol% C20), which has the same mole-fraction ratios of C4 and C20 as the water/C4/C20 mixture. It can be seen from Figure 2-4 that, at temperatures < 400 K, the three-phase envelope for the water/C4/C20 mixture tends to be closer to the two-phase envelope. This observation indicates that we can well approximate the phase behaviour of the water/C4/C20 mixture with that of the C4/C20 mixture at lower temperature. As temperature increases, the deviation between the three-phase envelope and two-phase envelope becomes enlarged, indicating a larger impact resulted from the presence of water on the phase behaviour of the C4/C20 mixture. As shown in Figure 2-4, there is a good agreement between the three-phase envelope obtained by applying the three-phase

free-water flash package and that obtained by applying the conventional three-phase flash package.

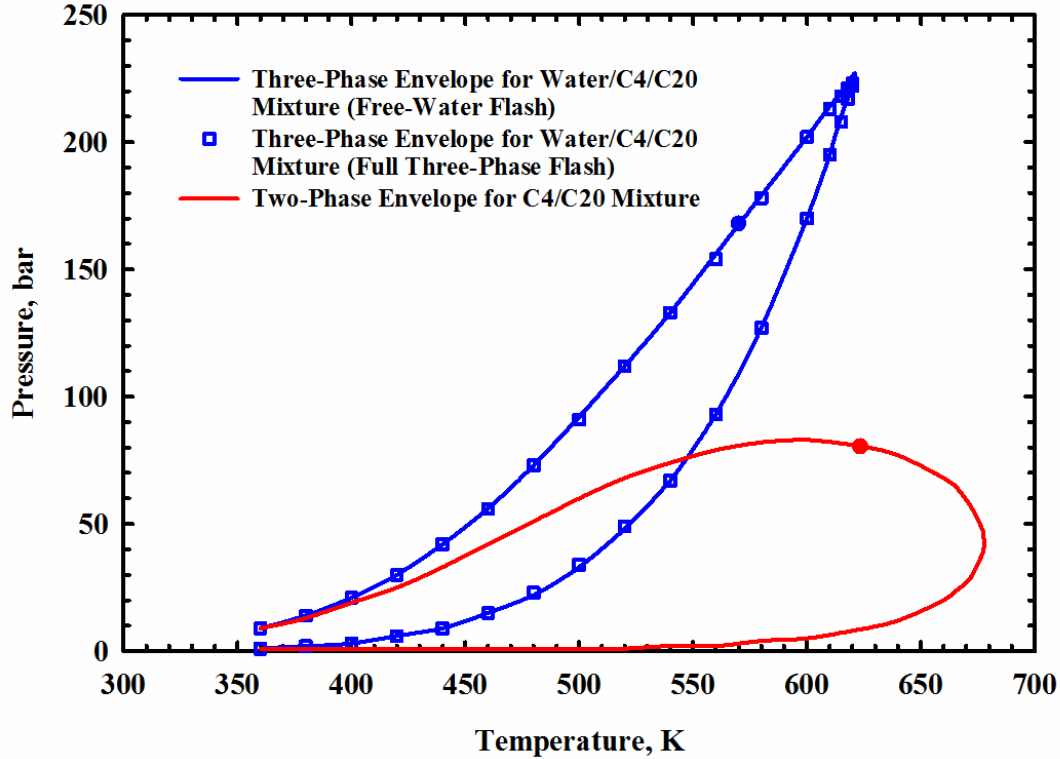


Figure 2-4 Calculated three-phase envelopes for the water/C4/C20 mixture and calculated two-phase envelopes for the C4/C20 mixture. Both the conventional three-phase flash and the three-phase free-water flash packages have been used to calculate the three-phase envelopes

Figure 2-5 compares the mole fractions of individual components in the hydrocarbon-rich phase that are calculated by using the two three-phase flash packages for the water/C4/C20 mixture at 50 bar. Figure 2-5a describes the variation of the mole fractions of individual components in the hydrocarbon-rich phase as temperature changes. In the three-phase region, it is obvious that, with an increasing temperature, more water tends to be dissolved in the hydrocarbon-rich phase. Such higher water fraction in the hydrocarbon-rich phase can actually help to reduce the viscosity of the hydrocarbon-rich phase.^[21] Figure 2-5b shows the absolute value of the absolute deviations between the mole fractions calculated

by the two three-phase flash packages. The largest absolute deviation is found to be $< 3 \times 10^{-6}$, which demonstrates that the free-water flash provides an accurate description of the phase equilibria as given by the conventional flash.

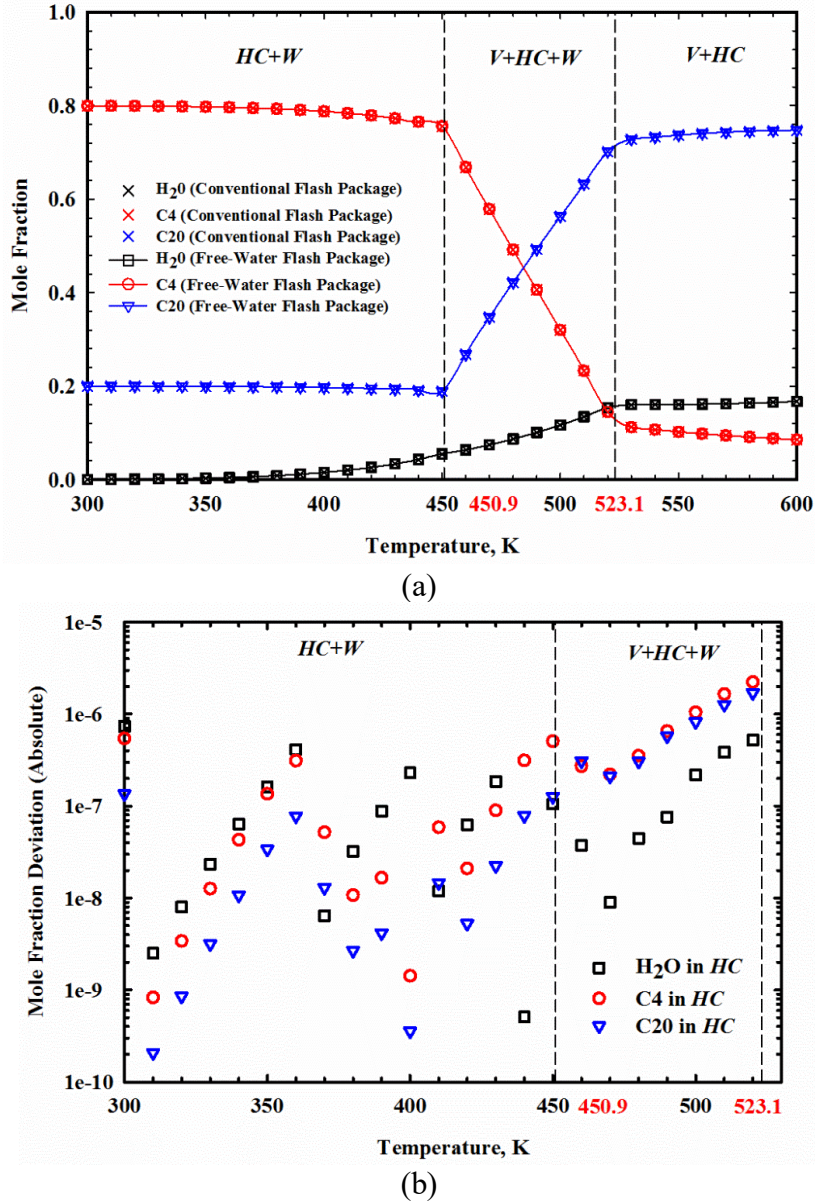
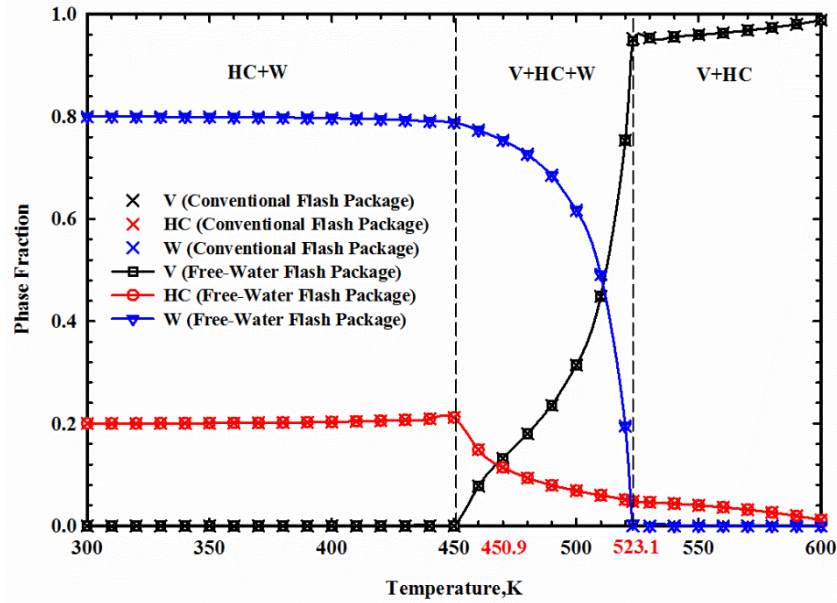
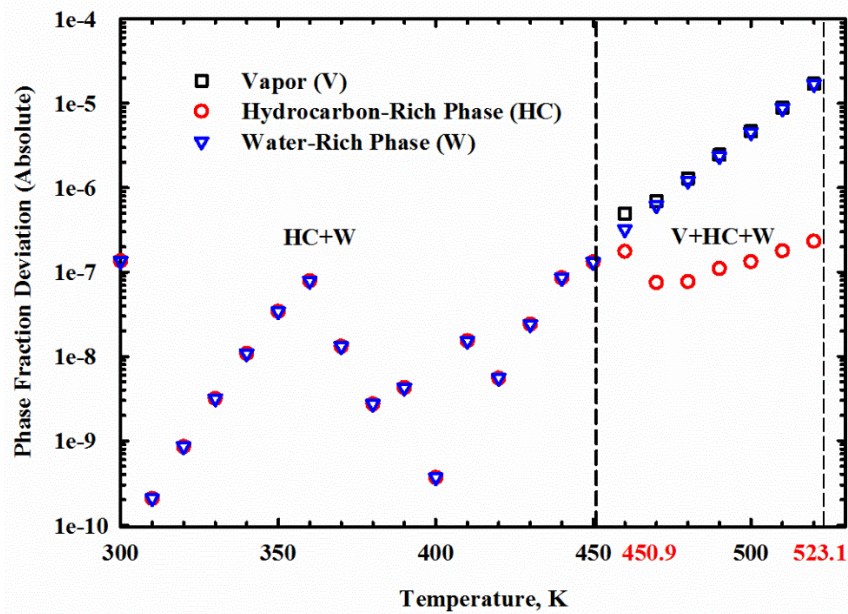


Figure 2-5 Comparison between the mole fractions of individual components in the hydrocarbon-rich phase obtained by applying the three-phase free-water flash package and those obtained by applying the conventional three-phase flash package for the water/C4/C20 mixture at 50 bar: (a) variation of the mole fractions of individual components in the hydrocarbon-rich phase as a function of temperature; (b) absolute deviations in the mole fractions of individual components that are calculated with the two three-phase flash packages

Figure 2-6 shows the phase fractions obtained from both the conventional three-phase flash package and the three-phase free-water flash package for the water/C4/C20 mixture at 50 bar. Figure 2-6a shows the variation of the phase fractions as a function of temperature. As shown in the figure, the three-phase equilibrium occurs at 450.9 K to 523.1 K. Figure 2-6b presents the absolute deviations between the calculated phase fractions using these two packages in the two-phase liquid-aqueous and three-phase vapour-liquid-aqueous regions. The absolute deviations are found to be $< 2 \times 10^{-5}$, which indicates that the free-water flash can provide accurate approximations to the phase fractions obtained by the conventional flash.



(a)



(b)

Figure 2-6 Comparison between the phase fractions obtained by applying the three-phase free-water flash package and those obtained by applying the conventional three-phase flash package for the water/C4/C20 mixture at 50 bar: (a) variation of the phase fractions as a function of temperature; (b) absolute deviations in the phase fractions that are calculated with the two three-phase flash packages

Figure 2-7 shows the comparison of the number of the outer-loop iterations required by the three-phase free-water flash algorithm and the conventional three-phase flash

algorithm for the water/C4/C20 mixture at 50 bar. It is shown in Figure 2-7 that the iteration times are reduced in the three-phase free-water flash algorithm. In addition to the reduced number of outer-loop iterations, less time is needed in the inner loop because the objective function in the inner loop of the three-phase flash algorithm contains only one unknown. Therefore, these two effects, i.e., reduction of both the number of outer-loop iterations and the time needed in the inner loop, contribute to a higher computational efficiency of the new algorithm than the conventional approach.

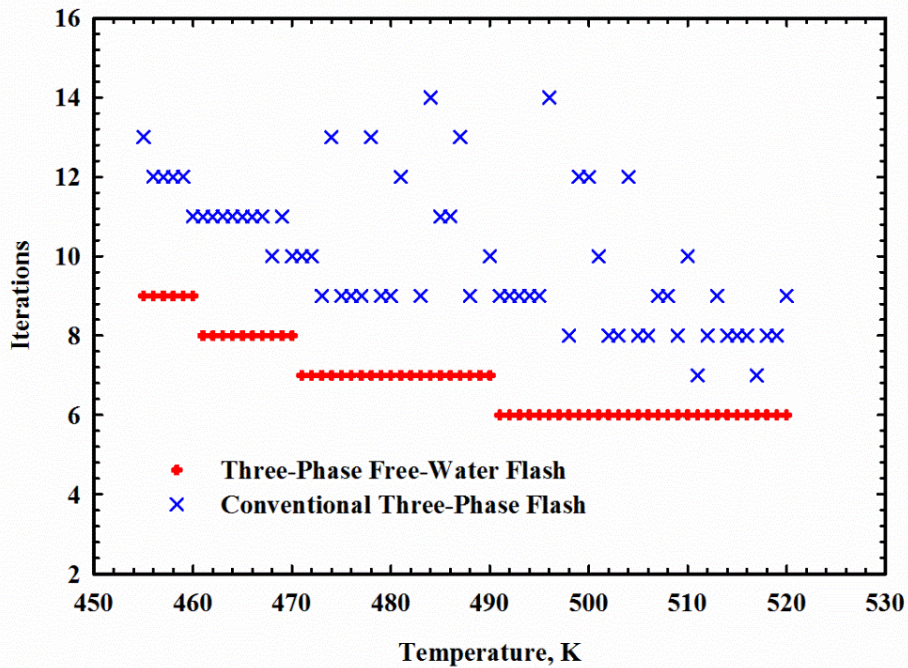


Figure 2-7 Comparison between the number of iterations in the outer loop required by the three-phase free-water flash algorithm and those required by the conventional three-phase flash algorithm for the water/C4/C20 mixture at 50 bar

Figure 2-8 compares the computational time required by one run of the three-phase free-water flash package and one run of the conventional three-phase flash package for the water/C4/C20 mixture at 50 bar. The interior-point method is used for solving the phase fractions in the three-phase free-water flash as well as in the conventional

three-phase flash. As shown in Figure 2-8, the total computational time is significantly reduced with the application of the three-phase free-water flash package. The total number of runs involved in this exercise is 150. We have saved about 7.6 seconds by using the three-phase free-water flash package to complete all the runs, instead of using the conventional three-phase flash package.

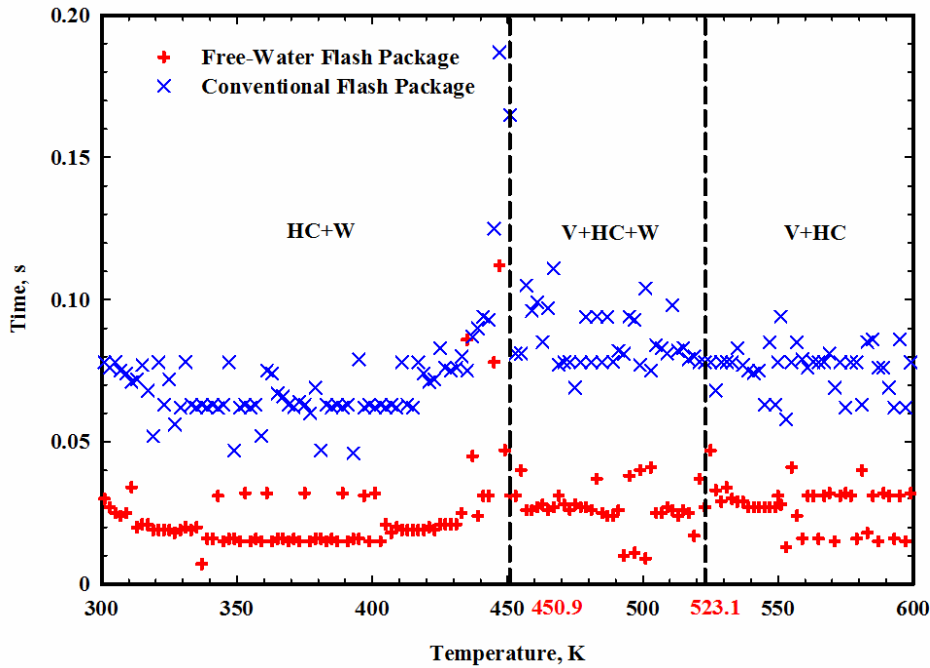
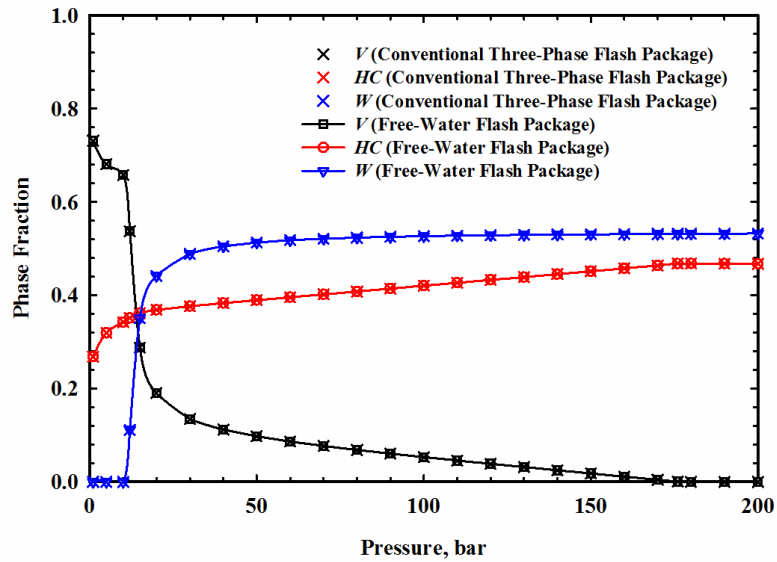


Figure 2-8 Comparison between the total computational time of one run of the three-phase free-water flash package and one run of the conventional three-phase flash package for the water/C4/C20 mixture at 50 bar

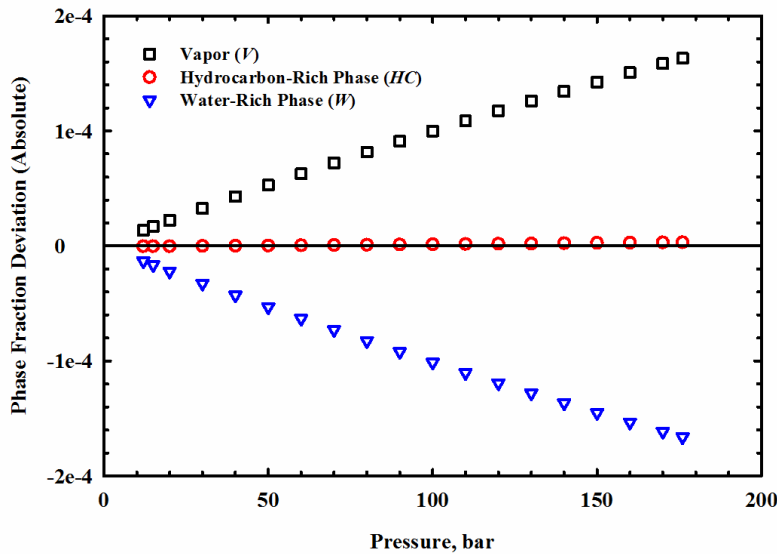
2.4.2 Water/N₂/C10/C20 Mixture

This water/N₂/C10/C20 mixture was also used by Lapene *et al.*^[14] Pressure is varied along an isothermal temperature of 450 K during the flash calculations. Figure 2-9 compares the phase fractions calculated with the three-phase free-water flash package and the conventional three-phase flash package. Figure 2-9a shows the variation of the phase fractions as a function of temperature, while Figure 2-9b shows the deviations between the phase fractions calculated by using the two three-phase flash algorithms. The deviations

are calculated by subtracting the phase fractions calculated by the three-phase free-water flash by those obtained by the conventional three-phase flash. The maximum absolute deviation is found to be $< 2 \times 10^{-4}$, again indicating a good agreement between the calculation results provided by the two three-phase flash algorithms.



(a)



(b)

Figure 2-9 Comparison between the phase fractions obtained by applying the three-phase free-water flash package and those obtained by applying the conventional three-phase flash package for the water/ N_2 / C_{10} / C_{20} mixture at 450 K: (a) variation of the phase fractions as a function of pressure; (b) deviations in the phase fractions that are calculated with the two three-phase flash packages

Figure 2-10 shows the comparison between the phase fractions obtained by applying the standalone three-phase free-water flash algorithm and those obtained by applying the conventional three-phase flash package. Temperature is held at 450 K. As indicated in this figure, physical phase fractions obtained by the standalone three-phase free-water flash algorithm only appear in the three-phase region. The temperatures, at which the calculated phase fractions by the standalone three-phase flash algorithm begin to escape from [0, 1], are corresponding to the two-phase/three-phase boundary temperature as predicted by the conventional three-phase flash package.

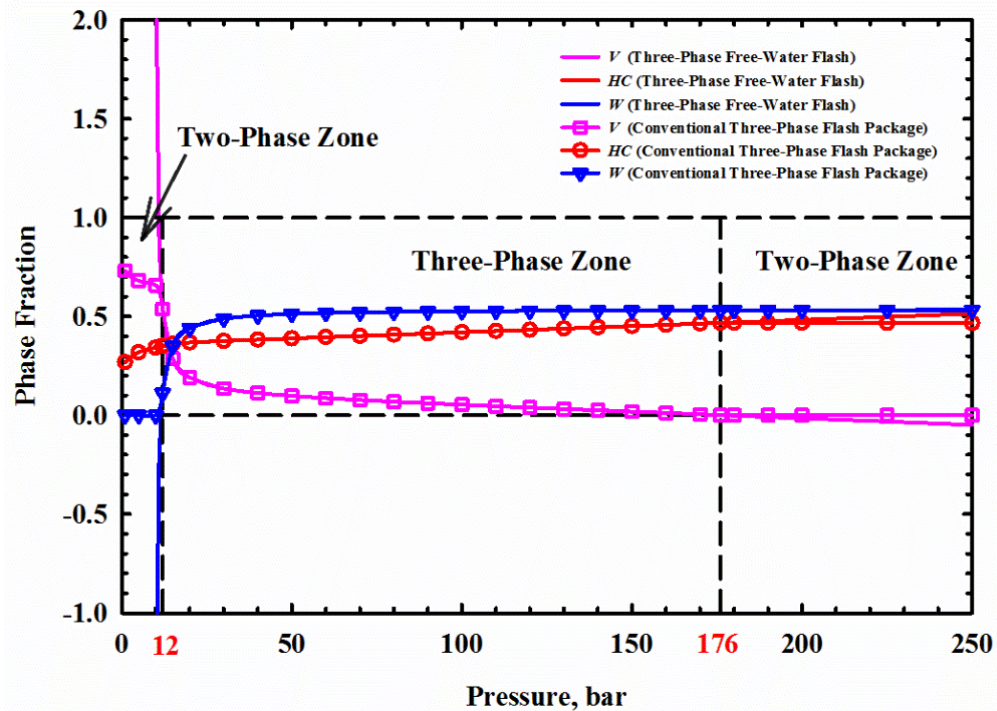
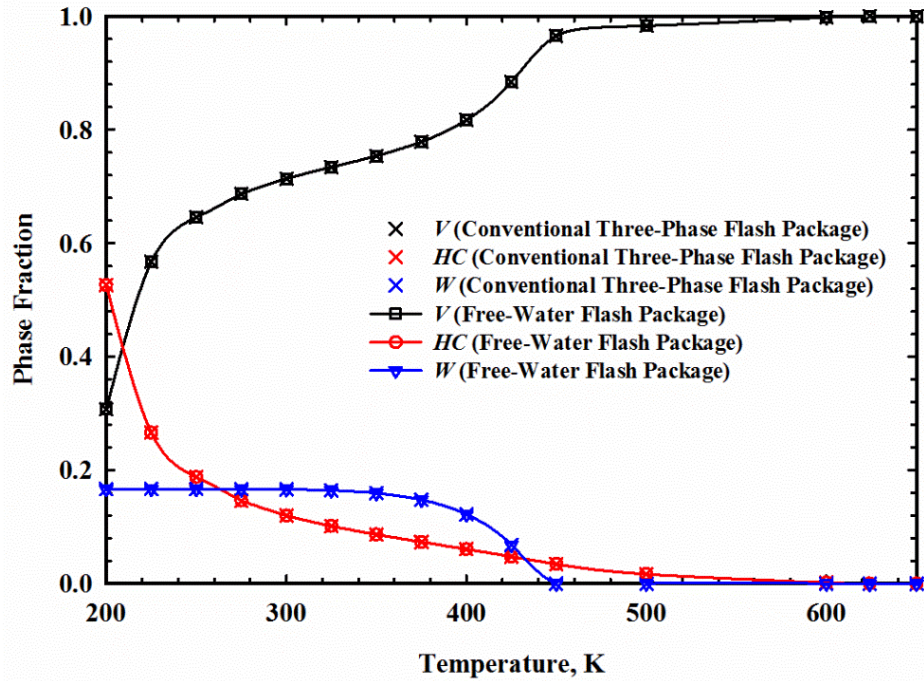


Figure 2-10 Comparison between the phase fractions obtained by applying the standalone three-phase free-water flash algorithm and those obtained by applying the conventional three-phase flash package for the water/ N_2 /C10/C20 mixture at 450 K

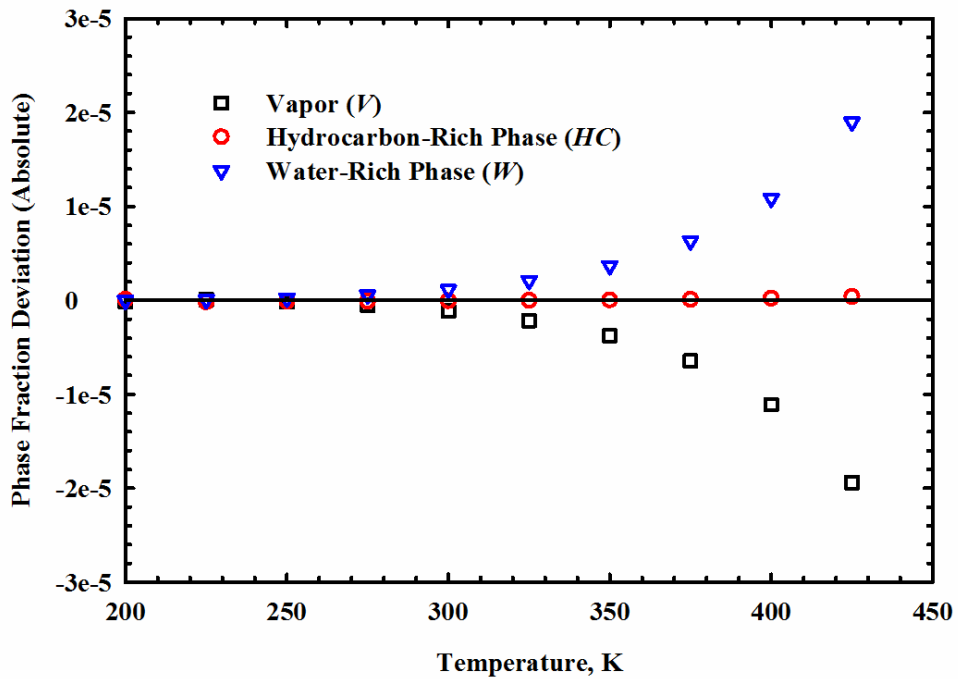
2.4.3 Water/Reservoir Fluid Mixture

This water/reservoir fluid mixture was also used by Lapene *et al.*^[14] Figure 2-11a

compares the phase fractions that are obtained by using the three-phase free-water flash package and the conventional three-phase flash package at 50 bar, while Figure 2-12a compares the phase fractions that are obtained with these two packages at 450 K. Figures 2-11b and 2-12b describe the absolute deviations between the results obtained by these two packages. As indicated by these figures, as for both the isobaric case (shown in Figure 2-11) and the isothermal case (shown in Figure 2-12), we can achieve a good agreement between the calculated phase fractions by the two flash methods.

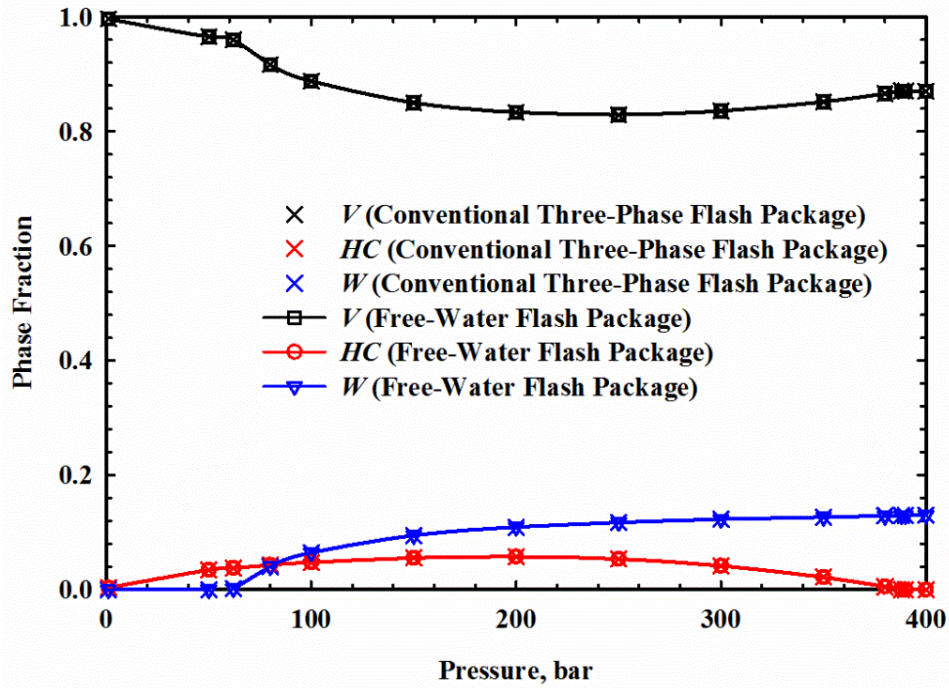


(a)

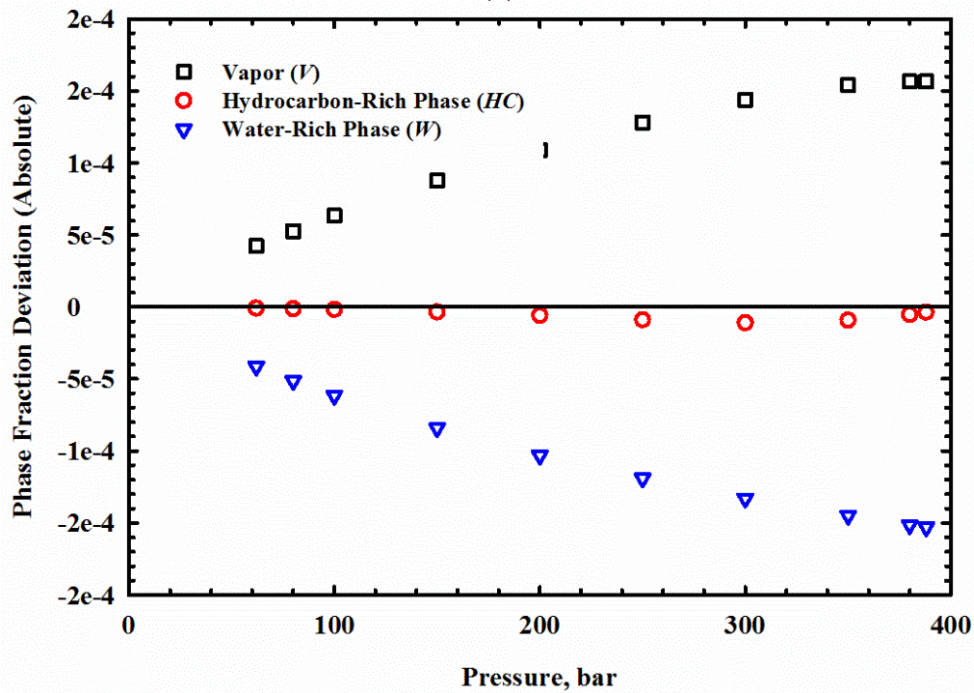


(b)

Figure 2-11 Comparison between the phase fractions obtained by applying the three-phase free-water flash package and those obtained by applying the conventional three-phase flash package for the water/reservoir fluid mixture at 50 bar: (a) variation of the phase fractions as a function of temperature; (b) deviations in the phase fractions that are calculated with the two three-phase flash packages



(a)



(b)

Figure 2-12 Comparison between the phase fractions obtained by applying the three-phase free-water flash package and those obtained by applying the conventional three-phase flash package for the water/reservoir fluid mixture at 450 K: (a) variation of the phase fractions as a function of pressure; (b) absolute deviations in the phase fractions that are calculated with the two three-phase flash packages

Table 2-2 shows the mole fractions of the hydrocarbon-rich phase and the water-rich phase obtained by applying the two two-phase flash algorithms at 450 K and 400 bar. Rather small deviations are found between the calculated compositions in the equilibrating two phases, confirming the good accuracy provided by the two-phase free-water flash. Table 2-3 shows the mole fractions in the three phases obtained by applying the two three-phase flash algorithms at 450 K and 200 bar. Again, the two three-flash algorithms provide very similar mole fractions in the three phases. It can be also observed from Tables 2-2 and 2-3 that, the mole fractions of non-water components in the water-rich phase, which are calculated with the conventional three-phase flash package, are nearly zero, supporting the free-water assumption.

Table 2-2 Comparison between the mole fractions obtained by applying the two-phase free-water flash and those obtained by applying the conventional two-phase flash for the water/reservoir fluid mixture at 450 K and 400 bar

Component	Conventional Two-Phase Flash		Two-Phase Free-Water Flash		Absolute Deviation	
	x_i (HC)	y_{i1} (W)	x_i (HC)	y_{i1} (W)	x_i (HC)	y_{i1} (W)
H ₂ O	0.042 445	0.999136	0.042 485	1	4.07E-05	0.000 864
N ₂	0.002 490	1.87E-06	0.002 489	0	4.40E-07	1.87E-06
CO ₂	0.034 422	0.000367	0.034 416	0	5.90E-06	0.000 367
C1	0.709 763	0.000489	0.709 637	0	0.000125	0.000 489
C2	0.076 039	6.08E-06	0.076 026	0	1.35E-05	6.08E-06
C3	0.031 508	7.09E-08	0.031 502	0	5.58E-06	7.09E-08
<i>i</i> -C4	0.006 512	1.33E-09	0.006 511	0	1.15E-06	1.33E-09
<i>n</i> -C4	0.011 875	2.81E-09	0.011 873	0	2.10E-06	2.81E-09
<i>i</i> -C5	0.005 267	9.51E-11	0.005 266	0	9.33E-07	9.51E-11
<i>n</i> -C5	0.005 842	5.24E-11	0.005 841	0	1.03E-06	5.24E-11
C6	0.008 332	9.17E-12	0.008 330	0	1.48E-06	9.17E-12
C7	0.011 013	1.17E-12	0.011 011	0	1.95E-06	1.17E-12
C8	0.010 247	5.25E-14	0.010 245	0	1.82E-06	5.25E-14
C9	0.009 098	2.14E-15	0.009 096	0	1.61E-06	2.14E-15
C10	0.006 416	7.54E-17	0.006 415	0	1.14E-06	7.54E-17
HVY1	0.015 802	1.92E-19	0.015 799	0	2.80E-06	1.92E-19
HVY2	0.010 822	1.68E-29	0.010 820	0	1.92E-06	1.68E-29
HVY3	0.002 107	1.35E-42	0.002 107	0	3.73E-07	1.35E-42

Table 2-3 Comparison between the mole fractions obtained by applying the three-phase free-water flash and those obtained by applying the conventional three-phase flash for the water/reservoir fluid mixture at 450 K and 200 bar

Component	Conventional Three-Phase Flash			Three-Phase Free-Water Flash			Absolute Deviation		
	y_{iV} (V)	x_i (HC)	y_{i1} (W)	y_{iV} (V)	x_i (HC)	y_{i1} (W)	y_{iV} (V)	x_i (HC)	y_{i1} (W)
H ₂ O	0.066 206	0.043 191	0.999 447	0.066 247	0.043 221	1	4.13E-05	2.99E-05	0.000 553
N ₂	0.002 537	0.000 913	9.81E-07	0.002 536	0.000 913	0	1.27E-07	1.17E-07	9.81E-07
CO ₂	0.034 472	0.021 624	0.000 244	0.034 499	0.021 643	0	2.69E-05	1.91E-05	0.000 244
C1	0.716 787	0.352 059	0.000 303	0.716 750	0.352 094	0	3.64E-05	3.51E-05	0.000 303
C2	0.075 345	0.058 626	4.86E-06	0.075 337	0.058 627	0	7.99E-06	3.81E-07	4.86E-06
C3	0.030 472	0.035 128	7.00E-08	0.030 469	0.035 127	0	3.81E-06	1.58E-06	7.00E-08
<i>i</i> -C4	0.006 191	0.008 811	1.53E-09	0.006 190	0.008 811	0	8.30E-07	5.16E-07	1.53E-09
<i>n</i> -C4	0.011 188	0.017 537	3.35E-09	0.011 187	0.017 536	0	1.54E-06	1.30E-06	3.35E-09
<i>i</i> -C5	0.004 830	0.009 700	1.32E-10	0.004 829	0.009 699	0	7.22E-07	9.43E-07	1.32E-10
<i>n</i> -C5	0.005 335	0.011 071	7.49E-11	0.005 335	0.011 070	0	8.09E-07	1.09E-06	7.49E-11
C6	0.007 276	0.020 623	1.53E-11	0.007 275	0.020 620	0	1.23E-06	2.83E-06	1.53E-11
C7	0.009 127	0.034 374	2.26E-12	0.009 125	0.034 368	0	1.71E-06	5.94E-06	2.26E-12
C8	0.008 022	0.038 785	1.13E-13	0.008 021	0.038 777	0	1.66E-06	7.87E-06	1.13E-13
C9	0.006 587	0.042 197	5.15E-15	0.006 586	0.042 187	0	1.52E-06	1.01E-05	5.15E-15
C10	0.004 298	0.034 797	1.95E-16	0.004 297	0.034 788	0	1.08E-06	9.47E-06	1.95E-16
HVY1	0.008 932	0.109 645	5.71E-19	0.008 929	0.109 609	0	2.64E-06	3.55E-05	5.71E-19
HVY2	0.002 363	0.129 484	6.09E-29	0.002 362	0.129 422	0	1.01E-06	6.26E-05	6.09E-29
HVY3	3.06E-05	0.031 434	2.48E-42	3.06E-05	0.031 416	0	1.12E-08	1.79E-05	2.48E-42

Figure 2-13 shows the calculated mole fractions of water in the hydrocarbon-rich phase by using the two flash packages at 50 bar. Again, a good agreement is achieved between these two flash packages. It is noted that, within the three-phase region, more water can be dissolved in the hydrocarbon-rich phase with temperature increasing. In particular, a temperature > 350 K leads to a more pronounced increase in the solubility of water in the hydrocarbon-rich phase. However, when temperature is > 442 K, the aqueous phase disappears, resulting in two-phase vapour-liquid equilibria. In the two-phase region, as temperature increases, water starts to evaporate from the hydrocarbon-rich phase into the vapour phase, causing a reduction of water fraction in the hydrocarbon-rich phase. In this case, the temperature of 442 K corresponds to the temperature point that provides the largest solubility of water in the hydrocarbon-rich phase.

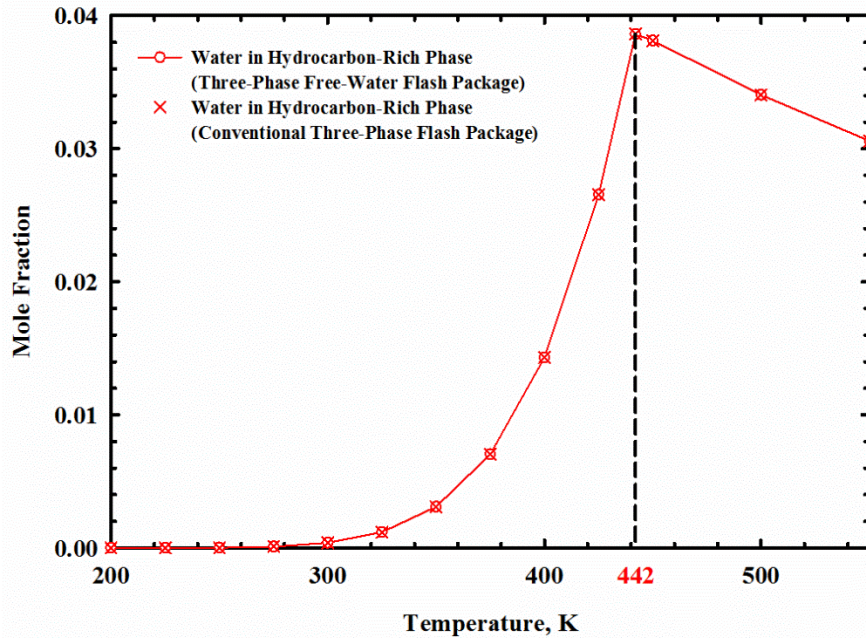
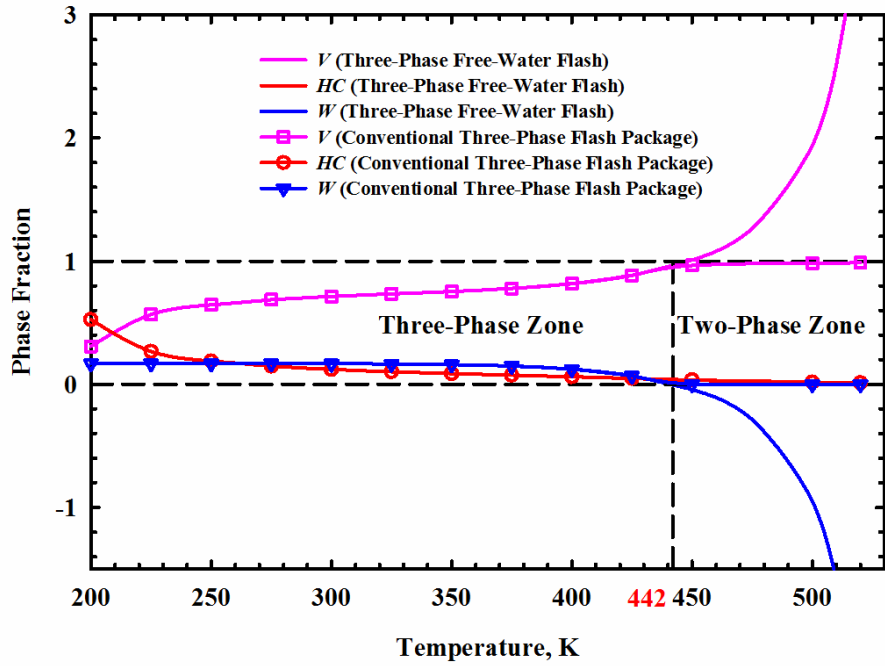
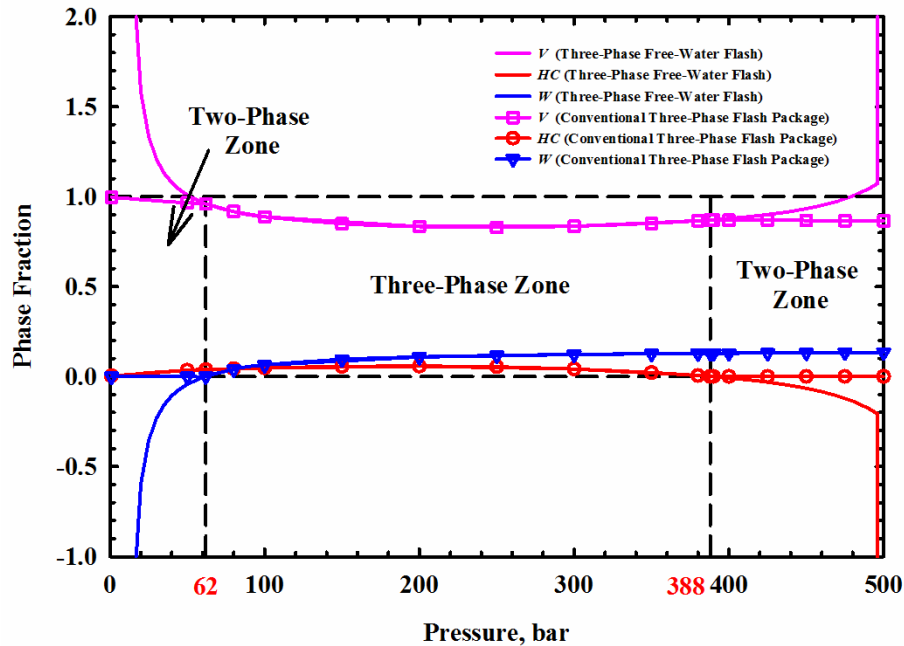


Figure 2-13 Comparison between the mole fractions of water in the hydrocarbon-rich phase obtained by applying the three-phase free-water flash package and those obtained by applying the conventional three-phase flash package for the water/reservoir fluid mixture at 50 bar

Figure 2-14a compares the phase fractions obtained by applying the standalone three-phase free-water flash against those obtained by applying the conventional three-phase flash package for the water/reservoir fluid mixture at 50 bar, while Figure 2-14b shows the same comparison at 450 K. It can be seen from Figure 2-14 that the calculation results given by the two algorithms coincide well with each other. Also, the two flash packages provide the same two-phase/three-phase boundary temperatures.



(a)



(b)

Figure 2-14 Comparison between the phase fractions obtained by applying the standalone three-phase free-water flash algorithm and those obtained by applying the conventional three-phase flash package for the water/reservoir fluid mixture: (a) at 50 bar; (b) at 450 K

2.5 Conclusions

Based on the free-water assumption, we simplify the objective function developed by

Okuno *et al.*^[18] for solving the phase fractions in the three-phase vapour-liquid-aqueous equilibrium, the two-phase vapour-aqueous equilibrium, or the two-phase liquid-aqueous equilibrium. As for the three-phase vapour-liquid-aqueous equilibrium considered in the newly developed algorithm, there is only one unknown in the objective function, while, as for the two-phase vapour-aqueous or liquid-aqueous equilibrium, the phase fractions can be analytically solved. We apply the method developed by Lapene *et al.*^[14] to initialize the equilibrium ratios required in both the three-phase free-water flash and the conventional two-phase flash, while a newly developed method for initializing the equilibrium ratios is applied in the two-phase free-water flash.

By incorporating these free-water flash algorithms, a free-water flash package is developed to enhance the computational efficiency associated with the multiphase flash computations. This flash package can be readily used to solve the number of present phases, phase fractions, and phase compositions in a multiphase equilibrium, i.e., a single-phase equilibrium, a two-phase equilibrium, or a three-phase vapour-liquid-aqueous equilibrium. We provide efficient criteria that help to determine how to switch from a three-phase equilibrium to a two-phase equilibrium without performing stability tests. Thereby, the number of stability tests is reduced in this flash package in comparison to the conventional full three-phase flash package; the reduced number of stability tests, together with the reduced number of variables in the free-water algorithms, result in a higher computational efficiency of the free-water flash package.

Example calculations demonstrate that the flash results obtained from the new two-phase/three-phase free-water flash algorithms are in good agreement with those obtained from the conventional flash algorithm. But it should be noted that the free-water

flash algorithm cannot be applied to the mixtures containing polar materials, such as alcohols, or other substances which tend to have a high solubility in the aqueous phase.

Nomenclature

c	number of components
err	error
f_{11}	fugacity of water component in the water-rich liquid phase
f_{1x}	fugacity of water component in the reference phase or hydrocarbon-rich phase in the three-phase flash
f_{ij}	fugacity of the i^{th} component in the j^{th} phase
f_{ix}	fugacity of the i^{th} component in the reference phase or hydrocarbon-rich phase in the three-phase flash
$iter$	iteration number
K_{11}	equilibrium ratio of water component in the water-rich liquid phase with respect to the reference phase
K_{1j}	equilibrium ratio of water component in the j^{th} phase with respect to the reference phase
K_{1y}	equilibrium ratio of water component in the vapour phase with respect to the reference phase
K_{ij}	equilibrium ratio of the i^{th} component in the j^{th} phase with respect to the reference phase
K_{iy}	equilibrium ratio of i^{th} component in the vapour phase with respect to the reference phase
M_w	molecular weight (g/mol)

N_p	number of phases
P	pressure (bar)
P_c	critical pressure (bar)
P_{sat}^w	saturation pressure of pure water (bar)
T	temperature (K)
T_c	critical temperature (K)
x_1	mole fraction of water component in the reference phase or hydrocarbon-rich phase in the three-phase flash
x_i	mole fraction of the i^{th} component in the reference phase or hydrocarbon-rich phase in the three-phase flash
y_1	mole fraction of water component in the vapour phase
y_{1j}	mole fraction of water component in the j^{th} phase
y_{1y}	mole fraction of water component in the vapour phase
y_{i1}	mole fraction of the i^{th} component in the water-rich liquid phase
y_{ij}	mole fraction of the i^{th} component in the j^{th} phase
z_1	mole fraction of water component in the feed
z_i	mole fraction of the i^{th} component in the feed

Greek Letters

β_1	phase fraction of the water-rich liquid phase
β_j	phase fraction of the j^{th} phase
β_x	phase fraction of the reference phase
β_y	phase fraction of the vapour phase

ε	tolerance
ϕ_{ix}	fugacity coefficient of the i^{th} component in the reference phase
ϕ_{ij}	fugacity coefficient of the i^{th} component in the j^{th} phase
ω	acentric factor

Subscripts

c	critical index
i	component index
j	phase index
x	reference phase index or hydrocarbon-rich phase index in the three-phase flash
y	vapour phase index

2.6 References

- [1] R.M. Butler, J. Can. Pet. Technol. **1994**, 33, 44.
- [2] S.K. Das, R.M. Butler, J. Petrol. Sci. Eng. **1998**, 21, 43.
- [3] M.J. Amani, M.R. Gray, J.M Shaw, Fluid Phase Equilibr. **2014**, 370, 75.
- [4] M. Arshad, H. Li, “Multiphase equilibria of solvent-steam-bitumen system within SAGD steam-chamber boundary,” *SPE Canada Heavy Oil Technical Conference*, Society of Petroleum Engineers, Calgary, 9-11 June **2015**.
- [5] C.H. Whitson, M.L. Michelsen, Fluid Phase Equilibr. **1989**, 53, 51.
- [6] C.F. Leibovici, J. Neoschil, Fluid Phase Equilibr. **1995**, 112, 217.
- [7] Z. Li, A. Firoozabadi, SPE J. **2012**, 17, 1096.
- [8] H.H. Rachford Jr., J.D.Rice, AIME Pet. Trans. **1952**, 195, 327.

- [9] L.E. Baker, A.C. Pierce, K.D. Luks, SPE J. **1982**, 22, 731.
- [10] M.L. Michelsen, Fluid Phase Equilibr. **1982**, 9, 1.
- [11] M.L. Michelsen, Fluid Phase Equilibr. **1982**, 9, 21.
- [12] K.H. Coats, SPE J. **1980**, 20, 363.
- [13] L.C. Young, R.E. Stephenson, SPE J. **1983**, 23, 727.
- [14] A. Lapene, D.V. Nichita, G. Debenest, M. Quintard, Fluid Phase Equilibr. **2010**, 297, 121.
- [15] Y. Tang, S. Saha, Ind. Eng. Chem. Res. **2003**, 42, 189.
- [16] C. Leibovici, J. Neoschil, Fluid Phase Equilibr. **1992**, 74, 303.
- [17] M.L. Michelsen, Comput. Chem. Eng. **1994**, 18, 545.
- [18] R. Okuno, R. Johns, K. Sepehrnoori, SPE J. **2010**, 15, 313.
- [19] C.F. Leibovici, D.V. Nichita, Fluid Phase Equilibr. **2008**, 267, 127.
- [20] D.Y. Peng, D.B. Robinson, Ind. Eng. Chem. Fund. **1976**, 15, 59.
- [21] C.A. Glandt, W.G. Chapman, SPE Res. Eng. **1995**, 10, 59.
- [22] G.M. Wilson, "A modified Redlich-Kwong equation of state, application to general physical data calculations," *65th National AIChE Meeting*, American Institute of Chemical Engineers, Cleveland, 4-7 March **1969**.
- [23] NIST Chemistry WebBook, 2017, NIST Standard Reference Database Number 69, Water Phase Change Data, <http://webbook.nist.gov>.
- [24] O.C. Bridgeman, E.W. Aldrich, J. Heat Transfer **1964**, 86, 279.

Appendix 2-A: Algorithm for the Two-Phase Free-Water Flash

For the two-phase free-water flash, the phase fraction can be analytically solved using Equation (9). Figure 2-A.1 shows the flow chart of this algorithm. PR EOS^[20] is used to calculate all thermodynamic properties. The detailed procedure of the algorithm is described as follows:

- 1) Initialize the compositions of the water-rich phase as follows:

$$y_{i1} = \begin{cases} 10^{-10}, & i \neq 1 \\ 1 - (c-1) \times 10^{-10}, & i = 1 \end{cases} \quad (2-A.1)$$

and the non-water-rich phase, i.e. hydrocarbon-rich phase or vapour phase, as follows:

$$x_i = 1/c \quad (2-A.2)$$

- 2) Calculate the equilibrium ratios as follows:

$$K_{i1} = \frac{y_{i1}}{x_i}, \quad i = 1, \dots, c \quad (2-A.3)$$

- 3) Set $iter = 1$, and $\varepsilon = 10^{-6}$. $iter$ is the iteration number, and ε is the tolerance.
- 4) Solve the Equation (2-9) to obtain the phase fraction of the water-rich phase.
- 5) Update the compositions in the two phases as follows:^[8]

$$x_i = \frac{z_i}{K_{i1}(1-\beta_1) + \beta_1}, \quad i = 1, \dots, c \quad (2-A.4)$$

$$y_{i1} = \frac{K_{i1}z_i}{K_{i1}(1-\beta_1) + \beta_1}, \quad i = 1, \dots, c \quad (2-A.5)$$

- 6) Calculate the fugacity of each component in each phase using PR EOS.^[20]
- 7) Update the equilibrium ratios as follows:

$$K_{i1} = K_{i1} \frac{f_{ix}}{f_{i1}}, \quad i = 1, \dots, c \quad (2-A.6)$$

8) Evaluate the fugacity error as follows:

$$err = \sqrt{\sum_{i=1}^c \left(\frac{f_{ix}}{f_{il}} - 1 \right)^2} \quad (2-A.7)$$

If $err < \varepsilon$ go to Step 9; otherwise, let $iter = iter + 1$ and go back to Step 4.

9) Calculate the phase fractions of the non-water-rich phase and output the phase fractions and compositions of all the phases.

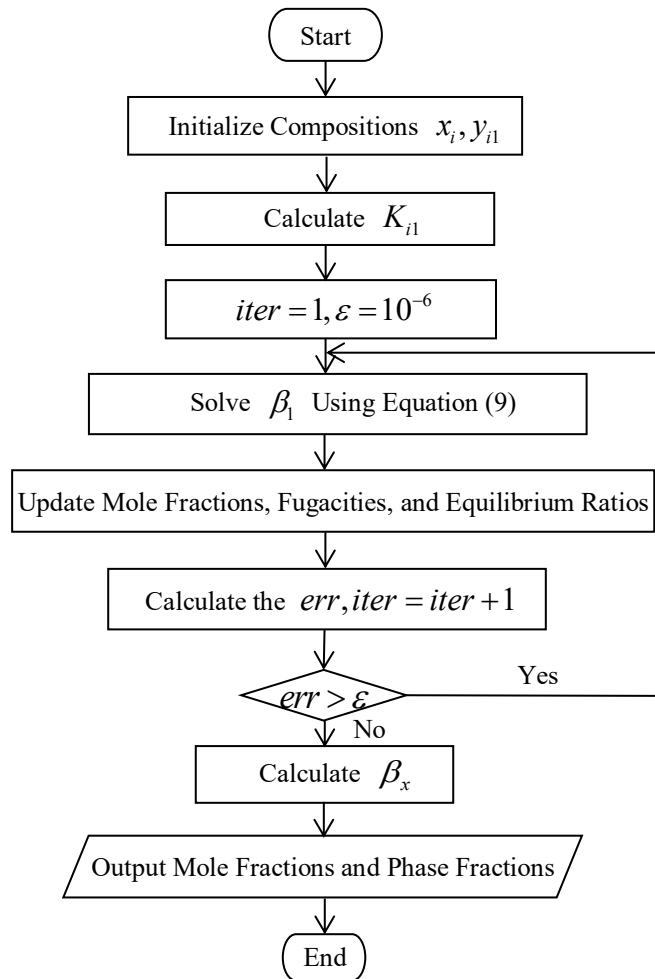


Figure 2-A.1 Flow chart of the two-phase free-water flash algorithm

Appendix 2-B: Algorithm for the Three-Phase Free-Water Flash

The three-phase free-water flash algorithm is based on the simplified objective function and constraints. Figure 2-B.1 shows the flow chart adopted by the algorithm. PR EOS^[20] is again used in this algorithm. This algorithm is primarily comprised of an outer loop and an inner loop. The outer loop is used to update the equilibrium ratios, while the inner loop is used to solve β_y using the interior-point method. The detailed procedure of the algorithm is described as follows:

- 1) Initialize the equilibrium ratios in the vapour phase with respect to the hydrocarbon-rich phase, K_{iy} , as follows:

$$K_{iy} = \frac{P_{ci}}{P} \exp \left[5.37(1 + \omega_i) \left(1 - \frac{T_{ci}}{T} \right) \right], i \neq 1 \quad (2-B.1)$$

$$K_{1y} = \frac{T}{T_{c1}} \frac{P_{c1}}{P} \quad (2-B.2)$$

where P and P_c represent pressure and critical pressure, respectively, bar; T and T_c represent temperature and critical temperature, respectively, K; and ω represents acentric factor. The initialization method is same as that referred by Lapene *et al.*^[14] Wilson equation^[22] is applied for the initialization of the equilibrium ratios for the non-water components.

- 2) Initialize the mole fractions of water in the vapour and hydrocarbon-rich phases as follows:^[13]

$$\begin{cases} y_1 = \frac{P_{sat}^w}{P} \\ x_1 = \frac{1}{K_{11}} \end{cases} \quad (2-B.3)$$

where x and y represents the compositions of the hydrocarbon-rich phase and the

vapour phase, respectively; K_{11} can be calculated using the equation $K_{11} = \frac{K_{1y}}{y_1}$; P_{sat}^w

represents the saturation pressure of pure water which can be calculated using the empirical formulas^[23] developed based on the data by Bridgeman and Aldrich.^[24]

- 3) Set $iter = 1$, and $\varepsilon = 10^{-6}$.
- 4) Calculate the feasible region formed by the constraints. If the feasible region is open, terminate this algorithm. When this algorithm is coupled in the flash package as shown in the Procedure of the Two-Phase and Three-Phase Free-Water Flash Algorithm, a two-phase flash will be conducted instead. If the value of $iter$ equals to one, go to Step 5; otherwise, go to Step 6.
- 5) If the left endpoint of the feasible region is smaller than zero, set it as zero. Initialize the vapour phase fraction using the average value of the two endpoints of the feasible region.
- 6) Solve the objective function to obtain the vapour phase fraction using the interior-point method.
- 7) Update the mole fractions of non-water components in the hydrocarbon-rich and vapour phases using Equations (2-B.4) and (2-B.5), respectively:

$$x_i = \frac{z_i}{(K_{iy} - K_{wy}^*)\beta_y + K_{wz}^*}, \quad i \neq 1 \quad (2-B.4)$$

$$y_i = \frac{K_{iy}z_i}{(K_{iy} - K_{wy}^*)\beta_y + K_{wz}^*}, \quad i \neq 1 \quad (2-B.5)$$

Update the mole fractions of water component in the hydrocarbon-rich and vapour phases using Equations (2-4) and (2-B.6), respectively:

$$y_1 = \frac{K_{1y}}{K_{11}} \quad (2-B.6)$$

8) Calculate the fugacity of each component in each phase using PR EOS.

9) Update the equilibrium ratios as follows:

$$\begin{cases} K_{iy} = K_{iy} \frac{f_{ix}}{f_{iy}}, i = 1, \dots, c \\ K_{11} = K_{11} \frac{f_{1x}}{f_{11}} \end{cases} \quad (2-B.7)$$

10) Evaluate the fugacity error as follows:

$$err = \sqrt{\sum_{i=1}^c \left(\frac{f_{ix}}{f_{iy}} - 1 \right)^2} \quad (2-B.8)$$

If $err < \varepsilon$ go to Step 11; otherwise, let $iter = iter + 1$ and go back to Step 4.

11) Calculate the phase fraction of the water-rich phase using Equation (2-B.9):

$$\beta_1 = \frac{z_1 + (x_1 - y_1)\beta_y - x_1}{1 - x_1} \quad (2-B.9)$$

Then calculate the phase fraction of the hydrocarbon-rich phase using Equation (2-7).

12) Output the phase fractions and compositions of all phases.

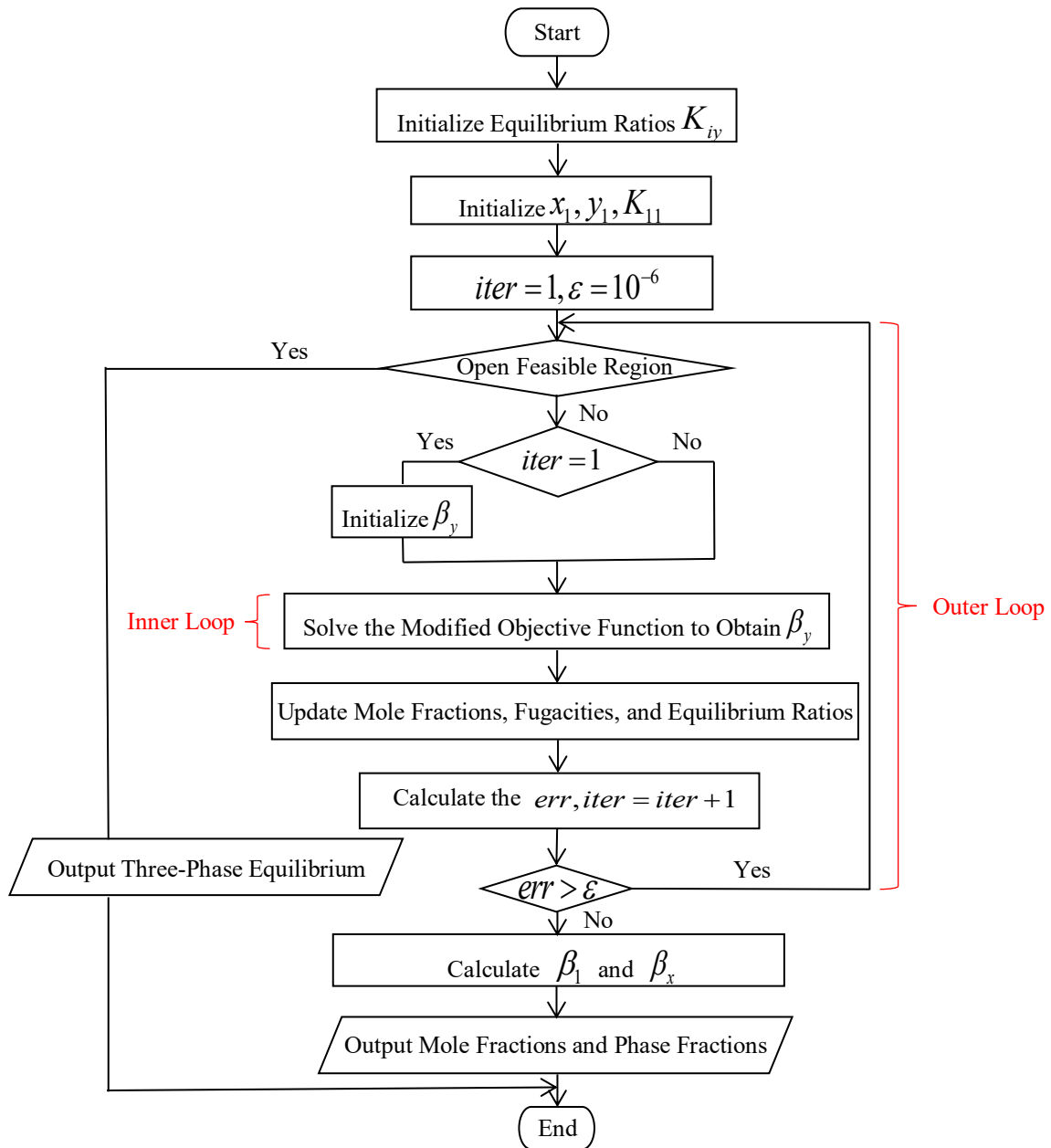


Figure 2-B.1 Flow chart of the three-phase free-water flash algorithm

Appendix 2-C: Component Properties and BIPs

Table C.1 shows component properties and feed composition for the water/C4/C20 mixture. The BIPs between water and hydrocarbon components are 0.5, while the BIPs between hydrocarbon components are set to zero. In this table, T_c represents critical temperature, K; P_c represents critical pressure, bar; ω represents acentric factor; M_w represents molecular weight, g/mol; and z represents mole fraction in the feed. Tables C.2 and C.3 show component properties, feed composition, and BIPs for the water/N₂/C10/C20 mixture. Tables C.4 and C.5 show component properties, feed composition, and BIPs for the water/reservoir fluid mixture. We set all the other BIPs, which are absent from Table C.5, to zero.

Table 2-C.1 Component properties and feed composition for the water/C4/C20 mixture

Component	T_c (K)	P_c (bar)	ω	z (mol%)	M_w (g/mol)
Water	647.0	220.5	0.3440	0.80	18
C4	425.2	38.0	0.1928	0.16	58
C20	782.0	14.6	0.8160	0.04	275

Table 2-C.2 Component properties and feed composition for the water/N₂/C10/C20 mixture by Lapene *et al.*^[14]

Component	T_c (K)	P_c (bar)	ω	z (mol%)	M_w (g/mol)
Water	647.0	220.5	0.344	0.55	18
N ₂	126.2	34.0	0.040	0.10	28
C10	622.0	25.3	0.443	0.10	134
C20	782.0	14.6	0.816	0.25	275

Table 2-C.3 BIPs between the components in the water/N₂/C10/C20 mixture by Lapene *et al.*^[14]

Component	Water	N ₂	C10	C20
Water	0	0.4778	0.5000	0.5000
N ₂	0.4778	0	0.1000	0.1000
C10	0.5000	0.1000	0	0
C20	0.5000	0.1000	0	0

Table 2-C.4 Component properties and feed composition for the water/reservoir fluid mixture by Lapene *et al.*^[14]

Component	T_c (K)	P_c (bar)	ω	z (mol%)	M_w (g/mol)
Water	647.37	221.20	0.3440	0.166 667	18.02
N ₂	126.20	33.94	0.0400	0.002 167	28.01
CO ₂	304.21	73.77	0.2250	0.030 000	44.01
C1	190.60	46.00	0.0115	0.617 667	16.04
C2	305.40	48.84	0.0908	0.066 167	30.07
C3	369.80	42.46	0.1454	0.027 417	44.10
<i>i</i> -C4	408.10	36.48	0.1760	0.005 667	58.12
<i>n</i> -C4	425.20	38.00	0.1928	0.010 333	58.12
<i>i</i> -C5	464.74	34.77	0.2235	0.004 583	71.94
<i>n</i> -C5	469.60	33.74	0.2273	0.005 083	72.15
C6	515.28	32.57	0.2637	0.007 250	84.99
C7	553.84	31.00	0.2897	0.009 583	97.87
C8	581.28	28.50	0.3245	0.008 917	111.54
C9	609.35	26.50	0.3791	0.007 917	126.10
C10	626.97	24.60	0.4363	0.005 583	140.14
HVY1	658.15	21.20	0.5200	0.013 750	179.30
HVY2	778.15	15.70	0.6500	0.009 417	290.60
HVY3	998.15	13.50	0.7200	0.001 833	450.00

Table 2-C.5 BIPs between the components in the water/reservoir fluid mixture by Lapene *et al.*^[14]

Component	Water	N₂	CO₂	C1	C2
Water	0	0.4778	0.1896	0.4850	0.4920
N ₂	0.4778	0	0.1000	0.1000	0.1000
CO ₂	0.1896	0.1000	0	0.1200	0.1200
C1	0.4850	0.1000	0.1200	0	0
C2	0.4920	0.1000	0.1200	0	0
C3	0.5525	0.1000	0.1200	0	0
<i>i</i> -C4	0.5000	0.1000	0.1200	0	0
<i>n</i> -C4	0.5000	0.1000	0.1200	0	0
<i>i</i> -C5	0.5000	0.1000	0.1200	0	0
<i>n</i> -C5	0.5000	0.1000	0.1200	0	0
C6	0.5000	0.1000	0.1200	0	0
C7	0.5000	0.1000	0.1200	0	0
C8	0.5000	0.1000	0.1200	0.0200	0
C9	0.5000	0.1000	0.1200	0.0300	0
C10	0.5000	0.1000	0.1200	0.0500	0.0200
HVY1	0.5000	0.1000	0.1200	0.0700	0.0400
HVY2	0.5000	0.1000	0.1200	0.0850	0.0500
HVY3	0.5000	0.1000	0.1200	0.0700	0.0400

CHAPTER 3 A ROBUST THREE-PHASE ISENTHALPIC FLASH ALGORITHM BASED ON FREE-WATER ASSUMPTION

A version of this chapter was presented at the ASME 2017 36th International Conference on Ocean, Offshore and Arctic Engineering conference, held on 25-30 June 2017 in Trondheim, Norway and has been accepted for publication in *Journal of Energy Resources Technology*.

Abstract

Isenthalpic flash is a type of flash calculation conducted at given pressure and enthalpy for a feed mixture. Multiphase isenthalpic flash calculations are often required in compositional simulations of steam-based enhanced oil recovery methods. Based on a free-water assumption that the aqueous phase is pure water, a robust and efficient algorithm is developed to perform isenthalpic three-phase flashes. Assuming the feed is stable, we first determine the temperature by solving the energy conservation equation. Then the stability test on the feed mixture is conducted at the calculated temperature and the given pressure. If the mixture is found unstable, two-phase and three-phase vapor-liquid-aqueous isenthalpic flash can be simultaneously initiated without resorting to stability tests. The outer loop is used to update the temperature by solving the energy conservation equation. The inner loop determines the phase fractions and compositions through a three-phase free-water isothermal flash. A two-phase isothermal flash will be initiated if an open feasible region in the phase fractions appears in any iteration during the three-phase flash or any of the ultimately calculated phase fractions from the three-phase flash do not belong to $[0,1]$. A number of example calculations for water/hydrocarbon mixtures are carried out, demonstrating that the proposed algorithm is accurate, efficient and robust.

3.1 Introduction

More efforts are required to recover heavy oil than light oil due to the high viscosity of the heavy oil [1]. To recover heavy oil, the main method relies on reducing the viscosity of heavy oil through heating or solvent dilution [1]. As one heating method, steam injection (such as steam-assisted gravity drainage (SAGD)) is widely implemented to enhance the oil recovery from heavy oil reservoirs [2-5]. One of the recovery mechanisms of steam injection is steam distillation which vaporizes/condensates light components in the heavy oil [6]. Vaporization/condensation of light components changes the compositions of the reservoir fluids and affects the oil recovery efficiency. Recently, the co-injection of solvent and steam has been proved to be a promising technology improving oil recovery. Three-phase vapor-liquid-aqueous equilibria of water/solvent/heavy-oil mixtures can readily occur when these mixtures are flowing in the reservoir and the production tubing [7, 8]. Accurate simulation of either steam injection or steam/solvent co-injection process requires detailed understanding of the in-situ phase behavior of water/solvent/heavy-oil mixtures throughout the heavy-oil reservoir and production tubing [9]. Experimental and modeling data of water/solvent/heavy-oil mixtures are recently provided by Zirrahi *et al.* [10-13].

Some thermal-compositional simulators use the K -values calculated by semi-empirical models to simulate the in-situ phase behavior in the reservoir [14, 15]. A more general thermal compositional simulator resorts to the use of a cubic equation of state (EOS) [9, 16-17]. Phase behavior and thermodynamic properties of the mixture at each grid and each time step can be well captured in

the EOS-based thermal simulators. As for the flash computation happening in each grid, the input variables used for conducting flash calculation in each grid of the reservoir model are usually feed composition, pressure, and enthalpy [9].

The calculation of phase behavior at the given feed composition, pressure, and enthalpy is the so-called isenthalpic flash [18]. One of the challenges in the multiphase isenthalpic flash is the absence of prior knowledge about the number of existing phases under flash conditions. Since the temperature is not known in advance in the isenthalpic flash [19], it is more complicated to determine the number of existing phases in the isenthalpic flash than the isothermal flash. Another challenge is caused by the appearance of the narrow-boiling region in which the total enthalpy is much sensitive to the change in the temperature [20]. The existence of the water-rich phase associated with the three-phase equilibria always tends to induce a narrow-boiling behavior [20]. Sometimes, the energy conservation equation is not converging in the narrow-boiling region. For the latter problem, Zhu and Okuno [21] modified the direct-substitution algorithm and developed a new isenthalpic flash algorithm that can avoid the convergence problem in the narrow-boiling region. In their algorithm, they first evaluate the condition number of the Jacobian matrix for the Rachford-Rice equation [22] and the energy conservation equation, and proposed a proper scheme to switch between the bisection method and the Newton method based on the condition number of the Jacobian matrix.

Michelsen [18] provided a stage-wise procedure for multiphase isenthalpic flash. The outer loop is

used to satisfy the energy conservation and feed temperature into the inner loop. The inner loop performs the stage-wise isothermal flash [23], which alternatingly implements the stability test and flash calculations. Agarwal *et al.* [20] proposed three schemes for the multiphase isenthalpic flash which are integrated with the conventional stability test as well. Scheme 1 is similar to the procedure provided by Michelsen [18]. Agarwal *et al.* [20] modified the method provided by Michelsen [18] by introducing a quasi-Newton successive substitution (QNSS) for updating K -values [24, 25] instead of the sole use of Newton iteration. The scheme 1 is considered to be robust and can handle the narrow-boiling behavior except for the mixture with one degree of freedom. However, due to the uncertain temperature in the isenthalpic flash, the stability test, which is time-consuming, needs be conducted with a considerable number of times. Scheme 2 solves the Rachford-Rice equation [22] and the energy conservation equation simultaneously. The number of phases is pre-assumed and needs to be added by one when the results obtained by the conventional stability test at the given pressure and solved temperature show the system is unstable. This scheme is considered to be three times faster than Scheme 1, but may fail in the narrow-boiling region due to the non-convergence of the energy conservation equation. Scheme 3 is a hybrid scheme involving 5 iterations of Scheme 2 after every iteration of Scheme 1.

Besides the stage-wise procedures for the multiphase isenthalpic flash, efforts are also devoted to proposing methods to reintegrate stability test and the isenthalpic flash. Gupta *et al.* [26] presented a method to simultaneously solve the Rachford-Rice equation, energy conservation equation, and stability equation in the inner loop, and use the outer loop to update K -values. Zhu and Okuno [27]

provided a formulation for multiphase isenthalpic flash with a rearranged design for integrating flash-stability calculations. Prior to every iteration for solving the Rachford-Rice equation and energy conservation equation, the number of existing phases is updated based on the stability test that performs a global minimization of the Gibbs free energy. The modified direct-substitution algorithm for multiphase isenthalpic flash provided by Zhu and Okuno [28] is applied in this formulation to solve the Rachford-Rice equation and energy conservation equation.

Heidari *et al.* [29] proposed a multiphase isenthalpic flash that combined the Scheme 3 of Agarwal *et al.* [20] and the free-water isothermal flash provided by Lapene *et al.* [30]. The free-water isothermal flash by Lapene *et al.* [30] can determine whether the existing phases are water-inclusive two phases or three phases without conducting stability test. The runs of conventional stability test are reduced, leading to an enhanced computational efficiency. However, when the two-phase equilibrium contains a water-rich phase, the initialization method for K -values in Lapene *et al.*'s method [30] may sometimes fail to give correct phase equilibrium results. Li and Li [31] developed a three-phase flash package based on the free-water assumption which assumes the water-rich phase is pure water [32]. This flash package can handle single-phase equilibrium, two-phase equilibrium, and three-phase vapor-liquid-aqueous equilibrium. This flash package provides an alternative method for switching between the two-phase and three-phase vapor-liquid-aqueous equilibria without resorting to stability test. An initialization method for the K -values, which is independent of the results of the stability test, is developed to ensure the efficiency and robustness of the isothermal flashes for two-phase equilibria involving a water-rich

phase.

The objective of this work is to develop an accurate, robust, and efficient three-phase isenthalpic flash algorithm for water/hydrocarbon mixtures based on the free-water assumption for the aqueous phase. We also aim to ensure that this scheme performs well for the three-phase vapor-liquid-aqueous equilibria where the narrow-boiling behavior appears. This multiphase isenthalpic flash can handle single-phase, two-phase, and three-phase vapor-liquid-aqueous equilibria that are frequently encountered in the thermal oil recovery processes. Phase appearances and disappearances can be readily handled by the new algorithm. We demonstrate the performance of the three-phase free-water isenthalpic flash via several example calculations.

3.2 Mathematical Formulation

The objective of isenthalpic flash is to find the T , β_j , and x_{ij} which give the maximum total entropy at the given P , z_i , and H_{spec} [18],

$$S_i = \sum_{j=1}^{N_p} \beta_j S_j \quad (3-1)$$

where the subscript i is the component index, and N_c is the number of components; The subscript j is the phase index, and N_p is the number of phases; T is temperature; β_j is the phase mole fraction of phase j ; x_{ij} is the mole fraction of component i in phase j ; P is pressure; z_i is mole fraction of component i in the feed; H_{spec} is the specified molar enthalpy; S_i is the total molar entropy; and S_j is the molar entropy of phase j . In our scheme, β_j and x_{ij} are solved in the inner loop by isothermal flash. For the isothermal flash, x_{ij} is updated in the outer loop until satisfying the chemical

potential,

$$f_{i1} = f_{i2} = \dots = f_{ij}, \quad i = 1, \dots, N_c, \quad j = 1, \dots, N_p \quad (3-2)$$

where f_{ij} represents the fugacity of component i in the phase j . β_j is solved in the inner loop based on the material balance,

$$z_i = \sum_{j=1}^{N_p} \beta_j x_{ij}, \quad i = 1, \dots, N_c \quad (3-3)$$

$$\sum_{j=1}^{N_p} \beta_j = 1 \quad (3-4)$$

In our case, based on the free-water assumption, we modify the objective function by Okuno *et al.* for performing three-phase vapor-liquid-aqueous isothermal flash calculations [31, 32],

$$\left\{ \begin{array}{l} \min : f(\beta_y) = - \sum_{i=2}^{N_c} z_i \ln \left| (K_{iy} - K_{wy}^*) \beta_y + K_{wz}^* \right| \\ \text{Subject to : } (K_{wy}^* - K_{iy}) \beta_y \leq \min \{ K_{wz}^* - z_i, K_{wz}^* - K_{iy} z_i \}, i \neq 1 \end{array} \right. \quad (3-5)$$

where

$$\left\{ \begin{array}{l} K_{wy}^* = \frac{1 - x_{1y}}{1 - x_{1x}} \\ K_{wz}^* = \frac{1 - z_1}{1 - x_{1x}} \end{array} \right. \quad (3-6)$$

Equation (3-6) refers to the “effective” equilibrium constants as defined by Tang and Saha [33].

The subscript x and y represent the hydrocarbon-rich phase and the vapor phase, respectively. We set the component 1 to be the water component. K_{iy} is the equilibrium ratios for the vapor phase with respect to the hydrocarbon-rich phase, i.e., the reference phase. K_{iy} is defined by

$K_{iy} = \frac{x_{iy}}{x_{ix}} = \frac{\phi_{ix}}{\phi_{iy}}$, $i = 1, \dots, N_c$, where ϕ represents the fugacity coefficient. β_w can be solved based on

β_y [30, 31],

$$\beta_w = \frac{z_1 + (x_{1x} - x_{1y})\beta_y - x_{1x}}{1 - x_{1x}} \quad (3-7)$$

where the subscript w represents the water-rich phase. As for the two-phase isothermal flash calculations, a modified objective function for flash computation provided by Okuno *et al.* [32] is applied,

$$\left\{ \begin{array}{l} \min : f(\beta_1) = -\sum_{i=1}^{N_c} z_i \ln |1 - (1 - K_{i1})\beta_1|, \quad i = 1, \dots, N_c \\ \text{Subject to : } (1 - K_{i1})\beta_1 \leq \min \{1 - z_i, 1 - K_{i1}z_i\}, \quad i = 1, \dots, N_c \end{array} \right. \quad (3-8)$$

where K_{i1} is defined by $K_{i1} = \frac{x_{i1}}{x_{i2}} = \frac{\phi_{i2}}{\phi_{i1}}$, $i = 1, \dots, N_c$. The subscript 1 represents the non-reference phase, while the subscript 2 represents the reference phase. T is updated by solving the energy conservation equation in the outer loop of the isenthalpic flash,

$$H_t = \sum_{j=1}^{N_p} \beta_j H_j = H_{spec} \quad (3-9)$$

where H_t is the total molar enthalpy, while H_j is the molar enthalpy of phase j . H_t is calculated by the method as proposed by Zhu and Okuno [21]. All of the thermodynamic properties are calculated by the Peng-Robinson EOS [34].

3.3 Algorithm

The algorithm discussed in this section is a modified three-phase isenthalpic flash based on the free-water assumption. This algorithm is developed to handle the multiphase equilibria including

single-phase, two-phase, and three-phase vapor-liquid-aqueous equilibria. The primary purpose of developing the three-phase isenthalpic flash algorithm is to enhance the computational efficiency of the algorithm by replacing the conventional stability test with an alternative analytical method for determining the number of existing phases.

Due to the narrow-boiling behavior in the three-phase vapor-liquid-aqueous zone which will cause convergence problem for the energy conservation equation, we need to avoid solving the Rachford-Rice equation and the energy conservation equation simultaneously. Therefore, we opt to use the outer loop to update temperature, while use inner loop to perform multiphase isothermal flash. However, if we perform the conventional multiphase isothermal flash in the inner loop, this scheme will be time-consuming; this is because in the conventional isothermal flash we need to conduct two times of the stability test in order to determine whether the number of existing phases is two or three. With the temperature updated in the outer loop, several runs of conventional isothermal flash are needed to achieve the convergence of the energy conservation equation. This will lead to a considerable number of stability tests.

In our scheme, we can efficiently identify the existence or non-existence of a one-phase equilibrium with the aid of the conventional stability test. $(N_c + 4)$ initial guesses of K -values are applied in the stability test to ensure the correctness of single-phase stability test [19]. Then, for the two-phase and three-phase vapor-liquid-aqueous equilibria, the inner loop of the isenthalpic flash implements parts of two-phase and three-phase equilibria calculations included in the isothermal

flash package proposed by Li and Li [31]. We can properly switch between the two-phase and three-phase equilibria in this isothermal flash package without resorting to the conventional stability test. Therefore, only one stability-test run needs to be executed in one run of the multiphase isenthalpic flash, which significantly reduces the number of stability test. This flash package also provides an efficient and robust method for initializing the K -values in both the two-phase and three-phase equilibria without using the results obtained by the stability test. The method of updating temperature in the outer loop is similar to that as proposed by Agarwal *et al.* [20]. Presented below is the stepwise procedure for implementing the new three-phase free-water isenthalpic flash algorithm. Figure 3-1 shows the flow chart of this algorithm.

- (1) Input P , z_i , H_{spec} , and component properties (such as critical temperature, T_c , critical pressure, P_c , acentric factor, ω , and binary interaction parameters (BIPs)). Set the upper temperature, T^U , the lower temperature, T^L , and the iteration number $iter=1$. Guess an initial temperature, T^I .
- (2) Assume the mixture is in a single phase, and solve T_1 using the energy conservation equation, Equation (3-15). The procedure for solving the energy conservation equation is similar to that as discussed in Steps (7) to (10).
- (3) Perform the conventional stability test by calculating the tangent plane distance at P and T_1 . If the mixture is stable, output one-phase equilibrium and T_1 . Otherwise, enter the inner loop to conduct isothermal flash for two-phase and three-phase vapor-liquid-aqueous equilibria [31]. The inner loop is covered in Steps (4) to (6).

- (4) Conduct three-phase free-water isothermal flash algorithm [31] at P and T^{iter} to solve for phase mole fractions and phase compositions. The initialization method of the three-phase free-water flash algorithm [31] is the same as that proposed by Lapene *et al.* [30]. The negative flash is allowed in this case [35].
- (5) If an open feasible region appears in any iteration or any of the ultimately calculated phase fractions do not belong to $[0, 1]$, go to Step (6). Otherwise, three-phase vapor-liquid-aqueous equilibrium will appear at P and T^{iter} and go to Step (7).
- (6) Conduct conventional two-phase isothermal flash and the mixture will split into two phases at P and T^{iter} . If the two-phase equilibrium does not contain a water-rich phase based on the criteria proposed by Li and Li [31], the Wilson equation [36] can be used to initialize K -values for the non-water component in the two-phase flash,

$$K_{iy} = \frac{P_{ci}}{P} \exp \left[5.37(1 + \omega_i) \left(1 - \frac{T_{ci}}{T} \right) \right], i \neq 1 \quad (3-10)$$

The Wilson equation can provide a satisfying initialization of the K -values between the vapor and hydrocarbon-rich phases for the non-water components, while the initialization given by Equation (3-11) for the water component proposed by Lapene *et al.* [30] can give a better initial value than the value provided by the Wilson equation based on our extensive testing,

$$K_{1y} = \frac{P_{c1}}{P} \frac{T}{T_{c1}} \quad (3-11)$$

Otherwise, the K -values are initialized by,

$$x_{il} = \begin{cases} 10^{-10}, & i \neq 1 \\ 1 - (N_c - 1) \times 10^{-10}, & i = 1 \end{cases} \quad (3-12)$$

$$x_{i2} = 1/N_c \quad (3-13)$$

$$K_{i1} = \frac{x_{i1}}{x_{i2}}, \quad i = 1, \dots, N_c \quad (3-14)$$

where the subscript 1 represents the non-reference phase which represents the water-rich phase in our case, while the subscript 2 represents the non-water-rich phase which is chosen as the reference phase in our case. This initialization method is based on the fact that little hydrocarbons can dissolve in the water-rich phase.

(7) Calculate the residual of the energy conservation equation, g_2^{iter} , as follows,

$$g_2^{iter} = H_t - H_{spec} \quad (3-15)$$

(8) Update T^{iter} . If $iter=1$, calculate the molar heat capacity of each phase, C_{pj} , and the total molar heat capacity, C_{pt} ,

$$C_{pt} = \sum_{j=1}^{N_p} \beta_j C_{pj} \quad (3-16)$$

Update the temperature by [20],

$$T^2 = T^1 + g_2^1 / C_{pt} \quad (3-17)$$

Otherwise, update the temperature by [20],

$$T^{iter+1} = T^{iter} - g_2^{iter} \frac{T^{iter} - T^{iter-1}}{g_2^{iter} - g_2^{iter-1}} \quad (3-18)$$

(9) Check if $T^L < T^{iter+1} < T^U$. If so, $iter=iter+1$ and go to Step (10). Otherwise, re-calculate T^{iter+1} by [20],

$$T^{iter+1} = T^{iter} - g_2^{iter} \frac{T^L - T^U}{g_2^L - g_2^U} \quad (3-19)$$

where g_2^L and g_2^U are the residual of the energy conservation equation at the lower

boundary temperature and the upper boundary temperature, respectively.

(10) If $abs(g_2^{iter-1}) < 10^{-6}$, output T^{iter-1} , phase mole fractions, and phase compositions.

Otherwise, go back to Step (4).

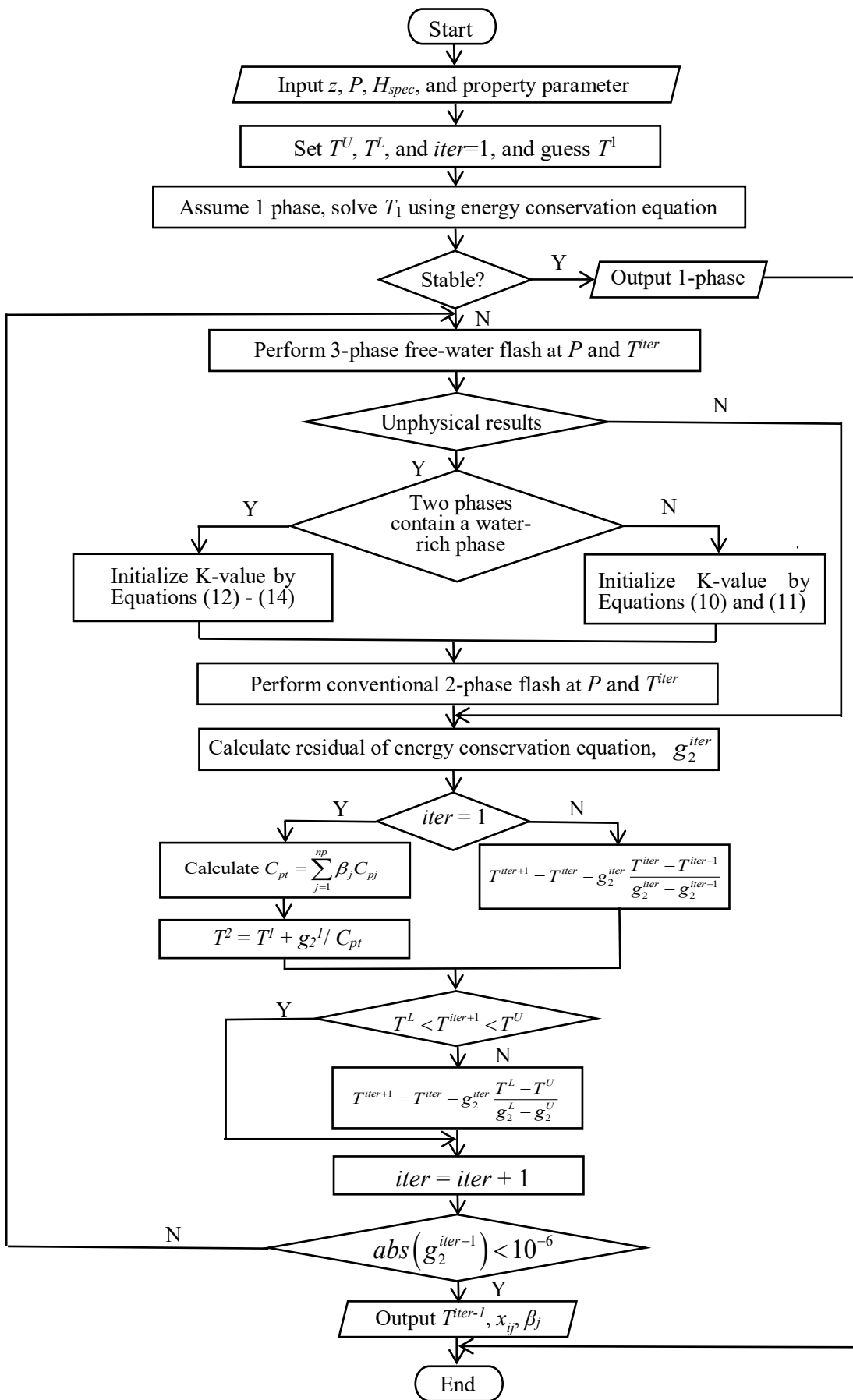


Figure 3-1 Flow chart of the multiphase isenthalpic flash algorithm based on the free-water assumption

3.4 Example Applications

We implement the newly developed three-phase isenthalpic flash algorithm to several water/hydrocarbon mixtures to test the robustness of this algorithm, especially, in the narrow-boiling regions. Each case is tested under a great number of pressure/enthalpy conditions. The details with regard to the calculations of the thermodynamic properties can refer to the formulations provided by Zhu and Okuno [21]. Appendix A provides all the values of the parameters needed in the calculations, including feed compositions, component properties, and BIPs. In the following text and figures, V represents the vapor phase, HC represents the hydrocarbon-rich phase, and W represents the water-rich phase.

3.4.1 Case 1 (Water/C3/C16 Mixture)

The water/C3/C16 mixture was also used by Zhu and Okuno [28]. This mixture is tested under 80 bar and different specified enthalpies. Figure 3-2 shows the comparison between temperatures obtained by the free-water isenthalpic flash algorithm in this work and those obtained by the Zhu and Okuno [28]. As shown in Figure 3-2, the calculated temperatures by these two works are in an excellent agreement. In the three-phase vapor-liquid-aqueous equilibrium zone, especially near the phase boundary between the three-phase and two-phase vapor-liquid equilibrium, the enthalpy is highly sensitive to the temperature change. This phenomenon is referred to as the narrow-boiling behavior. An extensive testing shows that our algorithm performs well in the narrow-boiling region.

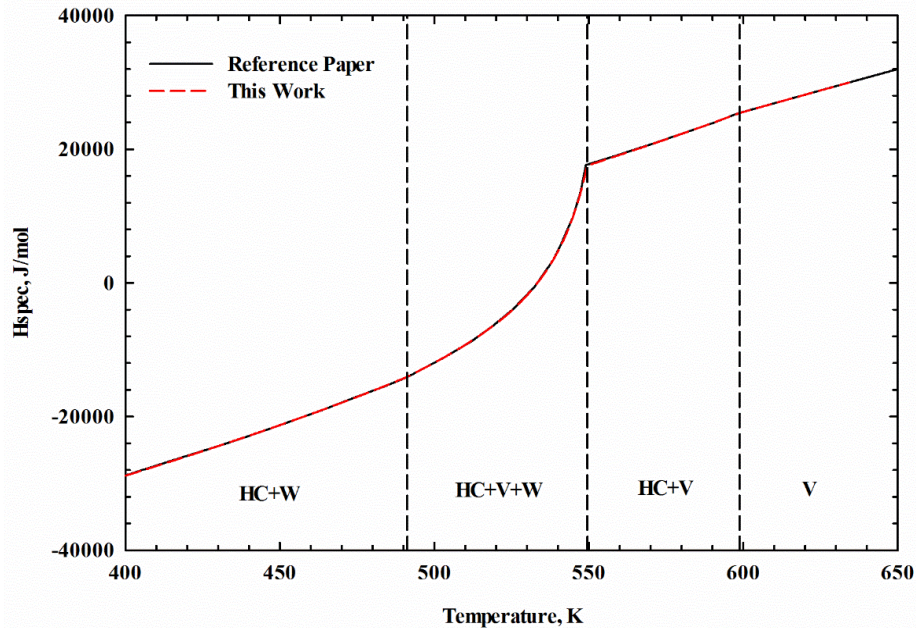
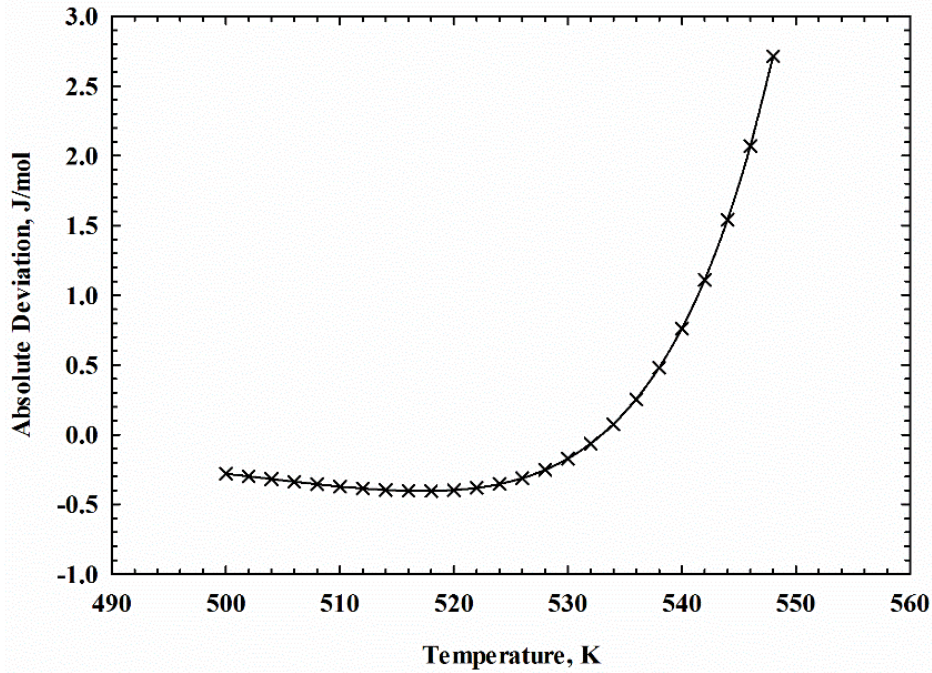
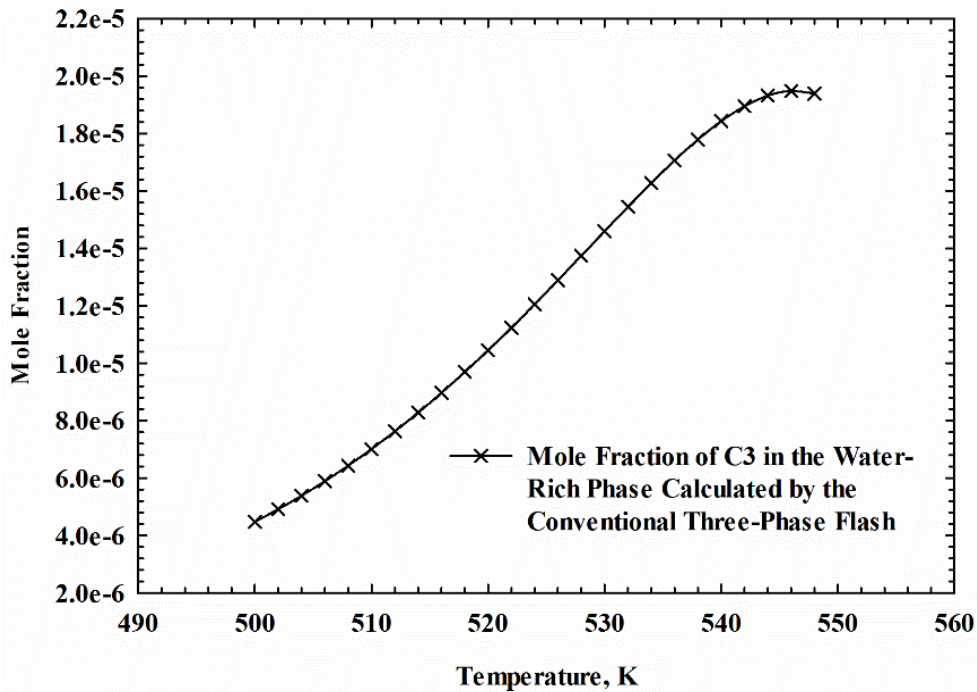


Figure 3-2 Case study 1 (water/C3/C16 mixture): comparison between temperatures obtained by the new isenthalpic flash algorithm and those obtained by the Zhu and Okuno [28] at 80 bar

As for this mixture at 80 bar and different temperatures, Figure 3-3 (a) shows the absolute deviations between the total molar enthalpies calculated by the conventional three-phase isothermal flash and those obtained by the three-phase free-water isothermal flash. Note that the absolute deviations tend to decrease first as a function of temperature below about 518 K, followed by a sharp increase as temperature further goes up towards the temperature that differentiates the two-phase vapor-liquid equilibrium and the three-phase equilibrium. Figure 3-3 (b) shows the variation in the mole fraction of C3 in the water-rich phase as calculated by the conventional three-phase isothermal flash. As shown in Figure 3-3 (b), the dissolution of C3 in the water-rich phase increases with an increase in temperature, which explains why the absolute deviations as shown in Figure 3-3 (a) shows a sharp increasing trend as temperatures goes beyond about 518 K.



(a)

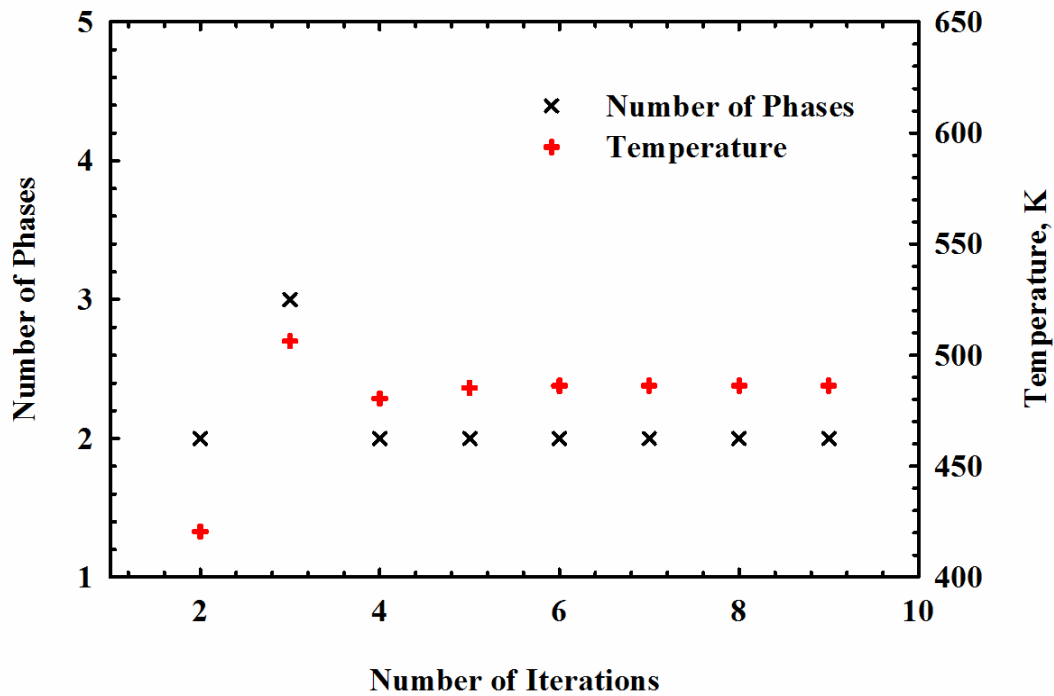


(b)

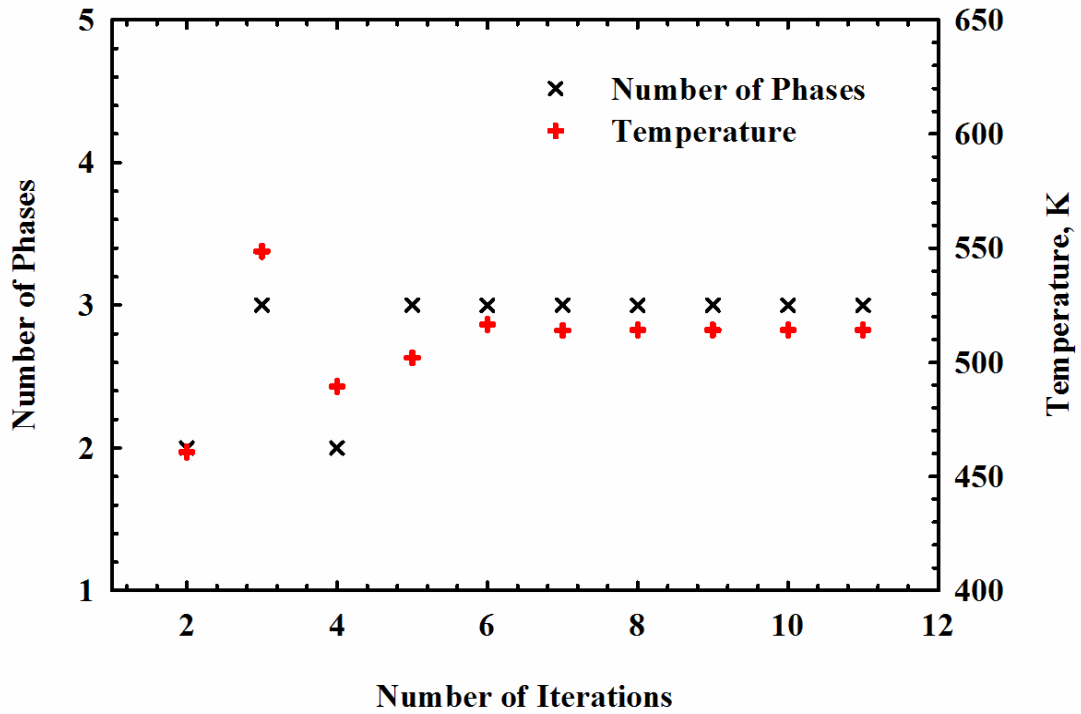
Figure 3-3 Case study 1 (water/C3/C16 mixture): (a) absolute deviations between the calculated total molar enthalpies obtained by the conventional three-phase isothermal flash and those obtained by the three-phase free-water isothermal flash at 80 bar and different temperatures; (b) mole fraction of C3 in the water-rich phase as calculated by the conventional three-phase

isothermal flash at 80 bar and different temperatures.

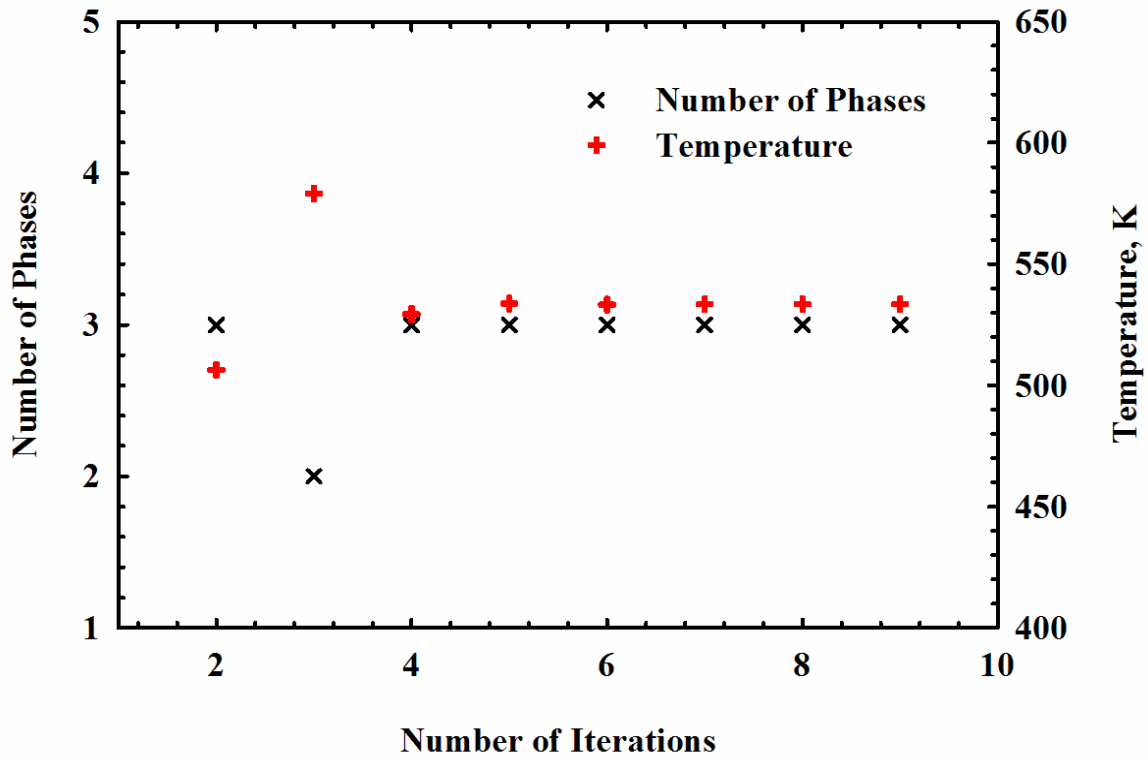
Figure 3-4 describes the evolution of the number of phases and temperatures as a function of the iteration number of the outer loop for the water/C3/C16 mixture at 80 bar and four different specified enthalpy values. These specified enthalpies are selected from the narrow-boiling region to illustrate the phase appearance and disappearance during the multiphase isenthalpic flash calculations. As shown in Figure 3-4, our multiphase isenthalpic flash algorithm can readily handle the phase appearance and disappearance as temperature varies since no convergence issue is encountered.



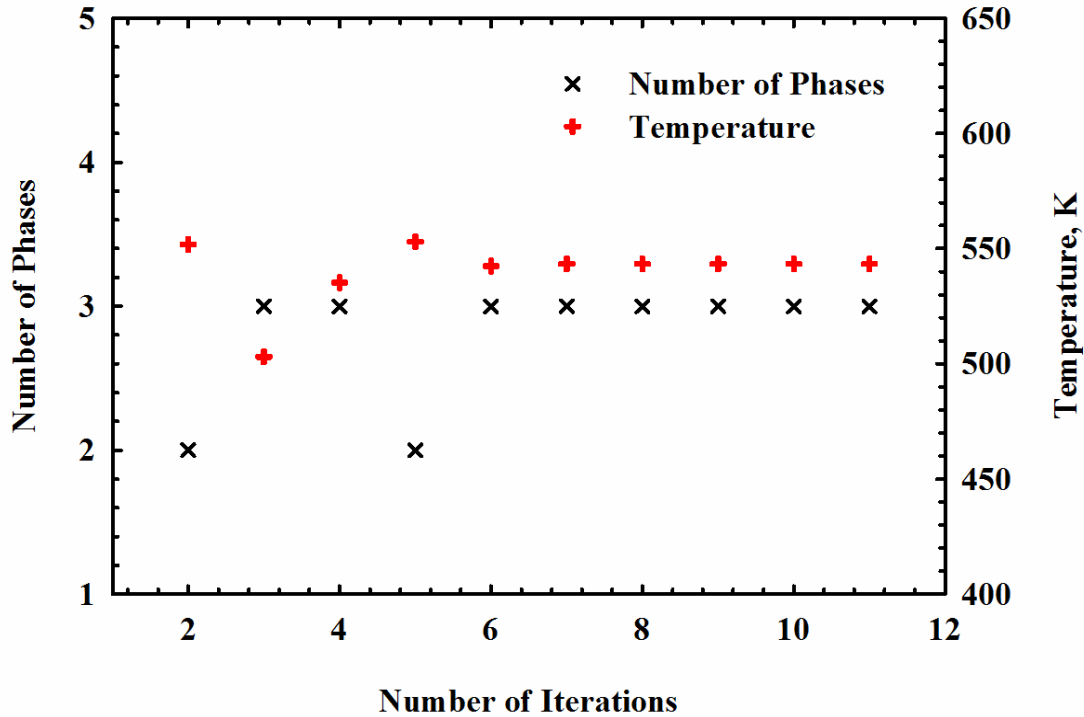
(a)



(b)



(c)



(d)

Figure 3-4 Case study 1 (water/C3/C16 mixture): evolution of the number of phases and temperatures as a function of the iteration number of the outer loop at 80 bar and four different values of the specified enthalpy: (a) $H_{spec} = -15000$ J/mol; (b) $H_{spec} = -8000$ J/mol; (c) $H_{spec} = 0$ J/mol; (d) $H_{spec} = 8000$ J/mol.

3.4.2 Case 2 (Water/Pseudo-Components Mixture)

This case study focuses on a water/hydrocarbon mixture that is comprised of water and four pseudo-components, which was also tested by Zhu and Okuno [28]. During the calculations, the pressure is set at 30 bar. Figure 3-5 shows the comparison between temperatures at different specified enthalpies obtained by the algorithm in this work and those obtained by Zhu and Okuno [28]. Again, a good agreement is observed between the calculated temperatures by these two methods.

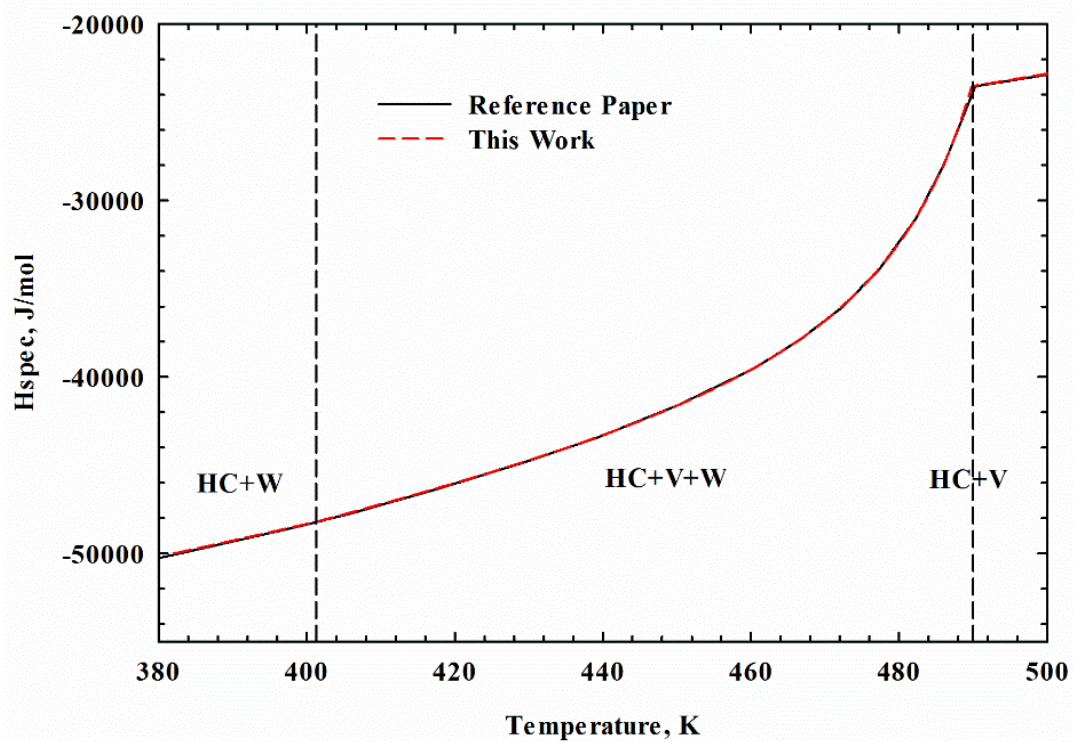


Figure 3-5 Case study 2 (water/pseudo-components mixture): comparison between temperatures obtained by the new isenthalpic flash algorithm and those obtained by the Zhu and Okuno [28] at 30 bar

Figure 3-6 presents the number of iterations at different calculated temperatures obtained by our multiphase isenthalpic flash algorithm. During the calculations, we set the T^U as 800 K, T^L as 200 K, and T^I as 300 K. Based on our extensive testing results, the initial temperature has little effect on the number of iterations required for the outer loop before convergence, while the upper and lower boundary temperatures have a relatively larger impact. As shown in Figure 3-6, the most obvious tendency is that the number of iterations becomes much larger when we are approaching the phase boundary between the three-phase and two-phase vapor-liquid equilibrium where the enthalpy is most sensitive to the temperature.

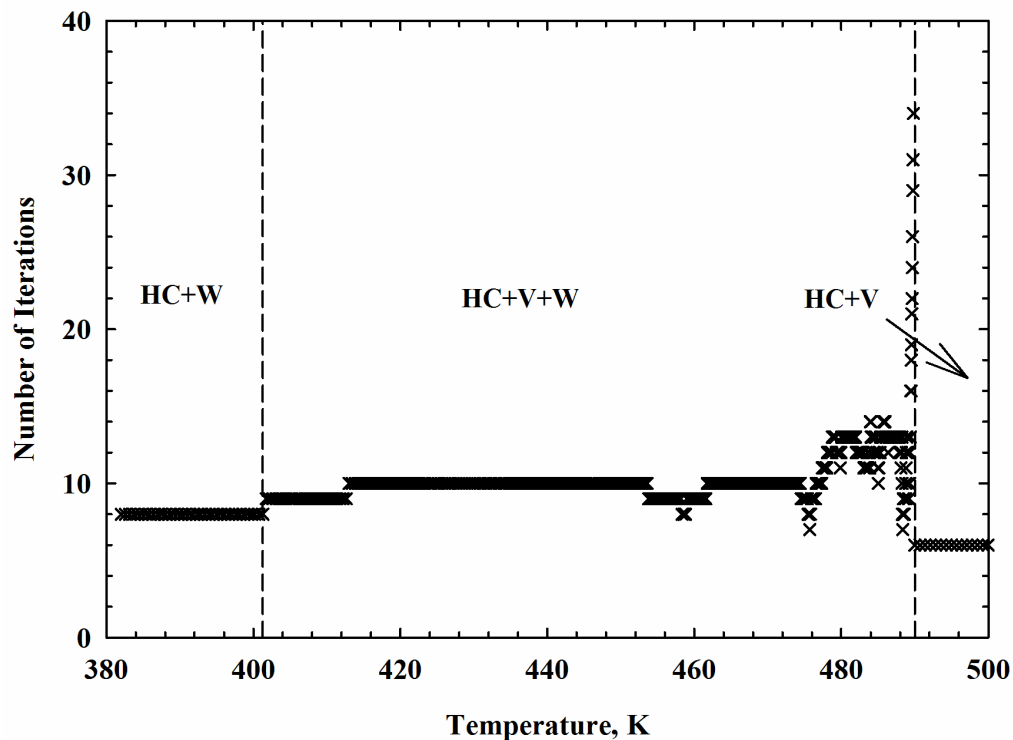
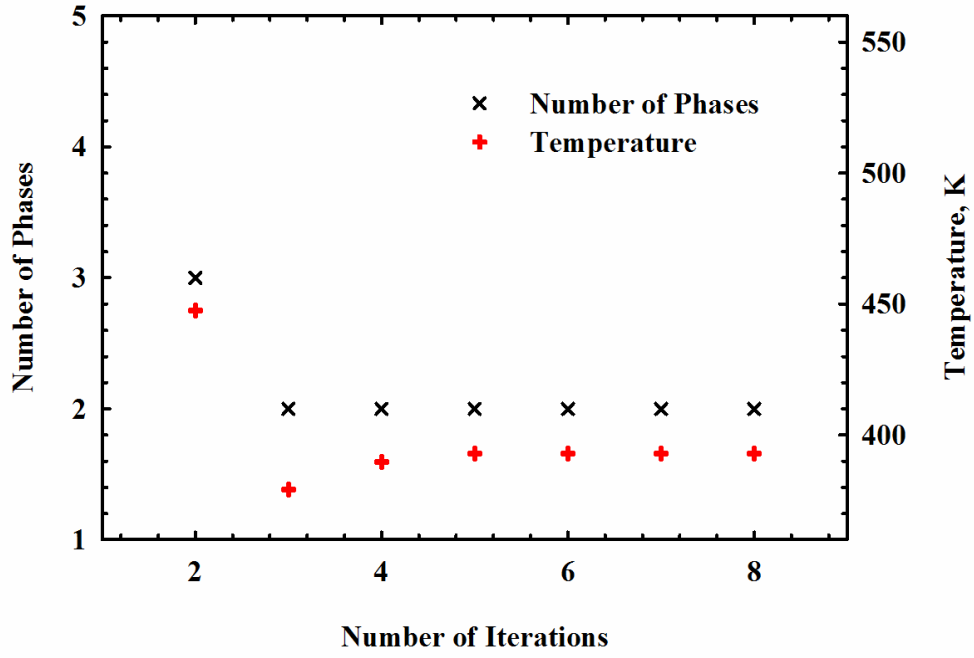


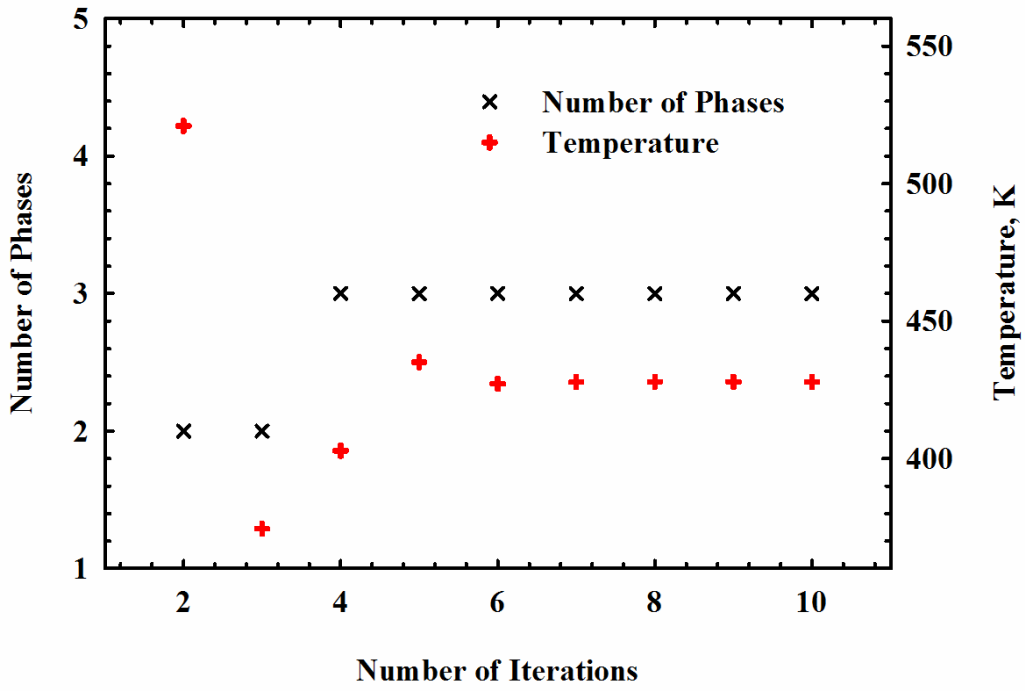
Figure 3-6 Case study 2 (water/pseudo-components mixture): variation in the number of iterations as a function of the calculated temperatures experienced by the new isenthalpic flash algorithm at 30 bar

Figure 3-7 shows the evolution of number of phases and temperatures as a function of the iteration number of the outer loop for this mixture at 30 bar and four different specified enthalpy values. These specified enthalpies are selected from the narrow-boiling region as well. From Figure 3-7, we can clearly observe how the phases appear or disappear during the isenthalpic flash calculations in the narrow-boiling region. As the specific enthalpy curve shown in Figure 3-5 moves closer to the narrow boiling region, we can see from Figure 3-7 that the number of the phases tend to be bouncing between 2 and 3. This instability raises the difficulty in performing the multiphase isenthalpic flash calculations, which translates to an increasing iteration number of the

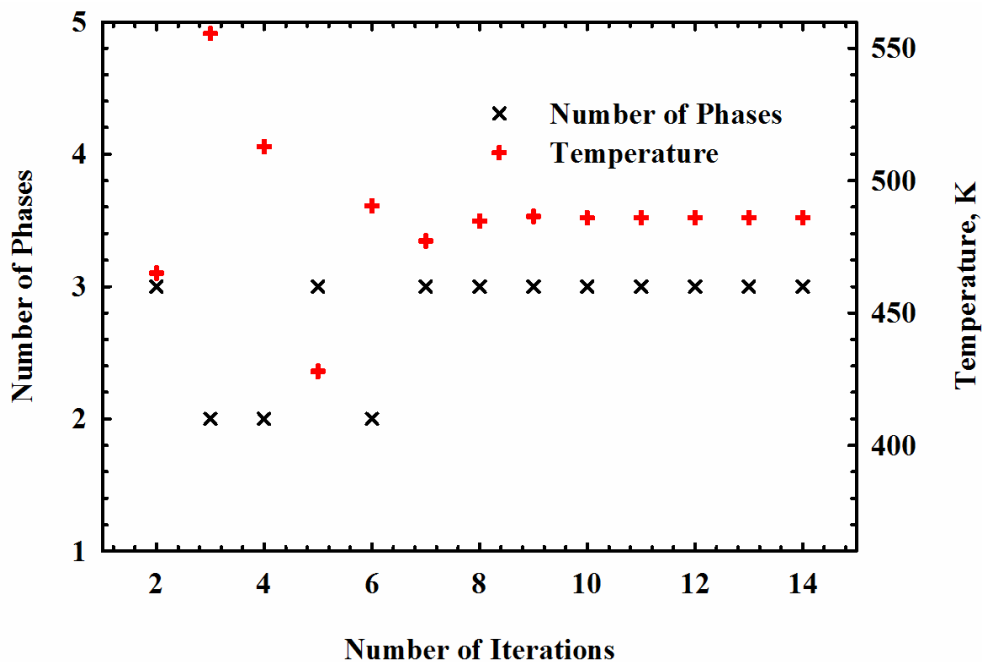
outer loop.



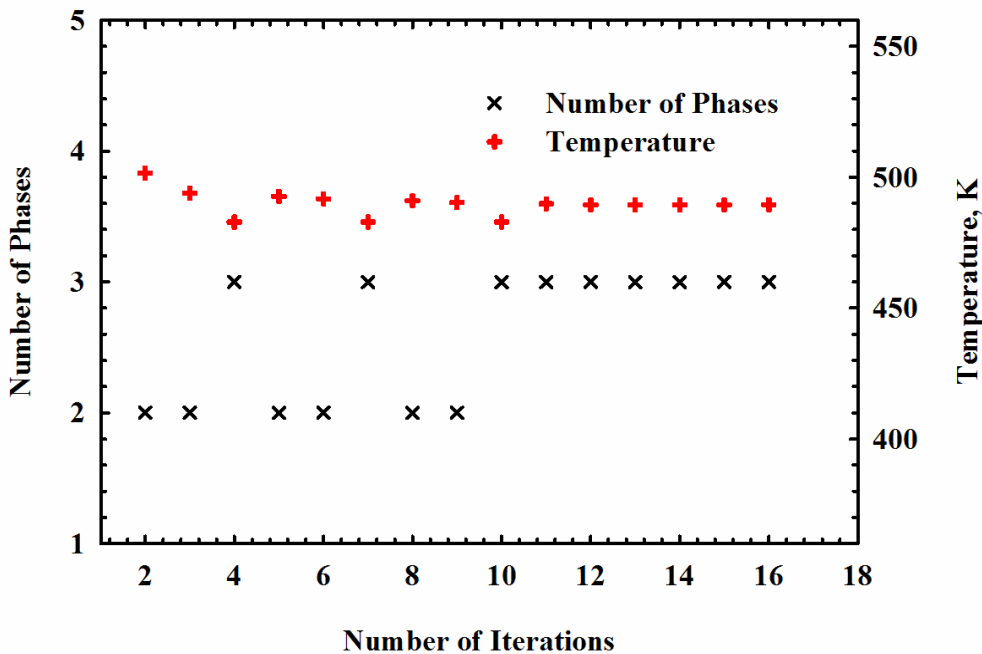
(a)



(b)



(c)

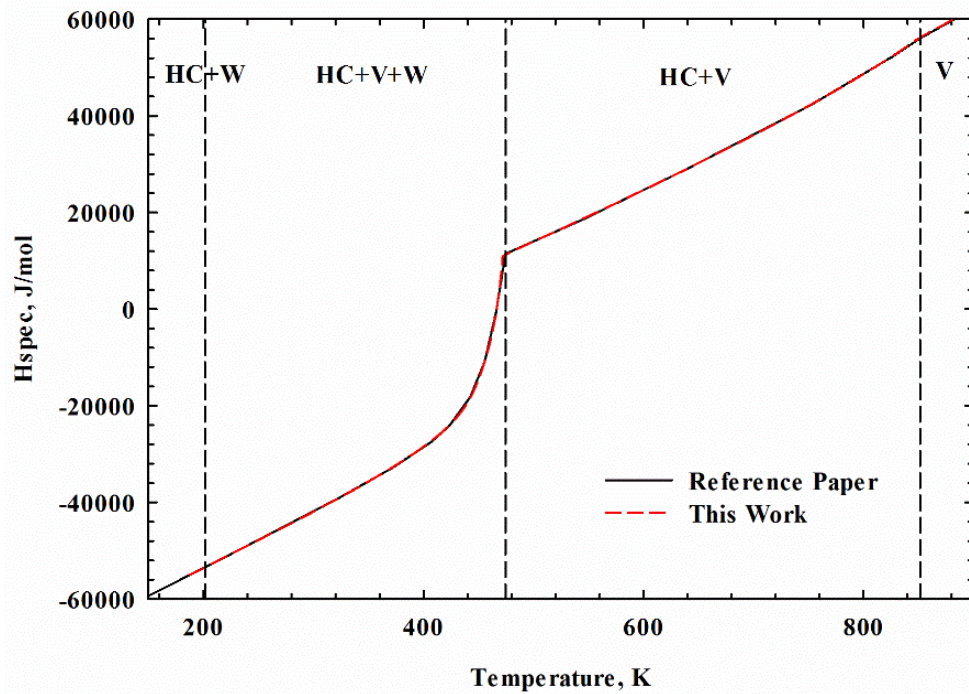


(d)

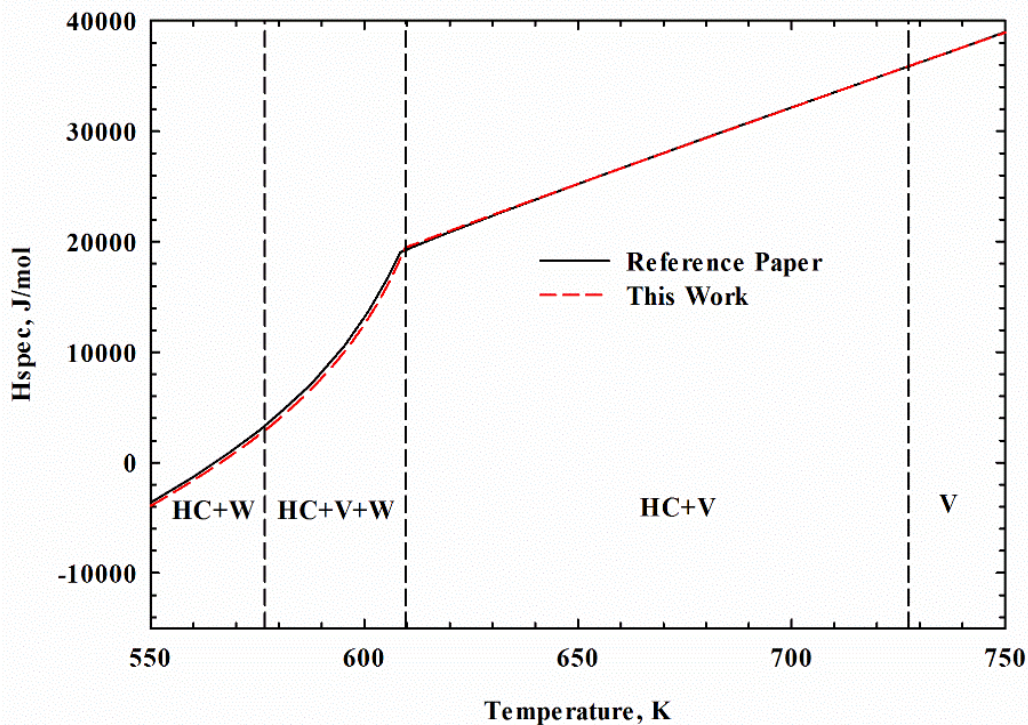
Figure 3-7 Case study 2 (water/pseudo-components mixture): evolution of the number of phases and temperatures as a function of the iteration number of the outer loop at 30 bar and four different values of the specified enthalpy: (a) $H_{spec} = -49000$ J/mol; (b) $H_{spec} = -45000$ J/mol; (c) $H_{spec} = -28000$ J/mol; (d) $H_{spec} = -24000$ J/mol.

3.4.3 Case 3 (Water/C1/C7/C_D Mixture)

This case study focuses on a water/hydrocarbon mixture containing 75% water, 8% C1, 15% n-C7, and 2% Athabasca (GCOS) dead bitumen (C_D). Zhu and Okuno [37] also used this mixture as an example. We conduct the multiphase isenthalpic flash calculations at several specified enthalpies at 20 bar and 210 bar, respectively. Figure 3-8 (a) shows the comparison between temperatures obtained by the new algorithm and those obtained by Zhu and Okuno [37] for this mixture at 20 bar and different specified enthalpies. Figure 3-8 (b) shows a similar comparison at 210 bar. A good agreement concurs between the calculated temperatures by these two algorithms at 20 bar. Nonetheless, we can observe some discrepancies between the calculated temperatures by these two algorithms at 210 bar. Such discrepancy is caused by the increasing dissolution of C1 in the water-rich phase at a higher pressure.



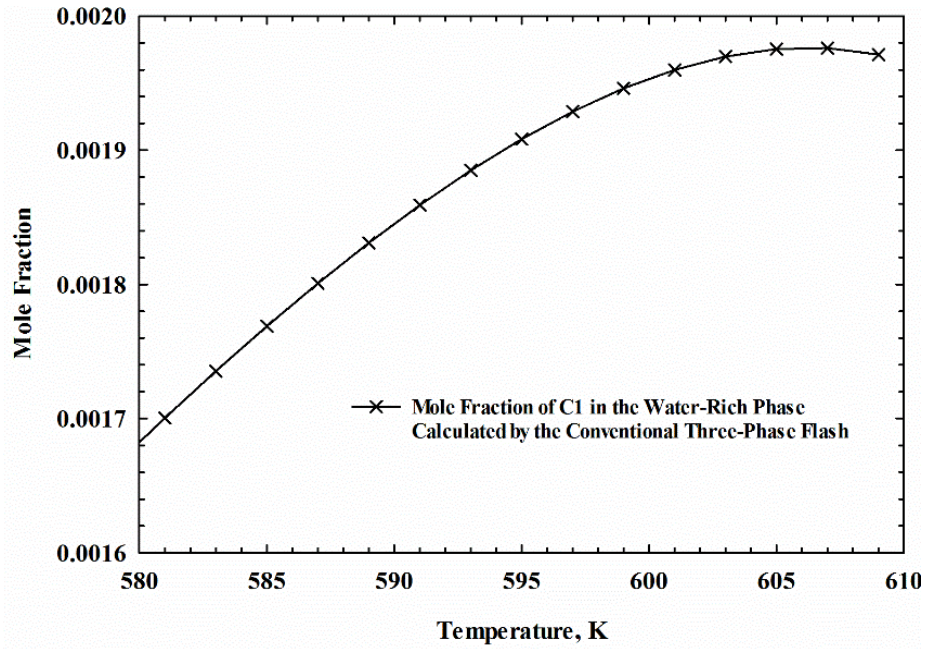
(a)



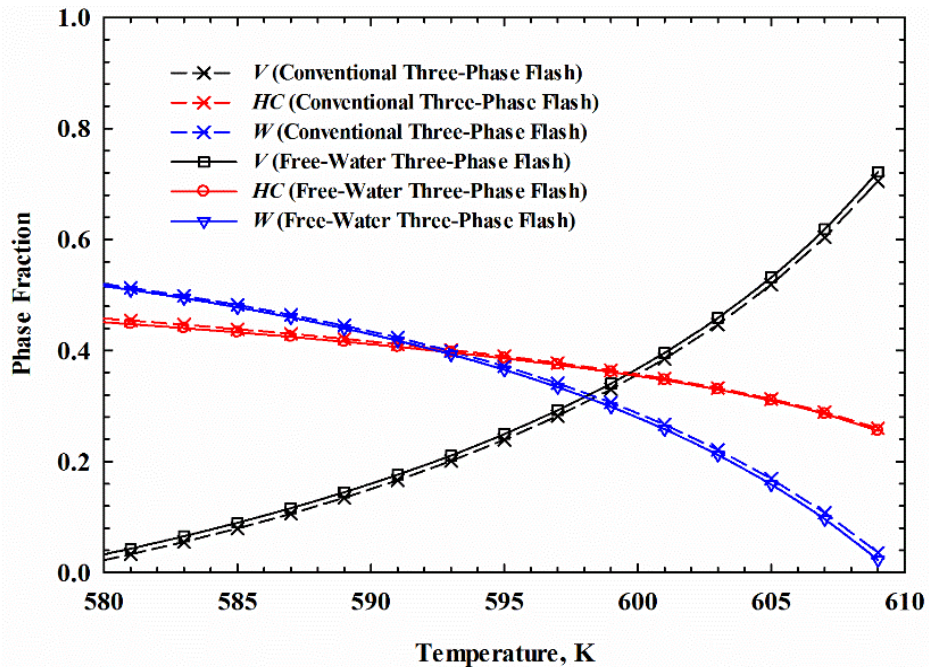
(b)

Figure 3-8 Case study 3 (Water/C1/C7/C_D mixture): comparison between temperatures obtained by the multiphase isenthalpic flash algorithm provided in this work and those obtained by the Zhu and Okuno [37], (a) at 20 bar and (b) at 210 bar.

As shown in Figure 3-9 (a), the mole fraction of C1 in the water-rich phase calculated by the conventional three-phase isothermal flash is larger than 0.0016. As temperature increases, the mole fraction of C1 in the water-rich phase becomes even larger, approaching 0.0020. Therefore, the C1 dissolved in the water-rich phase cannot be neglected at such high pressures, implying that the application of free-water assumption will lead to a larger approximation error. It is seen from Figure 3-9 (b) that a small discrepancy exists between the phase fractions obtained by the three-phase free-water isothermal flash and those obtained by the conventional three-phase isothermal flash. Fortunately, thermal recovery projects in Canadian heavy oil reservoirs are normally conducted under relatively low pressures, e.g., 20-40 bar. This means that our free-water isenthalpic algorithm can be potentially applicable to the thermal-recovery simulations for the majority of Canadian heavy oil reservoirs.



(a)



(b)

Figure 3-9 Case study 3 (Water/C1/C7/C_D mixture): (a) mole fraction of C1 in the water-rich phase calculated by the conventional three-phase isothermal flash at 210 bar and different temperatures; (b) comparison between the phase fractions obtained by the three-phase free-water isothermal flash and those obtained by the conventional three-phase isothermal flash at 210 bar and different temperatures.

Figure 3-10 describes the evolution of the number of iterations as a function of the calculated temperatures at 210 bar experienced by our new isenthalpic flash algorithm. During the calculations, we set T^U to be 800 K, T^L to be 200 K, and T^I to be 300 K. Similarly, we can see from Figure 3-10 that the number of iterations increases significantly when we are approaching the phase boundary between the three-phase and two-phase vapor-liquid equilibrium.

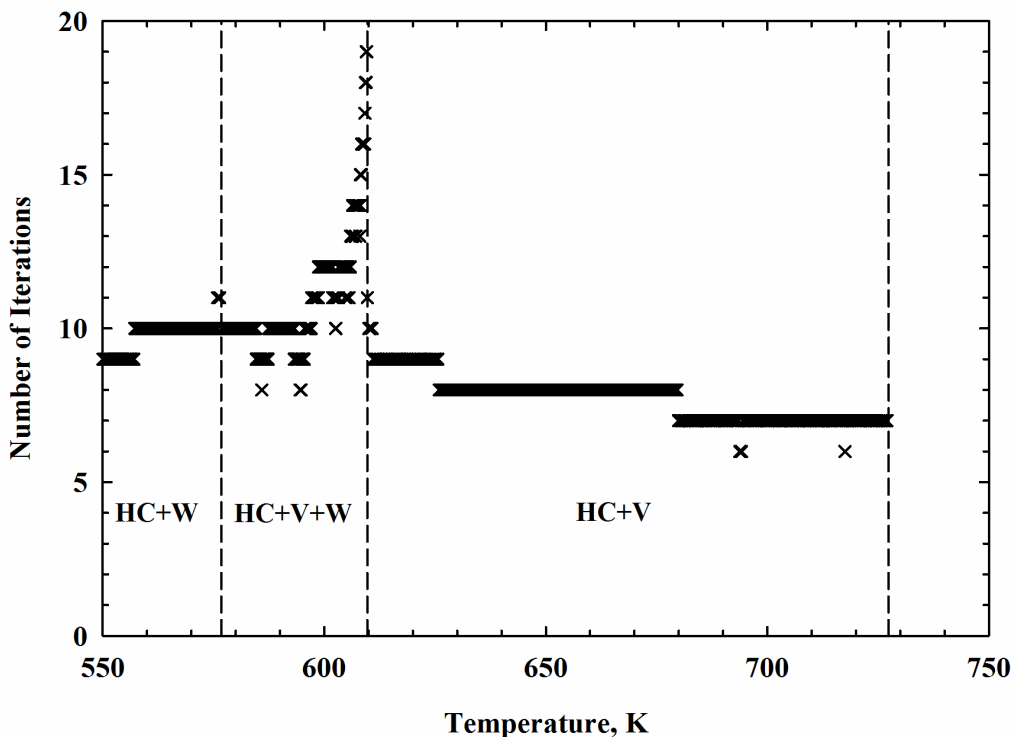


Figure 3-10 Case study 3 (Water/C1/C7/C_D mixture): evolution of the number of iterations as a function of the calculated temperatures at 210 bar as experienced by the new isenthalpic flash algorithm

3.5 Conclusions

In this paper, we present a robust and efficient three-phase isenthalpic flash algorithm based on the

free-water assumption for the aqueous phase if the aqueous phase exists. This isenthalpic flash algorithm can consider single-phase equilibria, two-phase equilibria, and three-phase vapor-liquid-aqueous equilibria. As demonstrated by the challenging case studies, this algorithm performs well in the narrow-boiling region except for the mixture with one degree of freedom and can readily handle the phase appearances and disappearances as temperature updates to satisfy the energy conservation equation. At low to medium pressures under which the thermal recovery processes are normally conducted, a good agreement can be observed between the flash results obtained by the new algorithm and those obtained by the conventional algorithm without imposing the free-water assumption. But it is worthwhile mentioning that this algorithm may cause intolerable errors if applied to the mixtures containing polar materials, such as alcohols, or the mixtures at given conditions under which the free-water assumption is not valid.

Nomenclature

C_{pj}	molar heat capacity of phase j
C_{pt}	total molar heat capacity
f_{ij}	fugacity of component i in phase j
g_2^{iter}	residual of the energy equation at a given temperature in each iteration
g_2^L	residual of the energy equation at the lower boundary temperature
g_2^U	residual of the energy equation at the upper boundary temperature

H_j	molar enthalpy of phase j
H_{spec}	specified molar enthalpy
H_t	total molar enthalpy
$iter$	number of iterations
K_{iy}	equilibrium ratio of component i for the vapor phase with respect to the reference phase
N_c	number of components
N_p	number of phases
P	pressure
P_c	critical pressure
S_j	molar entropy of phase j
S_t	total molar entropy
T	temperature
T_1	temperature calculated by the energy conservation equation assuming the feed is stable
T_c	critical temperature

T^{iter}	temperature in each iteration
T^L	the lower boundary temperature
T^U	the upper boundary temperature
x_{ij}	mole fraction of component i in phase j
z_i	mole fraction of component i in the feed
β_j	phase fraction of phase j
β_w	phase fraction of the water-rich phase
β_x	phase fraction of the hydrocarbon-rich phase
β_y	phase fraction of the vapor phase
ϕ	fugacity coefficient
ω	acentric factor

Subscripts

1	water component or non-reference phase
2	reference phase
c	critical property
i	component index

<i>j</i>	phase index
<i>spec</i>	specified value
<i>t</i>	total property
<i>w</i>	water-rich phase
<i>x</i>	hydrocarbon-rich phase
<i>y</i>	vapor phase

Superscripts

<i>iter</i>	iteration index
<i>L</i>	lower bound
<i>U</i>	upper bound

3.6 References

- [1] Naderi, K., and Babadagli, T., 2016, “Solvent selection criteria and optimal application conditions for heavy-oil/bitumen recovery at elevated temperatures: a review and comparative analysis,” *J. Energy Resour. Technol.*, **138**(1), pp. 012904. DOI: 10.1115/1.4031453
- [2] Prats, M., 1982, *Thermal recovery*, Society of Petroleum Engineers of AIME, New York: H.L. Doherty Memorial Fund of AIME.
- [3] Zheng, S., and Yang, D., 2017, “Experimental and theoretical determination of diffusion coefficients of CO₂-heavy oil systems by coupling heat and mass transfer,” *J. Energy Resour.*

Technol., **139**(2), pp. 022901. DOI: 10.1115/1.4033982

[4] Lee, H., Jin, J., Shin, H., and Choe, J., 2015, “Efficient prediction of SAGD productions using static factor clustering,” J. Energy Resour. Technol., **137**(3), pp. 032907. DOI: 10.1115/1.4029669

[5] Panwar, A., Trivedi, J.J., and Nejadi, S., 2015, “Importance of distributed temperature sensor data for steam assisted gravity drainage reservoir characterization and history matching within ensemble kalman filter framework,” J. Energy Resour. Technol., **137**(4), pp. 042902. DOI: 10.1115/1.4027763

[6] Willman, B.T., Valleroy, V.V., Runberg, G.W., Cornelius, A.J., and Powers, L.W., 1961, “Laboratory studies of oil recovery by steam injection,” J. Pet. Tech., **13**(7), pp. 681-690. DOI: 10.2118/1537-G-PA

[7] Utvik, O.H., Rinde, T., and Valle, A., 2001, “An experimental comparison between a recombined hydrocarbon-water fluid and a model fluid system in three-phase pipe flow,” J. Energy Resour. Technol., **123**(4), pp. 253-259. DOI: 10.1115/1.1410365

[8] Zaghoul J., Adewumi, M., and Ityokumbul, M.T., 2008, “Hydrodynamic modeling of three-phase flow in production and gathering pipelines,” J. Energy Resour. Technol., **130**(4), pp. 043004. DOI:10.1115/1.3000135

[9] Brantferger, K.M., Pope, G.A., and Sepehrnoori, K., 1991, “Development of a thermodynamically consistent, fully implicit, equation-of-state, compositional steamflood simulator,” Society of Petroleum Engineers Symposium on Reservoir Simulation, Anaheim, California. DOI: 10.2118/21253-MS

- [10] Zirrahi, M., Hassanzadeh, H., and Abedi, J., 2015, "Prediction of water solubility in petroleum fractions and heavy crudes using cubic-plus-association equation of state (CPA-EoS)," *Fuel*, **159**, pp. 894-899. DOI: 10.1016/j.fuel.2015.07.058
- [11] Zirrahi, M., Hassanzadeh, H., and Abedi, J., 2017, "Water content of light n-alkanes: New measurements and cub-plus-association equation of state modeling," *AIChE J.*, **63**(4), pp. 1384-1389. DOI: 10.1002/aic.15512
- [12] Zirrahi, M., Hassanzadeh, H., and Abedi, J., 2017, "Experimental and modeling studies of MacKay River bitumen and water," *J. Petrol. Sci. Eng.*, **151**, pp. 305-310. DOI: 10.1016/j.petrol.2017.01.013
- [13] Zirrahi, M., Hassanzadeh, H., and Abedi, J., 2017, "Experimental and modeling studies of water, light n-alkanes and MacKay River bitumen ternary systems," *Fuel*, **196**, pp. 1-12. DOI: 10.1016/j.fuel.2017.01.078
- [14] Grabowski, J.W., Vinsome, P.K., Lin, R.C., Behie, G.A., and Rubin, B., 1979, "A fully implicit general purpose finite-difference thermal model for in situ combustion and steam," Society of Petroleum Engineers Annual Technical Conference and Exhibition, Las Vegas, Nevada. DOI: 10.2118/8396-MS
- [15] Rubin, B., and Buchanan, W.L., 1985, "A general purpose thermal model," *SPE J.*, **25**(2), pp. 202-214. DOI: 10.2118/11713-PA
- [16] Ishimoto, K., Pope, G.A., and Sepchroori, K., 1987, "An equation-of-state steam simulator." *In Situ*, **11**(1), pp. 1-37.

- [17] Chien, M.C.H., Yardumian, H.E., Chung, E.Y., and Todd, W.W., 1989, "The formulation of a thermal simulation model in a vectorized, general purpose reservoir simulator," Society of Petroleum Engineers Symposium on Reservoir Simulation, Houston, Texas. DOI: 10.2118/18418-MS
- [18] Michelsen, M.L., 1987, "Multiphase isenthalpic and isentropic flash algorithms," Fluid Phase Equilibr., **33**(1-2), pp. 13-27. DOI: 10.1016/0378-3812(87)87002-4
- [19] Li, Z., and Firoozabadi, A., 2012, "General strategy for stability testing and phase-split calculation in two and three phases," SPE J., **17**(4), pp. DOI: 1096-1107. 10.2118/129844-PA
- [20] Agarwal, R.K., Li, Y.K., Nghiem, L.X., and Coombe, D.A., 1991, "Multiphase multicomponent isenthalpic flash calculations," J. Can. Pet. Tech., **30**(3), pp. 69-75. DOI: 10.2118/91-03-07
- [21] Zhu, D., and Okuno, R., 2014, "A robust algorithm for isenthalpic flash of narrow-boiling fluids," Fluid Phase Equilibr., **379**, pp. 26-51. DOI: 10.1016/j.fluid.2014.07.003
- [22] Rachford, H.H. Jr., and Rice, J.D., 1952, "Procedure for use of electronic digital computers in calculating flash vaporization hydrocarbon equilibrium (technical note 136)," Pet. Trans., AIME **195**, pp. 327-328. DOI: 10.2118/952327-G
- [23] Michelsen, M.L., 1982, "The isothermal flash problem. Part II. Phase-split calculation," Fluid Phase Equilibr., **9**(1), pp. 21-40. DOI: 10.1016/0378-3812(82)85002-4
- [24] Nghiem, L.X., 1983, "A new approach to quasi-Newton methods with application to compositional modeling," Society of Petroleum Engineers Reservoir Simulation Symposium, San

Francisco, California. DOI: 10.2118/12242-MS

[25] Nghiem, L.X., and Li, Y.K., 1984, "Computation of multiphase equilibrium phenomena with an equation of state," *Fluid Phase Equilibr.*, **17**(1), pp. 77-95. DOI: 10.1016/0378-3812(84)80013-8

[26] Gupta, A.K., Bishnoi, P.R., and Kalogerakis, N., 1990, "Simultaneous multiphase isothermal/isenthalpic flash and stability calculations for reacting/non-reacting systems," *Gas Sepa. Purif.*, **4**(4), pp. 215-222. DOI: 10.1016/0950-4214(90)80045-M

[27] Zhu, D., and Okuno, R., 2016, "Multiphase isenthalpic flash integrated with stability analysis," *Fluid Phase Equilibr.*, **423**, pp. 203-219. DOI: 10.1016/j.fluid.2016.04.005

[28] Zhu, D., and Okuno, R., 2015, "Robust isenthalpic flash for multiphase water/hydrocarbon mixtures," *SPE J.*, **20**(6), pp. 1350-1365. DOI: 10.2118/170092-PA

[29] Heidari, M., Nghiem, L.X., and Maini, B.B., 2014, "Improved isenthalpic multiphase flash calculations for thermal compositional simulators," *Society of Petroleum Engineers Heavy Oil Conference-Canada*, Calgary, Alberta. DOI: 10.2118/170029-MS

[30] Lapene, A., Nichita, D.V., Debenest, G., and Quintard, M., 2010, "Three-phase free-water flash calculations using a new modified Rachford-Rice equation," *Fluid Phase Equilibr.*, **297**(1), pp. 121-128. DOI: 10.1016/j.fluid.2010.06.018

[31] Li, R., and Li, H., 2018, "New two-phase and three-phase Rachford-Rice algorithms based on free-water assumption". *Can. J. Chem. Eng.*, **96** (1), pp. 390-403. DOI: 10.1002/cjce.23018

[32] Okuno, R., Johns, R., and Sepehrnoori, K., 2010, "A new algorithm for Rachford-Rice for

multiphase compositional simulation,” SPE J., **15**(2), pp. 313-325. DOI: 10.2118/117752-PA

[33] Tang, Y., and Saha, S., 2003, “An efficient method to calculate three-phase free-water flash for water-hydrocarbon systems,” Ind. Eng. Chem. Res., **42**(1), pp. 189-197. DOI: 10.1021/ie010785x

[34] Peng, D.Y., and Robinson, D.B., 1976, “A new two-constant equation of state,” Ind. Eng. Chem. Fund., 15(1), pp. 59-64.

[35] Whitson, C.H., and Michelsen, M.L., 1989, “The negative flash,” Fluid Phase Equilibr., 53, pp. 51-71. DOI: 10.1016/0378-3812(89)80072-X

[36] Wilson, G.M., 1969, “A modified Redlich-Kwong equation of state, application to general physical data calculations,” 65th National AIChE Meeting, Cleveland, Ohio.

[37] Zhu, D., and Okuno, R., 2015, “Analysis of narrow-boiling behavior for thermal compositional simulation,” Society of Petroleum Engineers Reservoir Simulation Symposium, Houston, Texas. DOI: 10.2118/173234-MS

Appendix 3-A: Component Properties and BIPs

Table 3-A.1, 3-A.3, and 3-A.5 show the component properties for the water/C3/C16 mixture used in Case 1, water/pseudo-components mixture used in Case 2, and water/C1/C7/C_D mixture used in Case 3, respectively. In these tables, z represents the mole fraction in the feed; T_c represents the critical temperature; P_c represents the critical pressure; ω represents the acentric factor; and C_{p1}^0 , C_{p2}^0 , C_{p3}^0 , and C_{p4}^0 are the coefficients used for calculating the molar enthalpy. Tables 3-A.2, 3-A.4, and 3-A.6 provide BIPs for the water/C3/C16 mixture used in Case 1, water/pseudo-components mixture used in Case 2, and water/C1/C7/C_D mixture used in Case 3, respectively.

Table 3-A.1 Component properties for the water/C3/C16 mixture [28]

Component	z (mol%)	T_c (K)	P_c (bar)	ω
H ₂ O	0.75	647.3	220.89	0.344
C3	0.15	369.8	42.46	0.152
C16	0.10	717.0	14.19	0.742
Component	C_{p1}^0 (J/mol·K)	C_{p2}^0 (J/mol·K ²)	C_{p3}^0 (J/mol·K ³)	C_{p4}^0 (J/mol·K ⁴)
H ₂ O	32.20	0.001907	1.06E-05	-3.596E-09
C3	-4.22	0.306300	-1.60E-04	3.215E-08
C16	-13.00	1.529000	-8.50E-04	1.850E-07

Table 3-A.2 BIPs between the components in the water/C3/C16 mixture [28]

Component	H ₂ O	C3	C16
H ₂ O	0	0.6841	0.3583
C3	0.6841	0	0
C16	0.3583	0	0

Table 3-A.3 Component properties for the water/pseudo-components mixture [28]

Component	z (mol%)	T_c (K)	P_c (bar)	ω
H ₂ O	0.50	647.300	220.89	0.344
PC1	0.15	305.556	48.82	0.098
PC2	0.10	638.889	19.65	0.535
PC3	0.10	788.889	10.20	0.891
PC4	0.15	838.889	7.72	1.085
Component	C_{P1}^0 (J/mol·K)	C_{P2}^0 (J/mol·K ²)	C_{P3}^0 (J/mol·K ³)	C_{P4}^0 (J/mol·K ⁴)
H ₂ O	32.200	0.001907	1.06E-05	-3.596E-09
PC1	-3.500	0.005764	5.09E-07	0
PC2	-0.404	0.000657	5.41E-08	0
PC3	-6.100	0.010930	1.41E-06	0
PC4	-4.500	0.008049	1.04E-06	0

Table 3-A.4 BIPs between the components in the water/pseudo-components mixture [28]

Component	H ₂ O	PC1	PC2	PC3	PC4
H ₂ O	0	0.71918	0.45996	0.26773	0.24166
PC1	0.71918	0	0	0	0
PC2	0.45996	0	0	0	0
PC3	0.26773	0	0	0	0
PC4	0.24166	0	0	0	0

Table 3-A.5 Component properties for the water/C1/C7/C_D mixture [37]

Component	z (mol%)	T_c (K)	P_c (bar)	ω
H ₂ O	0.75	647.3	220.89	0.344
C1	0.08	190.6	46.00	0.008
C7	0.15	540.2	27.36	0.351
C _D	0.02	1090.9	7.86	1.361
Component	C_{P1}^0 (J/mol·K)	C_{P2}^0 (J/mol·K ²)	C_{P3}^0 (J/mol·K ³)	C_{P4}^0 (J/mol·K ⁴)
H ₂ O	32.20	0.001907	1.06E-05	-3.596E-09
C1	19.30	0.052120	1.20E-05	-1.132E-08
C7	-5.15	0.676100	-3.70E-04	7.657E-08
C _D	-34.60	3.801000	-2.15E-03	0

Table 3-A.6 BIPs between the components in the water/C1/C7/C_D mixture [37]

Component	H₂O	C1	C7	C_D
H₂O	0	0.7560	0.5610	0.1000
C1	0.7560	0	0.0352	0
C7	0.5610	0.0325	0	0
C_D	0.1000	0	0	0

**CHAPTER 4 IMPROVED THREE-PHASE EQUILIBRIUM
CALCULATION ALGORITHM FOR WATER/HYDROCARBON
MIXTURES WITH A NEW INITIALIZATION SCHEME**

A version of this chapter has been accepted for publication in *Fuel*.

Abstract

Three-phase vapor-liquid-aqueous (VLA) equilibria can frequently appear in hydrocarbon reservoirs. The presence of the aqueous phase, which can commonly exist as a pure water phase, can dramatically increase the probability of encountering convergence issues in the three-phase equilibrium calculation algorithms. The primary reason is that there is a lack of good initial estimates of equilibrium ratios in both stability tests and flash calculations. In this research, we improve the three-phase VLA equilibrium calculation algorithm for water/hydrocarbon mixtures by developing a new scheme for initializing equilibrium ratios and also developing a new procedure for stability test. By applying this new initialization scheme, one can securely identify the aqueous-like stationary point on the tangent plane distance function. In our algorithm, convergence problems, which can frequently appear in the flash calculations of three-phase VLA equilibrium calculations, are avoided. We demonstrate the robustness and efficiency of the newly developed algorithm by showing a number of example calculations.

Keywords: Three-phase equilibrium, Stability test, Flash calculation, Initialization method, Robustness

4.1 Introduction

Three-phase vapor-liquid-aqueous (VLA) equilibria are frequently encountered in many hydrocarbon reservoirs. When one is conducting numerical simulations for such reservoirs with the aid of a compositional reservoir simulator, three-phase VLA equilibrium calculations should be conducted in each grid at each time step. A robust and efficient three-phase VLA equilibrium calculation algorithm is thereby becoming a prerequisite for accurately capturing the multiphase flow of water/hydrocarbon mixtures in hydrocarbon reservoirs [1, 2]. Three-phase VLA equilibrium calculation can be simplified as free-water three-phase equilibrium calculation if the aqueous phase can be considered as a pure water phase [3]; in most cases, this is a valid practice. But the free-water three-phase equilibrium calculation is not applicable to some reservoirs containing acid gases (such as CO_2 and H_2S). In such cases, the aqueous phase cannot be considered as a pure phase as the dissolution of the acid gases can be significant, especially at high pressure conditions [4, 5]; thus, a full three-phase equilibrium calculation is warranted.

Isothermal-isobaric phase equilibrium calculations aim to find a state at which the mixture has the lowest Gibbs free energy at the given feed composition, temperature, and pressure [6, 7]. In a multiphase equilibrium calculation, several kinds of phase equilibria may appear. For example, in a three-phase equilibrium calculation, the possible number of equilibrium phase can be one, two, or three. When the number of equilibrium phases is two, there will be three kinds of two-phase equilibria. However, we do not have a prior knowledge of the number of phases that are actually present. To determine the actual phase equilibrium, multiphase equilibrium

calculations are normally conducted in a stage-wise manner [6-8]. The most extensively adopted approach is to first perform stability test to determine if the number of phases needs to be increased by locating the stationary points of the tangent plane distance (TPD) function [6]; if any of the stationary points gives a negative TPD, we proceed with flash calculation with an increased number of phases to determine the phase fractions and phase compositions [7]. In this approach, the equilibrium ratios at the negative stationary point(s) yielded from the stability test are used to initialize the subsequent flash [7].

The aforementioned approach performs well when the largest number of present phases in the given system is two, while convergence problems are frequently encountered when that increases to three. This is partly because more stationary points can appear on the TPD function in three-phase equilibrium calculations than two-phase equilibrium calculations, leading to a higher chance of the negative stationary point(s) being hidden by positive ones. Thus, it is becoming more difficult for the stability tests to successfully detect the negative stationary point(s) in three-phase equilibrium calculations. To increase the chance of detecting the negative stationary points during stability test, multiple initial estimates of equilibrium ratios are required [6, 8-9]. Michelsen [6] suggested that the trial phase considered in the stability test can be initialized as a pure phase. Li and Firoozabadi [8] suggested that this method should be modified, since the pure phase may be largely distinct from the trial phase. For hydrocarbon fluids mixed with CO₂, they proposed to use $(c+4)$ initial estimates of equilibrium ratios for stability tests (where c represents the number of components) [8]. The initialization method proposed by Li and Firoozabadi [8]

works well in three-phase equilibrium calculations which do not involve the presence of an aqueous phase, but it may not perform well in three-phase VLA equilibrium calculations. This is because the presence of the aqueous phase skews the topography of the TPD function, leading to that the aqueous-like stationary point can frequently appears near the boundaries of the TPD surface. To find such aqueous-like stationary point near the boundaries of the TPD surface, Connolly [9] suggested that one should assign 99.9 mol% to water in the initial estimate of the trial phase, and let others equally share the remaining 0.1 mol%. When the pure water phase gives a local minimum value of the TPD function, this initialization method cannot detect the aqueous-like minimum point.

Another factor complicating the three-phase VLA calculation is that, in a three-phase VLA equilibrium calculation, multiple two-phase equilibria could be resulted from the two-phase flash calculations with different initial equilibrium-ratio estimates [10]. The true two-phase equilibrium should be the one having the minimum Gibbs free energy. Thereby, Gorucu and Johns [11] recommended that, to increase the chance of finding the true two-phase equilibrium or provide a better input for a subsequent three-phase flash, two-phase flash calculations should be performed several times with different initial estimates of equilibrium ratios, even if the results yielded by the first flash calculation seem physical; then the two-phase equilibrium, yielding the minimum Gibbs free energy, will be chosen to be applied in the subsequent calculations. To initialize the two-phase flashes, Gorucu and Johns [11] adopted the $(c+4)$ initial estimates of equilibrium ratios as proposed by Li and Firoozabadi [8] for initializing the stability

tests. However, this initialization method does not perform well in three-phase VLA equilibrium calculations, due to its possible failure in identifying the aqueous phase in two-phase flash calculations. It is also quite time-consuming to perform two-phase flash calculations in an exhaustive manner like this.

Many efforts have been invested in the past to develop a robust and efficient algorithm for performing three-phase VLA equilibrium calculations [2, 12-13]. Li and Nghiem [12] proposed a detailed three-phase VLA equilibrium calculation algorithm. Sabet and Gahrooei [13] modified this algorithm by adding a vapor-liquid (VL) stability test on the water-excluded feed. In these algorithms [12, 13], the vapor and oleic phases are modeled using the cubic equation of state (EOS), while the gas solubility in the aqueous phase is calculated by Henry's law [14]. This will result in an inconsistency of the thermodynamic properties among the aqueous phase and the vapor/liquid phases. Mortezaazadeh and Rasaeiuse [2] proposed a modified three-phase VLA equilibrium calculation algorithm. In their algorithm, all the thermodynamic properties are calculated by the Peng-Robinson (PR) EOS [15]. To have a precise description of the gas dissolution in the aqueous phase, the binary interaction parameters (BIPs) and α -function modified by Søreide and Whitson [16] are used to calculate the thermodynamic properties of the aqueous phase. In this algorithm, the presence of the aqueous phase is firstly checked by single-phase stability test; when conducting this single-phase stability test, the initial estimate of the trial phase, which is the same as that used by Connolly [9], is applied in an attempt to identify the aqueous-like stationary point on the TPD surface. But again, such initialization

method may fail to identify an aqueous-like stationary point in some cases. In addition, a negative aqueous-like stationary point may exist on the TPD surface, even if the aqueous phase will not appear in the actual phase equilibrium. Therefore, one cannot determine whether the aqueous phase will appear or not just based on the single-phase stability test. To ensure the robustness of their algorithm, Mortezaadeh and Rasaeiuse [2] suggested that several initial estimates of equilibrium ratios should be used in the two-phase VL flash calculations, which is similar to the recommendation made by Gorucu and Johns [11].

In this work, we improve the three-phase VLA equilibrium calculation algorithm with a new scheme to initialize equilibrium ratios in both stability tests and flash calculations. By applying this new initialization scheme, we can securely detect the aqueous-like stationary point on the TPD function. Moreover, convergence problems in flash calculations can be avoided with this new initialization scheme. By applying our improved algorithm, one can obtain correct phase equilibria in a more efficient way. The performance of the newly developed algorithm is demonstrated by using a large number of example calculations.

4.2 Theoretical Background

4.2.1 Phase Stability Test

Phase stability tests are applied to determine whether a mixture will reach a lower Gibbs free energy by splitting into two or more phases at a given temperature/pressure condition. A TPD function of the reduced molar Gibbs free energy is implemented in stability tests. The expression

of the TPD function is shown as follows [6],

$$g(\mathbf{y}) = \sum_{i=1}^c y_i [\ln \phi_i(\mathbf{y}) + \ln y_i - \ln \phi_i(\mathbf{z}) - \ln z_i] \quad (4-1)$$

where \mathbf{y} and \mathbf{z} represent the compositions of the trial phase and the test phase, respectively; $\phi_i(\mathbf{y})$ and $\phi_i(\mathbf{z})$ represent the fugacity coefficients of component i in the trial phase and the test phase, respectively; c is the number of components in the mixture; and the subscript i is the component index. In the single-phase stability test, \mathbf{z} represents the feed composition; while, in the two-phase stability test, \mathbf{z} represents the composition of either of the two phases yielded by the two-phase flash calculation (excluding the aqueous phase). If all the values of the TPD function are non-negative, the mixture will be considered to be stable. However, it is time-consuming to test all the possible compositions of the trial phase. Therefore, Michelsen [6] proposed that the mixture can be considered to be stable if all the values of stationary points on the TPD function are non-negative. The stationary points of the TPD function can be solved by the following equation [6],

$$\ln \phi_i(\mathbf{y}) + \ln y_i - \ln \phi_i(\mathbf{z}) - \ln z_i = k, \quad i = 1, \dots, c \quad (4-2)$$

where k is a constant representing the value of the stationary point. By introducing $Y_i = y_i e^{-k}$, the following equation can be obtained [6],

$$\ln \phi_i(\mathbf{Y}) + \ln Y_i - \ln \phi_i(\mathbf{z}) - \ln z_i = 0, \quad i = 1, \dots, c \quad (4-3)$$

The composition of the trial phase can be determined by $y_i = Y_i / \sum_{i=1}^c Y_i$. Based on the new variables Y_i , Michelsen [6] formulated an alternative version of the TPD function which was

unconstraint on Y_i (except $Y_i > 0$). The revised function is shown as follows [6],

$$g^*(\mathbf{y}) = 1 + \sum_{i=1}^c Y_i \left[\ln \phi_i(\mathbf{Y}) + \ln Y_i - \ln \phi_i(\mathbf{z}) - \ln z_i - 1 \right] \quad (4-4)$$

4.2.2 Flash Calculation

The convergence of flash calculations is subject to the material balance constraint and the constraint that the fugacities of each component in all phases present are equivalent [7]. In general, there are two iteration loops in the flash calculation algorithm. The outer loop is used to update equilibrium ratios in order to satisfy the equal-fugacity constraint, while the inner loop is used to calculate phase mole fractions by satisfying the material balance constraint (with equilibrium ratios provided by the outer loop). The successive substitution iteration (SSI) is applied in the outer loop, while either the bisection or the Newton method can be adopted in the inner loop [17, 18]. Rachford and Rice [19] developed the Rachford-Rice (RR) equation to solve phase mole fractions based on the material balance. The RR equation used for the two-phase flash calculation is provided as follows [19],

$$RR_y = \sum_{i=1}^c (y_i - x_i) = \sum_{i=1}^c \frac{z_i (K_{iy} - 1)}{1 + \beta_y (K_{iy} - 1)} = 0 \quad (4-5)$$

where x_i , y_i , and z_i represent the mole fraction of component i in the phase x , phase y , and feed, respectively; β_y represents the phase mole fraction of the phase y ; and K_{iy} represents the equilibrium ratio of component i in the phase y with respect to the phase x . K_{iy} can be described by the following equation,

$$K_{iy} = \frac{y_i}{x_i} = \frac{\phi_{ix}}{\phi_{iy}}, \quad i = 1, \dots, c \quad (4-6)$$

where ϕ_{ix} and ϕ_{iy} represent the fugacity coefficient of component i in the phase x and phase y , respectively. Phase compositions can be calculated by the following equations based on the material balance,

$$x_i = \frac{z_i}{1 + \beta_y (K_{iy} - 1)}; y_i = z_i K_{iy} \quad (4-7)$$

The RR equation can be also solved by minimizing a convex function [20-22]. For our three-phase VLA flash calculations, a modified RR equation proposed by Okuno *et al.* [22] is applied to solve phase mole fractions. The expression of the objective function and constraints is shown below [22],

$$\begin{cases} \min : f(\boldsymbol{\beta}) = -\sum_{i=1}^c z_i \ln |1 - (1 - K_{iy})\beta_y - (1 - K_{iw})\beta_w| \\ \text{Subject to : } \mathbf{a}_i^T \boldsymbol{\beta} \leq b_i, \quad i = 1, \dots, c \end{cases} \quad (4-8)$$

where $\mathbf{a}_i = [1 - K_{iy}; 1 - K_{iw}]$; $\boldsymbol{\beta} = [\beta_y; \beta_w]$; $b_i = \min \{1 - z_i, 1 - K_{iy}z_i, 1 - K_{iw}z_i\}$; w_i represents the mole fraction of component i in the phase w ; β_w represents the phase mole fraction of the phase w ; and K_{iw} represents the equilibrium ratio of component i in the phase w with respect to the phase x . K_{iw} is defined as follows,

$$K_{iw} = \frac{w_i}{x_i} = \frac{\phi_{ix}}{\phi_{iw}}, \quad i = 1, \dots, c \quad (4-9)$$

where ϕ_{iw} represents the fugacity coefficient of component i in the phase w . Phase compositions can be calculated as follows,

$$x_i = \frac{z_i}{1 + \beta_y (K_{iy} - 1) + \beta_w (K_{iw} - 1)}; y_i = z_i K_{iy}; w_i = z_i K_{iw} \quad (4-10)$$

4.2.3 Conventional Three-Phase Equilibrium Calculation Algorithm

The conventional three-phase equilibrium calculation algorithm refers to the most widely used stage-wise algorithm as described in [6-8]. The single-phase stability test is firstly performed in this conventional algorithm. If any of the stationary points gives a negative TPD, the two-phase flash calculation will be conducted. As suggested by Gorucu and Johns [11], two-phase flash calculations should be performed several times with multiple initial estimates of equilibrium ratios, even if the results yielded by the first two-phase flash calculation seem physical. The two-phase equilibrium with the minimum Gibbs free energy will be chosen for the subsequent calculations. Then, the two-phase stability test should be conducted. If the two-phase stability test shows the two-phase equilibrium is unstable, three-phase flash calculation should be performed. The equilibrium ratios at the negative stationary point(s) yielded from the stability test are used to initialize the subsequent flash [7]. In order to yield the correct phase equilibrium, it is essential to choose proper initial estimates of equilibrium ratios in both stability tests and flash calculations for different kind of mixtures, e.g. water/hydrocarbon mixtures.

4.3 Improved Three-Phase VLA equilibrium Calculation Algorithm with a New Initialization Scheme

In this section, a new initialization scheme and an improved three-phase VLA equilibrium calculation algorithm will be introduced. This new initialization scheme contains initialization methods for the single-phase stability test, two-phase flash calculation, and two-phase stability test, respectively. Possible phases considered in this algorithm are a vapor phase, a hydrocarbon-rich liquid phase, and an aqueous phase. In stability tests, the quasi-Newton

successive-substitution method [23] is implemented to detect the local stationary points of the TPD function. To increase the possibility of detecting the global minimum value of the TPD function, multiple initial estimates are required. We modify the equilibrium-ratios initialization methods proposed by Li and Firoozabadi [8] as follows,

$$K_i^{1-ST} = \left\{ K_i^{Wilson}, 1/K_i^{Wilson}, \sqrt[3]{K_i^{Wilson}}, 1/\sqrt[3]{K_i^{Wilson}}, K_i^{H_2O} \right\} \quad (4-11)$$

where K_i^{1-ST} is the initial equilibrium ratio of component i used for the single-phase stability

$$\text{test, } K_i^{H_2O} = \begin{cases} [1-10^{-15}]/z_i, & i = \text{H}_2\text{O} \\ [10^{-15}/(c-1)]/z_i, & i \neq \text{H}_2\text{O} \end{cases}, \text{ and } K_i^{Wilson} \text{ represents the equilibrium ratio of}$$

component i calculated by Wilson equation [24],

$$K_i^{Wilson} = \frac{P_{ci}}{P} \exp \left[5.37(1 + \omega_i) \left(1 - \frac{T_{ci}}{T} \right) \right] \quad (4-12)$$

where P and P_{ci} represent pressure and critical pressure of component i , respectively, bar; T and T_{ci} represent temperature and critical temperature of component i , respectively, K; and ω_i represents acentric factor of component i . This method is similar to the method proposed by Li and Firoozabadi [8], but the difference lies in the value of $K_i^{H_2O}$ that is used to detect the aqueous-like stationary point. The new initialization method as expressed by Equation (4-11) performs well in most cases. However, it fails when the pure water phase gives the local minimum value, which will be graphically illustrated in Section 4.4. Therefore, when an aqueous-like stationary point cannot be found by using the aforementioned initial estimates, the value of the TPD function at $K_i^{H_2O}$ can be regarded as the value of the aqueous-like stationary point; this step is an essential part of this new initialization method that helps to detect the

aqueous-like stationary point. For mixtures containing less or no acid gases, we can directly check the value of the TPD function at $K_i^{H_2O}$ instead of using $K_i^{H_2O}$ as an initial estimate to find the stationary point; this helps further simplify the stability tests. In addition, to avoid trivial computation, Nichita *et al.* [25] proposed that the solution can be considered trivial when the number of iterations is larger than 1000. Therefore, in our stability test algorithm, we will switch to the next initial estimate when the local minimum is found or the number of iterations is larger than 1000.

The two-phase stability test will be divided into two categories: (1) two-phase vapor/liquid stability test, which is used to test the existence of the vapor/liquid phase; and (2) two-phase aqueous stability test, which is used to test the existence of the aqueous phase. $\left\{ K_i^{Wilson}, 1/K_i^{Wilson}, \sqrt[3]{K_i^{Wilson}}, 1/\sqrt[3]{K_i^{Wilson}} \right\}$ [8] are applied to initialize the two-phase vapor/liquid stability test, while $K_i^{H_2O}$ is applied to initialize the two-phase aqueous stability test. Moreover, if an aqueous-like stationary point cannot be found by using $K_i^{H_2O}$ in the two-phase aqueous stability test, the value of the TPD function at $K_i^{H_2O}$ can be considered as the value of the aqueous-like stationary point and hence can be used to determine the stability of the tested phase. Same as mentioned above, for mixtures containing less or no acid gases, the value of the TPD function at $K_i^{H_2O}$ can be directly considered as the value of the aqueous-like stationary point.

In flash calculations, SSI is used in the outer loop. In the inner loop, the Newton method is

applied for the function-solving problem in two-phase flash calculations, while the interior-point method is applied for the minimization problem with constraints in three-phase flash calculations. Negative flash is allowed in flash calculations in order to ensure the robustness of this algorithm [20, 26]. The phase mole fractions are initialized by using the equally weighted mean of the vertices yielded by the constraints, as suggested by Okuno *et al.* [22]. In general, equilibrium ratios at stationary points yielded by the single-phase stability test will be used to initialize two-phase flash calculations. In our algorithm, when multiple stationary points are yielded by the single-phase stability test, we propose an approach to select which stationary point should be used to initialize the subsequent two-phase flash calculation. The selection approach is shown in the detailed procedures of our algorithm below. Only one stationary point is selected in our algorithm, avoiding running an unnecessarily high number of two-phase flash calculations in one run of the three-phase equilibrium calculation. For three-phase flash calculations, the initial values of equilibrium ratios are calculated based on the compositions of the two phases yielded by the two-phase flash calculation and the composition of the trial phase at the stationary point yielded by the two-phase stability test. When more than one real root are yielded by the cubic EOS, Evelein *et al.* [27] suggested that the compressibility factor, which gives the lowest Gibbs free energy, should be selected.

Figure 4-1 depicts the flow chart of the improved three-phase equilibrium calculation algorithm. The detailed procedures are listed below,

- (1) Conduct the single-phase stability test to detect the negative stationary points. Record the compositions of the trial phase at stationary points and the TPD values of stationary points. If any of the values of stationary points is negative, continue to Step (2). Otherwise, output the single-phase equilibrium.
- (2) Remove the stationary point with a composition where the mole fraction of the heaviest or the second heaviest hydrocarbon is larger than 0.5. Based on our extensive tests, the stationary point, which has a large fraction of the heaviest or the second heaviest hydrocarbon, is not a good initial estimate for the subsequent two-phase flash calculation in three-phase VLA equilibrium calculations. For the remaining stationary points, equilibrium ratios at the stationary point with the smallest TPD value are selected as the initial estimates for the two-phase flash calculation.
- (3) Conduct two-phase flash calculation.
- (4) If an aqueous phase is yielded from the two-phase flash calculation, conduct the two-phase vapor/liquid stability test and continue to Step (5). Otherwise, check if the single-phase stability test has a negative aqueous-like stationary point. If a negative aqueous-like stationary point appears, conduct the two-phase aqueous stability test and continue to Step (5). Otherwise, output the two-phase equilibrium calculation results.
- (5) If the two-phase stability test (as mentioned above) shows the two-phase equilibrium is unstable, conduct the three-phase VLA flash calculation and output the three-phase

equilibrium calculation results. Otherwise, output the two-phase equilibrium calculation results.

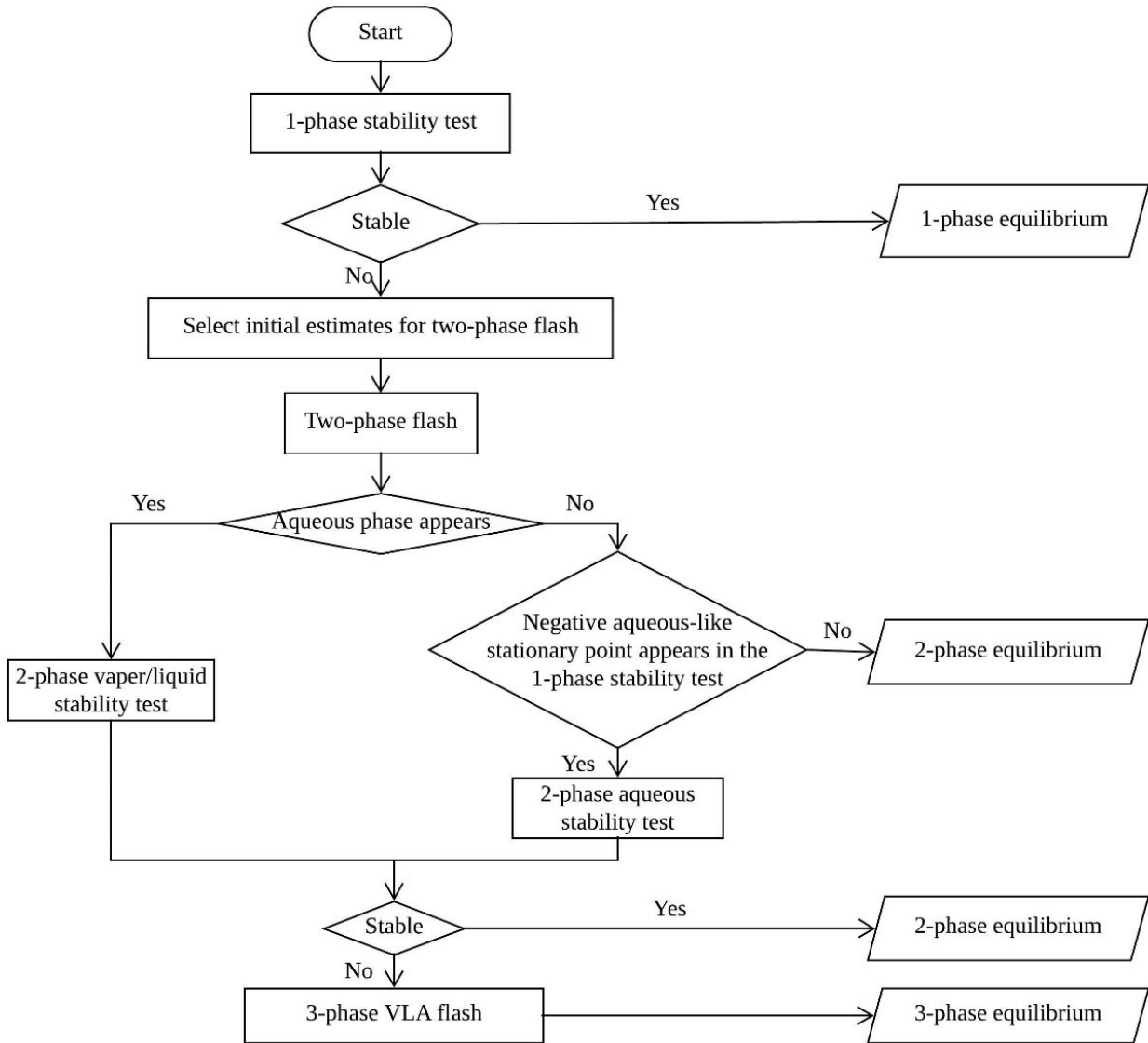


Figure 4-1 Flow chart of the improved three-phase VLA equilibrium calculation algorithm developed in this work

Table 4-1 compares the number of initial estimates of equilibrium ratios used in the newly developed algorithm and the conventional three-phase equilibrium calculation algorithm. To

apply the conventional three-phase equilibrium calculation algorithm to the water/hydrocarbon mixtures, K_i^{1-ST} are applied to initialize the single-phase and two-phase stability tests. Moreover, the multiple initial estimates used in the two-phase flash calculation are the equilibrium ratios at all the negative stationary points calculated by the single-phase stability test. As shown in this table, the numbers of initial estimates of equilibrium ratios used in the two-phase flash calculation and the two-phase stability test are reduced in our algorithm than in the conventional algorithm.

Table 4-1 Comparison between the number of initial estimates of equilibrium ratios used in the newly developed algorithm and the conventional three-phase equilibrium calculation algorithm

	Number of initial estimates of equilibrium ratios	
	Our algorithm	Conventional algorithm
Single-phase stability test	5	5
Two-phase flash calculation	1	Depends on how many negative stationary points are found in the single-phase stability test (≥ 1)
Two-phase stability test	4 (for the two-phase vapor/liquid stability test) or 1 (for the two-phase aqueous stability test)	5
Three-phase flash calculation	1	1

4.4 Example Calculations

We implement the improved three-phase VLA equilibrium calculation algorithm for multiple water/hydrocarbon mixtures to test its robustness. The equilibrium calculation algorithm is run hundreds of thousands of times for a given mixture at different temperature/pressure conditions.

But it is noted that although our algorithm has been validated by hundreds of thousands of example calculations, we cannot guarantee it can always converge to the correct equilibrium for all water/hydrocarbon mixtures at different temperature/pressure conditions. Appendix 4-A provides the critical properties, feed compositions, and BIPs needed in these calculations. PR EOS [15] combined with the van der Waals mixing rule is used to calculate all the thermodynamic properties. In addition, to accurately describe the gas solubility in the aqueous phase, the α -function and BIPs modified by Søreide and Whitson [16] are used for the calculations made to the aqueous phase. In the following figures, V represents the vapor phase, L represents the hydrocarbon-rich liquid phase, and A represents the aqueous phase.

4.4.1 Case 1 (Water/C3/C16 Mixture)

Figure 4-2 graphically shows the number of equilibrium phases in a pressure-temperature (PT) diagram for the water/C3/C16 mixture. The tested pressures are from 1 bar to 140 bar with a step size of 1 bar, while the tested temperatures are from 300 K to 650 K with a step size of 1 K. The total number of running the three-phase VLA equilibrium calculation algorithm is 49,140. As shown in this figure, this algorithm performs well in correctly identifying the phase equilibria.

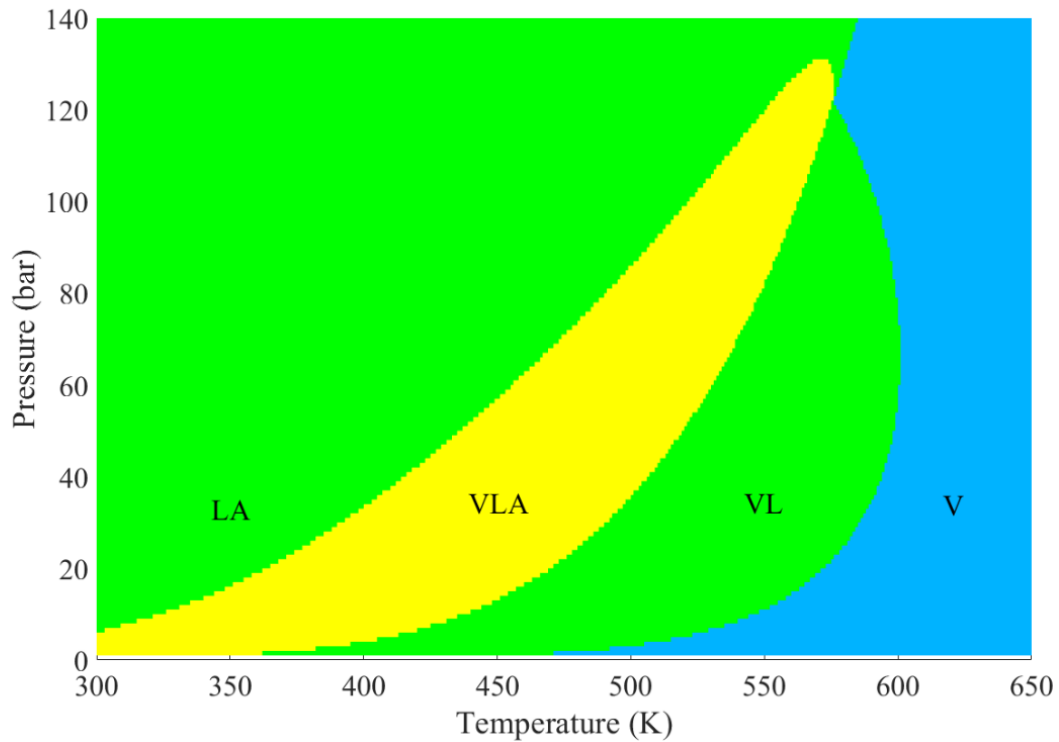


Figure 4-2 Number of equilibrium phases in a PT phase diagram for the water/C3/C16 mixture

The critical point of the water/C3/C16 mixture is at 130.37 bar and 569.89 K. Figure 4-3 graphically shows the number of equilibrium phases in a PT phase diagram for the water/C3/C16 mixture at the near critical region. The tested pressures are from 125 bar to 135 bar with a step size of 0.1 bar, while the tested temperatures are from 565 K to 575 K with a step size of 0.1 K. The total number of running the three-phase VLA equilibrium calculation algorithm is 10,201. As shown in this figure, this algorithm performs well in the near critical region.

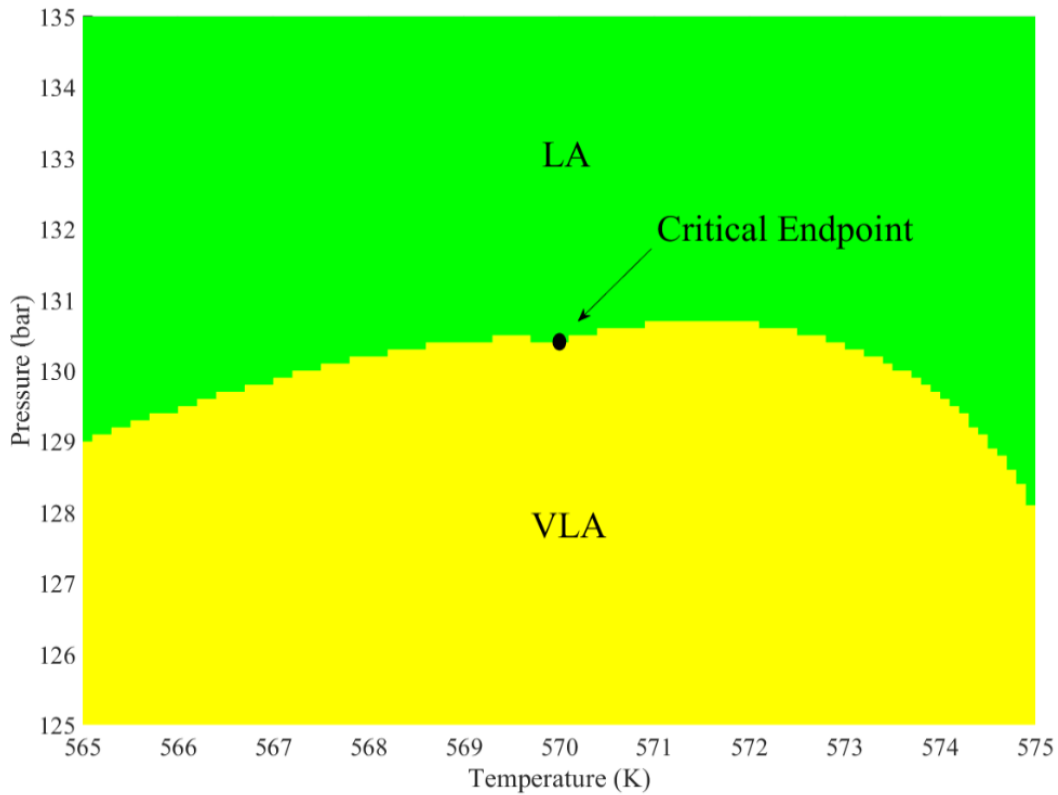


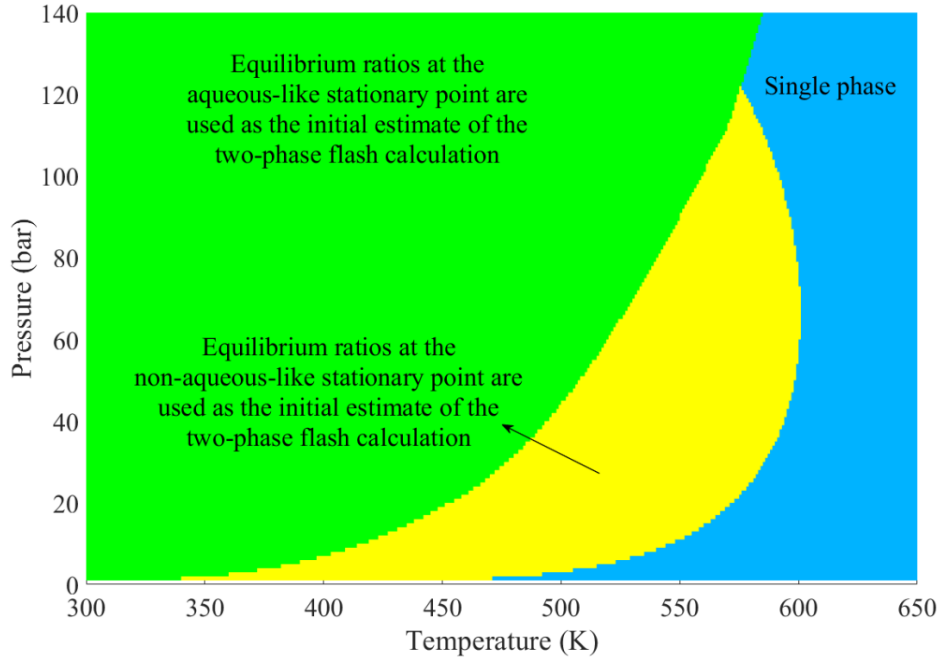
Figure 4-3 Number of equilibrium phases in a PT phase diagram for the water/C3/C16 mixture at the near critical region

As mentioned in Section 4.2.3, Gorucu and Johns [11] recommend using multiple initial estimates of equilibrium ratios in the two-phase flash calculation. Then, the two-phase equilibrium with the minimum Gibbs free energy will be chosen for the subsequent calculations in order to increase the chance of finding the true two-phase equilibrium or provide a better input for a subsequent three-phase flash. Here, we call the initial estimate, with which the two-phase flash calculation can yield a two-phase equilibrium with the minimum Gibbs free energy, as the “correct” initial estimate. It is obvious that the computational time will be reduced if one can know the “correct” initial estimate before conducting the two-phase flash calculation. In our

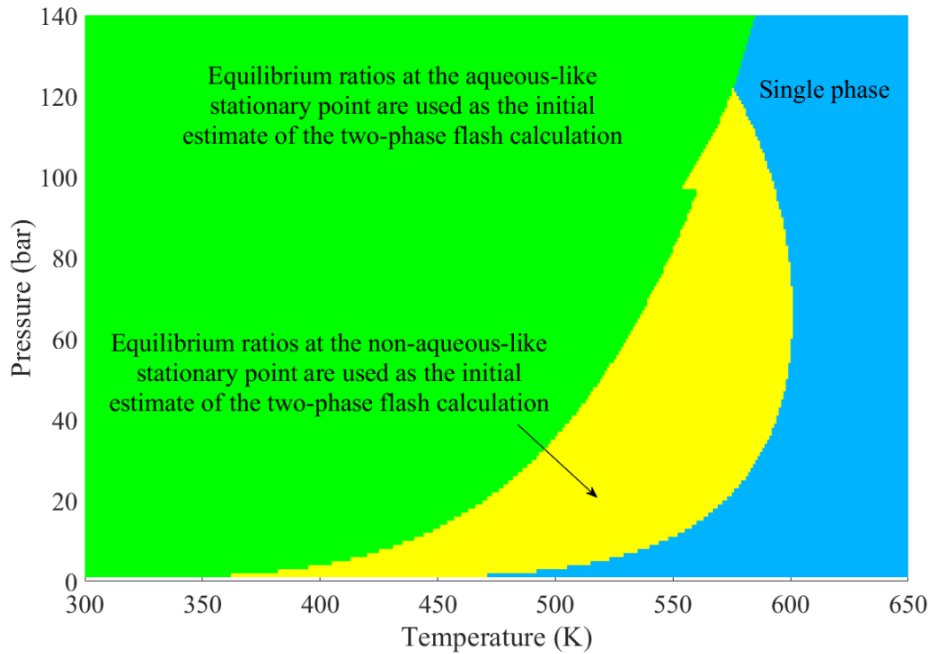
initialization scheme, this initial estimate can be almost detected prior to the two-phase flash based on the analytical method as shown in Section 4.3. Figure 4-4 shows the distribution of the initial estimates of equilibrium ratios used in two-phase flash calculations for the water/C3/C16 mixture. The initial estimates of equilibrium ratios can be classified into two categories: equilibrium ratios at the aqueous-like stationary point calculated by the single-phase stability test and equilibrium ratios at the non-aqueous-like stationary point calculated by the single-phase stability test. Figure 4-4a depicts the “correct” initial estimate of equilibrium ratios selected by applying the approach proposed by Gorucu and Johns [11]. The approach proposed by Gorucu and Johns [11] is used in the conventional three-phase equilibrium calculation algorithm. To apply this conventional algorithm to water/hydrocarbon mixtures, K_i^{1-ST} are applied to initialize both single-phase and two-phase stability tests. Moreover, the equilibrium ratios at all the negative stationary points calculated by the single-phase stability test are used to initialize the two-phase flash calculation. Figure 4-4b shows the initial estimate of equilibrium ratios selected by applying the approach developed in this algorithm; in this approach, only one set of the initial equilibrium-ratio estimates is needed. Figure 4-4c compares the boundary lines of different kinds of initial equilibrium-ratio estimates selected by the approach proposed by Gorucu and Johns [11] and those selected by our approach. As shown in Figure 4-4c, a similar distribution can be seen between the results shown in Figures 4a and 4b, indicating that a good initial estimate can be provided for the two-phase flash calculation by our method. Moreover, since only one set of equilibrium ratios is used to initialize the two-phase flash calculation in our algorithm, our

algorithm is more efficient compared with the algorithm proposed by Gorucu and Johns [11]

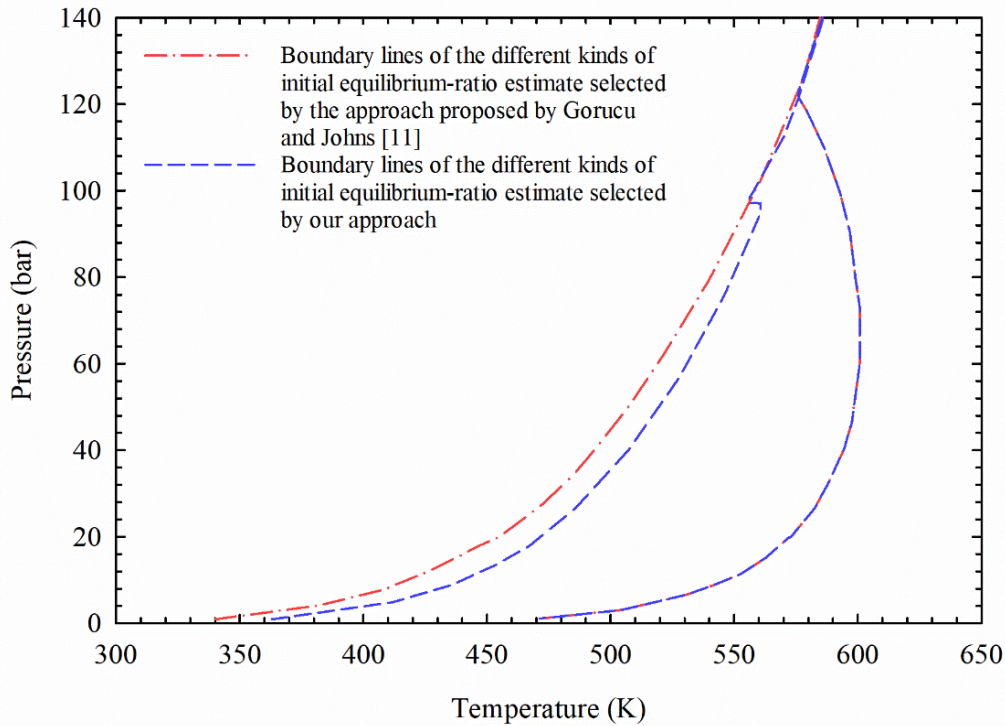
where multiple initial estimates are used.



(a)



(b)

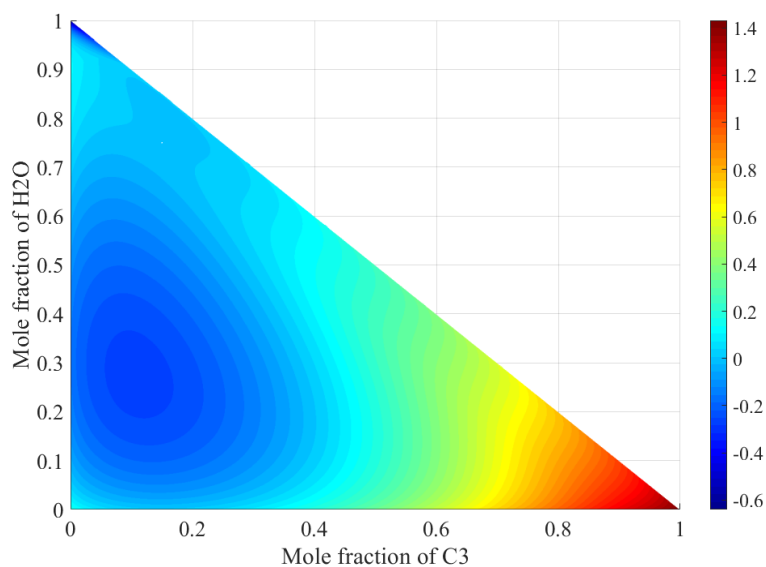


(c)

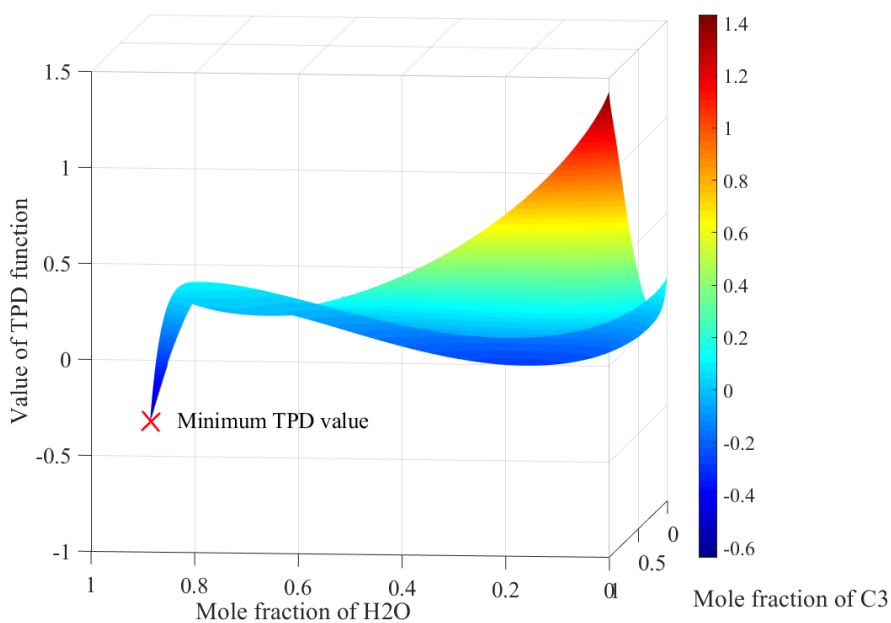
Figure 4-4 Distribution of the initial estimates of the equilibrium ratios used in two-phase flash calculations for the water/C3/C16 mixture by applying: (a) approach proposed by Gorucu and Johns [11]; (b) approach developed in this paper; and (c) comparison between the boundary lines of different kinds of initial equilibrium-ratio estimates selected by the approach proposed by Gorucu and Johns [11] and those selected by our approach.

Figure 4-5 illustrates the value of the TPD function for the water/C3/C16 mixture at 500 K and 80 bar. At 500 K and 80 bar, the mixture will split into three phases. As shown in Figure 4-5, there are three local minimum points. Two of them are stationary points, while the other one cannot be identified as a stationary point as the derivatives of TPD at this point are not zero. This minimum point is the global minimum point in this example calculation and appears when the trial phase is a pure water phase. It implies that when an aqueous-like stationary point cannot be found by using $K_i^{H_2O}$ as an initial estimate, it is necessary to check the value of the TPD function at

$K_i^{H_2O}$. Moreover, the convex region near the aqueous-like stationary point is very small, requiring that a large enough mole fraction of water in the trial phase should be set in $K_i^{H_2O}$.



(a)



(b)

Figure 4-5 Value of the TPD function for the water/C3/C16 mixture at 500 K and 80 bar: (a) top view; and (b) 3D diagram.

4.4.2 Case 2 (Water/C4/C20 Mixture)

Figure 4-6 graphically shows the number of equilibrium phases in a PT phase diagram for the water/C4/C20 mixture. The tested pressures are from 1 bar to 220 bar with a step size of 1 bar, while the tested temperatures are from 300 K to 650 K with a step size of 1 K. The three-phase VLA equilibrium calculation algorithm is conducted for 77,220 times. This algorithm performs well at most of temperature/pressure conditions. However, it fails in the red region shown in the Figure 4-6, due to the non-convergence of two-phase or three-phase flash calculations. This is because that the equality between the component fugacities of the aqueous phase and the non-aqueous phases cannot be established, which happens owing to the inconsistent BIPs used in the aqueous phase and non-aqueous phases. Future work is needed to address this issue. For this case, which contains three components with a large discrepancy of their properties,

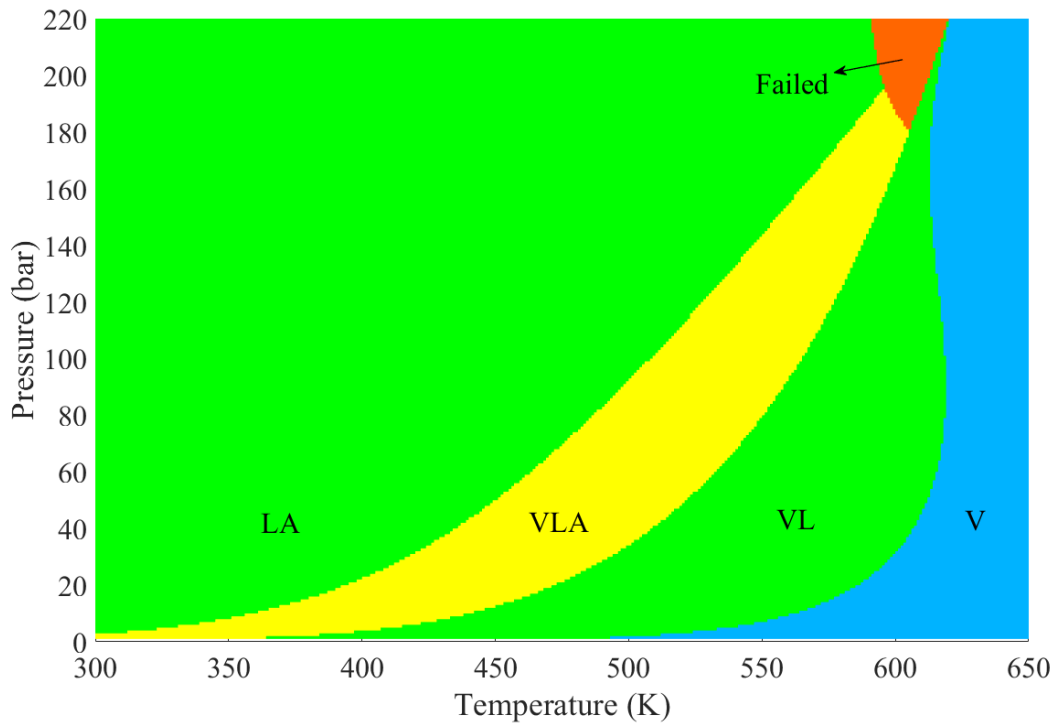
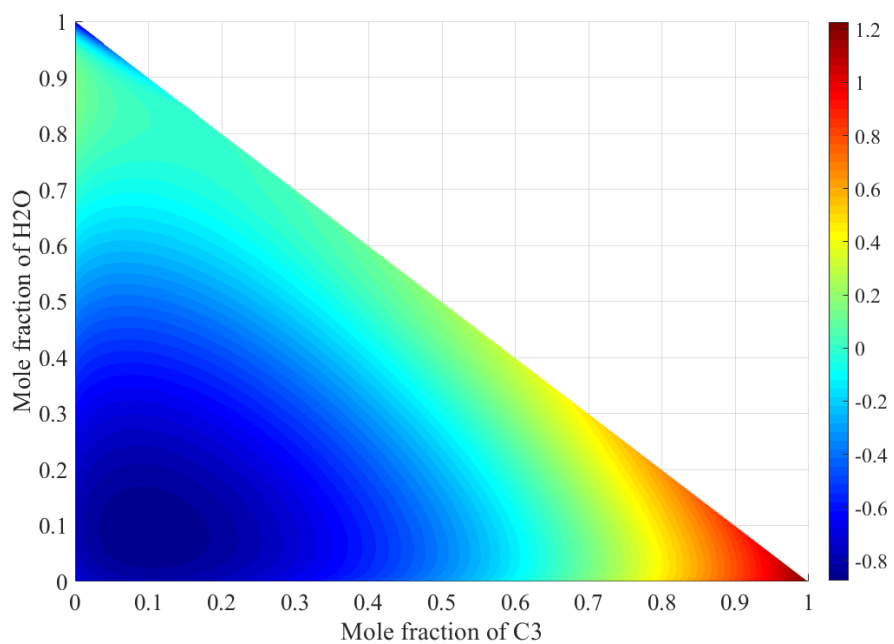
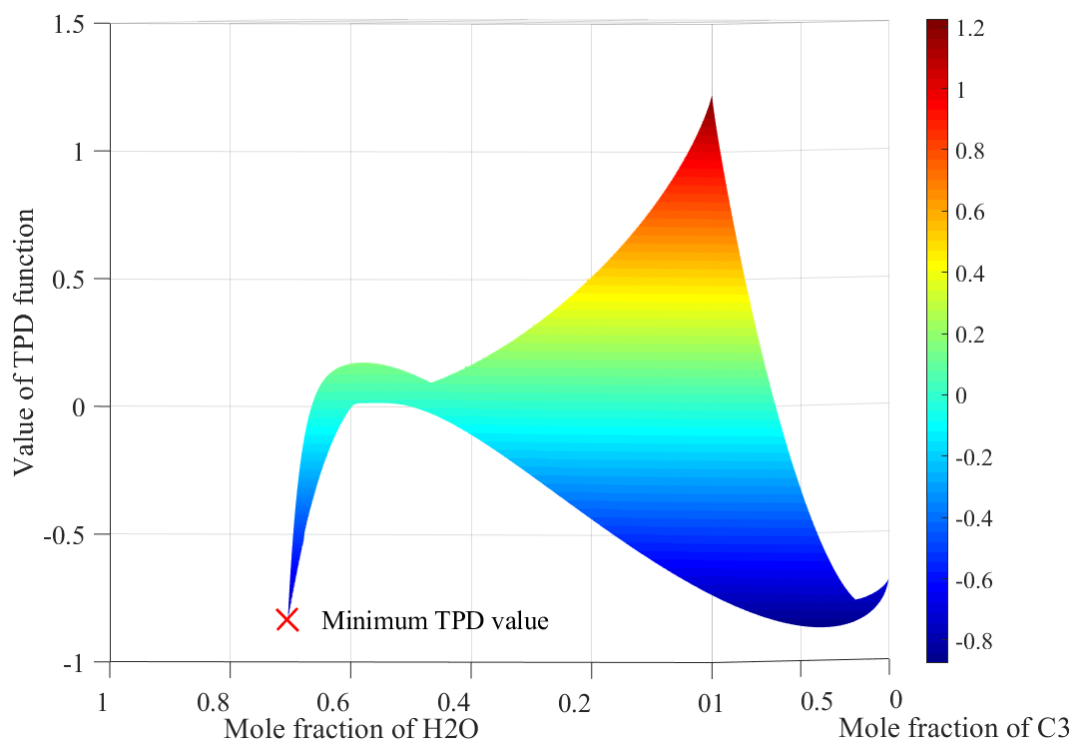


Figure 4-6 Number of equilibrium phases in a PT phase diagram for the water/C4/C20 mixture

Figure 4-7 shows a top view and a 3D view of the values of the TPD function for the water/C4/C20 mixture at 490 K and 100 bar. This mixture will split into a liquid phase and an aqueous phase at 490 K and 100 bar. Two local minima appear in Figure 4-7. One of the minimum points appears when the trial phase is a pure water phase. Therefore, this minimum point is not a stationary point. To obtain the value of the aqueous-like minimum point, we need to calculate the value of the TPD function at $K_i^{H_2O}$.



(a)



(b)

Figure 4-7 Value of the TPD function for the water/C4/C20 mixture at 490 K and 100 bar: (a) a top view; and (b) a 3D view.

4.4.3 Case 3 (Water/Pseudo-Components Mixture)

Figure 4-8 graphically describes the number of equilibrium phases in a PT phase diagram for the water/pseudo-components mixture. The pressures are set from 1 bar to 120 bar with a step size of 1 bar, while the temperature is set from 300 K to 800 K with a step size of 1 K. In total, we have run 60,120 equilibrium calculations to generate Figure 4-8. Again, this figure shows that this algorithm is very robust on identifying the correct phase equilibrium behavior.

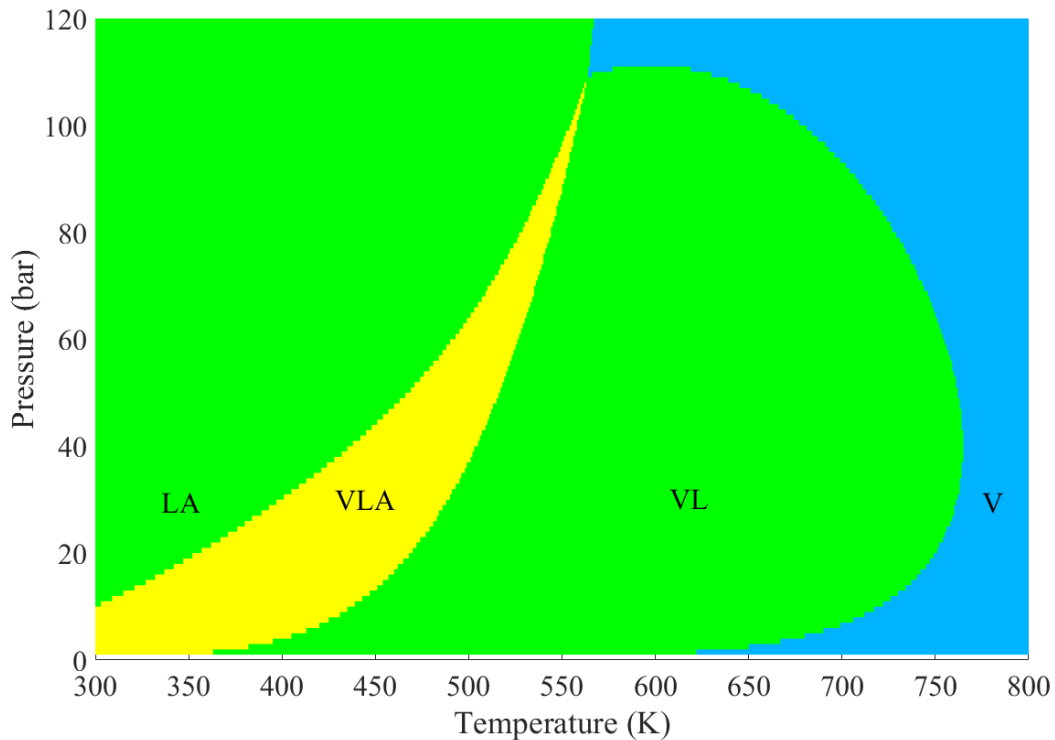


Figure 4-8 Number of equilibrium phases in a PT phase diagram for the water/pseudo-components mixture

Figure 4-9 depicts the comparison between the phase boundaries calculated by this study and those calculated by Zhu and Okuno [28] for the water/pseudo-components mixture. The phase

boundaries calculated in this paper is based on Figure 4-8. Therefore, the accuracy of the phase boundaries is within ± 1 bar and ± 1 K. As shown in this figure, similar phase boundaries can be yielded by our algorithm and by Zhu and Okuno [28]. The slight discrepancies between phase boundaries calculated by this study and those calculated by Zhu and Okuno [28] are caused by the different BIPs used in the aqueous phase.

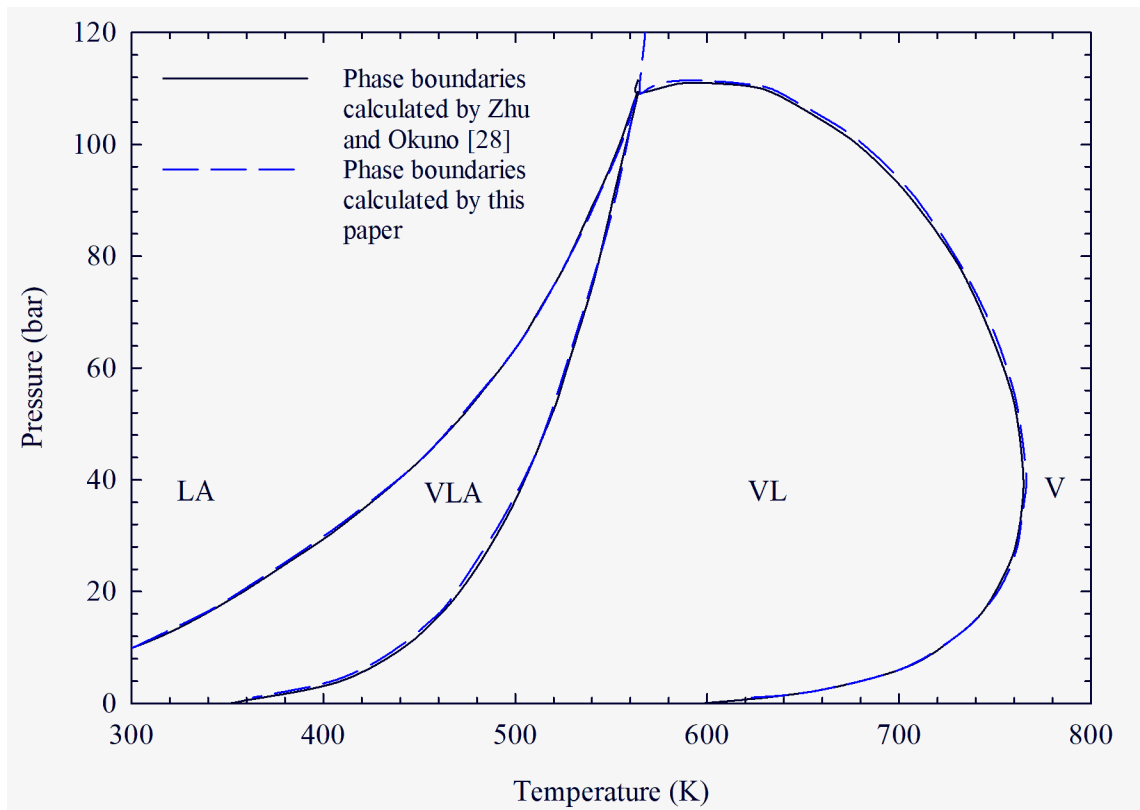
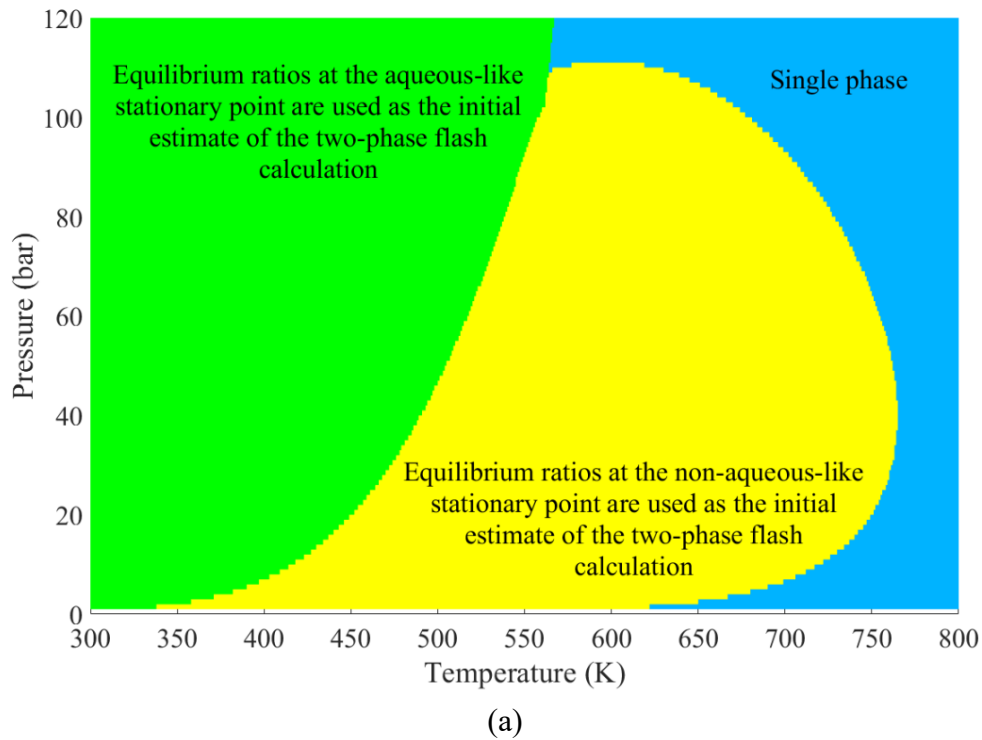
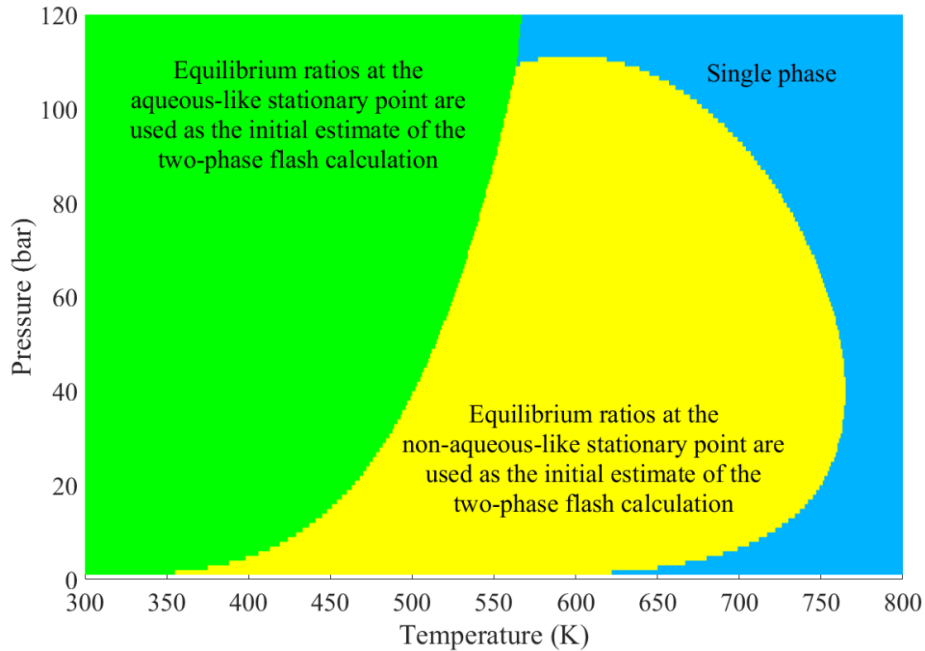


Figure 4-9 Comparison between the phase boundaries calculated by this study and those calculated by Zhu and Okuno [28] for the water/pseudo-components mixture

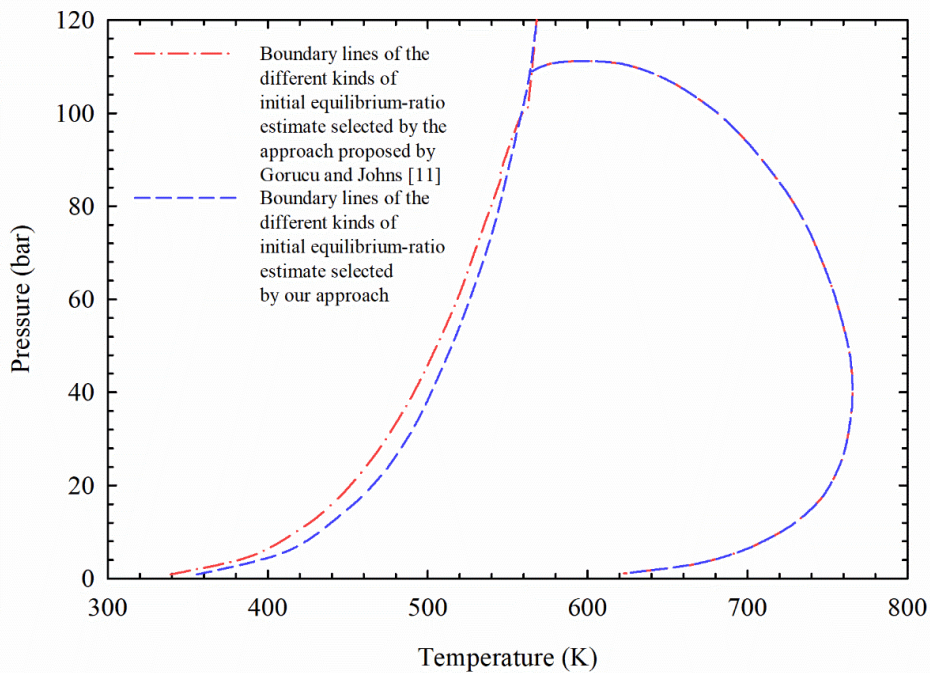
Figure 4-10 demonstrates the distribution of the initial estimates of equilibrium ratios used in two-phase flash calculations for the water/pseudo-components mixture. Figures 4-10a shows the initial estimate of equilibrium ratios selected by applying the approach proposed by Gorucu and

Johns [11], while Figure 4-10b shows the initial estimates of equilibrium ratios selected by applying the approach developed in this paper, respectively. The colors used in these figures have the same meaning as those in Figure 4-4. Figure 10c compares the boundary lines of different kinds of initial equilibrium-ratio estimate selected by the approach proposed by Gorucu and Johns [11] and those selected by our approach. Again, a similar distribution can be seen in Figure 4-10c, concluding that our approach can provide good initial estimates for two-phase flash calculations.





(b)



(c)

Figure 4-10 Distribution of the initial estimates of equilibrium ratios used in two-phase flash calculations for the water/pseudo-components mixture by applying: (a) approach proposed by Gorucu and Johns [11]; (b) approach developed in this paper; and (c) comparison between the boundary lines of different kinds of initial equilibrium-ratio estimates selected by the approach proposed by Gorucu and Johns [11] and those selected by our approach.

4.4.4 Case 4 (Water/C1/C7/C_D Mixture)

Figure 4-11 graphically describes the number of equilibrium phases in a PT phase diagram for the water/C1/C7/C_D mixture. C_D represents the Athabasca (GCOS) dead bitumen [29]. The tested pressures are varied from 1 bar to 240 bar with a step size of 1 bar, while the tested temperatures are varied from 300 K to 900 K with a step size of 1 K. The newly developed algorithm is run 144,240 times. As shown in Figure 4-11, our algorithm can converge to the correct phase equilibria in most cases. However, the algorithm fails in part of the two-phase LA equilibrium region as well as in part of the three-phase VLA equilibrium region. This is again caused by the inconsistency of the BIPs used in the aqueous phase and the non-aqueous phases.

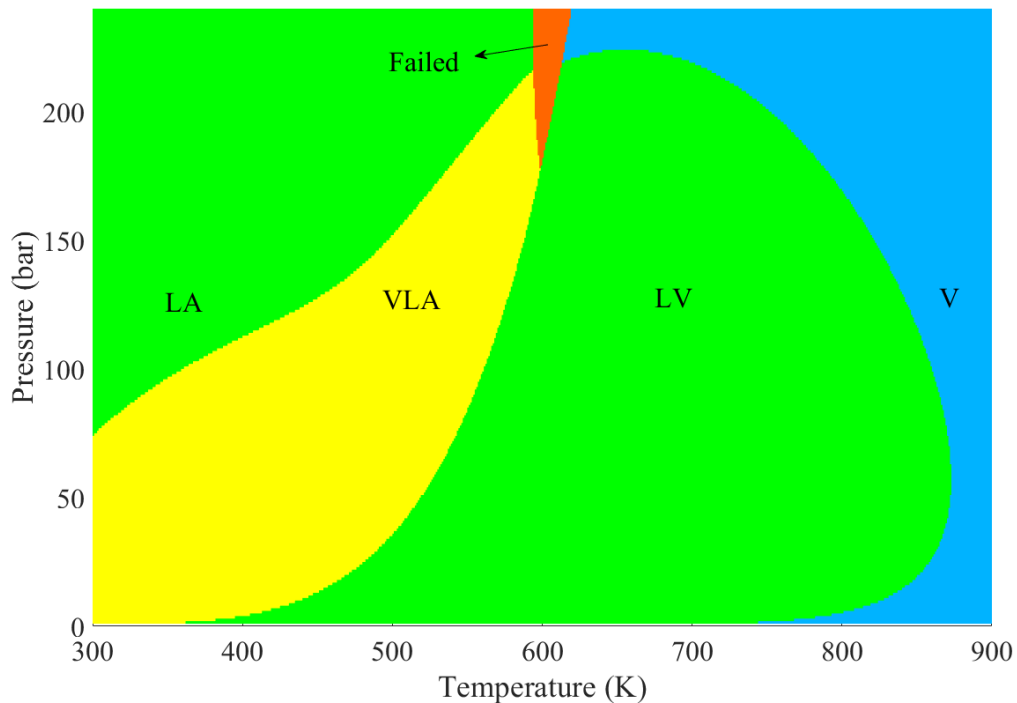


Figure 4-11 Number of equilibrium phases in a PT phase diagram for the water/C1/C7/C_D mixture

4.5 Conclusions

An improved three-phase VLA equilibrium calculation algorithm is proposed in this paper. A new scheme for initializing the equilibrium ratios is applied in this algorithm. The aqueous-like stationary point on the TPD function can be securely detected by using this new initialization scheme. Convergence problems are avoided in flash calculations with the application of our algorithm. Moreover, one can obtain a correct phase equilibrium in a more efficient way by using our algorithm with the new initialization scheme compared to the method documented in the literature [11]. The performance of the newly developed algorithm is validated by hundreds of thousands of example calculations. This algorithm performs well in most cases. However, it fails in part of the two-phase LA equilibrium region and in part of the three-phase VLA equilibrium region at high temperature/pressure conditions. The reason is that no equivalent fugacities between the aqueous phase and the non-aqueous phases can be found due to the inconsistency of the BIPs calculated by the Søreide and Wilson correlation [16] for the aqueous phase and the non-aqueous phases.

Nomenclature

c	number of components in the mixture
K_{iw}	equilibrium ratio of component i in the phase y with respect to the phase w
K_{iy}	equilibrium ratio of component i in the phase y with respect to the phase x
K_i^{1-ST}	initial equilibrium ratio of component i used in the single-phase stability test

P	pressure, bar
P_{ci}	critical pressure of component i , bar
T	temperature, K
T_{ci}	critical temperature of component i , K
w_i	mole fraction of component i in the phase w
x_i	mole fraction of component i in the phase x
y	compositions of the trial phase
y_i	mole fraction of component i in the trial phase or in the phase y
z	compositions of the test phase
z_i	mole fraction of component i in the test phase or in the feed

Greek Letters

β_w	phase mole fraction of the phase w
β_y	phase mole fraction of the phase y
ω_i	acentric factor of component i
ϕ_{iw}	fugacity coefficient of component i in the phase w
ϕ_{ix}	fugacity coefficient of component i in the phase x
ϕ_{iy}	fugacity coefficient of component i in the phase y
$\phi_i(y)$	fugacity coefficients of component i in the trial phase
$\phi_i(z)$	fugacity coefficients of component i in the test phase

Subscripts

c	critical index
i	component index
w	phase w
x	phase x
Y	phase y

4.6 References

- (1) A. Lapene, D.V. Nichita, G. Debenest, M. Quintard, Three-phase free-water flash calculations using a new Modified Rachford-Rice equation, *Fluid Phase Equilibr.* 297 (1) (2010) 121-128.
- (2) E. Mortezaadeh, M.R. Rasaei, A robust procedure for three-phase equilibrium calculations of water-hydrocarbon systems using cubic equations of state, *Fluid Phase Equilibr.* 450 (2017) 150-174.
- (3) Y. Tang, S. Saha, An efficient method to calculate three-phase free-water flash for water-hydrocarbon systems, *Ind. Eng. Chem. Res.*, 42 (2003) 189-197.
- (4) A. Dhima, J.C. de Hemptinne, G. Moracchini, Solubility of light hydrocarbons and their mixtures in pure water under high pressure, *Fluid Phase Equilibr.* 145 (1) (1998) 129-150.
- (5) A. Dhima, J.C. de Hemptinne, J. Jose, Solubility of hydrocarbons and CO₂ mixtures in water under high pressure, *Ind. Eng. Chem. Res.* 38 (8) (1999) 3144-3161.
- (6) M.L. Michelsen, The isothermal flash problem. Part I. Stability, *Fluid Phase Equilibr.* 9 (1) (1982) 1-19.

- (7) M.L. Michelsen, The isothermal flash problem. Part II. Phase-split calculation, *Fluid Phase Equilibr.* 9 (1) (1982) 21-40.
- (8) Z. Li, A. Firoozabadi, General strategy for stability testing and phase-split calculation in two and three phases, *SPE J.* 17 (4) (2012) 1096-1107.
- (9) M. Connolly, An isenthalpic-based compositional framework for nonlinear thermal simulation, PhD thesis, Stanford University, 2018.
- (10) L.E. Baker, A.C. Pierce, K.D. Luks, Gibbs energy analysis of phase equilibria, *SPE J.* 22 (05) (1982) 731-742.
- (11) S.E. Gorucu, R.T. Johns, Robustness of three-phase equilibrium calculations, *J. Petrol. Sci. Eng.* 143 (2016) 72-85.
- (12) Y.K. Li, L.X. Nghiem, Phase equilibria of oil, gas and water/brine mixtures from a cubic equation of state and Henry's law, *Can. J. Chem. Eng.* 64 (3) (1986) 486-496.
- (13) N. Sabet, H.R.E. Gahrooei, A new robust stability algorithm for three phase flash calculations in presence of water, *J. Nat. Gas. Sci. Eng.* 35 (2016) 382-391.
- (14) W. Henry, III. Experiments on the quantity of gases absorbed by water, at different temperatures, and under different pressures, *Phil. Trans. R. Soc. Lond.* 93 (1803) 29-274.
- (15) D.Y. Peng, D.B. Robinson, A new two-constant equation of state, *Ind. Eng. Chem. Fund.* 15 (1) (1976) 59-64.
- (16) I. Søreide, C.H. Whitson, Peng-Robinson predictions for hydrocarbons, CO₂, N₂, and H₂S with pure water and NaCl brine, *Fluid Phase Equilib.* 77 (1992) 217-240.

- (17) M.L. Michelsen, J. Mollerup, Thermodynamic modelling: fundamentals and computational aspects, 2004, Tie-Line Publications, ISBN 87-989961-1-8.
- (18) K.B. Haugen, A. Firoozabadi, L. Sun, Efficient and robust three-phase split computations, *AIChE J.* 57 (9) (2011) 2555-2565.
- (19) H.H. Rachford Jr., J.D. Rice, Procedure for use of electronic digital computers in calculating flash vaporization hydrocarbon equilibrium, *J. Pet. Tech.* 4 (10) (1952) 327-328.
- (20) M.L. Michelsen, Calculation of multiphase equilibrium, *Comput. Chem. Eng.* 18 (1994) 545-550.
- (21) C.F. Leibovici, D.V. Nichita, A new look at multiphase Rachford-Rice equations for negative flashes, *Fluid Phase Equilibr.* 267 (2) (2008) 127-132.
- (22) R. Okuno, R. Johns, K. Sepehrnoori, A new algorithm for Rachford-Rice for multiphase compositional simulation, *SPE J.* 15 (2) (2010) 313-325.
- (23) L.X. Nghiem, Y.K. Li, Computation of multiphase equilibrium phenomena with an equation of state, *Fluid Phase Equilibr.* 17 (1984) 77-95.
- (24) G.M. Wilson, A modified Redlich-Kwong equation of state, application to general physical data calculations, presented at the 65th National AIChE Meeting, Cleveland, Ohio, USA, 4-7 May, 1968.
- (25) D.V. Nichita, D. Broseta, F. Montel, Calculation of convergence pressure/temperature and stability test limit loci of mixtures with cubic equations of state, *Fluid Phase Equilibr.* 261 (1-2) (2007) 176-184.

- (26) C.H. Whitson, M.L. Michelsen, The negative flash, *Fluid Phase Equilibr.* 53 (1989) 51-71.
- (27) K.A. Evelein, R.G. Moore, R.A. Heidemann, Correlation of the phase behavior in the systems hydrogen sulfide-water and carbon dioxide-water, *Ind. Eng. Chem. Proc. Des. Dev.* 15 (3) (1976) 423-428.
- (28) D. Zhu, R. Okuno, Robust isenthalpic flash for multiphase water/hydrocarbon mixtures, *SPE J.* 20 (6) (2015) 1350-1365.
- (29) D. Zhu, R. Okuno, Analysis of narrow-boiling behavior for thermal compositional simulation, presented at the SPE Reservoir Simulation Symposium, Houston, Texas, USA, 23-25 February, 2015.
- (30) R. Li, H.A. Li, 2018. New two-phase and three-phase Rachford-Rice algorithms based on free-water assumption, *Can. J. Chem. Eng.* 96 (1) (2018) 390-403.

Appendix 4-A: Component Properties and BIPs

Tables 4-A.1, 4-A.3, 4-A.5, and 4-A.7 shows the component properties and feed compositions for the water/C3/C16 mixture used in Case 1, the water/C4/C20 mixture used in Case 2, water/pseudo-components mixture used in Case 3, and water/C1/C7/C_D mixture used in Case 4, respectively. Tables 4-A.2, 4-A.4, 4-A.6, and 4-A.8 provide BIPs used in the non-aqueous phases for the water/C3/C16 mixture used in Case 1, the water/C4/C20 mixture used in Case 2, water/pseudo-components mixture used in Case 3, and water/C1/C7/C_D mixture used in Case 4, respectively.

Table 4-A.1 Component properties and feed composition for the water/C3/C16 mixture [28]

Component	z (mol%)	T_c (K)	P_c (bar)	ω
H₂O	0.75	647.3	220.89	0.344
C3	0.15	369.8	42.46	0.152
C16	0.10	717.0	14.19	0.742

Table 4-A.2 BIPs between the components in the water/C3/C16 mixture [28]

Component	H₂O	C3	C16
H₂O	0	0.6841	0.3583
C3	0.6841	0	0
C16	0.3583	0	0

Table 4-A.3 Component properties and feed composition for the water/C4/C20 mixture [30]

Component	z (mol%)	T_c (K)	P_c (bar)	ω
Water	0.80	647.0	220.5	0.3440
C4	0.16	425.2	38.0	0.1928
C20	0.04	782.0	14.6	0.8160

Table 4-A.4 BIPs between the components in the water/C4/C20 mixture [30]

Component	H ₂ O	C4	C20
H ₂ O	0	0.5	0.5
C4	0.5	0	0
C20	0.5	0	0

Table 4-A.5 Component properties and feed composition for the water/pseudo-components mixture [28]

Component	<i>z</i> (mol%)	<i>T_c</i> (K)	<i>P_c</i> (bar)	<i>ω</i>
H ₂ O	0.50	647.300	220.89	0.344
PC1	0.15	305.556	48.82	0.098
PC2	0.10	638.889	19.65	0.535
PC3	0.10	788.889	10.20	0.891
PC4	0.15	838.889	7.72	1.085

Table 4-A.6 BIPs between the components in the water/pseudo-components mixture [28]

Component	H ₂ O	PC1	PC2	PC3	PC4
H ₂ O	0	0.71918	0.45996	0.26773	0.24166
PC1	0.71918	0	0	0	0
PC2	0.45996	0	0	0	0
PC3	0.26773	0	0	0	0
PC4	0.24166	0	0	0	0

Table 4-A.7 Component properties and feed composition for the water/C1/C7/C_D mixture [29]

Component	<i>z</i> (mol%)	<i>T_c</i> (K)	<i>P_c</i> (bar)	<i>ω</i>
H ₂ O	0.75	647.3	220.89	0.344
C1	0.08	190.6	46.00	0.008
C7	0.15	540.2	27.36	0.351
C _D	0.02	1090.9	7.86	1.361

Table 4-A.8 BIPs between the components in the water/C1/C7/C_D mixture [29]

Component	H ₂ O	C1	C7	C _D
H ₂ O	0	0.7560	0.5610	0.1000
C1	0.7560	0	0.0352	0
C7	0.5610	0.0325	0	0
C _D	0.1000	0	0	0

**CHAPTER 5 ROBUST THREE-PHASE VAPOR-LIQUID-ASPHALTENE
EQUILIBRIUM CALCULATION ALGORITHM FOR ISOTHERMAL CO₂
FLOODING APPLICATIONS**

A version of this chapter has been submitted to *Industrial & Engineering
Chemistry Research* for publication.

Abstract

CO₂ flooding is an effective enhanced oil recovery process for light oil reservoirs. Asphaltenes can easily precipitate during CO₂ flooding, leading to the appearance of three-phase vapor-liquid-asphaltene (VLS) equilibria. A prerequisite for accurately simulating the CO₂ flooding process is developing a robust three-phase VLS equilibrium calculation algorithm. In this study, we develop a robust and efficient three-phase VLS equilibrium calculation algorithm with the use of asphaltene-precipitation model proposed by Nghiem *et al.* [1]. To develop this algorithm, a two-phase flash calculation algorithm is first developed to split the mixture into an asphaltene phase and a non-asphaltene phase. Moreover, two different three-phase VLS flash calculation algorithms are developed and incorporated into our three-phase equilibrium calculation algorithm. New initialization approaches for both stability test and flash calculations are proposed. The performance of this three-phase VLS equilibrium calculation algorithm is tested by generating pressure-composition (P-X) diagrams for several reservoir fluids mixed with pure or impure CO₂.

5.1 Introduction

Carbon dioxide (CO₂) flooding is one of the most effective enhanced oil recovery processes for light oil reservoirs [2]. During CO₂ flooding, asphaltenes can easily precipitate due to the change in the composition of reservoir fluids or the change in pressure/temperature conditions [3, 4]. Therefore, three-phase vapor-liquid-asphaltene (VLS) equilibria can frequently appear in light oil reservoirs where CO₂ flooding is implemented. To have a better understanding of the CO₂ flooding process in light oil reservoirs, it is necessary to have a compositional simulator that is capable of handling three-phase VLS equilibria. In compositional simulations, phase equilibrium calculation will be conducted in each grid at each time step, implying that phase equilibrium calculations will be conducted at varying conditions. In a CO₂ flooding where reservoir temperature can be considered as constant, the varying conditions correspond to varying pressures and gas concentrations. Therefore, a prerequisite for building a robust compositional simulator is having an efficient and robust three-phase VLS equilibrium calculation algorithm, which performs well at varying pressures, varying gas concentrations and the given reservoir temperature.

To build such three-phase VLS equilibrium calculation algorithm, we first need to select a thermodynamic model that can describe the asphaltene-precipitation phenomenon. Over the last 30 years, there are many asphaltene-precipitation models proposed in the literature based on either colloidal theory or solubility theory [5]. In the colloidal theory, asphaltenes are regarded as colloidal particles with resins adsorbed onto their surfaces [6]. If enough resin desorbs, asphaltenes will deposit [7]. In the solubility theory, asphaltenes are assumed to be dissolved in crude oil [8]. If

the solubility falls below a certain value, asphaltenes begin to deposit. There are two main approaches in the solubility theory, i.e., regular solution model and equation of state (EOS) [5]. Since a large number of three-phase equilibrium calculations are required to be conducted in compositional simulations, we would like to select an asphaltene-precipitation model with relatively low mathematical complexity that can be readily incorporated into the three-phase VLS equilibrium calculation algorithm. In 1993, Nghiem *et al.* [1] developed an efficient thermodynamic model for asphaltene precipitation. In their model, vapor and liquid phases are modeled using a cubic EOS, while the precipitated asphaltenes are regarded as a pure dense phase. Moreover, they assumed that the heaviest component in crude oil can be divided into a precipitating component and a non-precipitating component. These two components have identical critical properties and acentric factors, but different binary interaction parameters (BIPs) with respect to light components. A good agreement can be seen between the experimental results and the results yielded by the model with some parameters estimated from experimental data.

One challenge in multiphase equilibrium calculations is how to determine the number of present phases in the system. Multiphase equilibrium calculations consist of phase stability test and flash calculations, which are normally conducted in a stage-wise manner [9-11]. Phase stability tests are conducted to determine whether the tested mixture is stable or will split into two or more phases [9], while flash calculations are performed at the given number of phases to calculate the phase mole fractions and phase compositions [10]. The most widely applied stage-wise method is alternately conducting phase stability tests and flash calculations [9]. For example, in a three-phase

equilibrium calculation, stability test is first conducted on the feed to check if a new phase needs to be introduced by locating the stationary points on the tangent plane distance (TPD) function [9]. If a negative value of the TPD function is found at any of the stationary points (implying that the feed is unstable), a two-phase flash calculation needs to be conducted; otherwise, the given mixture is considered to be stable as one phase. Then, stability test is again conducted on the phases yielded by the two-phase flash calculation. If those phases are unstable, a three-phase flash calculation is required to split the mixture into three phases; otherwise, the given mixture is considered to split into two phases.

However, convergence problems are frequently encountered in phase equilibrium calculations for three or more than three phases, even when one rigorously applies the aforementioned stage-wise procedure. One reason causing the convergence issue is that there may be several stationary points on the TPD surface in three-phase equilibrium calculations. Thus, in three-phase equilibrium calculations, there is a high chance that the stability test fails to detect the negative stationary point(s), since the negative stationary point(s) may be hidden by the non-negative one(s). To increase the possibility of detecting the negative stationary point(s), stability tests are required to be conducted with multiple sets of initial equilibrium ratios [9, 11]. For different types of fluids, different initialization methods might be required. For hydrocarbon fluids mixed with CO₂, Li and Firoozabadi [11] suggested that $(c+4)$ initial estimates of equilibrium ratios should be applied for stability tests (where c represents the number of components).

Another reason leading to the convergence problems encountered in three-phase equilibrium calculations is that multiple two-phase equilibria may be yielded by two-phase flash calculations that are conducted with different initial equilibrium ratios [12]. This requires one to first determine if the calculated two-phase equilibrium can be used for the subsequent calculations. Gorucu and Johns [13] recommended that the one with the minimum Gibbs free energy should be applied to the subsequent calculations. To yield the two-phase equilibrium with the minimum Gibbs free energy, Gorucu and Johns [13] suggested that two-phase flash calculations should be conducted several times with the use of different initial equilibrium ratios. However, it is time-consuming to repeat two-phase flash calculations for several times.

Another way to prevent yielding the trivial two-phase equilibrium and thereby having a chance of yielding a trivial three-phase equilibrium is to perform three-phase equilibrium calculations with an alternative stage-wise method. In this alternative stage-wise method, a three-phase flash calculation is first conducted. If any calculated phase fractions is negative, a two-phase flash calculation needs to be conducted [14, 15]. If any phase fractions calculated by the two-phase flash calculation is negative, the feed is considered to be stable as one phase. Li and Li [16] proposed that the results yielded by the three-phase flash calculation can provide a knowledge of the present phases in the two-phase equilibrium. Negative flash [14, 15, 17] should be allowed in this method. However, it is difficult to provide good initial estimates for equilibrium ratios in three-phase flash calculations [11]. Lapene *et al.* [18] developed a three-phase vapor-liquid-aqueous (VLA) flash calculation algorithm by assuming that the aqueous phase is pure water phase, i.e., the so-called

free-water assumption [19]. With this assumption, the equilibrium ratios of the aqueous phase with respect to the reference phase for all the non-aqueous components are zero. Therefore, the number of equilibrium ratio sets (which need to be initialized in the three-phase VLA flash calculation) is reduced, making it possible and easy to provide good initial estimates for equilibrium ratios. They provided efficient initialization method for equilibrium ratios in their three-phase VLA flash calculation algorithm. Li and Li [16] modified this three-phase flash calculation algorithm as well as the alternative stage-wise procedure. By integrating the modified three-phase flash calculation algorithm into the modified alternative stage-wise procedure, they developed an efficient and robust three-phase free-water vapor-liquid-aqueous (VLA) equilibrium calculation algorithm [16]. Since the assumption made on the asphaltene phase in the asphaltene-precipitation model proposed by Nghiem *et al.* [1] is similar to the free-water assumption, the number of equilibrium ratio sets in the three-phase VLS flash calculation can be also reduced when implementing the asphaltene-precipitation model proposed by Nghiem *et al.* [1]. Thus, it is possible for us to develop a robust three-phase VLS equilibrium calculation algorithm by taking advantage of the free-solid assumption. To our knowledge, such robust algorithm has not been reported in the literature.

In this work, we develop a robust three-phase VLS equilibrium calculation algorithm that is coupled with the asphaltene-precipitation model proposed by Nghiem *et al.* [1]. The key parameters used in this model are first adjusted based on experimental data. As previously mentioned, such asphaltene-precipitation model assumes that asphaltene phase only contains pure asphaltene. This assumption enables the appearance of the asphaltene phase to be checked simply

by comparing the fugacity of asphaltene component in the non-asphaltene phase against that in the asphaltene phase. The appearance of the non-asphaltene phase (i.e., vapor or liquid phase in this study) is determined by the phase stability test. New initialization methods for equilibrium ratios are provided for both stability test and flash calculations. To develop this three-phase VLS equilibrium calculation algorithm, we first develop a two-phase flash calculation algorithm used to split the mixture into an asphaltene phase and a non-asphaltene phase. Moreover, in order to enhance the robustness and efficiency of our three-phase VLS equilibrium calculation algorithm, two different three-phase VLS flash calculations algorithms are developed and incorporated into our three-phase VLS equilibrium calculation algorithm. The performance of the newly developed algorithm is tested by generating pressure-composition (P-X) diagrams for several real reservoir fluids mixed with pure or impure CO₂.

5.2 Mathematical Formulations

5.2.1 Thermodynamic Model

Nghiem *et al.* [1] proposed a thermodynamic model in which vapor and liquid phases are modeled using a cubic EOS, while asphaltene phase is considered as a pure dense phase only containing asphaltene. The fugacity of asphaltene in the asphaltene phase is calculated by the following equation [1],

$$\ln f_s = \ln f_s^* + \frac{V_s(P - P^*)}{RT} \quad (5-1)$$

where P and P^* represent the actual pressure and the reference pressure, respectively; f_s and f_s^*

represent the fugacities of asphaltene in the asphaltene phase at P and P^* , respectively; V_s represents the asphaltene molar volume; R represents the universal gas constant; T represents temperature; and the subscript s represents asphaltene phase. In this work, the Peng-Robinson (PR) EOS [20] is applied to model vapor and liquid phases.

5.2.2 Phase Stability Test

In this study, asphaltene precipitation can be simply checked by the following inequality [21],

$$\begin{cases} f_{cx} < f_{cs}, & \text{asphaltene phase does not exist} \\ f_{cx} \geq f_{cs}, & \text{asphaltene phase exists} \end{cases} \quad (5-2)$$

where f_{cx} and f_{cs} represent the fugacity of asphaltene component in the non-asphaltene phase calculated by PR EOS [20] and that in the asphaltene phase calculated by Equation (5-1), respectively, and the subscripts c , x , and s represent asphaltene component, non-asphaltene phase, and asphaltene phase, respectively. The appearance of vapor or liquid phase is checked by phase stability test [9]. The expression of the TPD function used in the stability analysis is shown as follows [9],

$$g(\mathbf{y}) = \sum_{i=1}^c y_i [\ln \phi_i(\mathbf{y}) + \ln y_i - \ln \phi_i(\mathbf{z}) - \ln z_i] \quad (5-3)$$

where \mathbf{y} and \mathbf{z} represent the compositions of the trial phase and the tested phase, respectively; $\phi_i(\mathbf{y})$ and $\phi_i(\mathbf{z})$ represent the fugacity coefficients of component i in the trial phase and the test phase, respectively; c is the number of components in the mixture; and the subscript i is component index. If the values of the TPD function are non-negative at any composition of the trial phase, the tested phase is considered to be stable. Michelsen proposed a stability test algorithm [9],

suggesting finding all stationary points on the TPD surface. If the values of all stationary points are non-negative, the tested phase can be considered to be stable. The stationary points on the TPD function can be detected by the following equation [9],

$$\ln \phi_i(\mathbf{y}) + \ln y_i - \ln \phi_i(\mathbf{z}) - \ln z_i = k, \quad i = 1, \dots, c \quad (5-4)$$

where k is the value of the stationary point (which is a constant). The detailed procedure for conducting stability test is provided by Michelsen [9]. In this work, the quasi-Newton successive-substitution method [22] is used in the stability test to search for the local stationary points. Moreover, multiple estimates of equilibrium ratios are used to initialize the stability test. **Section 5.3** will provide the detailed initialization method used in our stability tests.

5.2.3 Flash Calculation

Flash calculations aim to obtain phase fractions and phase compositions for a given mixture equilibrating at a given pressure/temperature condition and a given number of present phases [10]. The convergence of flash calculations is subject to the material balance constraint and the equal-fugacity constraint (i.e., the fugacities of each component in all present phases should be equivalent) [10].

5.2.3.1 Two-Phase Vapor-Liquid VL Flash Calculation

The equal-fugacity constraint for the two-phase VL flash calculation is shown as follows [10],

$$f_{ix} = f_{iy}, \quad i = 1, \dots, c \quad (5-5)$$

where f_{ix} and f_{iy} represent the fugacities of component i in liquid phase and vapor phase,

respectively, and the subscripts x and y represent liquid phase and vapor phase, respectively.

Rachford-Rice (RR) equation is developed to solve phase mole fractions based on the material balance [23]. RR equation used for the two-phase VL flash calculation is provided as follows [23],

$$RR = \sum_{i=1}^c (y_i - x_i) = \sum_{i=1}^c \frac{z_i (K_{iy} - 1)}{1 + \beta_y (K_{iy} - 1)} = 0 \quad (5-6)$$

where x_i , y_i , and z_i represent the mole fractions of component i in liquid phase, vapor phase, and feed, respectively; β_y represents the mole fraction of vapor phase; and K_{iy} represents the equilibrium ratio of component i in vapor phase with respect to liquid phase. K_{iy} can be calculated by,

$$K_{iy} = \frac{y_i}{x_i} = \frac{\phi_{ix}}{\phi_{iy}}, \quad i = 1, \dots, c \quad (5-7)$$

where ϕ_{ix} and ϕ_{iy} represent the fugacity coefficients of component i in liquid phase and vapor phase, respectively. Based on material balance, phase compositions can be calculated by [23],

$$x_i = \frac{z_i}{1 + \beta_y (K_{iy} - 1)}; \quad y_i = z_i K_{iy} \quad (5-8)$$

The two-phase VL flash calculation algorithm used in this research is the same as that provided by Michelsen [10]. The two-phase VL flash calculation algorithm is composed of two iteration loops. The outer loop aims to satisfy the equal-fugacity constraint by updating equilibrium ratios, while the inner loop solves RR equation to yield phase mole fractions and phase compositions. In this work, successive substitution iteration (SSI) is used in the outer loop, while Newton method is applied in the inner loop [24, 25].

5.2.3.2 Two-Phase Vapor/Liquid-Asphaltene V/L-S Flash Calculation

In two-phase V/L-S flash calculation, one of the present phases is the asphaltene phase. Based on the assumption that the asphaltene phase only contains asphaltene, the two-phase V/L-S flash calculation can be much simpler than the two-phase VL flash calculation. The equal-fugacity constraint for the two-phase V/L-S flash calculation can be simplified to one equation,

$$f_{cx} = f_{cs} \quad (5-9)$$

where f_{cx} and f_{cs} represent the fugacities of asphaltene in non-asphaltene phase and asphaltene phase, respectively, and the subscripts c , x , and s represent asphaltene component, non-asphaltene phase, and asphaltene phase, respectively. f_{cs} can be calculated based on Equation (5-1), while f_{cx} can be calculated based on PR EOS with a given composition of non-asphaltene phase. Based on the material balance, composition of non-asphaltene phase can be calculated by the following equation,

$$x_i = \begin{cases} z_i / (1 - \beta_s), & i = 1, \dots, c-1 \\ (z_i - \beta_s) / (1 - \beta_s), & i = c \end{cases} \quad (5-10)$$

where x_i and z_i represent the mole fractions of component i in non-asphaltene phase and feed, respectively, and β_s represents mole fraction of asphaltene phase. Therefore, the equal-fugacity constraint can be satisfied by updating β_s . **Appendix 5-A** provides the detailed procedure of the two-phase V/L-S flash calculation algorithm.

5.2.3.3 Three-Phase VLS Flash Calculation

The equal-fugacity constraints for the three-phase VLS flash calculation are given by [1],

$$f_{ix} = f_{iy}, \quad i = 1, \dots, c \quad (5-11)$$

$$f_{cx} = f_{cy} = f_{cs} \quad (5-12)$$

In this work, two algorithms are developed to conduct the three-phase VLS flash calculations. Both of them are incorporated into the three-phase VLS equilibrium calculation algorithm to enhance the robustness and efficiency of the new three-phase VLS equilibrium calculation algorithm. **Section 5.3** will provide the details about how to incorporate these two algorithms. The difference in these two algorithms lies in the method used for solving the phase compositions and phase fractions.

Li and Li [16] derived the objective function and constraints (used to solve phase mole fractions) for three-phase free-water VLA flash calculation by simplifying the objective function and constraints developed by Okuno *et al.* [26] based on the free-water assumption [19]. The objective function and constraints used in Algorithm #1 for three-phase VLS flash calculations is similar to that used in the three-phase free-water VLA flash calculation algorithm developed by Li and Li [16]. The objective function and constraints for three-phase VLS flash calculations can be expressed as follows [16],

$$\begin{cases} \min : f(\beta_y) = \sum_{i=1}^{c-1} -z_i \ln \left| (K_{iy} - K_{cy}^*) \beta_y + K_{cz}^* \right| \\ \text{Subject to : } (K_{cy}^* - K_{iy}) \beta_y \leq \min \{ K_{cz}^* - z_i, K_{cz}^* - K_{iy} z_i \}, i \neq c \end{cases} \quad (5-13)$$

where

$$\begin{cases} K_{cy}^* = \frac{1-y_c}{1-x_c} \\ K_{cz}^* = \frac{1-z_c}{1-x_c} \end{cases} \quad (5-14)$$

where x_c , y_c , and z_c represent the mole fractions of asphaltene component in liquid phase, vapor phase, and feed, respectively. As noted by Li and Li [16], there is only one unknown in the above objective function, i.e., phase mole fraction of vapor phase (β_y). Moreover, the constraints in Equation (5-14) form a reliable feasible region of β_y [16, 26]. The mole fractions of asphaltene phase and liquid phase can be solved by the following equations [16],

$$\beta_s = \frac{z_c + (x_c - y_c)\beta_y - x_c}{1 - x_c}; \beta_x = 1 - \beta_y - \beta_s \quad (5-15)$$

where β_x represents the mole fraction of liquid phase. The compositions of liquid and vapor phases can be calculated based on the following equations [16],

$$x_i = \begin{cases} \frac{z_i}{K_{iy} - K_{cy}^*\beta_y + K_{cz}^*}, i \neq c \\ \frac{1}{K_{is}}, i = c \end{cases}; y_i = K_{iy}x_i \quad (5-16)$$

where

$$K_{is} = \frac{s_i}{x_i} = \frac{\phi_{ix}}{\phi_{is}}, i = 1, \dots, c \quad (5-17)$$

where s_i represents the mole fraction of component i in asphaltene phase and ϕ_{is} represents the fugacity coefficient of component i in asphaltene phase. Based on the assumption that asphaltene phase only contains asphaltene, we can have,

$$s_i = \begin{cases} 1, i = c \\ 0, i \neq c \end{cases} \quad (5-18)$$

The procedures adopted by Algorithm #1 is similar to that of the three-phase free-water VLA flash calculation algorithm developed by Li and Li [16]. This algorithm can be simply summarized as two iteration loops (which is similar to the two-phase VL flash calculation algorithm). The outer loop is used to update equilibrium ratios for satisfying the equal-fugacity constraint by SSI, while the inner loop is used to calculate phase mole fractions and phase compositions by minimizing Equation (5-13) using the interior-point method. This algorithm is efficient; but the performance of Algorithm #1 relies on the quality of initial equilibrium ratios. In **Section 5.3**, we provide detailed initialization method for equilibrium ratios in Algorithm #1.

Algorithm #2 for three-phase VLS flash calculations is motivated by two-phase V/L-A flash calculation algorithm. In Algorithm #2, we perform two-phase VL flash calculations in the inner loop to satisfy Equation (5-11) in the equal-fugacity constraint, while the outer loop is used to update β_s to give a new feed used in the inner loop. Equation (5-12) in the equal-fugacity constraint should be satisfied in the outer loop. The feed used in the inner loop can be updated by,

$$z_{i2} = \begin{cases} z_i / (1 - \beta_s), & i = 1, \dots, c-1 \\ (z_i - \beta_s) / (1 - \beta_s), & i = c \end{cases} \quad (5-19)$$

where z_{i2} represents the mole fraction of component i in the feed used in the inner loop. Algorithm #2 is reliable when three-phase equilibrium actually appears; but it is time-consuming since several times of two-phase VL flash calculations are conducted in the inner loop. The detailed procedure of Algorithm #2 is summarized in **Appendix 5-B**.

5.3 Three-Phase VLS Equilibrium Calculation Algorithm

In this section, we will introduce the robust three-phase VLS equilibrium calculation algorithm. In order to ensure the robustness of the three-phase VLS equilibrium calculation algorithm, it is essential to have good initial values for both stability tests and flash calculations. In general, for different types of fluids, different initialization methods are required. To apply our algorithm to simulate CO₂ flooding in light oil reservoirs, we provide new initialization methods for equilibrium ratios in both stability tests and flash calculations.

The new initialization method for equilibrium ratios in stability tests is a modification of that proposed by Li and Firoozabadi [11]. This new method is shown as follows,

$$K_i^{ST} = \left\{ K_i^{Wilson}, 1/K_i^{Wilson}, \sqrt[3]{K_i^{Wilson}}, 1/\sqrt[3]{K_i^{Wilson}}, K_i^{CO_2-NS}, K_i^{CO_2-S} \right\} \quad (5-20)$$

where K_i^{ST} represents the initial equilibrium ratio of component i used for stability tests. The first four terms are the same as those proposed by Li and Firoozabadi [11]. K_i^{Wilson} represents the equilibrium ratio of component i calculated by Wilson equation [27],

$$K_i^{Wilson} = \frac{P_{ci}}{P} \exp \left[5.37(1 + \omega_i) \left(1 - \frac{T_{ci}}{T} \right) \right] \quad (5-21)$$

where P and P_{ci} represent pressure and the critical pressure of component i , respectively; T and T_{ci} represent temperature and the critical temperature of component i , respectively; and ω_i represents acentric factor of component i . $K_i^{CO_2-NS}$ and $K_i^{CO_2-S}$ can be calculated by the following equations, respectively,

$$K_i^{CO_2-NS} = \begin{cases} 0.8/z_i, & i = 2 \\ [0.2/(c-1)]/z_i, & i \neq 2 \end{cases} \quad (5-22)$$

$$K_i^{CO_2-S} = \begin{cases} 0.8 / z_i, & i = 2 \\ 10^{-8} / z_i, & i = c \\ \left[\left(0.2 - 10^{-8} \right) / (c - 2) \right] / z_i, & i \neq 2 \text{ and } c \end{cases} \quad (5-23)$$

where 2 and c represent components CO_2 and asphaltene, respectively. The new initialization method for equilibrium ratios in flash calculations will be introduced in the detailed procedure of the three-phase VLS equilibrium calculation algorithm. Figure 5-1 depicts the flow chart of this algorithm. The detailed procedure is listed below,

- (1) Using the new initialization method for equilibrium ratios as shown in Equation (5-20), conduct the stability test on the feed (z_i) to detect the negative stationary points. Record the compositions of the trial phases at all stationary points with negative TPD values as x_{0i} , x_{01i} , x_{02i} , etc. Note that x_{0i} corresponds to the smallest TPD value, while the last trial phase composition corresponds to the largest TPD value.
- (2) If negative stationary point exists, vapor or liquid phase may appear. If so, go to Step (5). Otherwise, continue to Step (3).
- (3) Check Inequality (5-2). If asphaltene phase exists, continue to Step (4); otherwise, output single-phase equilibrium.
- (4) Conduct two-phase V/L-S flash calculation and output two-phase V/L-S equilibrium.
- (5) Check Inequality (5-2). If asphaltene phase exists, go to Step (8); otherwise, continue to Step (6).
- (6) Conduct two-phase VL flash calculation to yield liquid-phase and vapor-phase compositions

(x_i^{2-VL} and y_i^{2-VL}) and mole fractions of liquid phase and vapor phase (β_x^{2-VL} and β_y^{2-VL}). The initial equilibrium ratios used in the two-phase VL flash calculation can be generated by the following equation,

$$K_{iy} = z_i / x_{i0}, \quad i = 1, \dots, c \quad (5-24)$$

(7) Check Inequality (5-2) again. If asphaltene phase does not exist, output two-phase VL equilibrium; otherwise, conduct three-phase VLS flash calculation Algorithm #1 and output three-phase VLS equilibrium. The initial equilibrium ratios used in the three-phase VLS flash calculation are given by,

$$K_{iy} = y_i^{2-VL} / x_i, \quad i = 1, \dots, c \quad (5-25)$$

where

$$x_i = \begin{cases} x_i^{2-VL} / (1 - 0.99 \times x_c^{2-VL}), & i \neq c \\ 0.01 \times x_i^{2-VL} / (1 - 0.99 \times x_c^{2-VL}), & i = c \end{cases} \quad (5-26)$$

(8) Conduct three-phase VLS flash calculation Algorithm #1 to yield liquid-phase, vapor-phase, and asphaltene-phase compositions (x_i^{3-1} , y_i^{3-1} , and s_i^{3-1}) and phase mole fractions of liquid phase, vapor phase, and asphaltene phase (β_x^{3-1} , β_y^{3-1} , and β_s^{3-1}). K_i^{Wilson} are used as the initial equilibrium ratios.

(9) If the results calculated by the three-phase VLS flash are physical, output three-phase VLS equilibrium; otherwise, continue to Step (10). This judging criterion is the same as that proposed by Li and Li [16]. As mentioned by Li and Li [16], the results of a three-phase flash calculation can be considered to be unphysical if an open feasible region (i.e., a region where

any of the endpoints is a pole) appears in any iteration or any of the ultimately calculated phase mole fractions do not fall into [0, 1].

- (10) If β_s^{3-1} can be calculated and $\beta_s^{3-1} < 0$, conduct two-phase VL flash with the initial equilibrium ratios calculated by the following equation,

$$K_{iy} = y_i^{3-1} / x_i^{3-1}, i = 1, \dots, c \quad (5-27)$$

Otherwise, conduct the two-phase VL flash with multiple initial equilibrium ratios calculated by the following equations,

$$K_{iy} = z_i / x_{-0i}, K_{iy} = z_i / x_{-01i}, \text{ etc. } i = 1, \dots, c \quad (5-28)$$

If multiple two-phase equilibria are yielded, select the one with the lowest Gibbs free energy.

The aforementioned two-phase VL flash will yield the liquid-phase and vapor-phase compositions (x_i^{2-VL} and y_i^{2-VL}) and mole fractions of liquid phase and vapor phase (β_x^{2-VL} and β_y^{2-VL}).

- (11) Conduct stability test and check Inequality (5-2) on the two phases yielded by the two-phase VL flash calculation. If both of these two phases are stable, output two-phase VL equilibrium; otherwise, conduct three-phase VLS flash calculation Algorithm #1 to yield liquid-phase, vapor-phase, and asphaltene-phase compositions (x_i^{3-2} , y_i^{3-2} , and s_i^{3-2}) and mole fractions of liquid phase, vapor phase, and asphaltene phase (β_x^{3-2} , β_y^{3-2} , and β_s^{3-2}). The initial equilibrium ratios used in the three-phase VLS flash calculation are the same as those expressed by Equation (5-25).

- (12) If the results calculated by the three-phase VLS flash are physical, output three-phase VLS

equilibrium; otherwise, conduct two-phase V/L-S flash calculation to yield non-asphaltene-phase and asphaltene-phase compositions ($x_i^{2-V/L-S}$ and $s_i^{2-V/L-S}$) and phase mole fractions of non-asphaltene phase and asphaltene phase ($\beta_x^{2-V/L-S}$ and $\beta_s^{2-V/L-S}$).

- (13) Conduct stability test on non-asphaltene phase obtained by the two-phase V/L-S flash calculation. If vapor or liquid phase will not appear, output two-phase V/L-S equilibrium; otherwise, conduct three-phase VLS flash calculation Algorithm #2 and output three-phase VLS equilibrium.

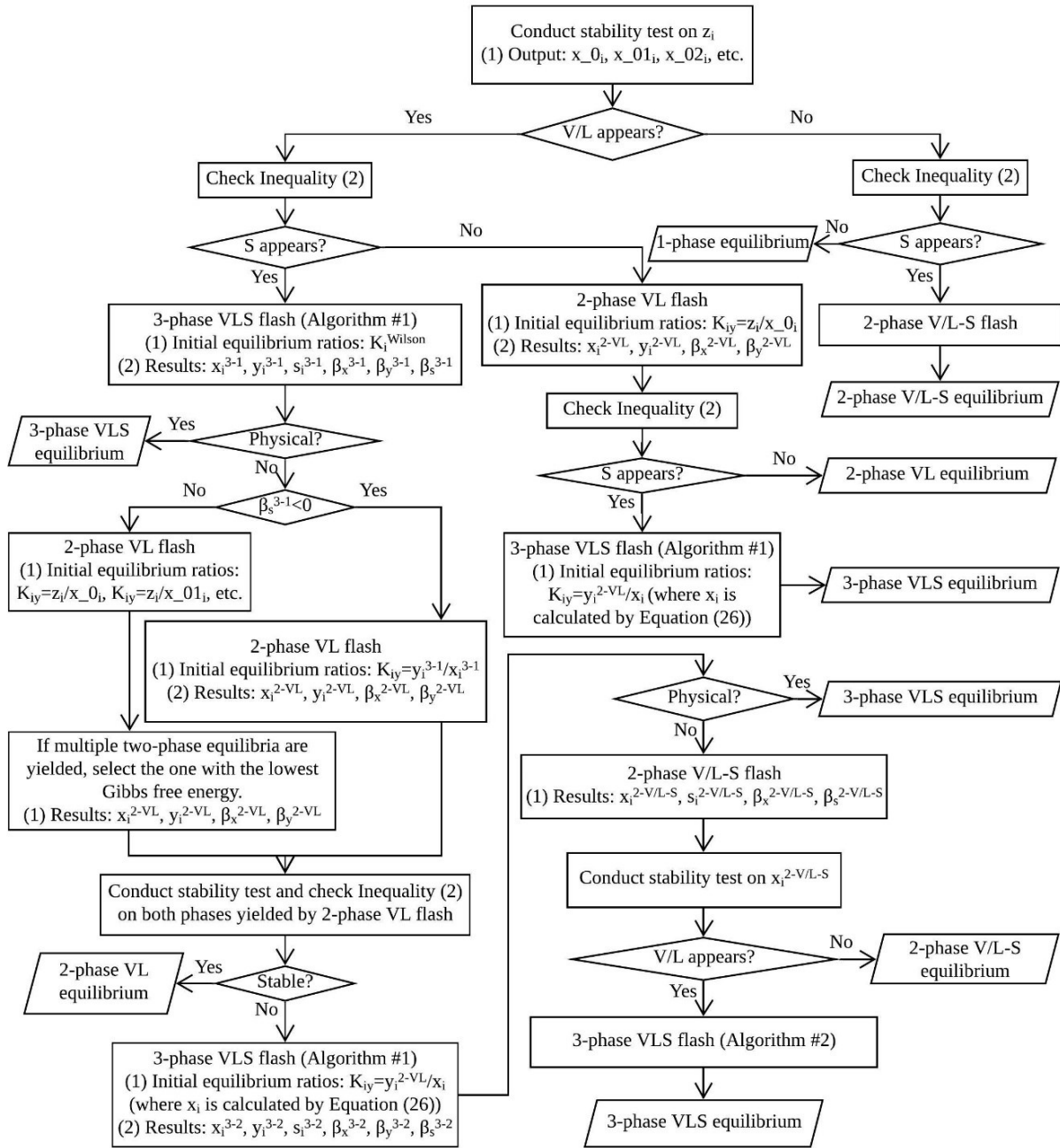


Figure 5-1 Flow chart of three-phase VLS equilibrium calculation algorithm. V: vapor phase; L: liquid phase; and S: solid asphaltene phase.

5.4 Results and Discussion

Two crude oil samples from Weyburn reservoir in Saskatchewan, Canada, are used to test the performance of the newly developed three-phase VLS equilibrium calculation algorithm. These

two oil samples are mixed with pure or impure CO₂. Srivastava *et al.* [4] provided detailed physical properties and compositions of these two oil samples. They also conducted experiments to obtain the asphaltene-precipitation data. In this work, we first use the asphaltene-precipitation data to adjust the key model parameters. Then, with the adjusted parameters, the three-phase VLS equilibrium calculation algorithm is applied to generate P-X phase diagrams for each oil sample mixed with pure or impure CO₂.

5.4.1 Oil Sample 1

Table 5-1 shows the compositions of oil sample 1 and injection gas [4]. Oil sample 1 is named as fluid W2 by Srivastava *et al.* [4]. Oil sample 1 has a gravity of 36°API [4]. Asphaltene content of oil sample 1 is measured to be 4 wt% [4].

Table 5-1 Compositions of oil sample 1 and injection gas [4]

Component	Oil sample 1	Gas (impure CO ₂)
N ₂	1.59	2.68
CO ₂	0.23	94.45
C1	4.54	2.87
C2	2.07	0
C3	4.41	0
<i>i</i> -C4	1.23	0
<i>n</i> -C4	2.59	0
<i>i</i> -C5	4.53	0
<i>n</i> -C5	4.96	0
C6+	73.85	0

5.4.1.1 Oil Characterization

The exponential distribution function proposed by Pedersen *et al.* [28] is applied to split the plus fraction. The lumping method is the same as that used by Srivastava *et al.* [4]. To get a

composition of oil sample 1 similar to that proposed by Srivastava *et al.* [4], the molecular weight of C6+ of oil sample 1 is set to be 195 g/mol. Kesler-Lee correlations [29, 30] are used to calculate the critical temperatures, critical pressures, and acentric factors of single carbon numbers (SCNs), while Riazi-Daubert correlation [31] is used to calculate the critical volumes of SCNs. The heaviest component is split into two components: a non-asphaltene component (i.e., C28A+ for oil sample 1) and an asphaltene component (i.e., C28B+ for oil sample 1). As mentioned by Nghiem *et al.* [1], these two components have identical critical properties and acentric factors, while the BIPs between C28B+ and other components are larger than the BIPs between C28A+ and other components. The mole fraction of asphaltene component can be calculated by the equation developed by Nghiem *et al.* [1],

$$z_{C28B+} = \frac{w_{C28B+} \cdot MW_{oil}}{MW_{C28B+}} \quad (5-29)$$

where z_{C28B+} represents the mole fraction of asphaltene component; w_{C28B+} represents the asphaltene content; and MW_{oil} and MW_{C28B+} represent the molecular weight of oil and C28B+, respectively. Table 5-2 summarizes the composition and component properties of oil sample 1. The critical properties and acentric factors of the first nine components are taken from the literature [32, 33], while the mole fractions and component properties of pseudo-components are calculated by this work.

Table 5-2 Composition and component properties of oil sample 1 [32, 33]

Component	Mole fraction (mol%)	Molecular weight (g/mol)	Critical temperature (K)	Critical pressure (bar)	Critical volume (m ³ /kmol)	Acentric factor
N ₂	1.59	28.01	126.20	34.40	0.0901	0.04
CO ₂	0.23	44.01	304.70	74.80	0.0940	0.23
C1	4.54	16.04	190.60	46.70	0.0993	0.01
C2	2.07	30.07	305.43	49.50	0.1479	0.10
C3	4.41	44.10	369.80	43.00	0.2029	0.15
<i>i</i> -C4	1.23	58.12	408.10	37.00	0.2627	0.18
<i>n</i> -C4	2.59	58.12	419.50	38.00	0.2547	0.20
<i>i</i> -C5	4.53	72.15	460.40	34.30	0.3058	0.23
<i>n</i> -C5	4.96	72.15	465.90	34.00	0.3040	0.24
C6-9	27.56	100.96	582.49	34.80	0.3869	0.32
C10-17	28.11	178.54	720.86	24.13	0.6475	0.54
C18-27	12.53	299.81	846.90	18.16	0.9254	0.75
C28A+	3.78	503.00	963.69	15.02	1.1550	0.93
C28B+	1.87	503.00	963.69	15.02	1.1550	0.93

5.4.1.2 Tuning of Key Model Parameters

Table 5-3 lists the adjustable parameters and their values used in our algorithm for oil sample 1 mixed with impure CO₂. In the thermodynamic model of asphaltene phase developed by Nghiem *et al.* [1], there are two adjustable parameters: f_s^* and V_s . In this work, we desire to match the experimental data of asphaltene precipitation for oil sample 1 under different gas concentrations at given temperature/pressure condition. Based on Equation (5-1), it is obvious that the changing of V_s will not affect the fugacity of asphaltene in the asphaltene phase when the pressure is fixed. Therefore, V_s cannot be adjusted based on the experimental data that are obtained at a fixed pressure. However, as mentioned by Nghiem and Coombe [21], V_s can be estimated based on the measured amounts of asphaltenes precipitated under different pressures. In our example

calculations, we do not tune V_s ; but the effect of this parameter on asphaltene precipitation is discussed in **Section 5.4.1.3**. Moreover, at the given temperature/pressure condition, f_s^* can be determined based on the critical gas concentration above which asphaltenes start to precipitate [1]. Therefore, in our case, we tune this parameter instead of f_s^* .

The BIPs between asphaltene component (C28B+) and other components should be adjusted as well. These BIPs can be calculated by the Chueh and Prausnitz model [34],

$$k_{ij} = 1 - \left[\frac{2v_{ci}^{1/6} v_{cj}^{1/6}}{v_{ci}^{1/3} + v_{cj}^{1/3}} \right]^\theta \quad (5-30)$$

where k_{ij} represents the BIP between component i and j ; v_{ci} and v_{cj} represent the critical volumes of component i and j , respectively; θ represents the exponential parameter; and the subscripts i and j represent components i and j , respectively. The same value of θ is used to calculate BIPs between asphaltene component (C28B+) and other components. This value can be tuned based on the experimental data. Based on our tests, the BIPs between CO₂ and hydrocarbon components (HCs) also need to be tuned to match the experimental data. Table 5-4 summarizes the BIPs used for oil sample 1. The BIPs between N₂ and other components except C28B+ are taken from the literature [33]. Moreover, during our tests, we find that the experimental data cannot be matched with the measured asphaltene content for oil sample 1. Nghiem and Coombe [21] also mentioned the effect of asphaltene content on asphaltene precipitation. Therefore, we tune the asphaltene content as well.

Table 5-3 Adjustable parameters and their values used in our algorithm for oil sample 1 mixed with impure CO₂

Parameter	Adjusted value
Critical gas concentration above which asphaltenes start to precipitate (mol%)	47
θ	3.8
BIP between CO ₂ and HCs	0.05
Asphaltene content (wt%)	6

Table 5-4 BIPs used for oil sample 1 calculations [33]

	N ₂	CO ₂	C28B+
N ₂	0	-0.0170	0.2836
CO ₂	-0.0170	0	0.2760
C1	0.0311	0.0500	0.2660
C2	0.0515	0.0500	0.1965
C3	0.0852	0.0500	0.1457
<i>i</i> -C4	0.1033	0.0500	0.1083
<i>n</i> -C4	0.0800	0.0500	0.1125
<i>i</i> -C5	0.0922	0.0500	0.0883
<i>n</i> -C5	0.1000	0.0500	0.0891
C6-9	0.1000	0.0500	0.0609
C10-17	0.1000	0.0500	0.0175
C18-27	0.1000	0.0500	0.0026
C28A+	0.1000	0.0500	0
C28B+	0.2836	0.2760	0

Figure 5-2 shows the comparison between the weight fractions of the precipitated asphaltenes as a function of gas concentration calculated by our algorithm with the adjusted parameters and those measured by Srivastava *et al.* [4]. The injection gas is an impure CO₂ stream, whose composition is shown in Table 1. The tested temperature and pressure are 61°C and 160 bar, respectively. As seen from Figure 5-2, a good agreement can be seen between the calculated weight fractions of the

precipitated asphaltenes and the measured counterparts, leading to the conclusion that our algorithm with the adjusted parameters can have a good description of the asphaltene precipitation phenomenon.

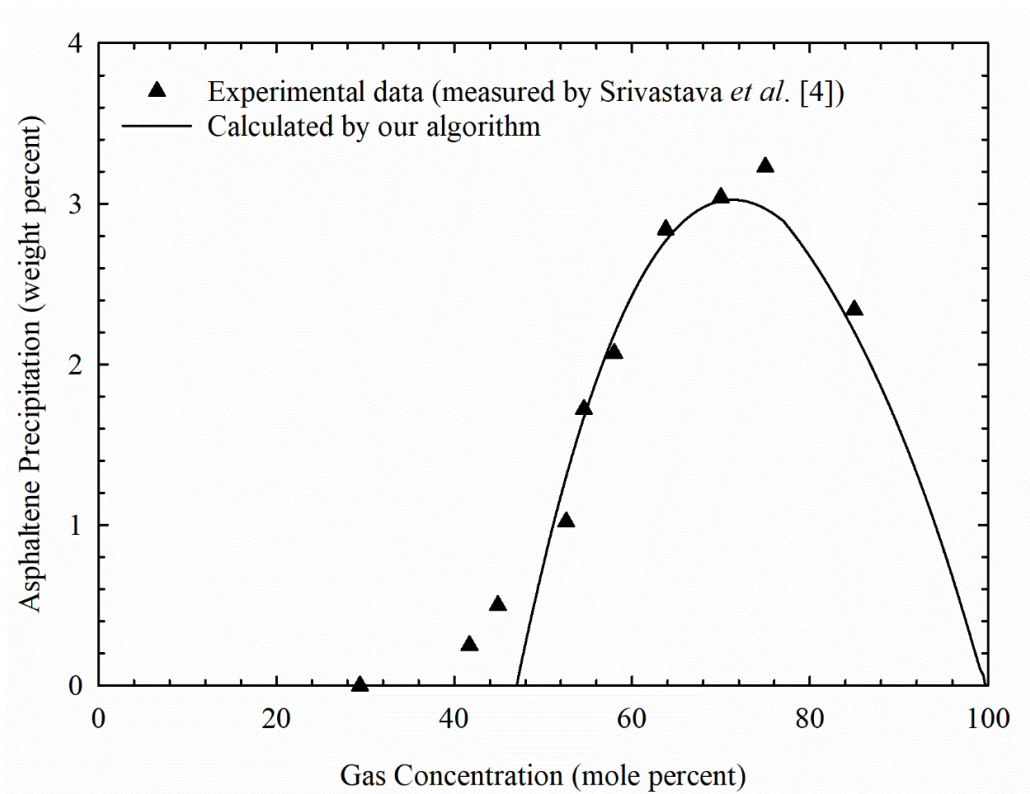


Figure 5-2 Comparison between the weight fractions of the precipitated asphaltenes as a function of gas concentration calculated by our algorithm with the adjusted parameters and those measured by Srivastava *et al.* [4] for oil sample 1 at 61°C and 160 bar

Figure 5-3 shows the effect of changing asphaltene content in oil sample 1 on the asphaltene precipitation under different gas concentrations. The three curves drawn in Figure 5-3 are generated by running the new three-phase VLS equilibrium algorithm under three different levels of asphaltene contents; other parameter values are the adjusted ones shown in Table 5-3. The asphaltene contents used to generate these three curves are 4 wt%, 5 wt%, and 6 wt%, respectively.

As shown in Figure 5-3, a change in the asphaltene content has a large effect on the asphaltene precipitation trends. A decrease in the asphaltene content will decrease the weight fractions of the precipitated asphaltenes, flattening the precipitation curve. As previously mentioned, the asphaltene content is measured to be 4 wt% by Srivastava *et al.* [4] However, the weight fractions of the precipitated asphaltenes calculated by our algorithm using 4 wt% asphaltene content are much smaller than the measured ones under a given gas loading. Therefore, to match the experimental data, we increase the asphaltene content in oil sample 1. As can be seen from Figure 5-3, using 6 wt% of asphaltene content in our calculations gives the best match with the experimental data.

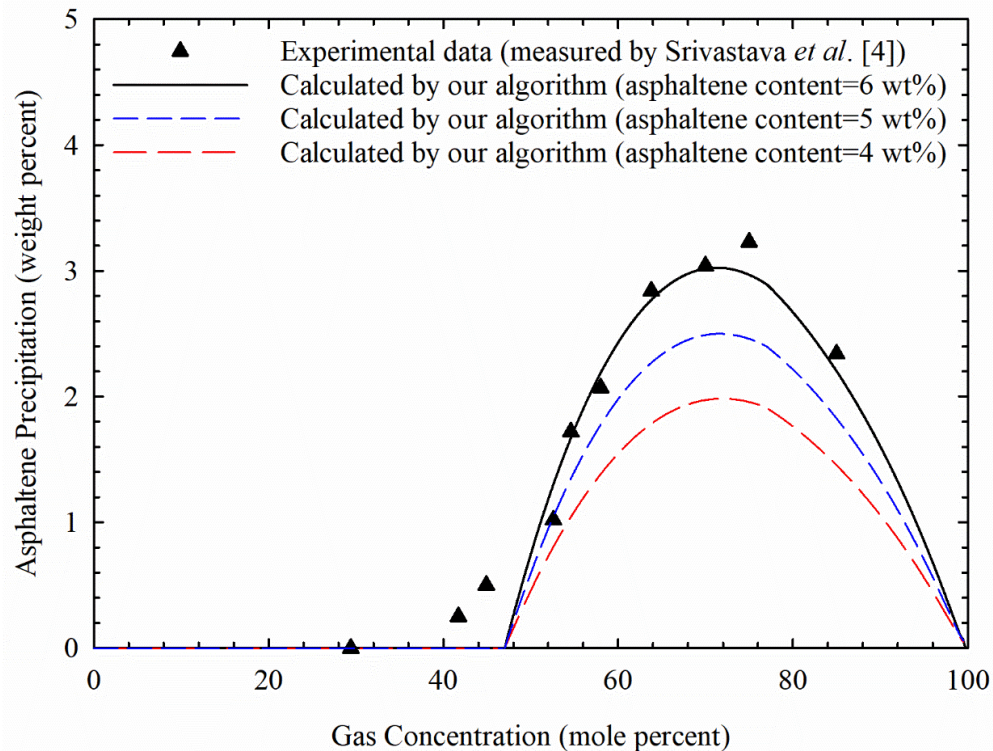


Figure 5-3 Effect of asphaltene content in oil sample 1 on asphaltene precipitation under different gas concentrations

Figure 5-4 shows the effect of the critical gas concentration, above which asphaltenes start to precipitate, on asphaltene precipitation under different gas concentrations. The three curves drawn in Figure 5-4 are calculated by our three-phase VLS equilibrium algorithm; we use the parameter values shown in Table 5-3 except the critical gas concentration (above which asphaltenes start to precipitate). The critical gas concentrations used to generate these three curves are 43 mol%, 47 mol%, and 50 mol%, respectively. As shown in Figure 5-4, an increase in the critical gas concentration tends to shift the left slope of the asphaltene precipitation curve to the right, but has negligible impact on the right slope of the asphaltene precipitation curve. In addition, an increase in the critical gas concentration tends to suppress the peak amount of the precipitated asphaltenes.

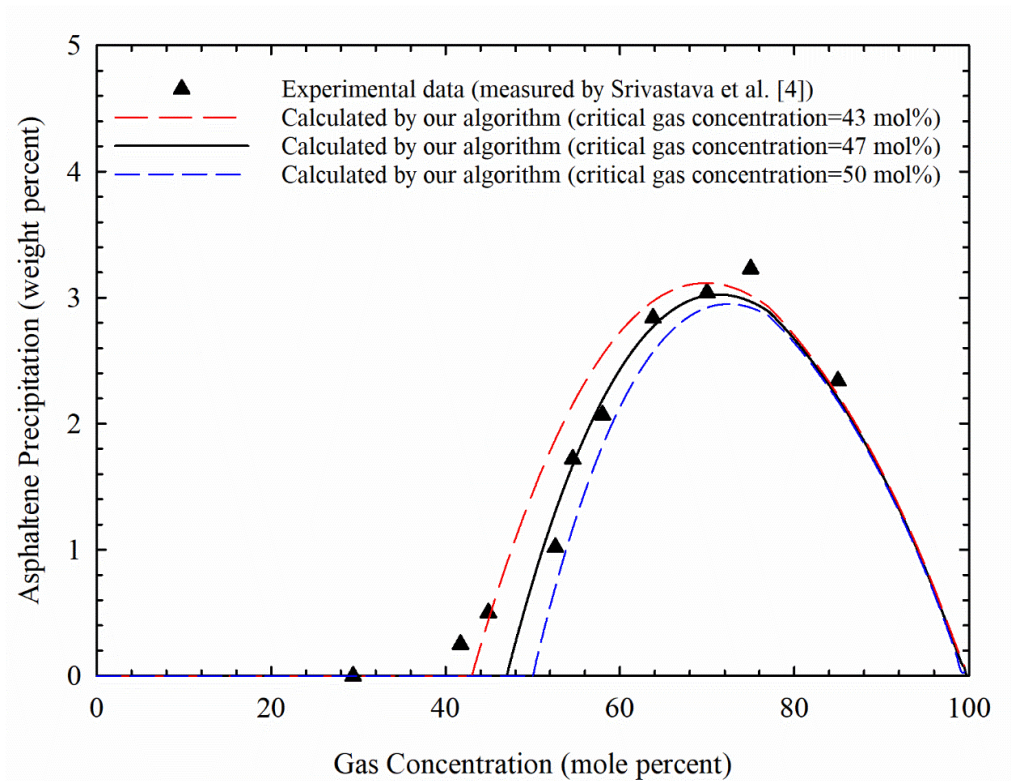


Figure 5-4 Effect of the critical gas concentration (above which asphaltenes start to precipitate) on asphaltene precipitation under different gas concentrations

Figure 5-5 depicts the effect of the exponential parameter (θ) on asphaltene precipitation under different gas concentrations. The three curves drawn in Figure 5-5 are calculated by our three-phase VLS equilibrium algorithm with the adjusted values of the parameters shown in Table 5-3 except the exponential parameter. The exponential parameter values used to generate these three curves are 3, 3.8, and 4.5, respectively. As seen from Figure 5-5, an increase in the exponential parameter value increases the amount of precipitated asphaltenes. Moreover, it tends to exert a larger effect on asphaltene precipitation in the region where the weight fractions of the precipitated asphaltenes increase with an increasing gas concentration, while it has smaller effect on asphaltene precipitation in the region where the weight fractions of the precipitated asphaltenes decrease with an increasing gas concentration.

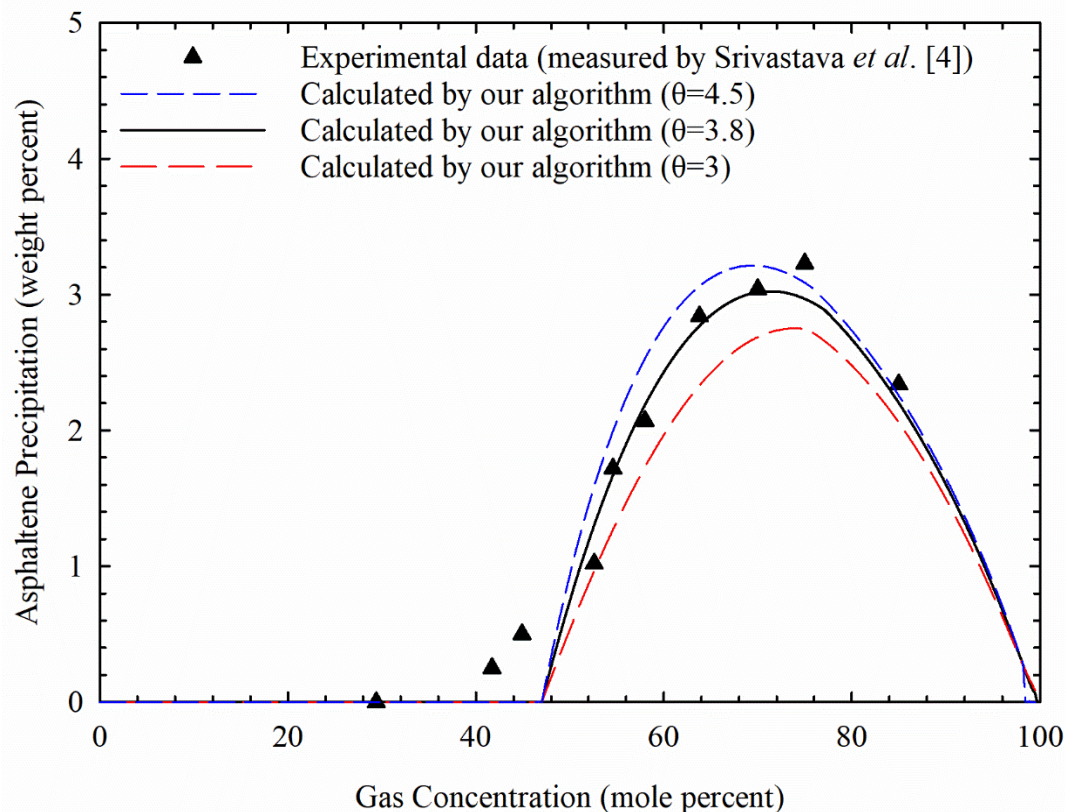


Figure 5-5 Effect of the exponential parameter (θ) on asphaltene precipitation under different gas concentrations

Figure 5-6 depicts the effect of the BIP between CO_2 and HCs on the asphaltene precipitation under different gas concentrations. The three curves drawn in Figure 5-6 are calculated by our three-phase VLS equilibrium algorithm with the adjusted values of the parameters shown in Table 5-3 except the BIP between CO_2 and HCs. The BIP between CO_2 and HCs used to generate these three curves are 0.02, 0.05, and 0.08, respectively. As Figure 5-6 shows, a decrease in the BIP between CO_2 and HCs increases the amount of the precipitated asphaltenes.

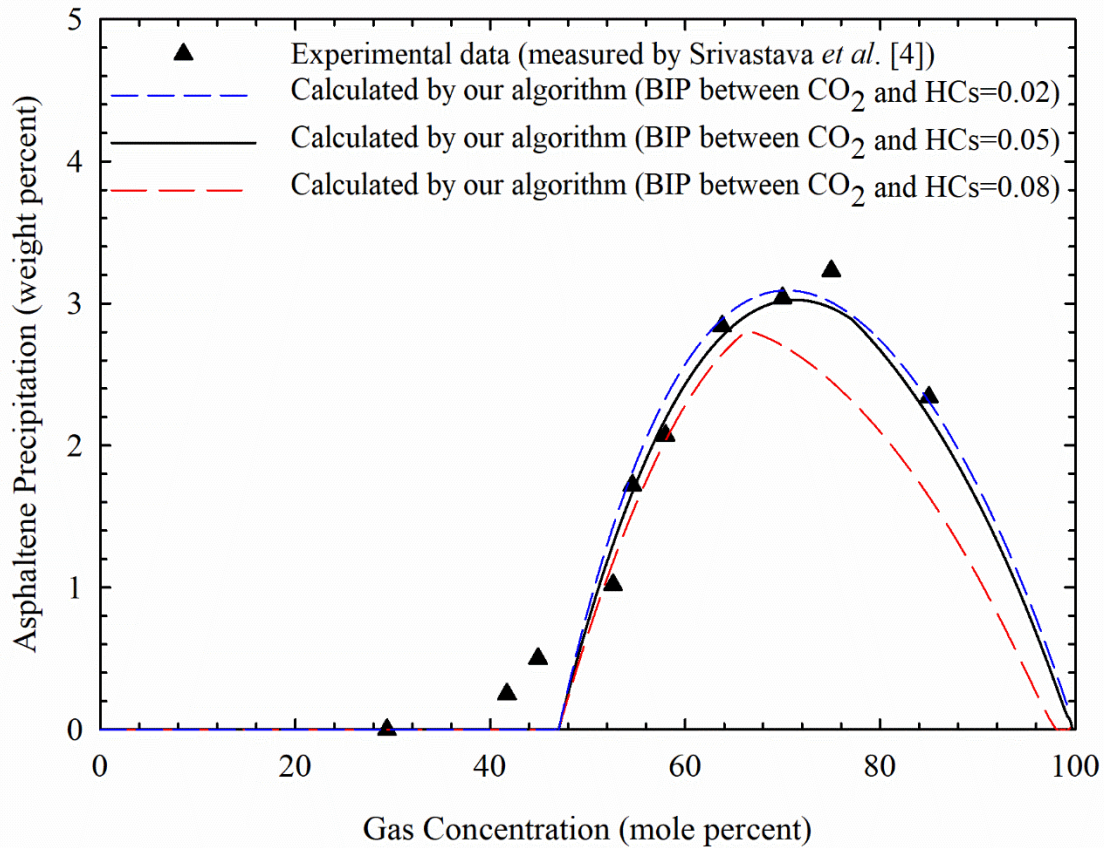


Figure 5-6 Effect of the BIP between CO₂ and HCs on the asphaltene precipitation under different gas concentrations

5.4.1.3 P-X Phase Diagram

In order to test the performance of the newly developed three-phase VLS equilibrium calculation algorithm, we apply this algorithm with the adjusted parameters to generate a P-X phase diagram for oil sample 1 mixed with impure CO₂. The composition of this impure CO₂ is shown in Table 5-1. Figure 5-7 depicts the calculation results. The temperature is set to be 61°C. V_s is calculated to be 0.4323 m³/kmol by PR EOS [20]. Pressure is varied from 1 bar to 250 bar with a step size of 0.25 bar, while the gas concentration is varied from 0 mol% to 99 mol% with a step size of 0.25 mol%. Our algorithm is run a total of 395,809 times to generate this P-X phase diagram. As shown

in Figure 5-7, this algorithm converges at all the tested points. The generated P-X phase diagram has smooth and continuous phase boundaries. Note that the line at the gas concentration of 99 mol% is not phase boundaries, since we do not conduct phase equilibrium calculations at gas concentrations larger than 99 mol%.

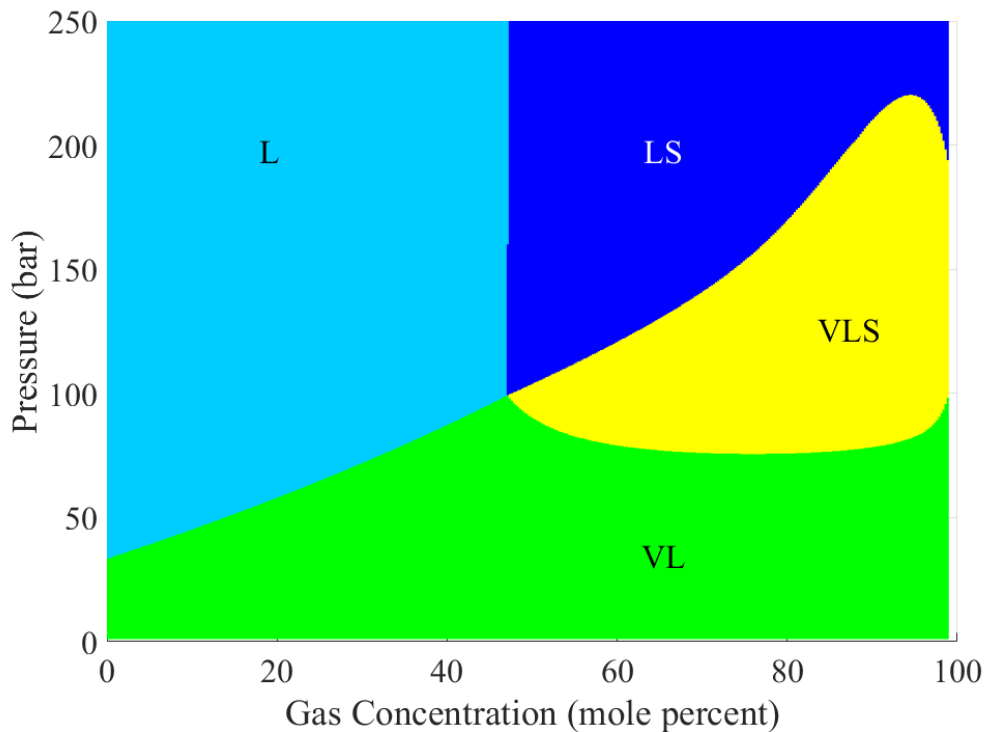
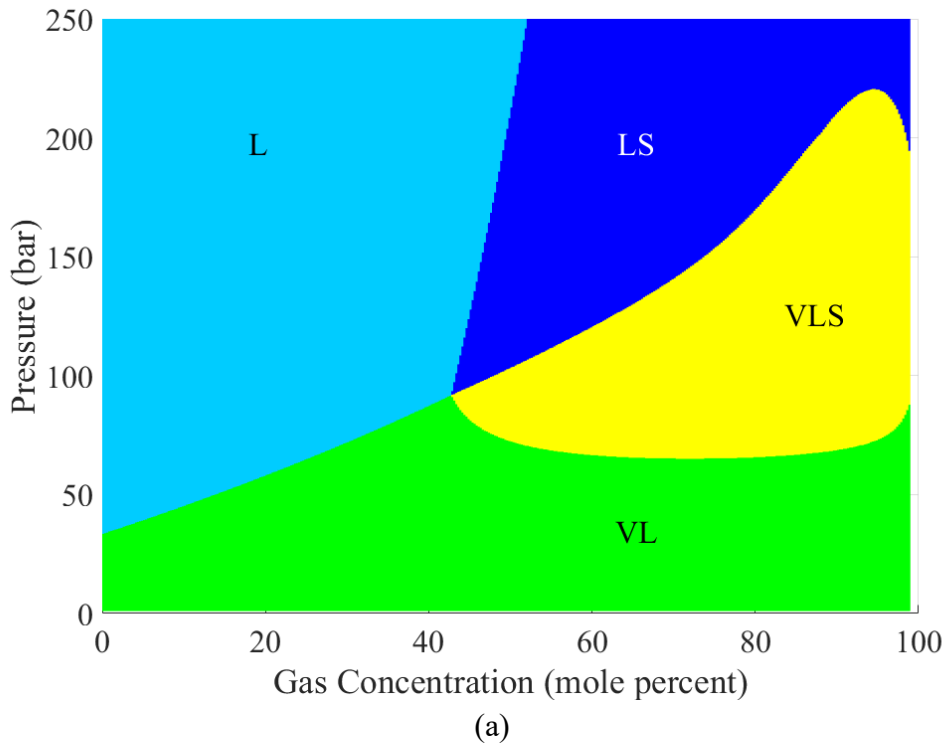
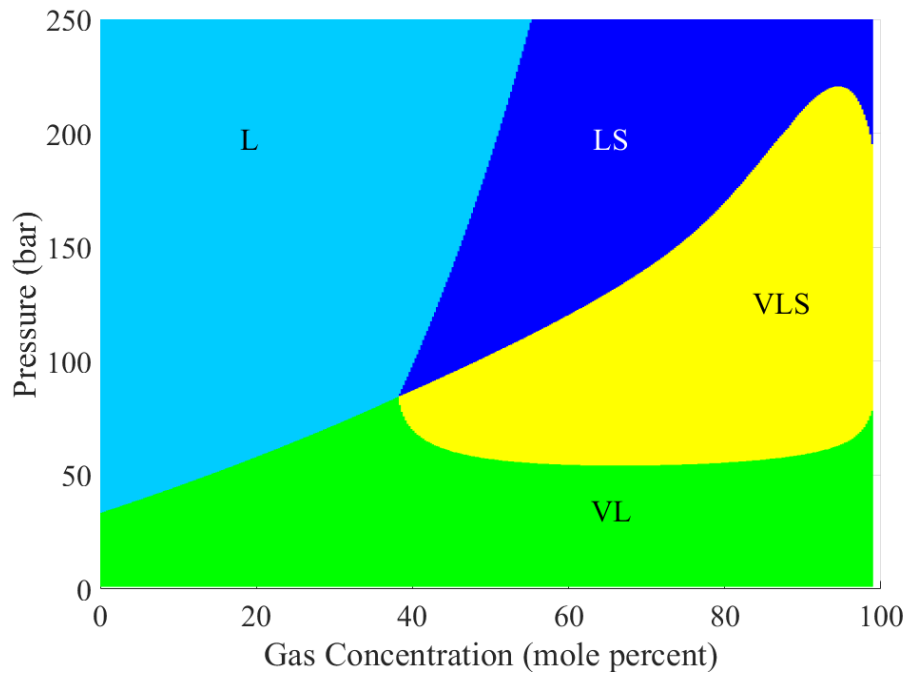


Figure 5-7 P-X phase diagram calculated by the three-phase VLS equilibrium calculation algorithm with the adjusted parameters for oil sample 1 mixed with impure CO₂ at 61°C. V: vapor phase; L: liquid phase; and S: solid asphaltene phase.

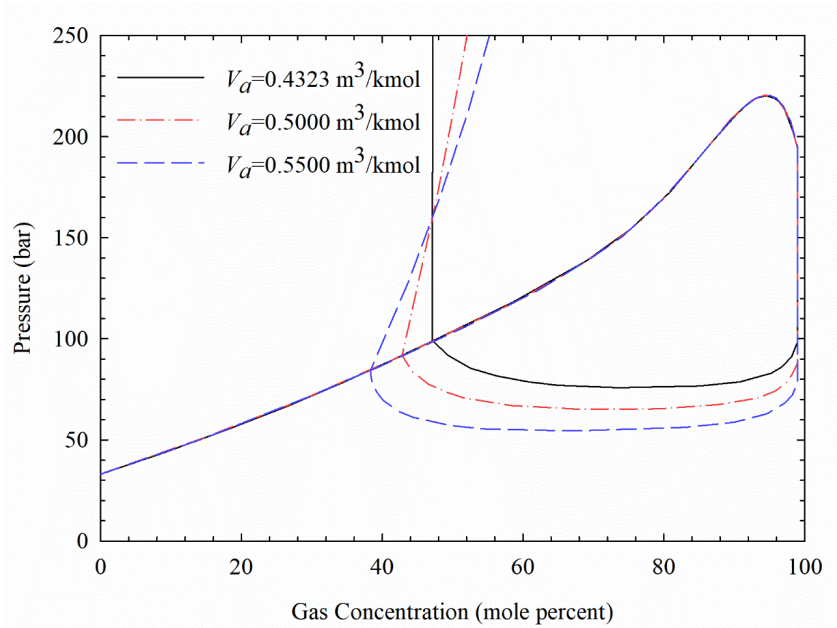
To show the effect of V_s on the resulting phase equilibria, we run our three-phase VLS equilibrium calculation algorithm with different V_s values to generate several P-X phase diagrams for oil sample 1 mixed with impure CO₂. Figure 5-8 shows the calculated P-X phase diagrams for oil sample 1 mixed with impure CO₂. Figure 5-8(a) and 5-8(b) depict the P-X phase diagram

generated by our algorithm with V_s set as 0.5000 m³/kmol and 0.5500 m³/kmol, respectively. For both phase diagrams, pressure is varied from 1 bar to 250 bar with a step size of 0.25 bar, while gas concentration is varied from 0 mol% to 99 mol% with a step size of 0.25 mol%. Again, Figures 5-8(a) and 5-8(b) show that our algorithm converges at all the tested points. Figure 5-8(c) shows the comparison of the different P-X phase boundaries yielded by our algorithm with different V_s values. As shown in Figure 5-8(c), if V_s increases, asphaltenes start to precipitate at a lower pressure and a smaller gas concentration. Moreover, under a constant pressure that is larger than the reference pressure P^* , the critical gas concentration (above which asphaltenes start to precipitate) increases as V_s increases.





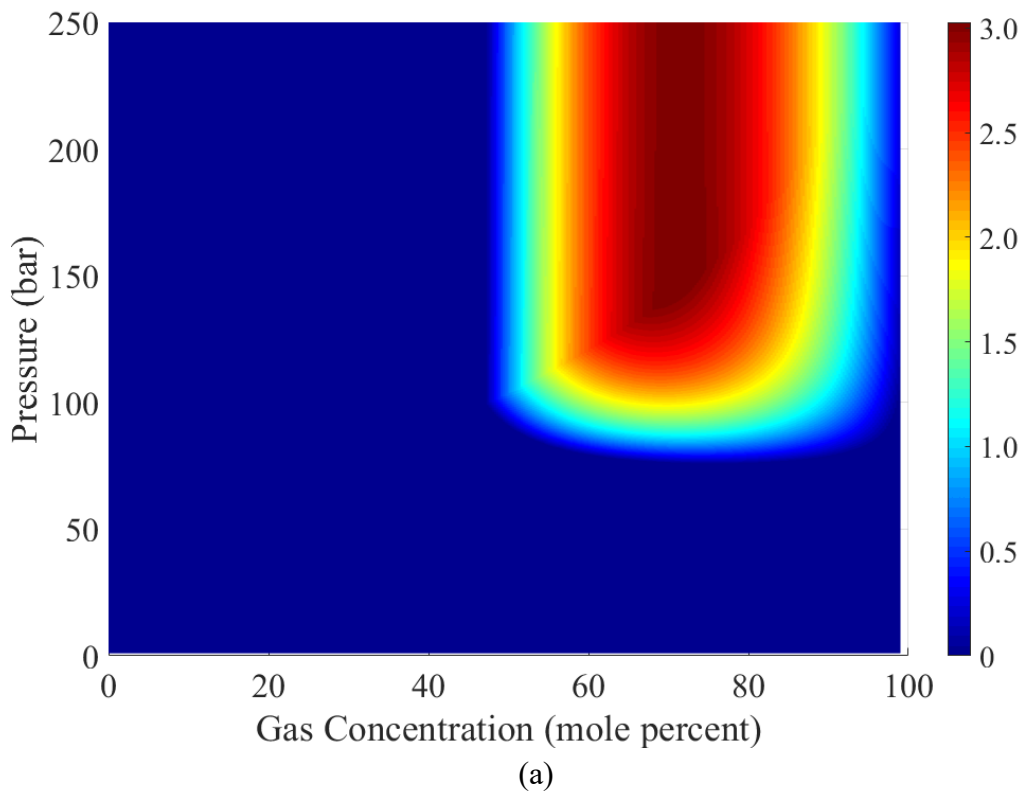
(b)

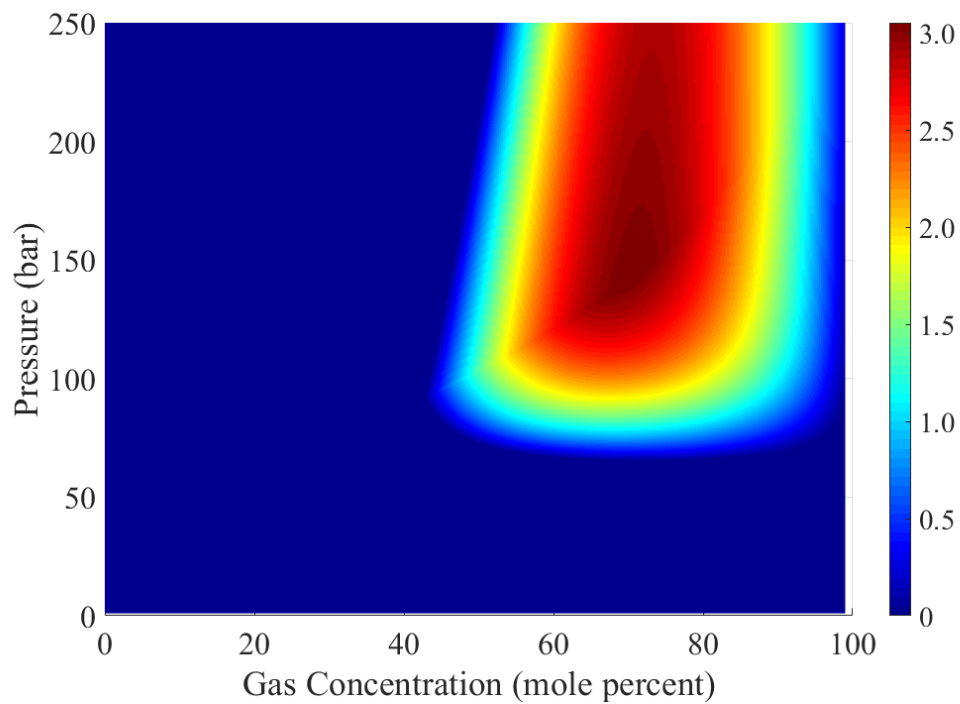


(c)

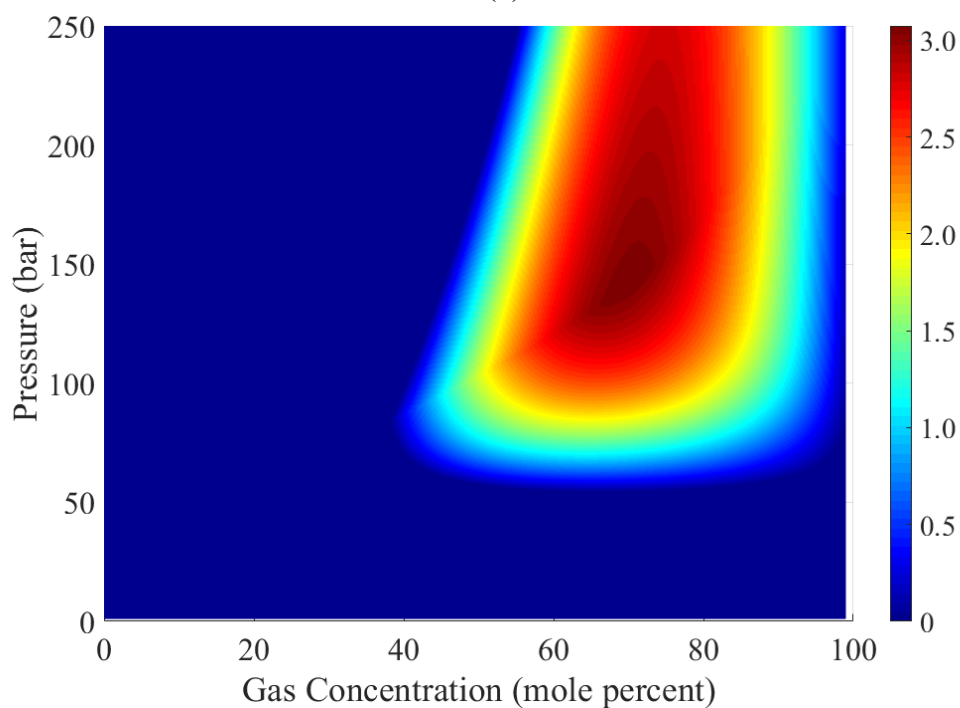
Figure 5-8 P-X phase diagrams for oil sample 1 mixed with impure CO₂ at 61°C yielded by our three-phase VLS equilibrium calculation algorithm with different V_s : (a) V_s is set to be 0.5000 m³/kmol; (b) V_s is set to be 0.5500 m³/kmol; and (c) comparison of the different P-X phase boundaries yielded by our algorithm with different V_s . V: vapor phase; L: liquid phase; and S: solid asphaltene phase.

Figure 5-9 shows the weight fractions of the precipitated asphaltenes calculated by our algorithm with different V_s as a function of pressure and gas concentration at 61°C. Figures 5-9(a), 5-9(b), and 5-9(c) are generated with V_s set as 0.4323 m³/kmol, 0.5000 m³/kmol, and 0.5500 m³/kmol, respectively. These figures show that V_s can significantly affect how much asphaltenes will get precipitated in the mixture. The weight fractions of the precipitated asphaltenes shown in the three figures in Figure 5-9 are continuous everywhere, which proves that our algorithm performs well at all the tested conditions.





(b)



(c)

Figure 5-9 Weight fractions (in wt%) of the precipitated asphaltenes calculated by our algorithm with different V_s as a function of pressure and gas concentration at 61°C: (a) V_s is set to be 0.4323 m³/kmol; (b) V_s is set to be 0.5000 m³/kmol; and (c) V_s is set to be 0.5500 m³/kmol.

5.4.2 Oil Sample 2

Table 5-5 depicts the compositions of oil sample 2 and three injection gas [4, 35]. Oil sample 2 is named as fluid W1 by Srivastava *et al.* [4]. Oil sample 2 has a gravity of 29°API [4]. The molecular weight of C6+ in oil sample 2 is measured to be 205 g/mol [35], while its asphaltene content is measured to be 4.9 wt% [4].

Table 5-5 Compositions of oil sample 2 and three injection gases [4, 35]

Component	Oil sample 2	Gas 1 (pure CO ₂)	Gas 2 (impure CO ₂)	Gas 3 (impure CO ₂)
N ₂	0.96	0	0	5.1
CO ₂	0.58	100	90.1	89.8
H ₂ S	0.3	0	0	0
C1	4.49	0	9.9	5.1
C2	2.99	0	0	0
C3	4.75	0	0	0
<i>i</i> -C4	0.81	0	0	0
<i>n</i> -C4	1.92	0	0	0
<i>i</i> -C5	1.27	0	0	0
<i>n</i> -C5	2.19	0	0	0
C6+	79.74	0	0	0

5.4.2.1 Oil Characterization

Table 5-6 summarizes the composition and component properties of oil sample 2. The critical properties and acentric factors of the first ten components are taken from the literature [32, 33], while the mole fractions and component properties of the pseudo-components are calculated by this work. The method used to determine the mole fractions and component properties of the pseudo-components for oil sample 2 are the same as that used for oil sample 1.

Table 5-6 Composition and component properties of oil sample 2 [32, 33]

Component	Mole fraction (mol%)	Molecular weight (g/mol)	Critical temperature (K)	Critical pressure (bar)	Critical volume (m ³ /kmol)	Acentric factor
N ₂	0.96	28.01	126.20	34.40	0.0901	0.04
CO ₂	0.58	44.01	304.70	74.80	0.0940	0.23
H ₂ S	0.30	34.08	373.60	90.60	0.0976	0.10
C1	4.49	16.04	190.60	46.70	0.0993	0.01
C2	2.99	30.07	305.43	49.50	0.1479	0.10
C3	4.75	44.10	369.80	43.00	0.2029	0.15
<i>i</i> -C4	0.81	58.12	408.10	37.00	0.2627	0.18
<i>n</i> -C4	1.92	58.12	419.50	38.00	0.2547	0.20
<i>i</i> -C5	1.27	72.15	460.40	34.30	0.3058	0.23
<i>n</i> -C5	2.19	72.15	465.90	34.00	0.3040	0.24
C6-9	27.93	101.12	579.68	34.34	0.3897	0.32
C10-17	29.94	179.18	717.68	23.72	0.6536	0.54
C18-27	14.43	300.79	843.53	17.74	0.9369	0.77
C28A+	5.80	513.00	963.33	14.39	1.1924	0.96
C28B+	1.64	513.00	963.33	14.39	1.1924	0.96

5.4.2.2 Tuning of Key Model Parameters

Table 5-7 lists the adjustable parameters and their values used in our algorithm for oil sample 2 mixed with pure CO₂. For oil sample 2, we find that the weight fractions of the precipitated asphaltenes measured by the experiments conducted by Srivastava *et al.* [4] can be well matched by those calculated by our algorithm using the asphaltene content measured by experiments and the adjusted parameter values given in Table 5-7. Therefore, we do not tune the asphaltene content in this case study. Table 5-8 summarizes the BIPs used for oil sample 2 calculations. The BIPs between N₂ and other components (except C28B+) and the BIPs between H₂S and other components (except C28B+) are taken from the literature [33].

Table 5-7 Adjustable parameters and their values used in our algorithm for oil sample 2 mixed with pure CO₂

Parameter	Adjusted value
Critical gas concentration above which asphaltenes start to precipitate (mol%)	46
θ	4.7
BIP between CO ₂ and HCs	0.07

Table 5-8 BIPs used for oil sample 2 calculations [33]

	N ₂	CO ₂	H ₂ S	C28B+
N ₂	0	-0.0170	0.1767	0.3447
CO ₂	-0.0170	0	0.0974	0.3359
H ₂ S	0.1767	0.0974	0	0.3280
C1	0.0311	0.0700	0.080	0.3245
C2	0.0515	0.0700	0.0833	0.2433
C3	0.0852	0.0700	0.0878	0.1828
i-C4	0.1033	0.0700	0.0474	0.1374
n-C4	0.0800	0.0700	0.0600	0.1426
i-C5	0.0922	0.0700	0.0600	0.1129
n-C5	0.1000	0.0700	0.0600	0.1139
C6-9	0.1000	0.0700	0.0600	0.0780
C10-17	0.1000	0.0700	0.0600	0.0233
C18-27	0.1000	0.0700	0.0600	0.0038
C28A+	0.1000	0.0700	0.0600	0
C28B+	0.3447	0.3359	0.3280	0

Figure 5-10 shows the comparison between the weight fractions of the precipitated asphaltenes as a function of gas concentration calculated by our algorithm with the adjusted parameters and those obtained by experiments conducted by Srivastava *et al.* [4]. The injection gas is Gas 1 (pure CO₂) in Table 5-1. The tested temperature and pressure are 59°C and 160 bar. As shown in Figure 5-10, a good agreement can be seen between the calculated weight fractions of the precipitated asphaltenes and those measured by experiments, except one point which corresponds to the

highest precipitation amount. As mentioned in **Section 5.4.1.2**, this discrepancy may be caused by the improper value of the asphaltene content assumed in the calculations. Since the calculated results only fail to match one experimental data point, we regard the measured asphaltene content is reliable and do not tune it in this case study. From Figure 5-10, we can again conclude that our algorithm with the adjusted parameters can have a good description of the asphaltene precipitation phenomenon.

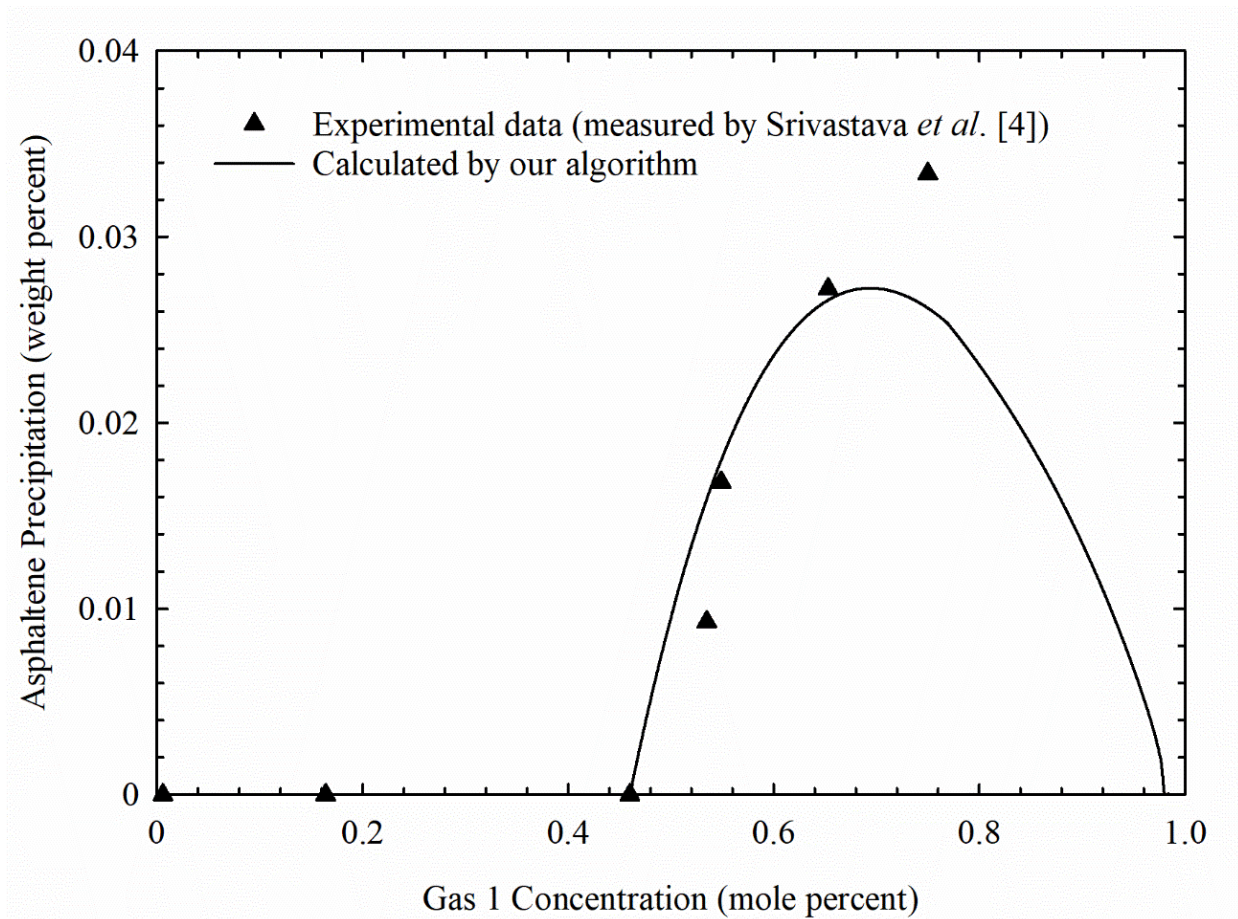


Figure 5-10 Comparison between the weight fractions of the precipitated asphaltenes as a function of gas concentration calculated by our algorithm with the adjusted parameters and those obtained by experiments conducted by Srivastava *et al.* [4] for oil sample 2 at 59°C and 160 bar

5.4.2.3 P-X Phase Diagram

Figure 5-11 depicts the P-X phase diagram calculated by the three-phase VLS equilibrium calculation algorithm with the adjusted parameters for oil sample 2 mixed with Gas 1 (pure CO₂). The temperature is set to be 59°C. V_s is calculated by the PR EOS to be 0.4505 m³/kmol [20]. The tested pressure is varied from 1 bar to 300 bar with a step size of 0.25 bar, while the tested gas concentration is varied from 0 mol% to 99 mol% with a step size of 0.25 mol%. This algorithm is run 475,209 times to generate the P-X phase diagram. Figure 5-11 shows that our three-phase VLS equilibrium calculation algorithm performs well at all the tested points. Note that there is a red region, named as Region 1, in Figure 5-11. This region is a three-phase VLS region. However, the liquid phase in this region is found to be very dense and more like an asphaltene phase. We think the reason underlying the appearance of this three-phase region is that the liquid phase cannot merge with the asphaltene phase due to the assumption that asphaltene phase is a pure asphaltene phase.

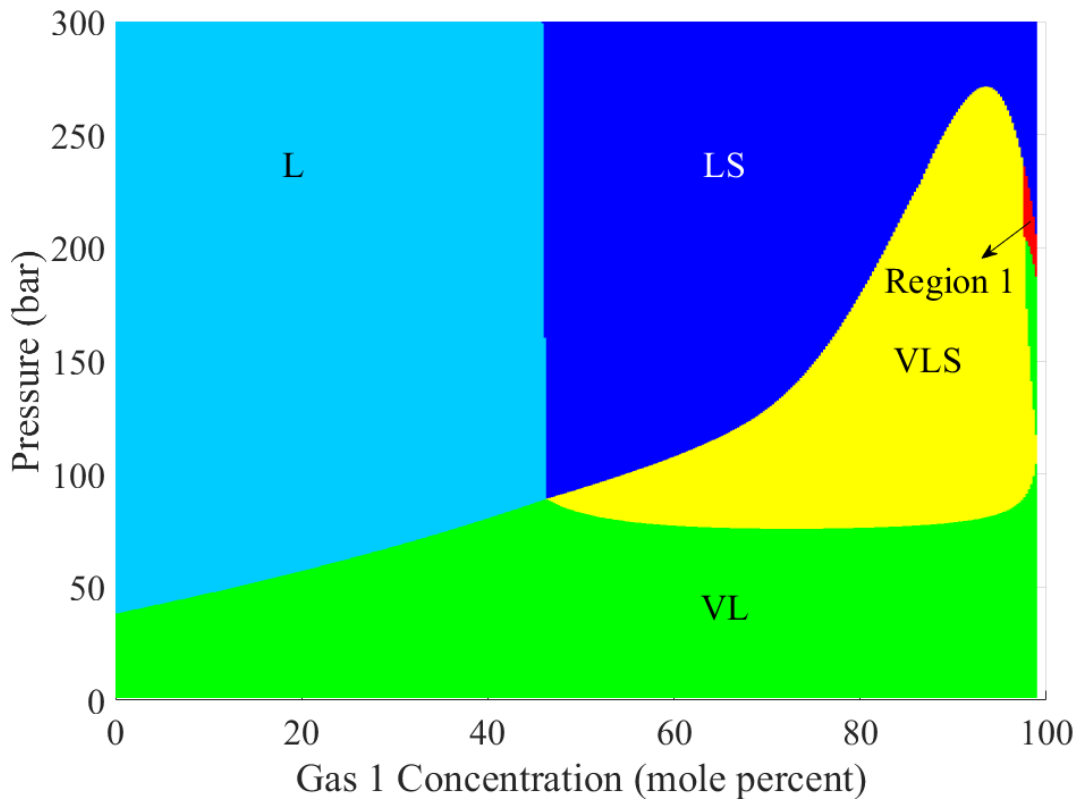
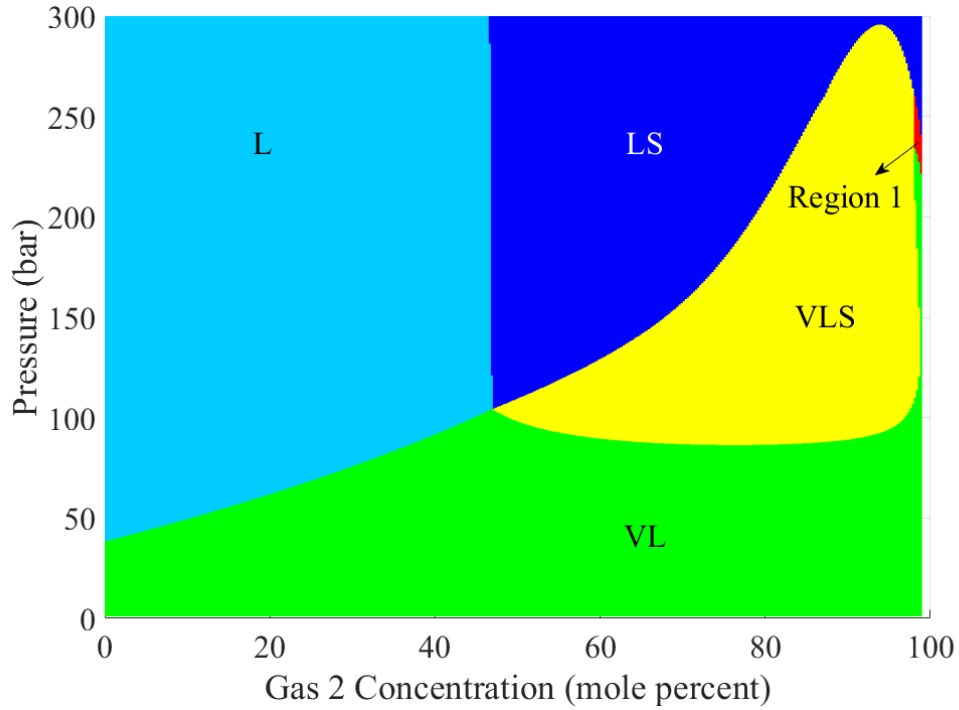


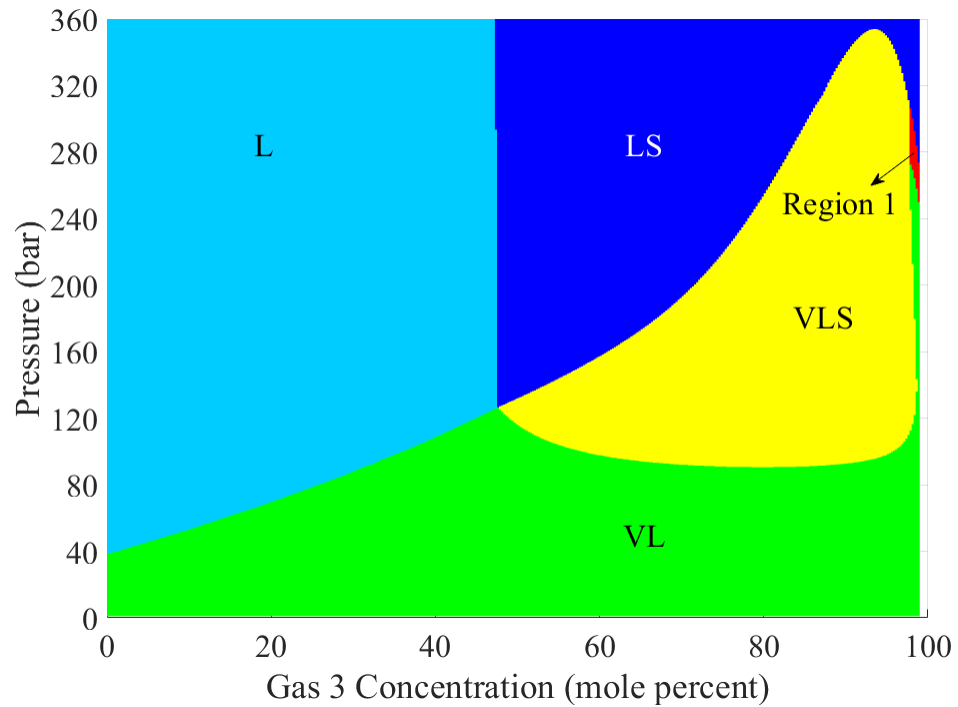
Figure 5-11 P-X phase diagram calculated by the three-phase VLS equilibrium calculation algorithm with the adjusted parameters for Oil sample 2 mixed with Gas 1 (pure CO₂) at 59°C. V: vapor phase; L: liquid phase; and S: solid asphaltene phase.

Figure 5-12 shows the P-X phase diagrams calculated by the three-phase VLS equilibrium calculation algorithm with the adjusted parameters for oil sample 2 mixed with impure CO₂. The temperature is set to be 59°C. V_s is calculated by the PR EOS to be 0.4505 m³/kmol [20]. The adjusted parameters used for modeling the phase behavior of oil sample 2 mixed with pure CO₂ are also applied for modeling the phase behavior of oil sample 2 mixed with impure CO₂. Figures 5-12(a) and 5-12(b) show the P-X phase diagrams generated for oil sample 2 mixed with Gas 2 and Gas 3, respectively. The tested pressure in Figure 5-12(a) is varied from 1 bar to 300 bar, while the

tested pressure in Figure 5-12(b) is varied from 1 bar to 360 bar. In both figures, a step size of 0.25 bar is used. Moreover, in both figures, the tested gas concentration is varied from 0 mol% to 99 mol% with a step size of 0.25 mol%. Our algorithm is run 475,209 times to generate Figures 5-12(a), while it is run 570,489 times to generate Figure 5-12(b). As shown in Figure 5-12, this algorithm performs well at all the tested points. Again, a special region (Region 1) appears in both figures.



(a)



(b)

Figure 5-12 P-X phase diagrams calculated by the three-phase VLS equilibrium calculation algorithm with the adjusted parameters for Oil sample 2 mixed with impure CO₂ at 59°C: (a) Gas 2 and (b) Gas 3. V: vapor phase; L: liquid phase; and S: solid asphaltene phase.

5.5 Conclusions

Based on the asphaltene-precipitation model proposed by Nghiem *et al.* [1], we develop a robust three-phase VLS equilibrium calculation algorithm. In this algorithm, new initialization methods for equilibrium ratios are provided for both stability test and flash calculation. To develop this three-phase VLS equilibrium calculation algorithm, a simple two-phase V/L-S flash calculation algorithm is first developed. Moreover, two three-phase VLS flash calculation algorithms are simultaneously developed to greatly ensure the robustness and efficiency of the three-phase VLS equilibrium calculation algorithm. Algorithm #1 is similar to the three-phase free-water VLA flash calculation algorithm developed by Li and Li [16]. It is more efficient but relies on the proper assignment of the initial equilibrium ratios. Algorithm #2 uses an outer loop to update the mole fraction of asphaltene phase and an inner loop to perform the two-phase VL flash calculation. This algorithm is more robust; but it is more time-consuming since several two-phase VL flash calculations are required to be conducted in the inner loop. Moreover, the prerequisite for conducting Algorithm #2 is that a three-phase VLS equilibrium actually appears.

We test the performance of this newly developed algorithm by several real reservoir fluids mixed with pure or impure CO₂. The parameters used in the asphaltene-precipitation model are first tuned to match the experimental asphaltene-precipitation data. With the adjusted parameters, our three-phase VLS equilibrium calculation algorithm is run hundreds of thousands of times to generate P-X phase diagrams for two crude oils mixed with pure or impure CO₂. Our algorithm performs well at all the test points. In general, four types of phase equilibria can be observed when

the crude oil is mixed with pure or impure CO₂: L equilibrium, LV equilibrium, LS equilibrium, and VLS equilibrium. When the gas concentration is very high, a small three-phase equilibrium region shows up between the two-phase VL equilibrium region and the two-phase LS equilibrium region. In this region, the three-phase equilibrium contains a vapor phase, an asphaltene phase, and a liquid phase which is very dense and more like an asphaltene phase. The appearance of this three-phase region can be attributed to the immiscibility of the dense liquid phase and the pure-asphaltene phase and the assumption that the asphaltene phase is assumed to be a pure phase.

Nomenclature

c	number of components or asphaltene component
f	fugacity
k	value of the stationary point (which is a constant) or BIP
K	equilibrium ratio
MW	molecular weight
P	pressure
R	universal gas constant
s	composition of the asphaltene phase
T	temperature
v	molar volume

V	molar volume
w	component weight fraction
x	composition of the liquid phase or non-asphaltene phase
$x_0, x_{01}, x_{02}, \dots$	compositions of the trial phase at negative stationary points
y	composition of the trial phase or vapor phase
z	composition of the tested phase or feed

Greek Letters

β	phase mole fraction
θ	exponential parameter
ω	acentric factor
Φ	fugacity coefficients

Subscript

2	component CO ₂
c	asphaltene component or critical properties
i	component index

j	component index
s	asphaltene phase
x	non-asphaltene phase or liquid phase
y	vapor phase

5.6 References

- [1] L.X. Nghiem, M.S. Hassam, R. Nutakki, A.E.D., George, Efficient modelling of asphaltene precipitation, presented at SPE Annual Technical Conference and Exhibition, Houston, Texas, USA, 3-6 October, 1993. SPE-26642-MS.
- [2] P.M. Jarrell, C.E. Fox, M.H. Stein, S.L. Webb, Practical aspects of CO₂ flooding (Vol. 22), 2002, Richardson, TX: Society of Petroleum Engineers, ISBN: 978-1-55563-096-6.
- [3] R.K. Srivastava, S.S. Huang, Laboratory investigation of Weyburn CO₂ miscible flooding, presented at Technical Meeting/Petroleum Conference of The South Saskatchewan Section, Regina, Saskatchewan, Canada, October 19-22, 1997.
- [4] R.K. Srivastava, S.S. Huang, M. Dong, Asphaltene deposition during CO₂ flooding, SPE Prod. Facil. 14 (04) (1999) 235-245. SPE-59092-PA.
- [5] S. Subramanian, S. Simon, J. Sjöblom, Asphaltene precipitation models: a review, J. Dispers. Sci. Technol. 37 (7) (2016) 1027-1049.

- [6] K. Leontaritis, G. Mansoori, Asphaltene flocculation during oil production and processing: A thermodynamic colloidal model, presented at SPE International Symposium on Oilfield Chemistry. San Antonio, Texas, USA, February 4-6, 1987. SPE-16258-MS.
- [7] M. Agrawala, H.W. Yarranton, An asphaltene association model analogous to linear polymerization, *Ind. Eng. Chem. Res.* 40 (21) (2001) 4664-4672.
- [8] P. David Ting, G.J. Hirasaki, W.G. Chapman, Modeling of asphaltene phase behavior with the SAFT equation of state, *Pet. Sci. Technol.* 21 (3-4) (2003) 647-661.
- [9] M.L. Michelsen, The isothermal flash problem. Part I. Stability, *Fluid Phase Equilibr.* 9 (1) (1982) 1-19.
- [10] M.L. Michelsen, The isothermal flash problem. Part II. Phase-split calculation, *Fluid Phase Equilibr.* 9 (1) (1982) 21-40.
- [11] Z. Li, A. Firoozabadi, General strategy for stability testing and phase-split calculation in two and three phases, *SPE J.* 17 (4) (2012) 1096-1107. SPE-129844-PA.
- [12] L.E. Baker, A.C. Pierce, K.D. Luks, Gibbs energy analysis of phase equilibria, *SPE J.* 22 (05) (1982) 731-742. SPE-9806-PA.
- [13] S.E. Gorucu, R.T. Johns, Robustness of three-phase equilibrium calculations, *J. Petrol. Sci. Eng.* 143 (2016) 72-85.
- [14] C.F. Leibovici, D.V. Nichita, A new look at multiphase Rachford-Rice equations for negative flashes, *Fluid Phase Equilibr.* 267 (2) (2008) 127-132.

- [15] M.L. Michelsen, Calculation of multiphase equilibrium, *Comput. Chem. Eng.* 18 (1994) 545-550.
- [16] R. Li, H.A. Li, New two-phase and three-phase Rachford-Rice algorithms based on free-water assumption, *Can. J. Chem. Eng.* 96 (1) (2018) 390-403.
- [17] C.H. Whitson, M.L. Michelsen, The negative flash, *Fluid Phase Equilibr.* 53 (1989) 51-71.
- [18] A. Lapene, D.V. Nichita, G. Debenest, M. Quintard, Three-phase free-water flash calculations using a new modified Rachford-Rice equation, *Fluid Phase Equilibr.* 297 (1) (2010) 121-128.
- [19] Y. Tang, S. Saha, An efficient method to calculate three-phase free-water flash for water-hydrocarbon systems, *Ind. Eng. Chem. Res.*, 42 (2003) 189-197.
- [20] D.Y. Peng, D.B. Robinson, A new two-constant equation of state, *Ind. Eng. Chem. Fund.* 15 (1) (1976) 59-64.
- [21] L.X. Nghiem, D.A. Coombe, Modelling asphaltene precipitation during primary depletion. *SPE J.* 2 (02) (1997) 170-176. SPE-36106-PA.
- [22] L.X. Nghiem, Y.K. Li, Computation of multiphase equilibrium phenomena with an equation of state. *Fluid Phase Equilibr.* 17 (1) (1984) 77-95.
- [23] H.H. Rachford, Jr., J.D. Rice, Procedure for use of electronic digital computers in calculating flash vaporization hydrocarbon equilibrium, *J. Pet. Tech.* 4 (10) (1952) 327-328.
- [24] K.B. Haugen, A. Firoozabadi, L. Sun, Efficient and robust three-phase split computations, *AIChE J.* 57 (9) (2011) 2555-2565.

- [25] M.L. Michelsen, J. Mollerup, Thermodynamic modelling: fundamentals and computational aspects, 2004, Tie-Line Publications, ISBN 87-989961-1-8.
- [26] R. Okuno, R. Johns, K. Sepehrnoori, A new algorithm for Rachford-Rice for multiphase compositional simulation, SPE J. 15 (2) (2010) 313-325. SPE-117752-PA.
- [27] G.M. Wilson, A modified Redlich-Kwong equation of state, application to general physical data calculations, presented at the 65th National AIChE Meeting, Cleveland, Ohio, USA, 4-7 May, 1968.
- [28] K.S. Pedersen, A. Fredenslund, P. Thomassen, Properties of oils and natural gases (Vol. 5), 1989, Gulf Publishing Co.
- [29] M.G. Kesler, B.I. Lee, Improve prediction of enthalpy of fractions, Hydro. Proc. 55 (1976) 153.
- [30] B.I. Lee, M.G. Kesler, A generalized thermodynamic correlation based on three-parameter corresponding states. AIChE J. 21(3) (1975) 510-527.
- [31] M. Riazi, Simplify property predictions, Hydro. Proc. 59 (1980) 115-116.
- [32] A. Kariman Moghaddam, A.H. Saeedi Dehaghani, Modeling of asphaltene precipitation in calculation of minimum miscibility pressure, Ind. Eng. Chem. Res. 56 (25) (2017) 7375-7383.
- [33] PVTsim Nova 3.3, Calsep A/S, Copenhagen, Denmark, 2019.
- [34] P.L. Chueh, J.M. Prausnitz, Vapor-liquid equilibria at high pressures: Calculation of partial molar volumes in nonpolar liquid mixtures, AIChE J. 13 (6) (1967) 1099-1107.

[35] M. Dong, S. Huang, S.B. Dyer, F.M. Mourits, A comparison of CO₂ minimum miscibility pressure determinations for Weyburn crude oil. *J. Petrol. Sci. Eng.* 31 (1) (2001) 13-22.

Appendix 5-A: Two-Phase V/L-S Flash Calculation Algorithm

Figure 5-A.1 depicts the flow chart of the two-phase V/L-S flash calculation algorithm. The detailed procedure of this algorithm is given below,

- (1) Input the pressure (P), temperature (T), feed (z_i), and thermodynamic properties of each component (T_{ci} , P_{ci} , and ω_i).
- (2) Initialize phase mole fraction of asphaltene phase (β_s) and set its tolerance (tol) to be 10^{-6} .
- (3) Calculate the composition of non-asphaltene phase (x_i) using Equation (5-10) and calculate the fugacity of each component in non-asphaltene phase (f_{ix}) based on PR EOS.
- (4) Calculate the absolute relative error (err) between the fugacities of asphaltene component in the non-asphaltene phase (f_{cx}) and the asphaltene phase (f_{cs}) using the following equation,

$$err = \frac{|f_{cs} - f_{cx}|}{f_{cs}} \quad (5-A.1)$$

- (5) If $err > tol$, update mole fraction of asphaltene phase (β_s) and go back to Step (3); otherwise, output the calculated phase mole fractions and phase compositions.

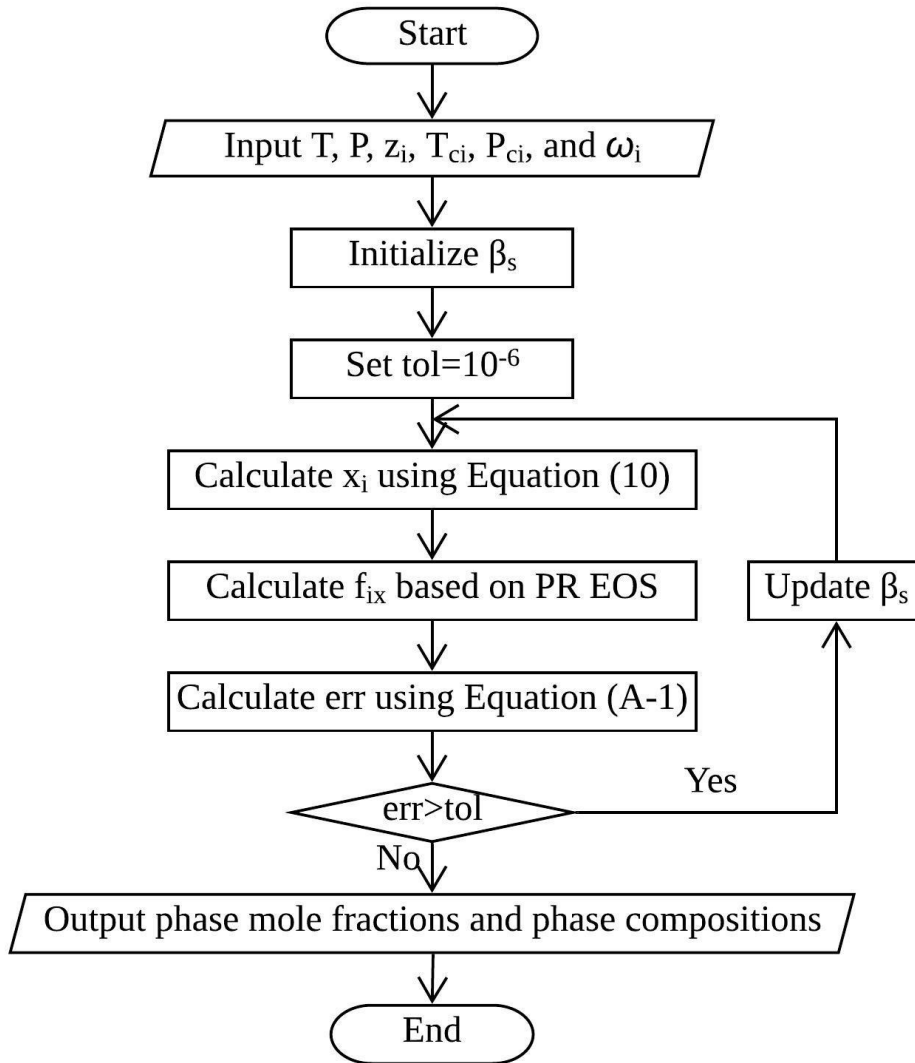


Figure 5-A.1 Flow chart of the two-phase V/L-S flash calculation algorithm

Appendix 5-B: Three-Phase VLS Flash Calculation Algorithm #2

Figure 5-B.1 depicts the flow chart of the three-phase VLS flash calculation Algorithm #2. The detailed procedure of this algorithms is summarized below,

- (1) Input the pressure (P), temperature (T), feed (z_i), and thermodynamic properties of each component (T_{ci} , P_{ci} , and ω_i).
- (2) Initialize mole fraction of asphaltene phase (β_s) and set its tolerance (tol) to be 10^{-6} .
- (3) Calculate the composition of non-asphaltene phase (z_{i2}) using Equation (5-19).
- (4) Conduct two-phase VL flash calculation to calculate phase mole fractions of liquid phase and vapor phase (β_x and β_y) and compositions of liquid and vapor phases (x_i and y_i).
- (5) Calculate the fugacities of each component in liquid and vapor phases (f_{ix} and f_{iy}) based on PR EOS.
- (6) Calculate the absolute relative error (err) between the fugacities of asphaltene component in the non-asphaltene phase (f_{cx}) and asphaltene phase (f_{cs}) using Equation (5-A.1).
- (7) If $err > tol$, update mole fraction of asphaltene phase (β_s) and go back to Step (3); otherwise, update phase mole fractions of liquid phase and vapor phase (β_x and β_y) by the following equation and output the calculated phase fractions and phase compositions,

$$\beta_x = \beta_x \times (1 - \beta_s); \beta_y = \beta_y \times (1 - \beta_s) \quad (5-B.1)$$

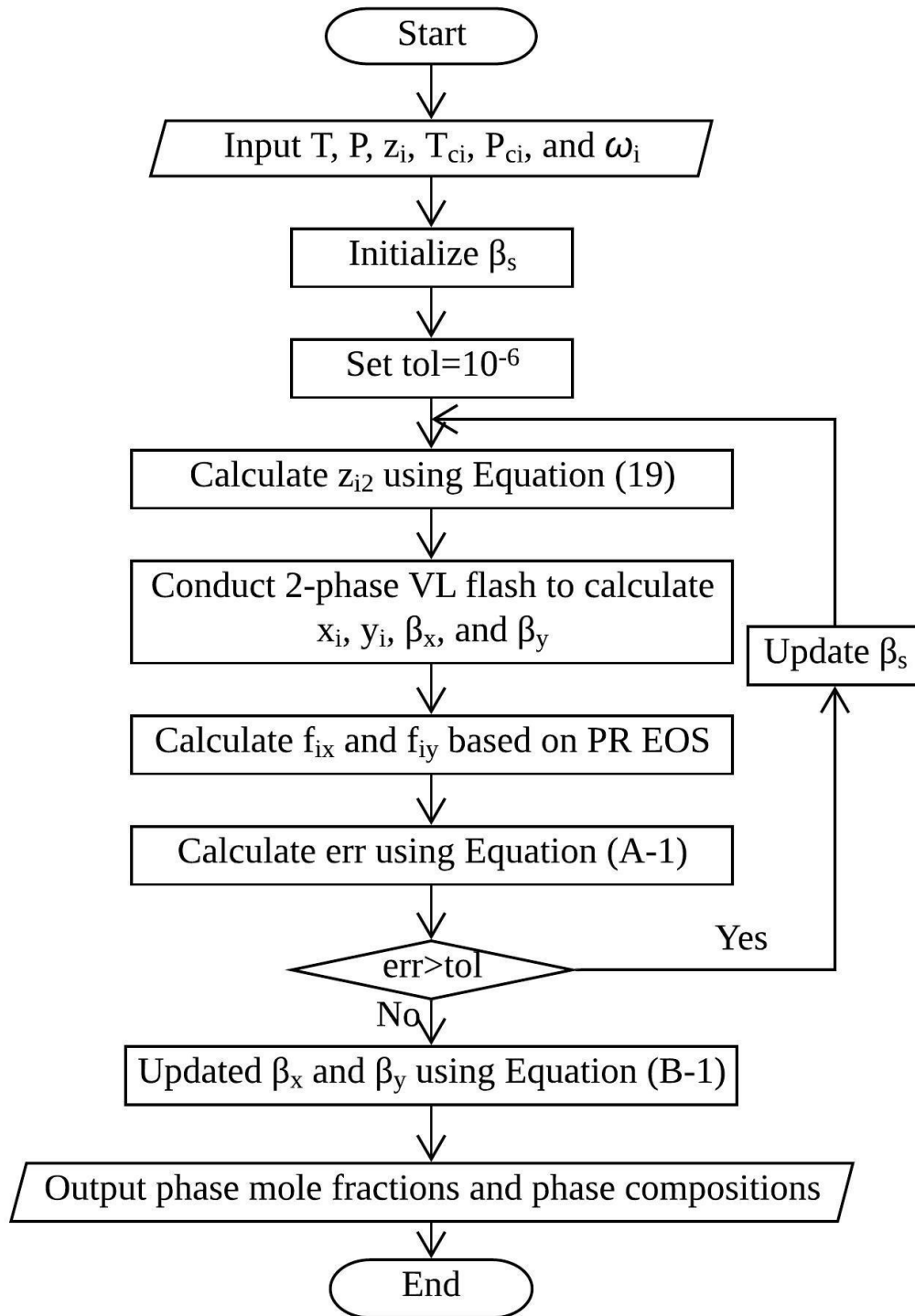


Figure 5-B.1 Flow chart of the three-phase VLS flash calculation Algorithm #2

**CHAPTER 6 A MODIFIED MULTIPLE-MIXING-CELL ALGORITHM
FOR MINIMUM MISCIBILITY PRESSURE PREDICTION WITH THE
CONSIDERATION OF ASPHALTENE-PRECIPIATION EFFECT**

A version of this chapter was presented as a poster at the 20th International Conference on Petroleum Phase Behavior and Fouling, held on 2-6 June 2019 in Kanazawa, Japan and has been submitted to *Industrial & Engineering Chemistry Research* for publication.

Abstract

Minimum miscibility pressure (MMP) is one of the most important design parameters in CO₂ flooding. Recent experimental studies show that the precipitation of asphaltenes in light oils can increase the MMP between injection gas and crude oil. To model the asphaltene-precipitation effect on MMP calculations, we develop a three-phase multiple-mixing-cell (MMC) algorithm by considering three-phase vapor-liquid-asphaltene (VLS) equilibria. This algorithm is developed by modifying the MMC method proposed by Ahmadi and Johns (2011). The three-phase VLS equilibrium calculation algorithm developed by Li and Li (2019) is integrated into the two-phase MMC algorithm. In the modified three-phase MMC algorithm, the first contact is conducted on two cells containing injection gas and reservoir oil. A three-phase equilibrium calculation is first conducted. If asphaltene phase appears, the mixture composition needs to be updated by excluding the precipitated asphaltenes. Then, negative two-phase flash will be conducted on the mixture with the updated composition. Considering that gas moves faster than liquid, the equilibrium vapor phase is always put ahead of the equilibrium liquid phase. A number of contacts are performed by mixing the neighbouring cells until all key tie lines are obtained. MMP is the pressure where the minimum key tie line length becomes zero. The modified algorithm provides a simple way to model the effect of asphaltene precipitation on MMP, since it is independent of relative permeability, volume of cells, and volume of injected gas, but only relies on the three-phase equilibrium calculations. Several example calculations are carried out to demonstrate the performance of our algorithm. The MMPs predicted by our algorithm and those predicted by the

two-phase MMC algorithm are both compared with the MMPs measured by experiments. For all tested examples, the MMPs predicted by our algorithm are larger than those predicted by the MMC algorithm without considering asphaltene-precipitation effect.

6.1 Introduction

Carbon dioxide (CO₂) flooding is a widely applied enhanced oil recovery process in light oil reservoirs [1]. In the design of CO₂ flooding, it is essential to precisely predict the minimum miscibility pressure (MMP) between CO₂ and reservoir fluid. At MMP, we can theoretically achieve 100% oil recovery from the reservoir. Asphaltene precipitation is common during CO₂ flooding due to the dynamic variations in the composition of reservoir fluids [2, 3]. Recent experimental studies reveal that the asphaltene deposition can increase the measured MMPs between the reservoir fluid and the injection gas [4]. Therefore, in order to obtain an accurate MMP between CO₂ and reservoir fluid, an MMP prediction method considering asphaltene-precipitation effect is required.

There are many experimental or computational methods that have been developed to determine MMPs. The most common experimental method for determining MMP is slim tube test [5]. It is considered to be reliable for MMP determination, since it can capture the dynamic flow interactions in porous media by considering the phase behavior of reservoir fluids. However, it is an expensive and time-consuming test. Moreover, Johns *et al.* [6] pointed out that slim tube experiments may fail to give an accurate MMP due to the limited number of experimental data points and the existence of dispersion phenomenon. Another common experimental method for determining MMP is multi-contact experiment. For miscibility achieved via a vaporizing or condensing drive during gas flooding, the multi-contact experiment can provide a precise MMP. However, the miscibility of most gas flooding processes is achieved via a combined condensing

and vaporizing drive, making the MMP measured by the multi-contact experiment less accurate [7, 8].

Since the experimental method for MMP determination is expensive and time-consuming, many attempts are made to develop computational methods for MMP determination based on equation of state (EOS). There are three main computational methods for MMP determination: slim tube compositional simulation, method of characteristics (MOC), and multiple mixing cell (MMC) method. Slim tube compositional simulation models the slim tube experiment in a numerical manner. The MMP can be developed at the inflection point on the recovery factor curve as a function of pressure [9]. Compared with other computational methods, one of the drawbacks of this computational method is its high computational demand. The MOC method is developed to analytically solve the $c-1$ key tie lines (where c represents the number of the component in the given mixture) [8, 10-12]. MMP is the minimum pressure where any of the key tie lines has a length of zero. However, the MOC method is complex and could easily converge to a wrong key tie line [13].

There are several published MMC approaches. Two MMC approaches are widely used. The first approach is a simplification of the slim tube compositional simulation by ignoring the flow equations [14, 15]. In this approach, a series of cells initially filled with oil are connected with each other. Then, a specified volume of gas is injected into the first cell. A two-phase equilibrium calculation is required to be conducted on the mixture in the first cell at the given

temperature/pressure condition. The excess volume will be moved to the second cell and mixed with the initial oil in the second cell. The same transfer is made on the following cells. After finishing the first injection, another injection will be conducted until a given volume of gas is injected. The aforementioned calculations will be conducted at different pressures. The oil recovery factor at each pressure should be recorded. Jaubert *et al.* [14] regarded the pressure, where 97% oil recovery is achieved, to be MMP. To model asphaltene-precipitation effect on MMPs, Moghaddam and Dehaghani [16] developed an MMP determination algorithm by extending the MMC method proposed by Jaubert *et al.* [14].

Another MMC approach is proposed by Ahmadi and Johns [17]. In this method, the first contact is conducted between two cells that are filled with injection gas and oil. By applying the negative two-phase flash calculation [18, 19], additional two cells will be obtained. The equilibrium gas phase is always put ahead of the equilibrium liquid phase considering that the gas phase moves faster than the liquid phase. A number of contacts are conducted by mixing the neighbouring cells until all $c-1$ key tie lines are obtained. The aforementioned calculations should be conducted at different pressures. The minimum tie line length is required to be recorded at each pressure. The MMP is the pressure where the minimum tie line length becomes zero. This MMC method provides a simple way to predict MMP, since it is independent of relative permeability, volume of cells, and volume of injected gas. The performance of this method only relies on the robustness of two-phase flash calculation algorithm. But currently the original MMC algorithm developed by Ahmadi and Johns [17] cannot accommodate the asphaltene precipitation phenomenon, and

thereby cannot model the effect of asphaltene precipitation on the MMP.

In this study, we develop an MMC algorithm considering asphaltene-precipitation effect by modifying the MMC method proposed by Ahmadi and Johns [17]. In the revised MMC algorithm, before each contact, we first perform a three-phase VLS equilibrium calculation to check if the asphaltene phase will appear. The three-phase VLS equilibrium calculation algorithm used in our algorithm is the one recently developed by Li and Li [20] with the application of the asphaltene-precipitation model proposed by Nghiem *et al.* [21]. If asphaltene phase appears, the asphaltene phase is considered to be deposited in the cell containing the liquid phase. Then, the composition of the mixture of the fluids in two neighbouring cells will be updated by excluding the asphaltene phase. Afterwards, a two-phase flash calculation is conducted on the mixture with the updated composition. Example calculations are conducted for several real fluid mixtures to test the performance of the newly developed algorithm. The MMPs predicted by our algorithm, together with those predicted by the MMC algorithm without considering asphaltene-precipitation effect, are both compared with the MMPs measured by slim tube experiments.

6.2 Thermodynamic Model

For two-phase flash calculations, Peng-Robinson (PR) EOS [22] is applied. PR EOS can be expressed as [22],

$$P = \frac{RT}{V-b} - \frac{a}{V(V+b)+b(V-b)} \quad (6-1)$$

where P represents pressure; T represents temperature; V represents molar volume; R represents

the universal gas constant; and a and b represent the attraction parameter and repulsion parameter, respectively. a and b can be calculated by [22],

$$a = 0.45724 \frac{R^2 T_c^2}{P_c} \alpha(T_r, \omega) \quad (6-2)$$

$$b = 0.07780 \frac{RT}{P_c} \quad (6-3)$$

where P_c represents critical pressure; T_c represents critical temperature; ω represents acentric factor; and T_r represents reduced temperature (which can be calculated by $T_r = \frac{T}{T_c}$). The

α -function in Equation (6-2) can be expressed as [23],

$$\alpha = \begin{cases} \left[1 + (0.37464 + 1.54226\omega - 0.26992\omega^2)(1 - T_r^{0.5}) \right]^2, & \omega < 0.49 \\ \left[1 + (0.379642 + 1.48503\omega - 0.164423\omega^2 + 0.016666\omega^3)(1 - T_r^{0.5}) \right]^2, & \omega \geq 0.49 \end{cases} \quad (6-4)$$

For a mixture, the van der Waals mixing rule is used,

$$a = \sum_{i=1}^c \sum_{j=1}^c x_i x_j (1 - k_{ij}) \sqrt{a_i a_j} \quad (6-5)$$

$$b = \sum_{i=1}^c x_i b_i \quad (6-6)$$

where c represents the number of components in the mixture; x represents component mole fraction; k_{ij} represent the binary interaction parameter (BIP) between components i and j ; and the subscripts i and j represent components i and j , respectively. The detailed procedure for conducting two-phase flash calculation is proposed by Michelsen [24].

For the three-phase VLS equilibrium calculation algorithm proposed by Li and Li [20], the

asphaltene-precipitation model developed by Nghiem *et al.* [21] is applied. In this model, asphaltene phase is considered as a pure dense phase only containing asphaltene. The fugacity of asphaltene in the asphaltene phase is calculated by [21],

$$\ln f_s = \ln f_s^* + \frac{V_s(P - P^*)}{RT} \quad (6-7)$$

where P and P^* represent the actual pressure and the reference pressure, respectively; f_s and f_s^* represent the fugacities of asphaltene in the asphaltene phase at P and P^* , respectively; V_s represents the asphaltene molar volume; and the subscript s represents asphaltene phase. As mentioned above, for vapor and liquid phases, PR EOS [22] is applied.

Li and Li [20] provided the details of the three-phase VLS equilibrium calculation algorithm. In their three-phase VLS equilibrium calculation algorithm, the appearance of asphaltene phase is checked by comparing the fugacity of asphaltene component in the non-asphaltene phase against that in the asphaltene phase, while the appearance of non-asphaltene phase (i.e., vapor or liquid phase) is determined by stability test. The detailed procedure of stability test is proposed by Michelsen [25]. If neither of these two cases appears, the tested mixture is stable. If only asphaltene phase appears, a two-phase vapor/liquid-asphaltene flash calculation is required. If only non-asphaltene phase appears, a two-phase vapor-liquid flash calculation needs to be conducted. After that, the results yielded by the two-phase flash calculation should be again checked if the asphaltene phase will appear. If it appears, a three-phase flash calculation needs to be conducted. If both asphaltene and non-asphaltene phases may appear, a three-phase flash

calculation is first conducted. If the results yielded by the three-phase flash calculation are unphysical, a two-phase flash calculation is then conducted. Moreover, the stability of the results yielded by the two-phase flash calculation should be checked. If it is unstable, a three-phase flash calculation should be again conducted. Two different three-phase VLS flash calculation algorithms are developed and incorporated into the three-phase equilibrium calculation algorithm to ensure its robustness and efficiency. To simulate CO₂ flooding in light oil reservoirs, new initialization approaches for both stability tests and flash calculations are proposed in their work [20].

6.3 MMC Algorithm Considering Asphaltene-Precipitation Effect

Figure 6-1 depicts the schematic of the contact method adopted by the MMC method that considers the asphaltene-precipitation effect. This MMC algorithm is a modification of the MMC algorithm developed by Ahmadi and Johns [17]. The detailed procedure for conducting this modified MMC algorithm is summarized as follows,

- (1) Fill two cells with the injection gas (G) and reservoir oil (O), respectively. Put the cell filled with the injection gas in the upstream, while put the cell filled with the reservoir oil in the downstream.
- (2) Mix the injection gas and the reservoir oil. The composition of the mixture can be calculated by the following equation,

$$Z_i = O_i + \alpha(G_i - O_i), \quad i = 1, \dots, c \quad (6-8)$$

where Z_i , G_i , and O_i represent the mole fractions of component i in the gas-oil mixture,

injection gas, and oil, respectively; α represents the mole fraction of gas phase; c represents the number of components; and the subscript i represents the component index. As mentioned by Ahmadi and Johns [17], the value of α will not affect the final results. In our test, α is set to be 0.5.

(3) Conduct three-phase VLS equilibrium calculation on the gas-oil mixture at the given temperature/pressure condition. The three-phase VLS equilibrium calculation algorithm developed by Li and Li [20] is applied in this MMC algorithm. The asphaltene-precipitation model used in their algorithm is the one developed by Nghiem *et al.* [21]. In that model, Nghiem *et al.* [21] assumed that the asphaltene phase only contain asphaltene component. Based on such assumption, the composition of asphaltene phase can be simply expressed as follows,

$$S_i = \begin{cases} 1, & i = c \\ 0, & i \neq c \end{cases} \quad (6-9)$$

where S_i represents the mole fraction of component i in the asphaltene phase and component c represents the asphaltene component. The possible phases yielded by the three-phase equilibrium calculation will be an equilibrium liquid phase (X), an equilibrium vapor phase (Y), and an asphaltene phase (S). If asphaltene phase appears based on the three-phase equilibrium calculations, we assume that it will deposit and not participate in the subsequent calculations. Therefore, the composition of the mixture can be updated by the following equation,

$$Z_i = \begin{cases} Z_i / (1 - \beta_s), & i = 1, \dots, c - 1 \\ (Z_i - \beta_s) / (1 - \beta_s), & i = c \end{cases} \quad (6-10)$$

where β_s represents the mole fraction of asphaltene phase calculated by the three-phase VLS equilibrium calculation algorithm. If the asphaltene phase does not appear, the composition of the mixture will not change.

- (4) Conduct two-phase flash calculation on the gas-oil mixture with the updated composition at the given temperature/pressure condition. The negative flash [18, 19] is allowed in this MMC algorithm. PR EOS is used in two-phase flash calculations [22]. The two-phase flash calculation will give us an equilibrium liquid phase (X) and an equilibrium vapor phase (Y). Based on the fact that gas moves faster than the liquid, the equilibrium vapor phase will be put ahead of the equilibrium liquid phase. The aforementioned steps show the procedure of the first contact. The tie line length between the equilibrium liquid phase and the equilibrium vapor phase requires to be recorded for each contact. It can be calculated by the following equation,

$$TL = \sqrt{\sum_{i=1}^c (X_i - Y_i)^2} \quad (6-11)$$

where TL represents the tie line length and X_i and Y_i represent the mole fractions of component i in the equilibrium liquid phase and equilibrium vapor phase, respectively.

- (5) There are two contacts in the second contact. One is conducted on the mixture of the injection gas and the equilibrium liquid phase, while the other is conducted on the mixture of the fresh oil and the equilibrium vapor phase. Similar to the first contact, the three-phase VLS

equilibrium calculation is first conducted on the mixture to check whether the asphaltene phase will appear or not. If the asphaltene phase appears, the composition of the mixture needs to be updated by excluding the precipitated asphaltene. Two-phase flash calculation is subsequently conducted on the updated mixture. Both of these two contacts will give us an equilibrium liquid phase and an equilibrium vapor phase. Together with the injection gas and the fresh oil, there will be six cells. These cells are schematically shown in Figure 6-1.

- (6) Additional contacts between the neighbouring cells are required until all $c-1$ key tie lines are developed. Note that, in the N^{th} contact, the contacts will be conducted N times. These contacts will be numbered from 1 to N in a left-to-right order as shown in Figure 6-1. As mentioned by Ahmadi and Johns [17], the key tie line is considered to be fully developed if the same values of tie line lengths are yielded by three neighbouring contacts. The minimum tie line length should be recorded.

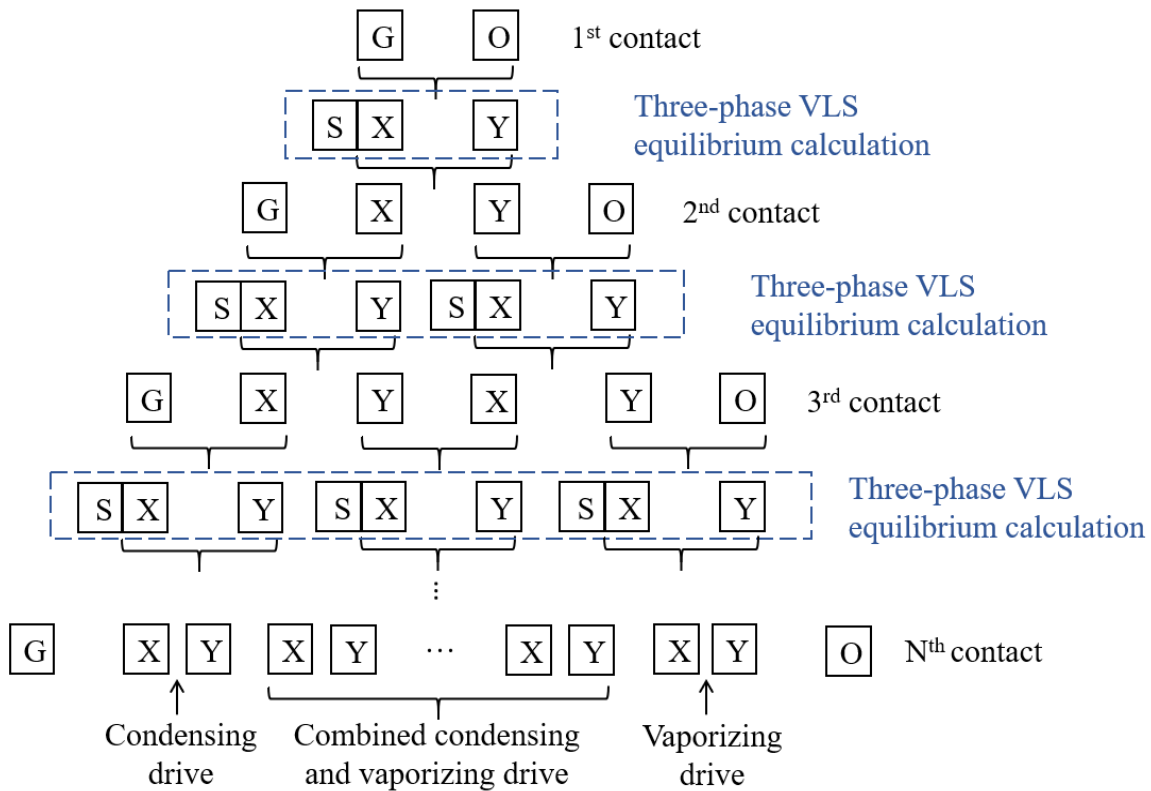


Figure 6-1 Schematic of the contact method adopted by the MMC method considering asphaltene-precipitation effect. G: injection gas; O: oil; X: equilibrium liquid phase; Y: equilibrium vapor phase; S: solid asphaltene phase; and 1st contact, 2nd contact, 3rd contact, ..., and Nth contact: contact times.

This MMC algorithm is performed to develop the minimum tie line length at the given temperature/pressure conditions. As shown in Figure 6-1, in this MMC algorithm, the condensing drive occurs at the downstream, while the vaporizing drive occurs at the upstream. In the middle of this development, the miscibility is developed by a combined condensing and vaporizing drive. To obtain the MMP, the MMC algorithm is required to be conducted at different pressures. As pressure increases, the developed minimum tie line length will decrease. In this work, MMP is estimated by the power-law extrapolation using the minimum tie line lengths at the last several

pressures by [17],

$$TL^n = aP + b \quad (6-12)$$

where n represents the exponential parameter; P represents pressure; and a and b are constants representing the slope and the intercept of y -axis, respectively. The values of a , b , and n can be finalized when the correlation coefficient exceeds 0.999. The MMP is the pressure at which the minimum tie line length becomes zero. This MMC algorithm only relies on the performance of three-phase VLS equilibrium calculations and two-phase flash calculations. In comparison with other methods used to estimate MMP which also relies on relative permeability, volume of cells, and volume of injected gas, the revised MMC algorithm provides a simple way for modeling the effect of asphaltene precipitation on MMP.

6.4 Results and Discussion

In this work, three oil and gas samples from Weyburn reservoir in Saskatchewan, Canada, are used to test the performance of the newly developed MMC algorithm that couples the asphaltene-precipitation effect. Both of the MMPs predicted by our algorithm and those predicted by the MMC algorithm proposed by Ahmadi and Johns [17] without considering asphaltene-precipitation effect are compared with the MMPs measured by slim tube experiments conducted by Dong *et al.* [26]. Table 6-1 lists the compositions of Fluid W1 and three injection gases [3, 26]. Fluid W1 has a gravity of 29°API [3] and a molecular weight of C6+ of 205 g/mol [26]. The asphaltene content of Fluid W1 is measured to be 4.9 wt% [3].

Table 6-1 Compositions of Fluid W1 and three injection gases [3, 26]

Component	Fluid W1	Gas 1 (pure CO₂)	Gas 2 (impure CO₂)	Gas 3 (impure CO₂)
N ₂	0.96	0	0	5.1
CO ₂	0.58	100	90.1	89.8
H ₂ S	0.30	0	0	0
C1	4.49	0	9.9	5.1
C2	2.99	0	0	0
C3	4.75	0	0	0
<i>i</i> -C4	0.81	0	0	0
<i>n</i> -C4	1.92	0	0	0
<i>i</i> -C5	1.27	0	0	0
<i>n</i> -C5	2.19	0	0	0
C6+	79.74	0	0	0

Table 6-2 depicts the composition and component properties of Fluid W1. The critical properties and acentric factor of the first ten components are cited from literatures [16, 27], while the mole fractions and component properties of pseudo-components are calculated by Li and Li [20].

Table 6-2 Composition and component properties of Fluid W1 [16, 20, 27]

Component	Mole fraction (mol%)	Molecular weight (g/mol)	Critical temperature (K)	Critical pressure (bar)	Critical volume (m³/kmol)	Acentric factor
N ₂	0.96	28.01	126.20	34.40	0.0901	0.04
CO ₂	0.58	44.01	304.70	74.80	0.0940	0.23
H ₂ S	0.30	34.08	373.60	90.60	0.0976	0.10
C1	4.49	16.04	190.60	46.70	0.0993	0.01
C2	2.99	30.07	305.43	49.50	0.1479	0.10
C3	4.75	44.10	369.80	43.00	0.2029	0.15
<i>i</i> -C4	0.81	58.12	408.10	37.00	0.2627	0.18
<i>n</i> -C4	1.92	58.12	419.50	38.00	0.2547	0.20
<i>i</i> -C5	1.27	72.15	460.40	34.30	0.3058	0.23
<i>n</i> -C5	2.19	72.15	465.90	34.00	0.3040	0.24
C6-9	27.93	101.12	579.68	34.34	0.3897	0.32
C10-17	29.94	179.18	717.68	23.72	0.6536	0.54
C18-27	14.43	300.79	843.53	17.74	0.9369	0.77
C28A+	5.80	513.00	963.33	14.39	1.1924	0.96
C28B+	1.64	513.00	963.33	14.39	1.1924	0.96

To apply the asphaltene-precipitation model developed by Nghiem *et al.* [21] in the three-phase VLS equilibrium calculations, Li and Li [20] tuned some key model parameters in the asphaltene-precipitation model by matching the asphaltene precipitation data measured by Srivastava *et al.* [3] for Fluid W1. Table 6-3 summarizes the adjustable parameters and their values adjusted by Li and Li [20] for Fluid W1 mixed with pure CO₂.

Table 6-3 Adjustable parameters and their adjusted values used in three-phase VLS equilibrium calculation algorithm for Fluid W1 mixed with pure CO₂ [20]

Parameter	Adjusted value
Critical gas concentration above which asphaltenes start to precipitate (mol%)	46
θ (exponential parameter in Equation (13))	4.7
BIP between CO ₂ and HCs	0.07

Table 6-4 shows the BIPs used by Li and Li [20] for Fluid W1. The BIPs between N₂ and other components (except C28B+) and that between H₂S and other components (except C28B+) are taken from literature [27]. The BIPs between asphaltene component (C28B+) and other components are calculated by the Chueh and Prausnitz model [28],

$$k_{ij} = 1 - \left[\frac{2v_{ci}^{1/6}v_{cj}^{1/6}}{v_{ci}^{1/3} + v_{cj}^{1/3}} \right]^{\theta} \quad (6-13)$$

where v_c represents critical molar volume; θ represents the exponential parameter; and the subscripts i and j represent components i and j , respectively. BIPs between asphaltene component (C28B+) and other components are calculated by the same value of θ .

Table 6-4 BIPs used for Fluid W1 [20, 27]

	N ₂	CO ₂	H ₂ S	C28B+
N ₂	0	-0.0170	0.1767	0.3447
CO ₂	-0.0170	0	0.0974	0.3359
H ₂ S	0.1767	0.0974	0	0.3280
C1	0.0311	0.0700	0.080	0.3245
C2	0.0515	0.0700	0.0833	0.2433
C3	0.0852	0.0700	0.0878	0.1828
<i>i</i> -C4	0.1033	0.0700	0.0474	0.1374
<i>n</i> -C4	0.0800	0.0700	0.0600	0.1426
<i>i</i> -C5	0.0922	0.0700	0.0600	0.1129
<i>n</i> -C5	0.1000	0.0700	0.0600	0.1139
C6-9	0.1000	0.0700	0.0600	0.0780
C10-17	0.1000	0.0700	0.0600	0.0233
C18-27	0.1000	0.0700	0.0600	0.0038
C28A+	0.1000	0.0700	0.0600	0
C28B+	0.3447	0.3359	0.3280	0

Figure 6-2 shows the pressure-composition (P-X) diagram generated by Li and Li [20] for Fluid W1 mixed with Gas 1 at 59°C. As mentioned by Li and Li [20], this P-X phase diagram is generated by running the three-phase VLS equilibrium calculation algorithm (proposed in their work) a total of 475,209 times at different pressures and gas concentrations. As shown in Figure 6-1, their algorithm performs well at all the tested conditions. Note that no asphaltene precipitates at lower pressures. For Fluid W1 mixed with Gas 2 and 3, similar P-X phase diagrams are generated by Li and Li [20].

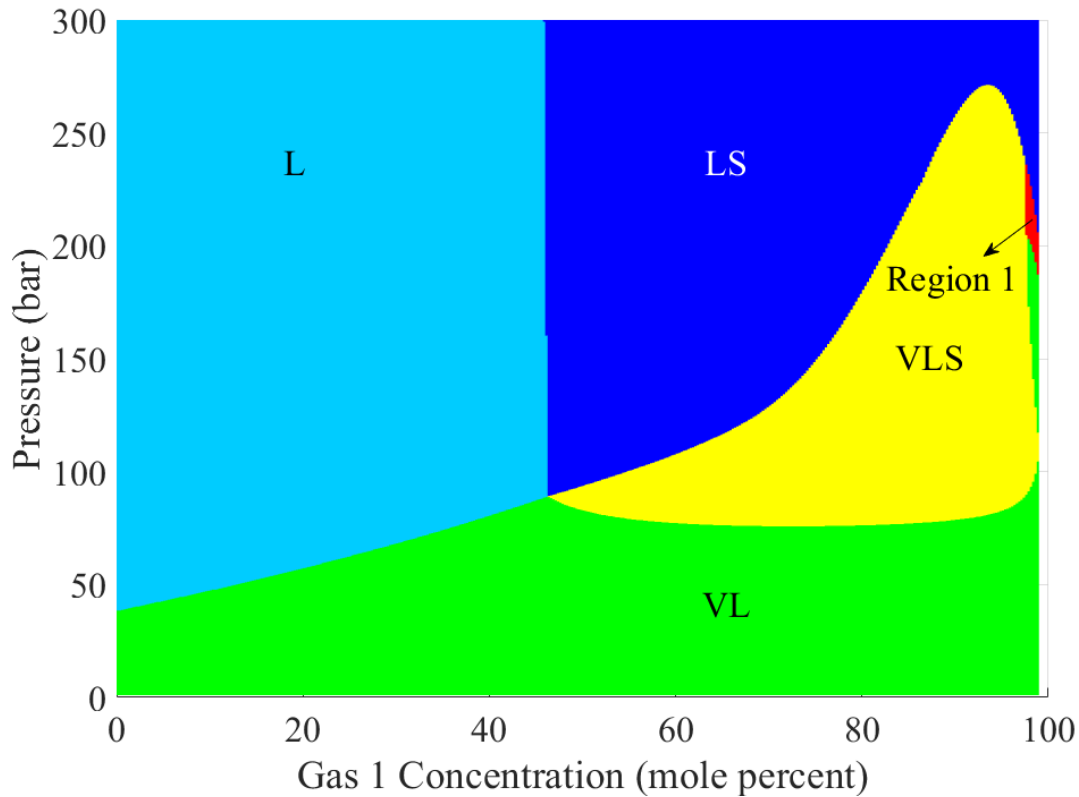
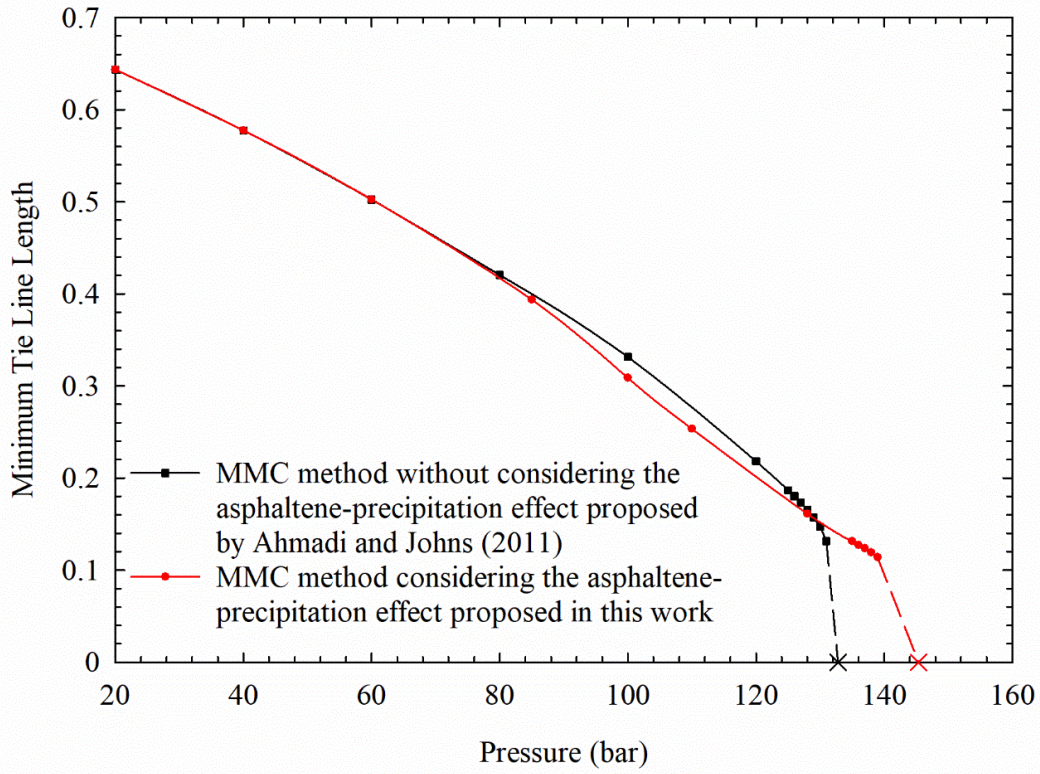


Figure 6-2 P-X phase diagram generated by Li and Li [20] for Fluid W1 mixed with Gas 1 (pure CO₂) at 59°C. V: vapor phase; L: liquid phase; S: solid asphaltene phase; and Region 1: three-phase VLS equilibrium region where the liquid phase is very dense and more like an asphaltene phase.

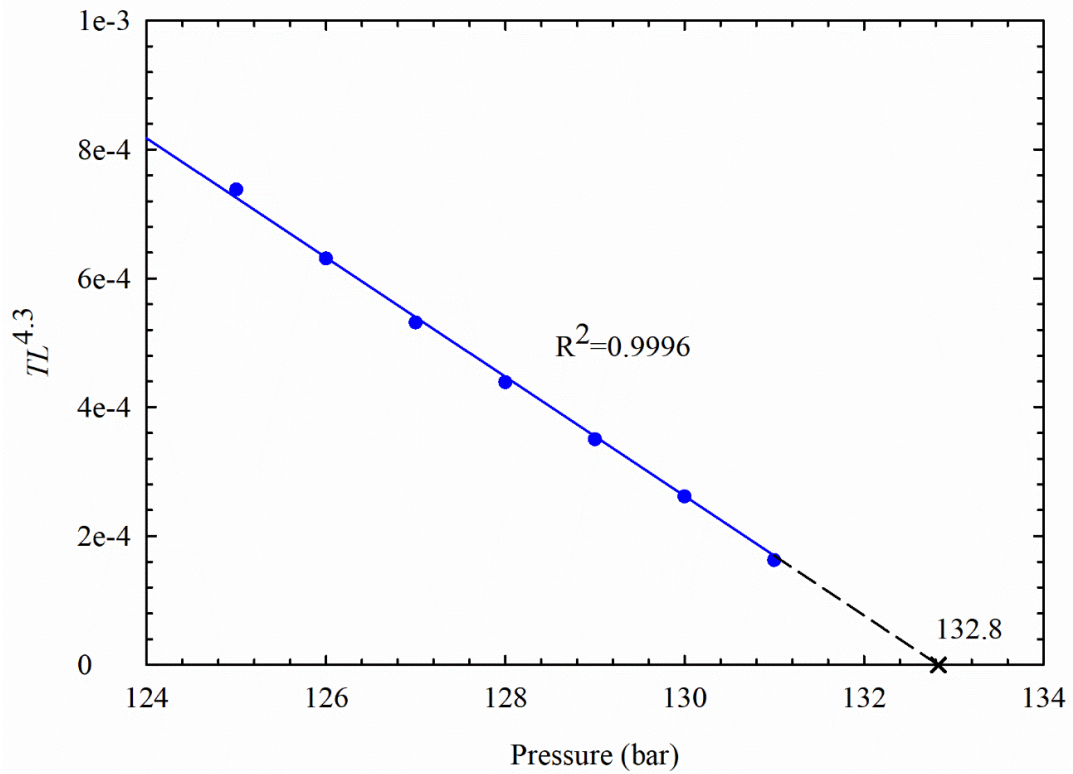
6.4.1 Case Study 1: Fluid W1 Displaced by Gas 1 (Pure CO₂)

Figure 6-3 shows the variation of the minimum tie lie lengths at different pressures for Fluid W1 displaced by Gas 1 at 59°C. Figure 6-3(a) depicts the comparison of the minimum tie lie lengths with and without considering the asphaltene-precipitation effect. In Figure 6-3(a), the black line represents the results calculated by the MMC method developed by Ahmadi and Johns [17] without considering asphaltene-precipitation effect, while the red line presents the results yielded by our MMC algorithm considering asphaltene-precipitation effect. As shown in Figure 6-3(a), at

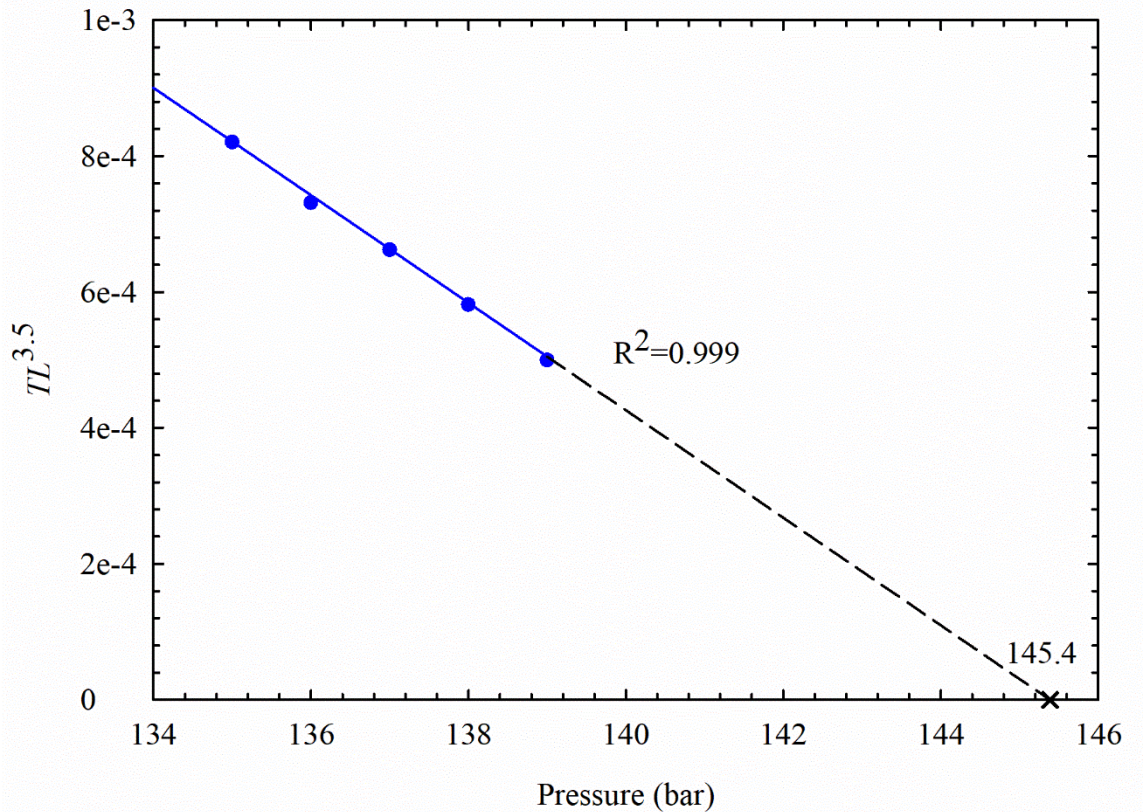
lower pressures (where no asphaltene precipitates), the minimum tie line lengths calculated by our algorithm are the same as those calculated by the MMC method proposed by Ahmadi and Johns [17]; while at higher pressures (where asphaltene precipitates), the minimum tie line lengths calculated by our algorithm are smaller than those calculated by the MMC method proposed by Ahmadi and Johns [17]. Moreover, MMP yielded by our MMC algorithm (which is 145.4 bar) is larger than that yielded by the algorithm proposed by Ahmadi and Johns [17] (which is 132.8 bar). These MMPs are estimated by the power-law extrapolation as shown in Equation (6-12). Figures 6-3(b) and 6-3(c) present the extrapolation of the minimum tie line lengths yielded by the MMC method proposed by Ahmadi and Johns [17] and that yielded by the MMC method proposed by this work, respectively. The exponential parameter (n) used in Figure 6-3(b) is 4.3, while that used in Figure 6-3(c) is 3.5.



(a)



(b)



(c)

Figure 6-3 Variation of the minimum tie line lengths as a function of pressure for Fluid W1 displaced by Gas 1 at 59°C: (a) comparison of the minimum tie line lengths yielded by the MMC method proposed by Ahmadi and Johns [17] and those yielded by the MMC method proposed by this work; (b) extrapolation of the minimum tie line lengths yielded by the MMC method proposed by Ahmadi and Johns [17]; and (c) extrapolation of the minimum tie line lengths yielded by the MMC method proposed by this work.

Figure 6-4 depicts the variation of the tie line length calculated by our MMC algorithm as a function of contact number for Fluid W1 displaced by Gas 1 at 59°C and 110 bar. Profiles of tie line lengths yielded at different contact times are shown in Figure 6-4. As seen in Figure 6-4, the key tie lines are gradually developed as contact time increases, demonstrating that our algorithm performs well in detecting the key tie lines. The shortest key tie line is nearly developed after the

25th contact, whereas it is considered to be fully developed after the 100th contact. As shown in Figure 6-4, the shortest key tie line is the crossover tie line in the middle of the contacts, indicating that the miscibility of Fluid W1 and Gas 1 will be generated by a combined condensing and vaporizing drive.

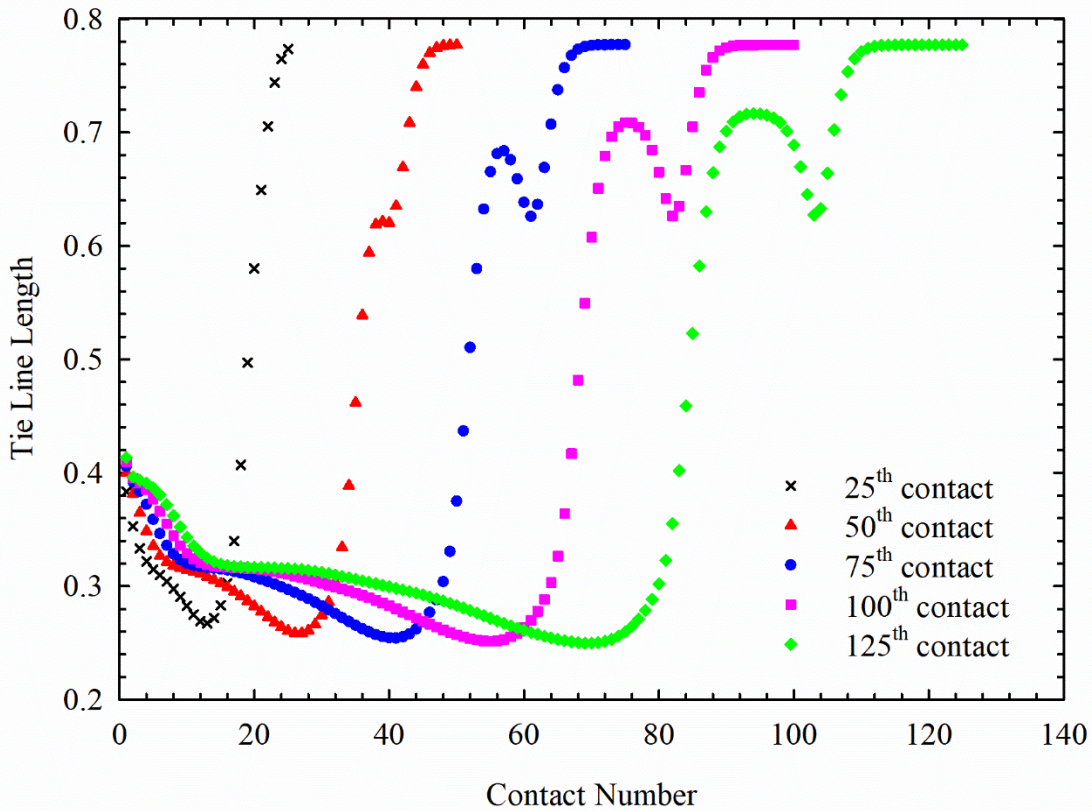
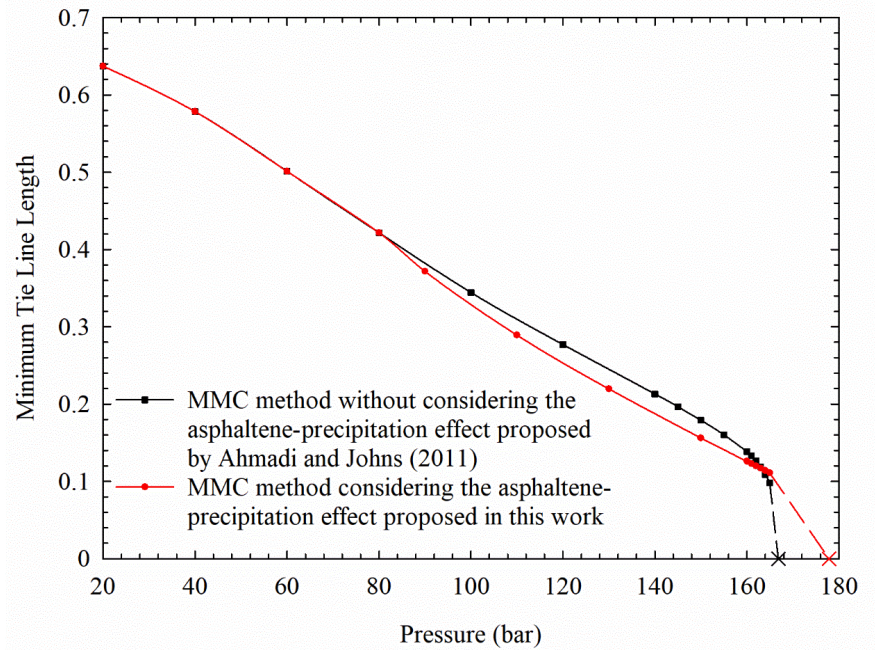


Figure 6-4 Variation of the tie line length calculated by our MMC algorithm as a function of contact number for Fluid W1 displaced by Gas 1 at 59°C and 110 bar

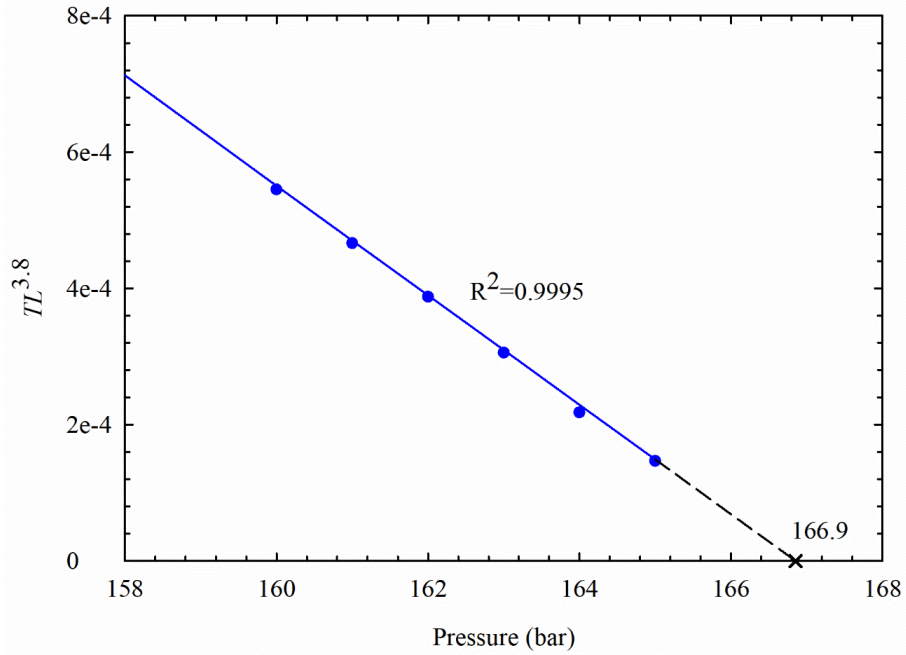
6.4.2 Case Study 2: Fluid W1 Displaced by Gas 2 (Impure CO₂)

Figure 6-5 shows the variation of the minimum tie lie lengths as a function of pressure for Fluid W1 displaced by Gas 2 at 59°C. Figure 6-5(a) depicts the comparison of the minimum tie lie

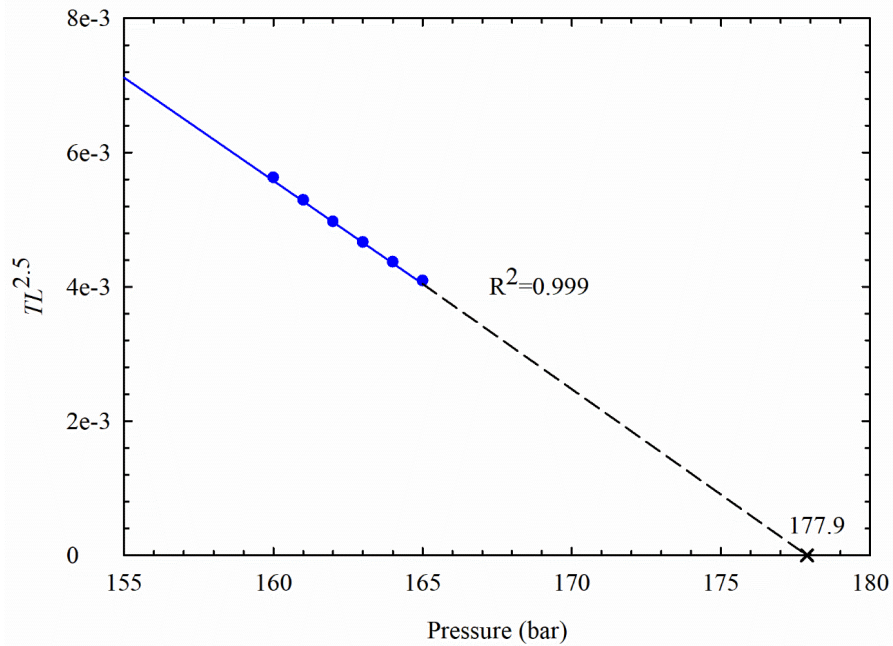
lengths with and without considering the asphaltene-precipitation effect. Similar to Figure 6-3(a), the same minimum tie line lengths are calculated by these two algorithms at lower pressures (where no asphaltene precipitates); while at higher pressures (where asphaltene precipitates), smaller minimum tie line lengths are calculated by our algorithm compared with those calculated by the MMC method proposed by Ahmadi and Johns [17]. Again, our MMC algorithm predicts a larger MMP (i.e., 177.9 bar) than that predicted by the algorithm proposed by Ahmadi and Johns [17] (i.e., 166.9 bar). The power-law extrapolation as shown in Equation (6-12) is adopted to predict these MMPs. Figures 5(b) and 5(c) present the extrapolation of the minimum tie line lengths yielded by the MMC method proposed by Ahmadi and Johns [17] and that yielded by the MMC method proposed by this work, respectively. The exponential parameters (n) used in Figures 6-5(b) and 6-5 (c) are 3.8 and 2.5, respectively.



(a)



(b)



(c)

Figure 6-5 Variation of the minimum tie lie lengths as a function of pressure for Fluid W1 displaced by Gas 2 at 59°C: (a) comparison of the minimum tie lie lengths yielded by the MMC method proposed by Ahmadi and Johns [17] and those yielded by the MMC method proposed by this work; (b) extrapolation of the minimum tie lie lengths yielded by the MMC method proposed by Ahmadi and Johns [17]; and (c) extrapolation of the minimum tie lie lengths yielded by the MMC method proposed by this work.

Figure 6-6 presents the variation of the tie line length calculated by our MMC algorithm as a function of contact number for Fluid W1 displaced by Gas 2 at 59°C and 110 bar. Figure 6-6 contains profiles of tie line lengths generated at different contact times. As contact time increases, the key tie lines are gradually detected. As shown in Figure 6-6, at the 25th contact, the shortest key tie line is almost developed. In this calculation, we consider the shortest key tie line to be fully developed at the 100th contact. Same as shown in Figure 6-4, the shortest key tie line appears at the middle of this development, indicating that a combined condensing and vaporizing drive dominates the gas flooding process.

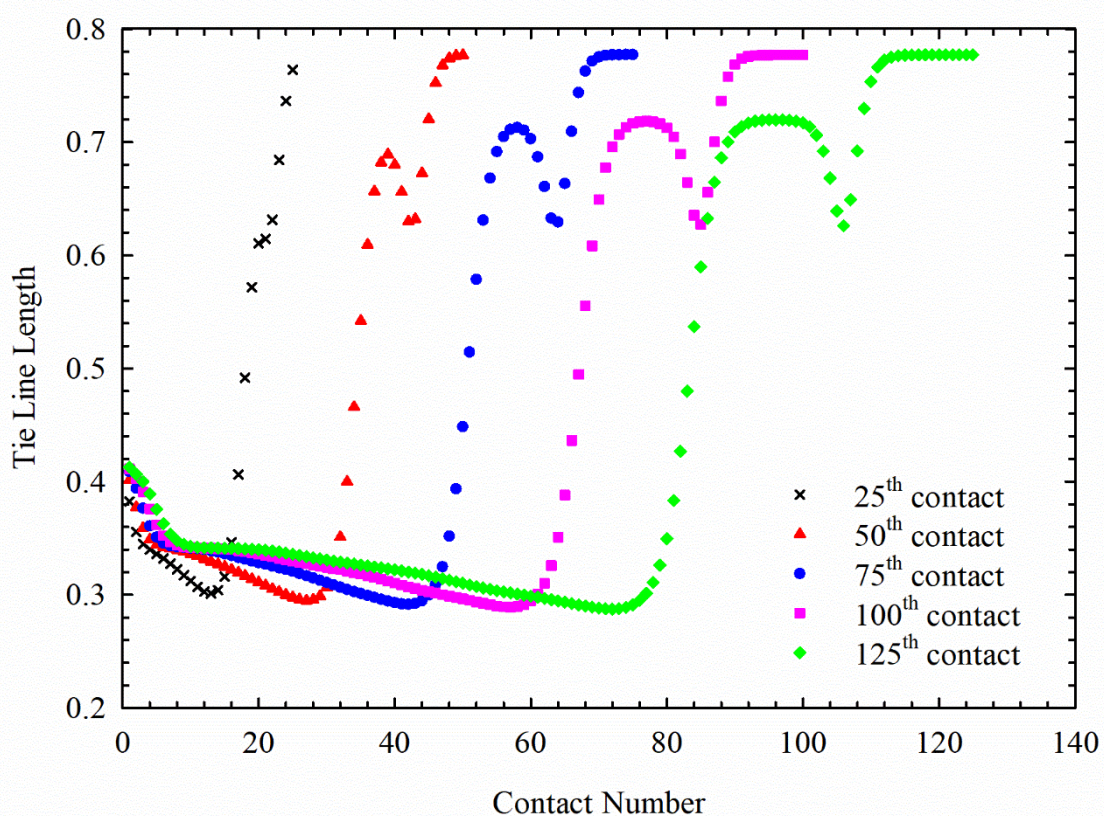


Figure 6-6 Variation of the tie line length calculated by our MMC algorithm as a function of contact number for Fluid W1 displaced by Gas 2 at 59°C and 110 bar

Figure 6-7(a) shows the variation of the weight fractions of precipitated asphaltene calculated by our MMC algorithm as a function of contact number for Fluid W1 displaced by Gas 2 at 59°C and 110 bar. Profiles of the weight fractions of precipitated asphaltene yielded by different contact times are presented in Figure 6-7(a). Figure 6-7(b) depicts the weight fractions of precipitated asphaltene and the tie line lengths calculated by our MMC algorithm as a function of contact number when the total contact number is 100. The weight fraction of precipitated asphaltene shown in Figure 7 is calculated by dividing the weight of precipitated asphaltene by the weight of the mixture (obtained after mixing the neighbouring cells). As seen in Figure 6-7(a), asphaltene only precipitates in the middle of the displacement. Moreover, as shown in Figure 6-7(b), asphaltene precipitation occurs near the contact number where the shortest tie line is developed. Thus, the asphaltene precipitation will have an obvious effect on the minimum tie line length.

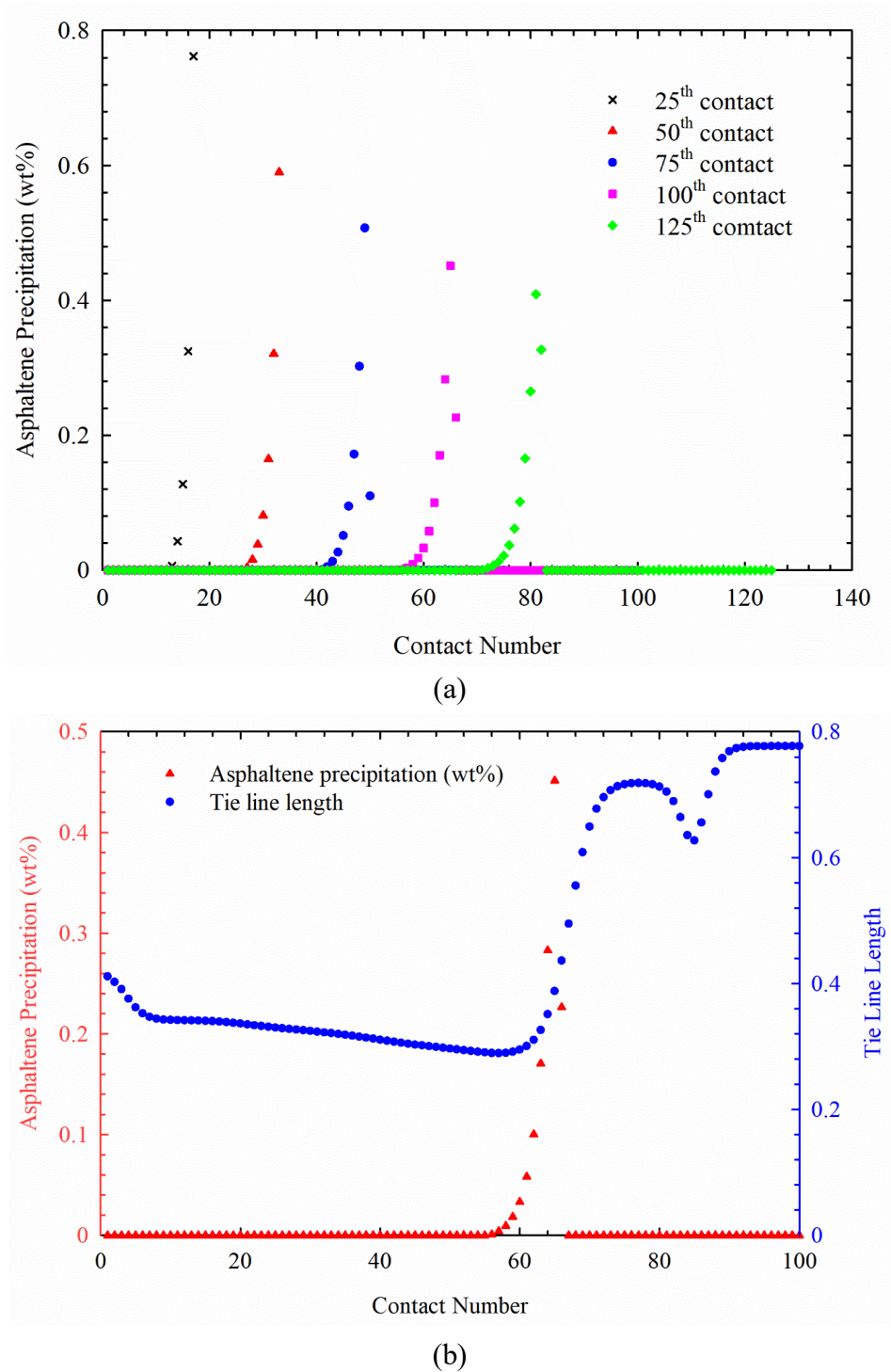
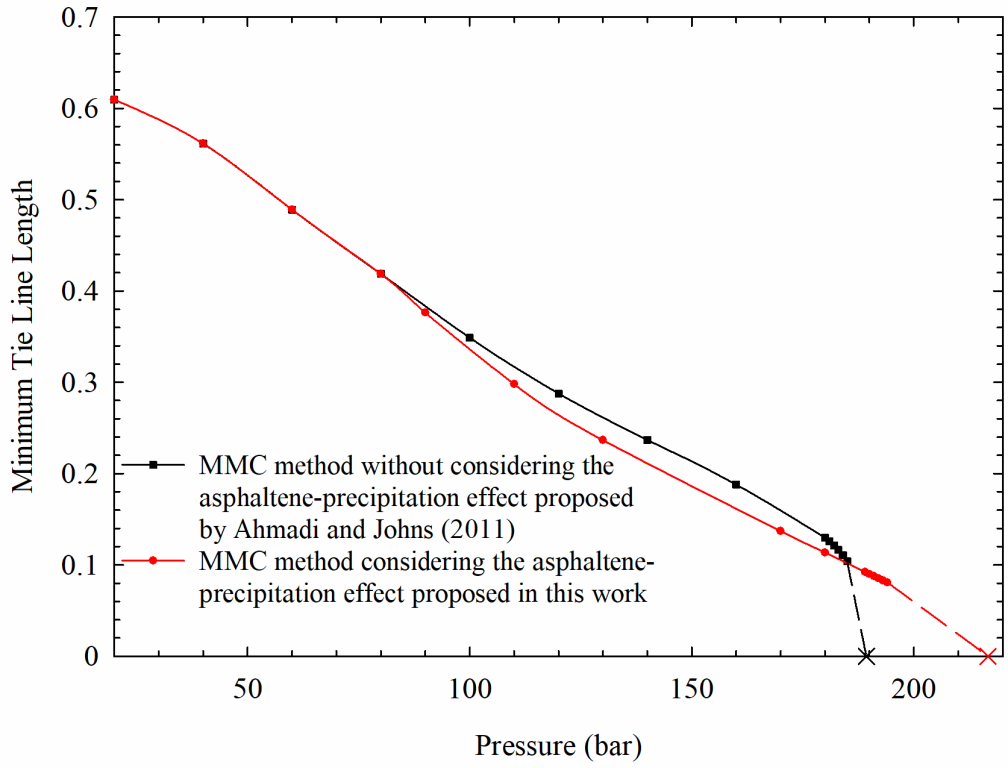


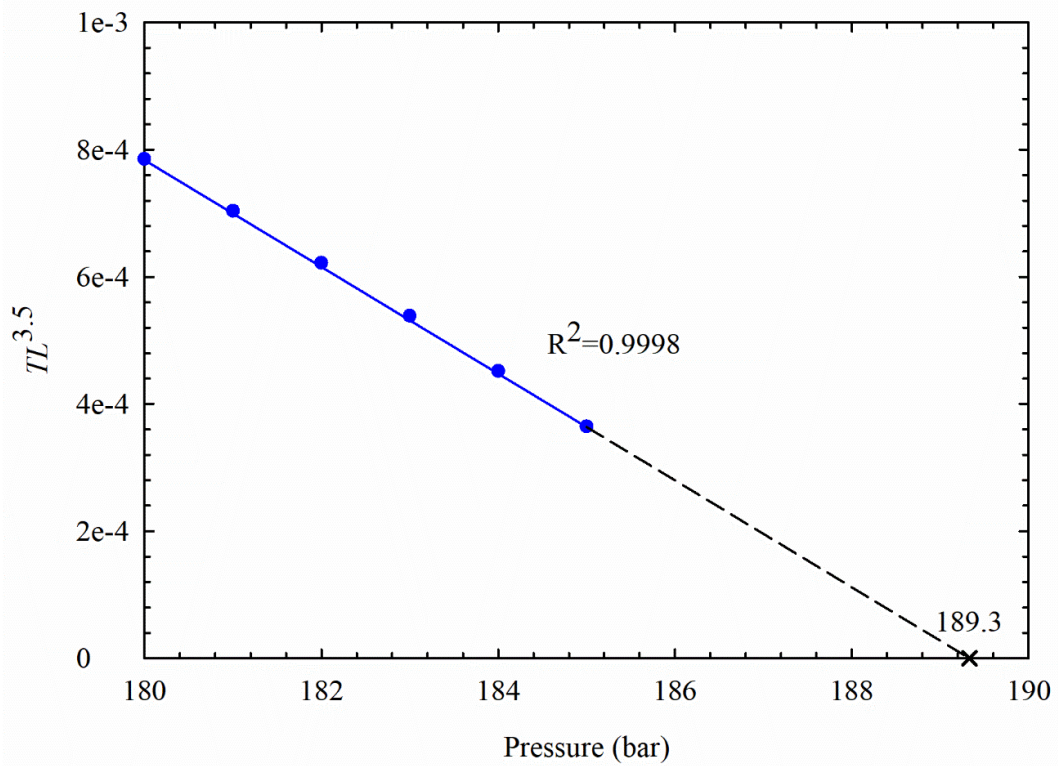
Figure 6-7 Fluid W1 displaced by Gas 2 at 59°C and 110 bar: (a) Variation of the weight fractions of precipitated asphaltene calculated by our MMC algorithm as a function of contact number in different contact times. (b) Weight fractions of precipitated asphaltene and tie line lengths calculated by our MMC algorithm as a function of contact number when the total contact number is 100.

6.4.3 Case Study 3: Fluid W1 Displaced by Gas 3 (Impure CO₂)

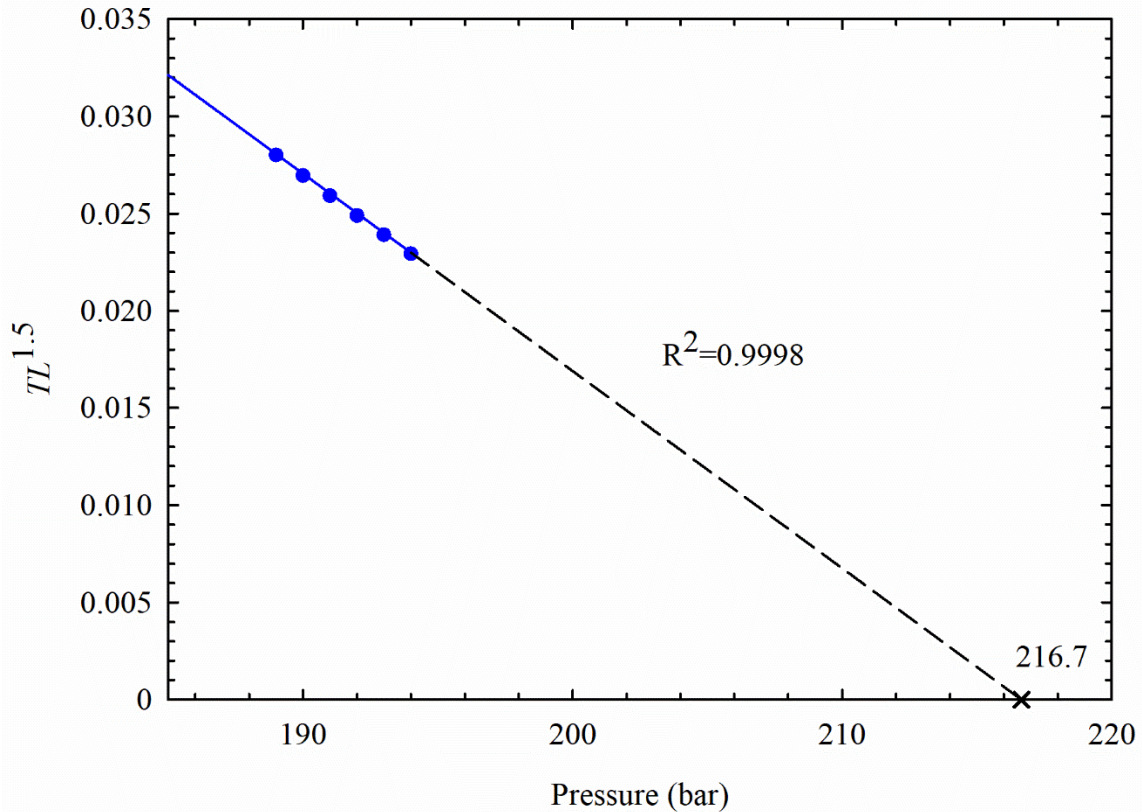
Figure 6-8 shows the variation of the minimum tie line lengths as a function of pressure for Fluid W1 displaced by Gas 3 at 59°C. Figure 6-8(a) depicts the comparison of the minimum tie line lengths with and without considering the asphaltene-precipitation effect. Again, at lower pressures (where no asphaltene precipitates), the same minimum tie line lengths are calculated by these two algorithms, while at higher pressures (where asphaltene precipitates), smaller minimum tie line lengths are calculated by our algorithm compared with those calculated by the MMC method proposed by Ahmadi and Johns [17]. Similar to the findings made in case studies 1 and 2, MMP yielded by our MMC algorithm (which is 216.7 bar) is larger than that yielded by the algorithm proposed by Ahmadi and Johns [17] (which is 189.3 bar). Equation (6-12) is applied to estimate the MMPs. Figures 6-8(b) and 6-8(c) shows the extrapolation of the minimum tie line lengths yielded by the MMC method proposed by Ahmadi and Johns [17] and that yielded by the MMC method proposed by this work, respectively. The exponential parameter (n) used in Figures 6-8(b) and 6-8(c) are 3.5 and 1.5, respectively.



(a)



(b)



(c)

Figure 6-8 Variation of minimum tie line lengths as a function of pressure for Fluid W1 displaced by Gas 3 at 59°C: (a) comparison of the minimum tie line lengths yielded by the MMC method proposed by Ahmadi and Johns [17] and those yielded by the MMC method proposed by this work; (b) extrapolation of the minimum tie line lengths yielded by the MMC method proposed by Ahmadi and Johns [17]; and (c) extrapolation of the minimum tie line lengths yielded by the MMC method proposed by this work.

Figure 6-9 depicts the variation of the tie line length calculated by our MMC algorithm as a function of contact number for Fluid W1 displaced by Gas 3 at 59°C and 110 bar. Profiles of the tie line lengths developed by different contact times are summarized in Figure 6-9. Figure 6-9 shows the gradual development of the key tie lines as contact times increases. The shortest key tie line almost appears after the 25th contact, whereas the fully development of the shortest key tie line is considered to occur after the 100th contact. As shown in Figure 6-9, the development of the shortest

key tie line occurs in the middle of the displacement. Again, this indicates that the miscibility between Fluid W1 and Gas 3 is developed by a combined condensing and vaporizing drive.

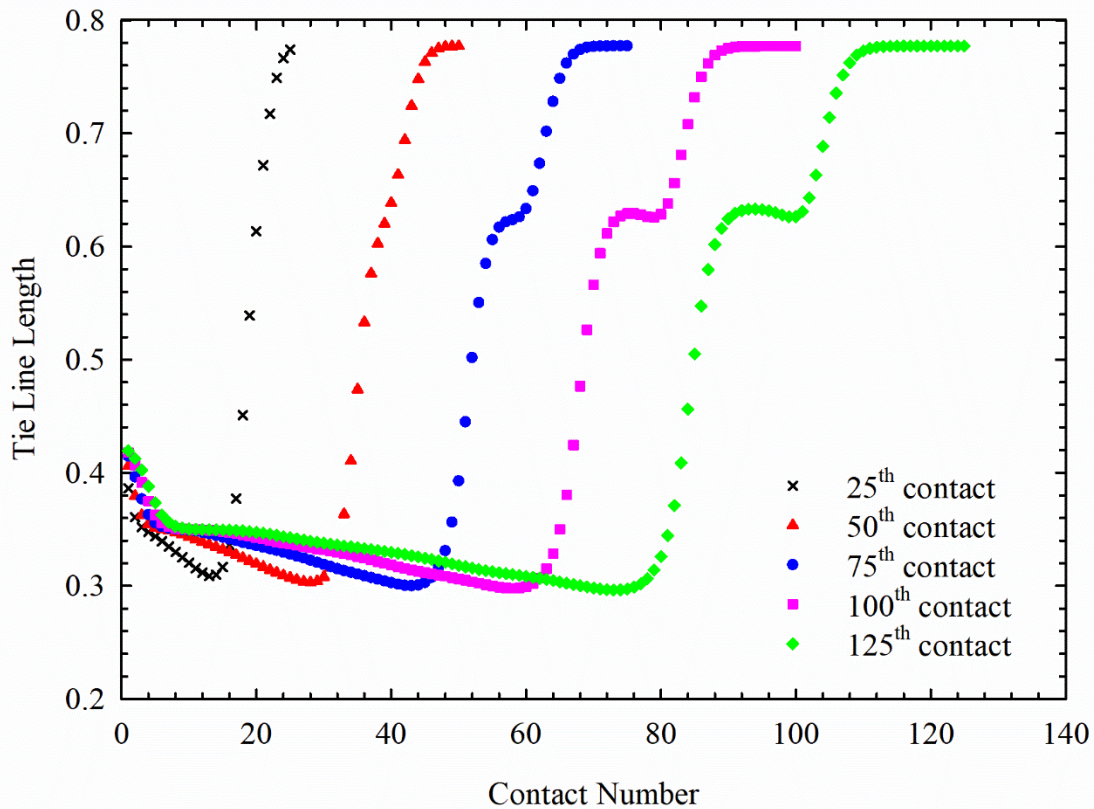
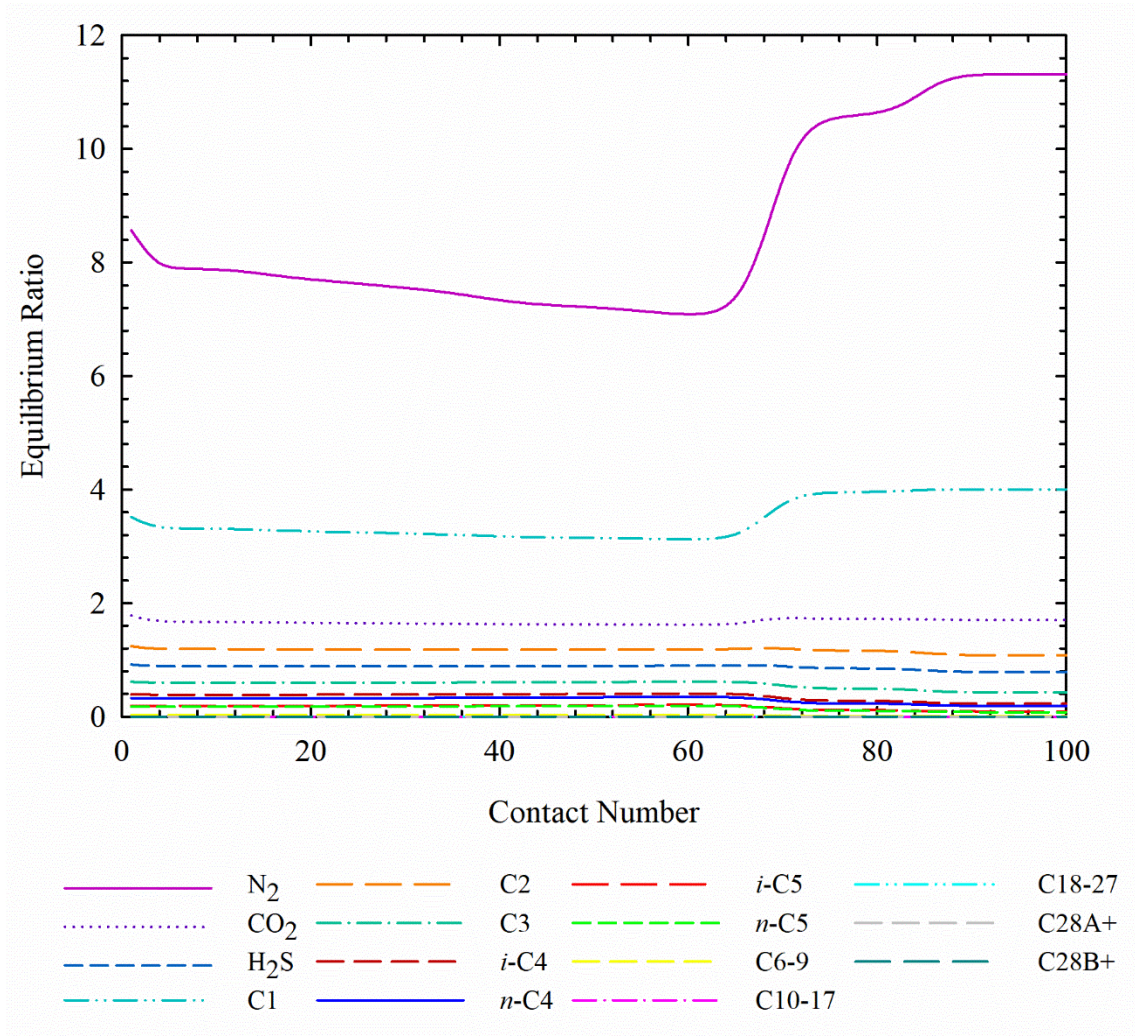


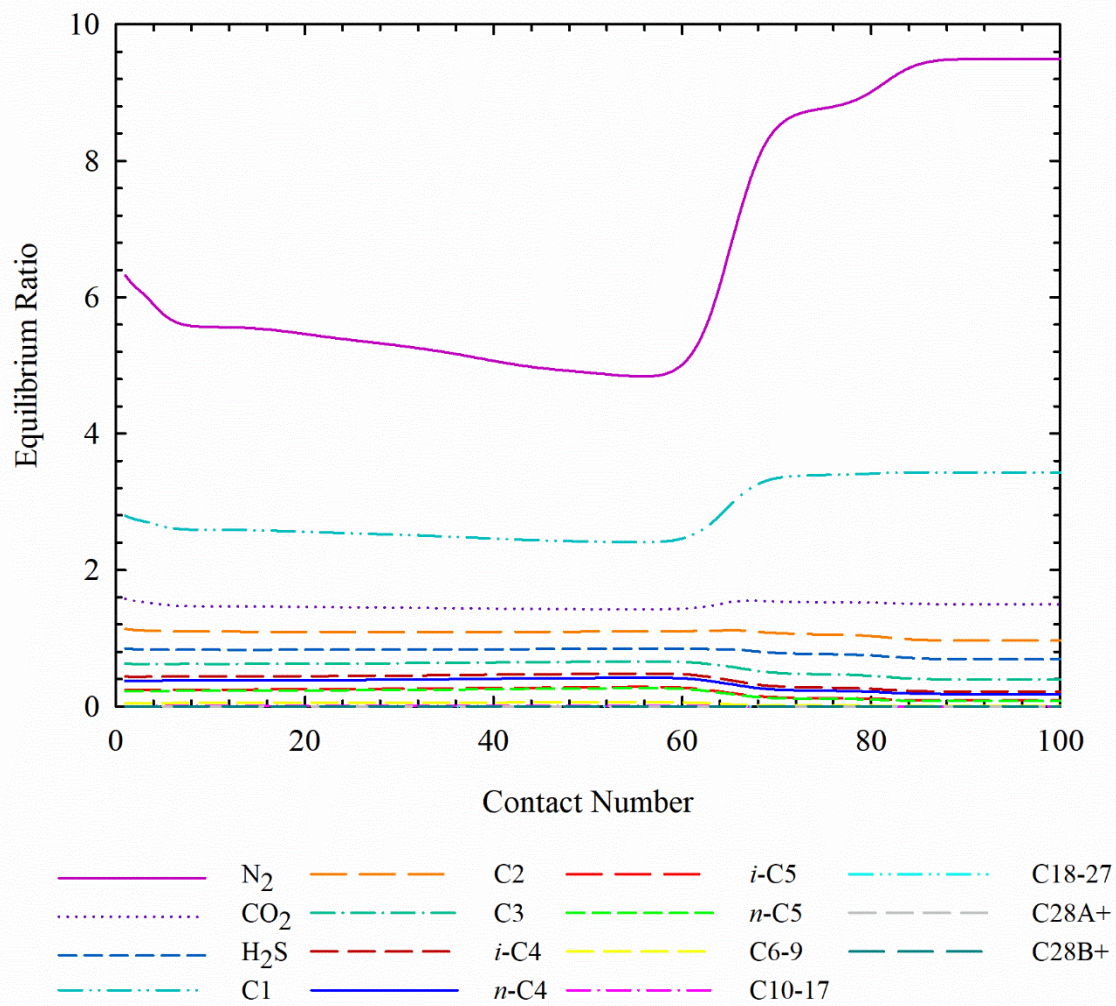
Figure 6-9 Variation of the tie line length calculated by our MMC algorithm as a function of contact number for Fluid W1 displaced by Gas 3 at 59°C and 110 bar

Figure 6-10 depicts the variation of the vapor-liquid equilibrium ratios of each component calculated by the two-phase flash calculation in our MMC algorithm as a function of contact number for Fluid W1 displaced by Gas 3 at 59°C at different pressures. The tested pressures for Figures 6-10(a), 6-10(b), 6-10(c), and 6-10(d) are 90 bar, 110 bar, 170 bar, and 193 bar, respectively. These four figures in Figure 6-10 are all generated at the 100th contact. As seen from Figure 6-10, the values of the equilibrium ratios move closer to 1 as pressure increases. The

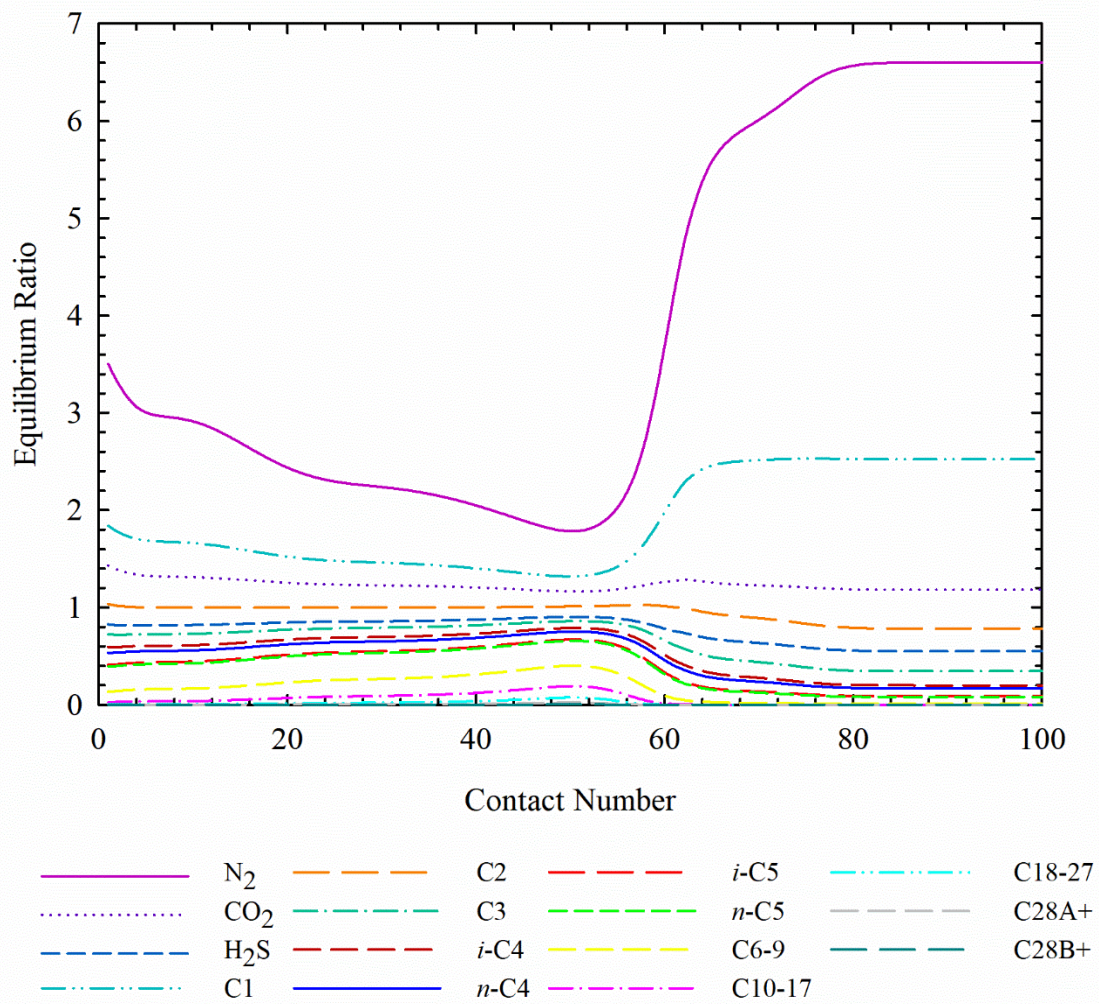
equilibrium ratios are clustering towards 1 at the contact number where the shortest tie line is developed.



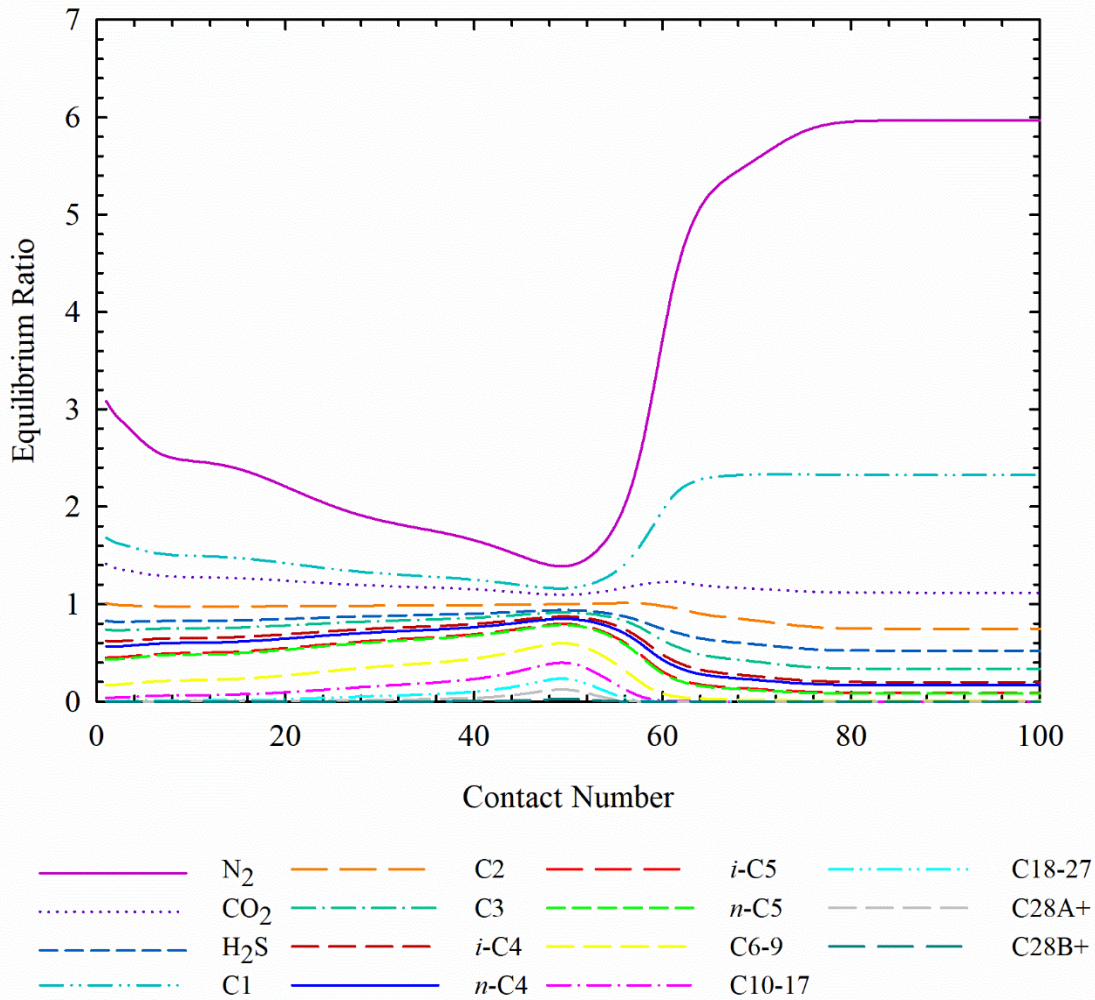
(a)



(b)



(c)



(d)

Figure 6-10 Variation of the vapor-liquid equilibrium ratios calculated by the two-phase flash calculation in our MMC algorithm as a function of contact number for Fluid W1 displaced by Gas 3 at 59°C: (a) 90 bar; (b) 110 bar; (c) 170 bar; and (d) 193 bar.

6.4.4 Comparison of Measured and Predicted MMPs

Table 6-5 compares the measured and predicted MMPs for Fluid W1 displaced by three gases at 59°C. The absolute relative error shown in Table 6-5 is calculated by,

$$ARE = \frac{|MMP_{measured} - MMP_{predicted}|}{MMP_{measured}} \square 100\% \quad (6-14)$$

where ARE represents absolute relative error between the measured and predicted MMPs, $MMP_{measured}$ and $MMP_{predicted}$ represent the measured and predicted MMPs, respectively. The experimental data are measured by Dong *et al.* [26] through slim tube experiments. As shown in Table 5, for Fluid W1 displaced by Gas 2 and Gas 3, the MMPs predicted by the algorithm proposed by this work are larger than the measured ones, while the MMPs predicted by the algorithm proposed by Ahmadi and Johns [17] are smaller than the measured ones. For these two cases, the MMPs predicted by our algorithm are closer to the measured ones compared with those predicted by the algorithm proposed by Ahmadi and Johns [17], indicating that our algorithm can provide a more accurate predicted MMP when asphaltene precipitates during the CO₂ flooding process. However, for Fluid W1 displaced by Gas 1, both of the predicted MMPs are larger than the measured one. Moreover, for this case, the ARE between the MMP predicted by Ahmadi and Johns [17] and the measured one is smaller than that between the MMP predicted by this work and the measured one. This may be caused by several factors, e.g., the values of the key parameters used in the three-phase VLS equilibrium calculation algorithm, the characterization of the undefined cut, the BIPs used, etc. Note that, as seen in Table 6-5, all MMPs predicted by our algorithm considering the asphaltene-precipitation effect are larger than those predicted by the algorithm proposed by Ahmadi and Johns [17] without considering the asphaltene-precipitation effect. This is consistent with the experimental study that asphaltene precipitation tends to increase MMP [4]. As previously mentioned, Kariman Moghaddam and Saeedi Dehaghani [16] proposed an algorithm to predict MMPs with the consideration of

asphaltene-precipitation effect by extending the MMC method developed by Jaubert *et al.* [14]. Table 6-5 summarizes the MMPs predicted by Kariman Moghaddam and Saeedi Dehaghani [16] as well. As shown in Table 6-5, all the MMPs predicted by Kariman Moghaddam and Saeedi Dehaghani [16] are smaller than those predicted by our algorithm. The ARE yielded by the algorithm developed by Kariman Moghaddam and Saeedi Dehaghani [16] is smaller than that by our algorithm for Fluid W1 displaced by Gas 1, while the AREs yielded by the algorithm developed by Kariman Moghaddam and Saeedi Dehaghani [16] are larger than those by our algorithm for Fluid W1 displaced by Gas 2 and 3.

Table 6-5 Comparison of measured and predicted MMPs for Fluid W1 displaced by three gases at 59°C

Injection gas	Measured MMP (bar) [26]	Predicted MMP (bar)			ARE (%)		
		Algorithm proposed by this work	Algorithm proposed by Ahmadi and Johns [17]	Algorithm proposed by Kariman Moghaddam and Saeedi Dehaghani [16]	Algorithm proposed by this work	Algorithm proposed by Ahmadi and Johns [17]	Algorithm proposed by Kariman Moghaddam and Saeedi Dehaghani [16]
Gas 1	128	145.4	132.8	128.2	13.59	3.75	0.16
Gas 2	175	177.9	166.9	159.1	1.66	4.63	9.09
Gas 3	212	216.7	189.3	192.8	2.22	10.71	9.06

6.5 Conclusions

In this study, we develop an MMC algorithm considering asphaltene-precipitation effect by modifying the MMC method proposed by Ahmadi and Johns [17]. The main modification is that

the three-phase VLS equilibrium calculation algorithm developed by Li and Li [20] is conducted before each contact to check if the asphaltene phase will appear. If asphaltene phase appears, the composition of the mixture of the fluids in two neighbouring cells needs to be updated by excluding the asphaltene phase. The two-phase flash calculation should be conducted on the mixture with the updated composition. Both the MMPs predicted by our algorithm and those predicted by the MMC algorithm without considering asphaltene-precipitation effect are compared with the MMPs measured by slim tube experiments conducted by Dong *et al.* [26] for three real reservoir fluids. The comparison results show that the MMPs predicted by our algorithm are larger than those predicted by the MMC algorithm without considering asphaltene-precipitation effect for all tested examples, which is the same as the experimental results that the asphaltene precipitation will increase MMPs [4]. Moreover, for Fluid W1 displaced by Gas 2 and Gas 3, the MMPs predicted by our algorithm are closer to the MMPs measured by experiments compared with the MMPs predicted by the MMC algorithm without considering asphaltene-precipitation effect. For Fluid W1 displaced by Gas 1, the MMP predicted by the original MMC algorithm without considering the asphaltene-precipitation effect is closer to the measured one compared to the MMP predicted by our new MMC algorithm; and both of the predicted MMPs by the original MMC algorithm and our new MMC algorithm are larger than the measured one.

Nomenclature

a	attraction parameter in PR EOS or slope
b	repulsion parameter in PR EOS or intercept of y -axis
c	number of components or asphaltene component
$error$	absolute relative error between measured and predicted MMPS
f	fugacity
G_i	mole fraction of component i in the injection gas
k	BIP
MMP	MMP
n	exponential parameter
O_i	component mole fraction in oil
R	universal gas constant
S	component mole fraction in asphaltene phase
TL	tie line length
v	molar volume
V	molar volume
x	component mole fraction in mixture
X	component mole fraction in equilibrium liquid phase
Y	component mole fraction in equilibrium vapor phase
Z	component mole fraction in gas-oil mixture

Greek Letters

α	gas phase mole fraction or α -function
β	phase mole fraction
ω	acentric factor
θ	exponential parameter

Superscript

*	reference parameter
---	---------------------

Subscript

c	critical property
i	component index
j	component index
<i>measured</i>	measured value
<i>predicted</i>	predicted value
r	reduced parameter
s	asphaltene phase

6.6 References

[1] P.M. Jarrell, C.E. Fox, M.H. Stein, S.L. Webb, Practical aspects of CO₂ flooding (Vol. 22),

- 2002, Richardson, TX: Society of Petroleum Engineers, ISBN: 978-1-55563-096-6.
- [2] R.K. Srivastava, S.S. Huang, Laboratory investigation of Weyburn CO₂ miscible flooding, presented at Technical Meeting/Petroleum Conference of The South Saskatchewan Section, Regina, Saskatchewan, Canada, October 19-22, 1997.
- [3] R.K. Srivastava, S.S. Huang, M. Dong, Asphaltene deposition during CO₂ flooding, SPE Prod. Facil. 14 (04) (1999) 235-245. SPE-59092-PA.
- [4] A.M. Elsharkawy, F.H. Poettmann, R.L. Christiansen, Measuring minimum miscibility pressure: slim-tube or rising-bubble method? presented at SPE/DOE Enhanced Oil Recovery Symposium, Tulsa, Oklahoma, USA, April 22-24, 1992. SPE-24114-MS.
- [5] W.F. Yellig, R.S. Metcalfe, Determination and prediction of CO₂ minimum miscibility pressures, J. Pet. Technol., 32 (01) (1980) 160-168. SPE-7477-PA.
- [6] R.T. Johns, P. Sah, R. Solano, Effect of dispersion on local displacement efficiency for multicomponent enriched-gas floods above the minimum miscibility enrichment, SPE Res. Eval. & Eng. 5 (01) (2002) 4-10. SPE-75806-PA.
- [7] A.A. Zick, A combined condensing/vaporizing mechanism in the displacement of oil by enriched gases, presented at SPE annual technical conference and exhibition, New Orleans, Louisiana, USA, October 5-8, 1986. SPE-15493-MS.
- [8] R.T. Johns, B. Dindoruk, F.M. Orr Jr., Analytical theory of combined condensing/vaporizing gas drives. Soc. Pet. Eng. Adv. Tech. Series, 1 (02) (1993) 7-16. SPE-24112-PA.
- [9] R.S. Metcalfe, D.D. Fussell, J.L. Shelton, A multicell equilibrium separation model for the

- study of multiple contact miscibility in rich-gas drives, SPE J. 13 (03) (1973) 147-155. SPE-3995-PA.
- [10] R.T. Johns, F.M. Orr Jr., Miscible gas displacement of multicomponent oils, SPE J. 1 (01) (1996) 39-50. SPE-30798-PA.
- [11] Y. Wang, F.M. Orr Jr., Analytical calculation of minimum miscibility pressure, Fluid Phase Equilibr. 139 (1-2) (1997) 101-124.
- [12] K. Jessen, M.L. Michelsen, E.H. Stenby, Global approach for calculation of minimum miscibility pressure, Fluid Phase Equilibr. 153 (2) (1998) 251-263.
- [13] H. Yuan, R.T. Johns, Simplified method for calculation of minimum miscibility pressure or enrichment, SPE J. 10 (04) (2005) 416-425. SPE-77381-PA.
- [14] J.N. Jaubert, L. Wolff, E. Neau, L. Avaullee, A very simple multiple mixing cell calculation to compute the minimum miscibility pressure whatever the displacement mechanism, Ind. Eng. Chem. Res. 37 (12) (1998) 4854-4859.
- [15] G.B. Zhao, H. Adidharma, B. Towler, M. Radosz, Using a multiple-mixing-cell model to study minimum miscibility pressure controlled by thermodynamic equilibrium tie lines, Ind. Eng. Chem. Res. 45 (23) (2006) 7913-7923.
- [16] A. Kariman Moghaddam, A.H. Saeedi Dehaghani, Modeling of asphaltene precipitation in calculation of minimum miscibility pressure, Ind. Eng. Chem. Res. 56 (25) (2017) 7375-7383.
- [17] K. Ahmadi, R.T. Johns, Multiple-mixing-cell method for MMP calculations, SPE J. 16 (04) (2011) 733-742. SPE-116823-PA.

- [18] C.H. Whitson, M.L. Michelsen, The negative flash, *Fluid Phase Equilibr.* 53 (1989) 51-71.
- [19] C.F. Leibovici, D.V. Nichita, A new look at multiphase Rachford-Rice equations for negative flashes, *Fluid Phase Equilibr.* 267 (2) (2008) 127-132.
- [20] R. Li, H.A. Li, Robust three-phase vapor-liquid-asphaltene equilibrium calculation algorithm for isothermal CO₂ flooding application, manuscript submitted to *Ind. Eng. Chem. Res.*
- [21] L.X. Nghiem, M.S. Hassam, R. Nutakki, A.E.D., George, Efficient modelling of asphaltene precipitation, presented at SPE Annual Technical Conference and Exhibition, Houston, Texas, USA, 3-6 October, 1993. SPE-26642-MS.
- [22] D.Y. Peng, D.B. Robinson, A new two-constant equation of state, *Ind. Eng. Chem. Fund.* 15 (1) (1976) 59-64.
- [23] D.B. Robinson, D.Y. Peng, The characterization of the heptanes and heavier fractions for the GPA Peng-Robinson programs. GPA Research Report 28, 1978.
- [24] M.L. Michelsen, The isothermal flash problem. Part II. Phase-split calculation, *Fluid Phase Equilibr.* 9 (1) (1982) 21-40.
- [25] M.L. Michelsen, The isothermal flash problem. Part I. Stability, *Fluid Phase Equilibr.* 9 (1) (1982) 1-19.
- [26] M. Dong, S. Huang, S.B. Dyer, F.M. Mourits, A comparison of CO₂ minimum miscibility pressure determinations for Weyburn crude oil. *J. Petrol. Sci. Eng.* 31 (1) (2001) 13-22.
- [27] PVTsim Nova 3.3, Calsep A/S, Copenhagen, Denmark, 2019.
- [28] P.L. Chueh, J.M. Prausnitz, Vapor-liquid equilibria at high pressures: Calculation of partial

molar volumes in nonpolar liquid mixtures, AIChE J. 13 (6) (1967) 1099-1107.

CHAPTER 7 CONCLUSIONS, CONTRIBUTIONS AND RECOMMENDATIONS

7.1 Conclusions and Scientific Contributions to the Literature

In this dissertation, we develop robust and efficient three-phase equilibrium calculation algorithms for the three-phase vapor-liquid-aqueous (VLA) and vapor-liquid-asphaltene (VLS) equilibria. Moreover, the three-phase VLS equilibrium calculation algorithm is applied to predict minimum miscibility pressure (MMP) with the consideration of asphaltene-precipitation effect.

The main conclusions of this thesis are summarized as follows:

Chapter 2:

Based on the free-water assumption (Tang and Saha 2003), we simplify the objective function (used to solve the phase fractions) developed by Okuno *et al.* (2010) for the three-phase VLA flash calculation and the two-phase vapor/liquid-aqueous flash calculation. Note that, in our three-phase free-water VLA flash calculation algorithm, there is only one unknown in the objective function; while, in the two-phase free-water vapor/liquid-aqueous (V/L-A) flash calculation algorithm, the phase fractions can be analytically solved. The initialization method developed by Lapene *et al.* (2010) is applied to initialize the equilibrium ratios required in both the three-phase free-water flash calculation and the two-phase vapor-liquid (VL) flash calculation, while a new initialization method is developed to initialize the equilibrium ratios for the two-phase free-water V/L-A flash calculation.

By incorporating these two aforementioned free-water flash calculation algorithms, a three-phase free-water VLA equilibrium calculation algorithm is developed to enhance the computational efficiency. In this algorithm, we provide efficient criteria that help to determine how to switch from a three-phase equilibrium to a two-phase equilibrium without performing stability tests. Thereby, the number of stability tests is reduced in this three-phase free-water VLA equilibrium calculation algorithm comparing to the conventional full three-phase equilibrium calculation algorithm; the reduced number of stability tests, together with the reduced number of variables in the flash calculations, result in a higher computational efficiency of our algorithm.

Example calculations demonstrate that the calculation results yielded by the newly developed algorithm are in good agreement with those yielded by the conventional three-phase equilibrium calculation algorithm. But it should be noted that our algorithm may fail to give an accurate result when it is applied to the mixtures containing polar materials, such as alcohols, or other substances which tend to have a high solubility in the aqueous phase.

Chapter 3:

In this chapter, we present a robust and efficient three-phase isenthalpic equilibrium calculation algorithm based on the free-water assumption. This three-phase isenthalpic equilibrium calculation algorithm can consider single-phase equilibria, two-phase equilibria, and three-phase VLA equilibria. As demonstrated by the challenging case studies, this algorithm performs well in the narrow-boiling region except for the mixture with one degree of freedom and can readily

handle the phase appearances and disappearances as temperature updates to satisfy the energy conservation equation. At low to medium pressures under which the thermal recovery processes are normally conducted, a good agreement can be observed between the flash results obtained by the new algorithm and those obtained by the conventional algorithm without imposing the free-water assumption. Moreover, this algorithm is more efficient than the existing three-phase isenthalpic equilibrium calculation algorithms. Because this algorithm is robust and efficient, it is possible to be incorporated into thermal/compositional simulators. However, it is worthwhile mentioning that this algorithm may cause intolerable errors if applied to the mixtures containing polar materials, such as alcohols, or the mixtures at given conditions under which the free-water assumption is not valid.

Chapter 4:

An improved three-phase VLA equilibrium calculation algorithm is proposed in this paper. A new scheme used to initialize the equilibrium ratios is applied in this algorithm. The aqueous-like stationary point on the TPD surface can be securely detected by using this new initialization scheme. Convergence problems are avoided in the flash calculations with the application of our algorithm. Moreover, one can obtain a correct phase equilibrium in a more efficient way by using our algorithm with the new initialization scheme compared to the method proposed by Gorucu and Johns (2016). This algorithm is applicable to scenarios where the three-phase free-water VLA equilibrium calculation algorithm cannot work. The performance of the newly developed algorithm is validated by hundreds of thousands of example calculations. Pressure-temperature

(P-T) phase diagrams are generated by this algorithm. The computational results show that our algorithm performs well in most cases. However, it fails in part of the two-phase liquid-aqueous (LA) equilibrium region and in part of the three-phase VLA equilibrium region at high temperature/pressure conditions. The reason is that no equivalent fugacities between the aqueous phase and the non-aqueous phases can be found due to the inconsistency of the BIPs set for the non-aqueous phases and those calculated by the Søreide and Wilson correlation (Søreide and Wilson 1992) for the aqueous phase.

Chapter 5:

By adopting the asphaltene-precipitation model proposed by Nghiem *et al.* (1993), we develop a robust three-phase VLS equilibrium calculation algorithm. In this algorithm, new initialization methods of equilibrium ratios are provided for both stability test and flash calculation. To develop this three-phase VLS equilibrium calculation algorithm, a simple two-phase vapor/liquid-asphaltene (V/L-S) flash calculation algorithm is first developed. Moreover, two three-phase VLS flash calculation algorithms are developed to ensure the robustness and efficiency of the three-phase VLS equilibrium calculation algorithm. Algorithm #1 is similar to the three-phase free-water VLA flash calculation algorithm developed by Li and Li (2018). It is more efficient; but relies on the initial equilibrium ratios. Algorithm #2 uses the outer loop to update the asphaltene-phase mole fraction, while it uses inner loop to perform the two-phase VL flash calculation. This algorithm is more robust; but it is more time-consuming since several two-phase

VL flash calculations are required to be conducted in the inner loop. Moreover, the prerequisite of conducting this algorithm is that the three-phase VLS equilibrium actually appears.

The performance of this newly developed algorithm is tested by several real reservoir fluids mixed with pure or impure CO₂. The key model parameters of the asphaltene-precipitation model are first adjusted by experimental data of asphaltene precipitation. The effects of these parameters on the asphaltene precipitation phenomenon with the change of gas concentration are discussed. With the adjusted key model parameters, our three-phase VLS equilibrium calculation algorithm is conducted hundreds of thousands of times at different pressures and gas concentrations to generate a pressure-composition (P-X) diagram. It performs well at all test points. Note that, there is a small three-phase equilibrium region between the two-phase VL equilibrium region and the two-phase liquid-asphaltene (LS) equilibrium region when the gas concentration is very high. In this region, the three-phase equilibrium contains a vapor phase, an asphaltene phase, and a liquid phase which is very dense and more like an asphaltene phase. The reason of the appearance of this three-phase region may be that the liquid phase cannot merge with the asphaltene phase due to the assumption made on the asphaltene phase (i.e., asphaltene phase is a pure dense phase).

Chapter 6:

In this chapter, we develop a multiple-mixing-cell (MMC) algorithm considering asphaltene-precipitation effect by modifying the MMC method proposed by Ahmadi and Johns (2011). The main modification is that the three-phase VLS equilibrium calculation algorithm

developed by Li and Li (2019) is conducted before each contact to check if the asphaltene phase will appear. If asphaltene phase appears, the composition of the mixture of the fluids in two neighbouring cells needs be updated by excluding the asphaltene phase. The two-phase flash calculation should be conducted on the mixture with the updated composition. Both the MMPs predicted by our algorithm and those predicted by the MMC algorithm without considering asphaltene-precipitation effect are compared with the MMPs measured by slim tube experiments conducted by Dong *et al.* (2001) for three real reservoir fluids. The comparison results show that the MMPs predicted by our algorithm are larger than those predicted by the MMC algorithm without considering asphaltene-precipitation effect for all tested examples, which is the same as the experimental results that the asphaltene precipitation will increase MMPs. Moreover, for Fluid W1 displaced by Gas 2 and Gas 3, the MMPs predicted by our algorithm are closer to the MMPs measured by experiments compared with the MMPs predicted by the MMC algorithm without considering asphaltene-precipitation effect. For Fluid W1 displaced by Gas 1, the MMP predicted by the original MMC algorithm without considering the asphaltene-precipitation effect is closer to the measured one compared to the MMP predicted by our new MMC algorithm; and both of the predicted MMPs by the original MMC algorithm and our new MMC algorithm are larger than the measured one.

7.2 Suggested Future Work

- In this thesis, we develop robust and efficient three-phase equilibrium calculation algorithms for the three-phase vapor-liquid-aqueous (VLA) and vapor-liquid-asphaltene

(VLS) equilibria. In the future, we would like to apply them to compositional simulators for simulating the fluid flow in both wellbores and reservoirs.

- As mentioned in Chapter 4, at the high pressure and temperature conditions, our algorithm fails to detect the actual phase equilibria. The possible reason is that no equivalent fugacities between the aqueous phase and the non-aqueous phases can be found due to the inconsistency of the BIP set used for the non-aqueous phases and those calculated by the Søreide and Wilson correlation for the aqueous phase (Søreide and Wilson 1992). The objective of using the BIPs calculated by the Søreide and Wilson correlation (Søreide and Wilson 1992) is to precisely describe the gas dissolution in the aqueous phase, since the original Peng-Robinson equation of state (PR EOS) (Peng and Robinson 1976) cannot precisely capture it. Therefore, we recommend incorporating other EOS models, which can precisely describe the gas dissolution in the aqueous phase (e.g. perturbed-chain statistical associating fluid theory (PC-SAFT) (Gross and Sadowski 2001) and cubic-plus-association (CPA) EOS (Li and Firoozabadi 2009)), into our improved three-phase VLA equilibrium calculation algorithm in order to have an accurate description of the gas dissolution in aqueous phase as well as have a consistent thermodynamic model for all the three phases.
- In Chapter 5, the asphaltene-precipitation model proposed by Nghiem *et al.* (1993) is applied in our three-phase VLS equilibrium calculation algorithm. However, this algorithm assumes that the asphaltene phase is a pure dense phase containing only

asphaltene component. There are many other asphaltene-precipitation models which can have a more accurate description of the asphaltene precipitation phenomenon (e.g. PC-SAFT (Gross and Sadowski 2001) and CPA EOS (Li and Firoozabadi 2009)). Therefore, in the future, we can combine other more accurate asphaltene-precipitation models into our algorithm to have a more precise description of the VLS equilibria together with the asphaltene precipitation phenomenon.

- Moreover, four-phase vapor-liquid-aqueous-asphaltene equilibria can commonly appear in reservoirs containing water and asphaltenic oil. It is worthwhile of developing a robust and efficient four-phase vapor-liquid-aqueous-asphaltene equilibrium calculation algorithm, which is, however, much more complex and requires a much more careful design of the algorithm configuration.

7.3 References

- Ahmadi, K., and Johns, R.T., 2011, Multiple-mixing-cell method for MMP calculations, *SPE J.* **16** (04): 733-742.
- Dong, M., Huang, S., Dyer, S.B., and Mourits, F.M., 2001, A comparison of CO₂ minimum miscibility pressure determinations for Weyburn crude oil, *J. Petrol. Sci. Eng.* **31** (1): 13-22.
- Gorucu, S.E., and Johns, R.T., 2016, Robustness of three-phase equilibrium calculations, *J. Petrol. Sci. Eng.* **143**: 72-85.
- Gross, J., and Sadowski, G., 2001, Perturbed-chain SAFT: An equation of state based on a perturbation theory for chain molecules, *Ind. Eng. Chem. Res.* **40** (4): 1244-1260.

- Lapene, A., Nichita, D.V., Debenest, G., and M., Quintard, 2010, Three-phase free-water flash calculations using a new Modified Rachford-Rice equation, *Fluid Phase Equilibr.* **297** (1):121-128.
- Li, Z., and Firoozabadi, A., 2009, Cubic-plus-association equation of state for water-containing mixtures: Is “cross association” necessary? *AIChE J.* **55** (7): 1803-1813.
- Li, R., and H.A. Li, 2018, New two-phase and three-phase Rachford-Rice algorithms based on free-water assumption, *Can. J. Chem. Eng.* **96** (1): 390-403.
- Li, R. and Li, H., 2019, Robust three-phase vapor-liquid-asphaltene equilibrium calculation algorithm for isothermal CO₂ flooding, manuscript submitted to *Ind. Eng. Chem. Res.*
- Okuno, R., Johns, R.T., and Sepehrnoori, K., 2010, A new algorithm for Rachford-Rice for multiphase compositional simulation., *SPE J.* **15** (02): 313-325.
- Peng, D.Y., and Robinson, D.B., 1976, A new two-constant equation of state, *Ind. Eng. Chem. Fundam.* **15** (1): 59-64.
- Søreide, I., and Whitson, C.H., 1992, Peng-Robinson predictions for hydrocarbons, CO₂, N₂, and H₂S with pure water and NaCl brine, *Fluid Phase Equilib.* **77**: 217-240.
- Tang, Y., and Saha, S., 2003, An efficient method to calculate three-phase free-water flash for water-hydrocarbon systems, *Ind. Eng. Chem. Res.* **42** (1): 189-197.

BIBLIOGRAPHY

- Agarwal, R.K., Li, Y.K., Nghiem, L.X., and Coombe, D.A., 1991, Multiphase multicomponent isenthalpic flash calculations, *J. Can. Pet. Tech.* **30** (3): 69-75.
- Agrawala, M., and Yarranton, H.W., 2001, An asphaltene association model analogous to linear polymerization, *Ind. Eng. Chem. Res.* **40** (21): 4664-4672.
- Ahmadi, K., and Johns, R.T., 2011, Multiple-mixing-cell method for MMP calculations, *SPE J.* **16** (04): 733-742. SPE-116823-PA.
- Amani, M.J., Gray, M.R., and Shaw, J.M., 2014, The phase behavior of Athabasca bitumen + toluene + water ternary mixtures, *Fluid Phase Equilibr.* **370**: 75-84.
- Baker, L.E., Pierce, A.C., and Luks, K.D., 1982, Gibbs energy analysis of phase equilibria, *SPE J.* **22** (05): 731-742. SPE-9806-PA.
- Brantferger, K.M., Pope, G.A., and Sepehrnoori, K., 1991, Development of a thermodynamically consistent, fully implicit, equation-of-state, compositional steamflood simulator, presented at SPE Symposium on Reservoir Simulation, Anaheim, California. SPE-21253-MS.
- Bridgeman, O.C., and Aldrich, E.W., 1964, Vapor pressure tables for water, *J. Heat Transfer* **86** (2): 279-286.
- Butler, R.M., 1994, Steam-assisted gravity drainage: concept, development, performance and future. *J. Can. Pet. Technol.* **33** (02): 44-50.
- Chien, M.C.H., Yardumian, H.E., Chung, E.Y., and Todd, W.W., 1989, The formulation of a thermal simulation model in a vectorized, general purpose reservoir simulator, presented at

- SPE Symposium on Reservoir Simulation, Houston, Texas. SPE-18418-MS.
- Chueh, P.L., and Prausnitz, J.M., 1967, Vapor-liquid equilibria at high pressures: Calculation of partial molar volumes in nonpolar liquid mixtures, *AIChE J.* **13** (6): 1099-1107.
- Coats, K.H., 1980, An equation of state compositional model, *SPE J.* **20** (05): 363-376. SPE-8284-PA.
- Connolly, M., 2018, An isenthalpic-based compositional framework for nonlinear thermal simulation, PhD thesis, Stanford University.
- Das, S.K., and Butler, R.M., 1998, Mechanism of the vapor extraction process for heavy oil and bitumen, *J. Petrol. Sci. Eng.* **21** (1-2): 43-59.
- David Ting, P., Hirasaki, G.J., and Chapman, W.G., 2003, Modeling of asphaltene phase behavior with the SAFT equation of state, *Pet. Sci. Technol.* **21** (3-4): 647-661.
- Dhima, A., de Hemptinne, J.C., and Moracchini, G., 1998, Solubility of light hydrocarbons and their mixtures in pure water under high pressure, *Fluid Phase Equilibr.* **145** (1): 129-150.
- Dhima, A., de Hemptinne, J.C., and Jose, J., 1999, Solubility of hydrocarbons and CO₂ mixtures in water under high pressure, *Ind. Eng. Chem. Res.* **38** (8): 3144-3161.
- Dong, M., Huang, S., Dyer, S.B., and Mourits, F.M., 2001, A comparison of CO₂ minimum miscibility pressure determinations for Weyburn crude oil, *J. Petrol. Sci. Eng.* **31** (1): 13-22.
- Elsharkawy, A.M., Poettmann, F.H., and Christiansen, R.L., 1992, Measuring minimum miscibility pressure: slim-tube or rising-bubble method? presented at SPE/DOE Enhanced Oil Recovery Symposium, Tulsa, Oklahoma. SPE-24114-MS.

- Evelein, K.A., Moore, R.G., and Heidemann, R.A., 1976, Correlation of the phase behavior in the systems hydrogen sulfide-water and carbon dioxide-water, *Ind. Eng. Chem. Proc. Des. Dev.* **15** (3): 423-428.
- Glandt, C.A., and Chapman, W.G., 1995, The effect of water dissolution on oil viscosity, *SPE Res. Eng.* **10** (01): 59-64. SPE-24631-PA.
- Gorucu, S.E., and Johns, R.T., 2016, Robustness of three-phase equilibrium calculations, *J. Petrol. Sci. Eng.* **143**: 72-85.
- Grabowski, J.W., Vinsome, P.K., Lin, R.C., Behie, G.A., and Rubin, B., 1979, A fully implicit general purpose finite-difference thermal model for in situ combustion and steam, presented at SPE Annual Technical Conference and Exhibition, Las Vegas, Nevada. SPE-8396-MS.
- Gross, J., and Sadowski, G., 2001, Perturbed-chain SAFT: An equation of state based on a perturbation theory for chain molecules, *Ind. Eng. Chem. Res.* **40** (4): 1244-1260.
- Gupta, A.K., Bishnoi, P.R., and Kalogerakis, N., 1990, Simultaneous multiphase isothermal/isenthalpic flash and stability calculations for reacting/non-reacting systems, *Gas Sepa. Purif.* **4** (4): 215-222.
- Haugen, K.B., Firoozabadi, A., and Sun, L., 2011, Efficient and robust three-phase split computations, *AIChE J.* **57** (9): 2555-2565.
- Heidari, M., Nghiem, L.X., and Maini, B.B., 2014, Improved isenthalpic multiphase flash calculations for thermal compositional simulators, presented at SPE Heavy Oil Conference-Canada, Calgary, Alberta. SPE-170029-MS.

- Henry, W., 1803, III. Experiments on the quantity of gases absorbed by water, at different temperatures, and under different pressures, *Phil. Trans. R. Soc. Lond.* **93**: 29-274.
- Ishimoto, K., Pope, G.A., and Sepchrnoori, K., 1987, An equation-of-state steam simulator, *In Situ* **11**(1): 1-37.
- Jarrell, P.M., Fox, C.E., Stein, M.H., and Webb, S.L., 2002, Practical aspects of CO₂ flooding (Vol. 22), Richardson, TX: Society of Petroleum Engineers, ISBN: 978-1-55563-096-6.
- Jaubert, J.N., Wolff, L., Neau, E., and Avaullee, L., 1998, A very simple multiple mixing cell calculation to compute the minimum miscibility pressure whatever the displacement mechanism, *Ind. Eng. Chem. Res.* **37** (12): 4854-4859.
- Jessen, K., Michelsen, M.L, and Stenby, E.H., 1998, Global approach for calculation of minimum miscibility pressure, *Fluid Phase Equilibr.* **153** (2): 251-263.
- Johns, R.T., Dindoruk, B., and Orr Jr., F.M., 1993, Analytical theory of combined condensing/vaporizing gas drives, *Soc. Pet. Eng. Adv. Tech. Series.* **1** (02): 7-16. SPE-24112-PA.
- Johns, R.T., and Orr Jr., F.M., 1996, Miscible gas displacement of multicomponent oils, *SPE J.* **1** (01): 39-50. SPE-30798-PA.
- Johns, R.T., Sah, P., and Solano, R., 2002, Effect of dispersion on local displacement efficiency for multicomponent enriched-gas floods above the minimum miscibility enrichment, *SPE Res. Eval. & Eng.* **5** (01): 4-10. SPE-75806-PA.
- Kariman Moghaddam, A., and Saeedi Dehaghani, A.H., 2017, Modeling of asphaltene

- precipitation in calculation of minimum miscibility pressure, *Ind. Eng. Chem. Res.* **56** (25): 7375-7383.
- Kesler, M.G., and Lee, B.I., 1976, Improve prediction of enthalpy of fractions, *Hydro. Proc.* **55**: 153.
- Lee, B.I., and Kesler, M.G., 1975, A generalized thermodynamic correlation based on three-parameter corresponding states, *AIChE J.* **21** (3): 510-527.
- Lee, H., Jin, J., Shin, H., and Choe, J., 2015, Efficient prediction of SAGD productions using static factor clustering, *ASME J. Energy Resour. Technol.* **137** (3): 032907.
- Leibovici, C.F., and Nichita, D.V., 2008, A new look at multiphase Rachford-Rice equations for negative flashes, *Fluid Phase Equilibr.* **267** (2): 127-132.
- Leontaritis, K., and Mansoori, G., 1987, Asphaltene flocculation during oil production and processing: A thermodynamic colloidal model, presented at SPE International Symposium on Oilfield Chemistry, San Antonio, Texas. SPE-16258-MS.
- Lapene, A., Nichita, D.V., Debenest, G., and Quintard, M., 2010, Three-phase free-water flash calculations using a new modified Rachford-Rice equation, *Fluid Phase Equilibr.* **297** (1): 121-128.
- Li, R., and Li, H.A., 2018, New two-phase and three-phase Rachford-Rice algorithms based on free-water assumption, *Can. J. Chem. Eng.* **96** (1): 390-403.
- Li, R. and Li, H.A., 2018, A robust three-phase isenthalpic flash algorithm based on free-water assumption, *J. Energy Resour. Technol.* **140** (3): 032902.

- Li, R. and Li, H.A., 2019, Improved three-phase equilibrium calculation algorithm for water/hydrocarbon mixtures, *Fuel* **244**: 517-527.
- Li, R., and Li, H.A., 2019, Robust three-phase vapor-liquid-asphaltene equilibrium calculation algorithm for isothermal CO₂ flooding application, manuscript submitted to *Ind. Eng. Chem. Res.*
- Li, R., and Li, H.A., 2019, A modified multiple-mixing-cell algorithm for minimum miscibility pressure prediction with the consideration of asphaltene-precipitation effect, manuscript submitted to *Ind. Eng. Chem. Res.*
- Li, Y.K., and Nghiem, L.X., 1986, Phase equilibria of oil, gas and water/brine mixtures from a cubic equation of state and Henry's law, *Can. J. Chem. Eng.* **64** (3): 486-496.
- Li, Z., and Firoozabadi, A., 2012, General strategy for stability testing and phase-split calculation in two and three phases, *SPE J.* **17** (4): 1096-1107. SPE-129844-PA.
- Metcalf, R.S., Fussell, D.D., and Shelton, J.L., 1973, A multicell equilibrium separation model for the study of multiple contact miscibility in rich-gas drives, *SPE J.* **13** (03): 147-155. SPE-3995-PA.
- Michelsen, M.L., 1982a, The isothermal flash problem. Part I. Stability, *Fluid Phase Equilibr.* **9** (1): 1-19.
- Michelsen, M.L., 1982b, The isothermal flash problem. Part II. Phase-split calculation, *Fluid Phase Equilibr.* **9** (1): 21-40.
- Michelsen, M.L., 1987, Multiphase isenthalpic and isentropic flash algorithms, *Fluid Phase*

Equilibr. **33** (1-2): 13-27.

Michelsen, M.L., 1994, Calculation of multiphase equilibrium, *Comput. Chem. Eng.* **18**: 545-550.

Michelsen, M.L., and Mollerup, J., 2004, Thermodynamic modelling: fundamentals and computational aspects, Tie-Line Publications, ISBN 87-989961-1-8.

Mortezazadeh, E., and Rasaei, M.R., 2017, A robust procedure for three-phase equilibrium calculations of water-hydrocarbon systems using cubic equations of state, *Fluid Phase Equilib.* **450**: 150-174.

Naderi, K., and Babadagli, T., 2016, Solvent selection criteria and optimal application conditions for heavy-oil/bitumen recovery at elevated temperatures: a review and comparative analysis, *J. Energy Resour. Technol.* **138** (1): 012904.

Nghiem, L.X., 1983, A new approach to quasi-Newton methods with application to compositional modeling, presented at SPE Reservoir Simulation Symposium, San Francisco, California. SPE-12242-MS.

Nghiem, L.X., and Coombe, D.A., 1997, Modelling asphaltene precipitation during primary depletion, *SPE J.* **2** (02): 170-176. SPE-36106-PA.

Nghiem, L.X., Hassam, M.S., Nutakki, R., and George, A.E.D., 1993, Efficient modelling of asphaltene precipitation, presented at SPE Annual Technical Conference and Exhibition, Houston, Texas. SPE-26642-MS.

Nghiem, L.X., and Li, Y.K., 1984, Computation of multiphase equilibrium phenomena with an equation of state, *Fluid Phase Equilibr.* **17** (1): 77-95.

- Nichita, D.V., Broseta, D., and Montel, F., 2007, Calculation of convergence pressure/temperature and stability test limit loci of mixtures with cubic equations of state, *Fluid Phase Equilibr.* **261** (1-2): 176-184.
- NIST Chemistry WebBook, 2017, NIST Standard Reference Database Number 69, Water Phase Change Data, <http://webbook.nist.gov>.
- Okuno, R., Johns, R., and Sepehrnoori, K., 2010, A new algorithm for Rachford-Rice for multiphase compositional simulation, *SPE J.* **15** (2): 313-325. SPE-117752-PA.
- Panwar, A., Trivedi, J.J., and Nejadi, S., 2015, Importance of distributed temperature sensor data for steam assisted gravity drainage reservoir characterization and history matching within ensemble Kalman filter framework, *J. Energy Resour. Technol.* **137** (4): 042902.
- Pedersen, K.S., Fredenslund, A., and Thomassen, P., 1989, Properties of oils and natural gases (Vol. 5), Gulf Publishing Co.
- Peng, D.Y., and Robinson, D.B., 1976, A new two-constant equation of state, *Ind. Eng. Chem. Fund.* **15** (1): 59-64.
- Prats, M., 1982, Thermal recovery, SPE of AIME, New York: H.L. Doherty Memorial Fund of AIME.
- PVTsim Nova 3.3, Calsep A/S, Copenhagen, Denmark, 2019.
- Rachford Jr., H.H., and Rice, J.D., 1952, Procedure for use of electronic digital computers in calculating flash vaporization hydrocarbon equilibrium, *J. Pet. Tech.* **4** (10): 327-328.
- Riazi, M., 1980, Simplify property predictions, *Hydro. Proc.* **59**: 115-116.

- Robinson, D.B., and Peng, D.Y., 1978, The characterization of the heptanes and heavier fractions for the GPA Peng-Robinson programs. *GPA Research Report 28*.
- Rubin, B., and Buchanan, W.L., 1985, A general purpose thermal model, *SPE J.* **25** (2): 202-214. SPE-11713-PA.
- Sabet, N., and Gahrooei, H.R.E., 2016, A new robust stability algorithm for three phase flash calculations in presence of water, *J. Nat. Gas. Sci. Eng.* **35**: 382-391.
- Søreide, I., and Whitson, C.H., 1992, Peng-Robinson predictions for hydrocarbons, CO₂, N₂, and H₂S with pure water and NaCl brine, *Fluid Phase Equilib.* **77**: 217-240.
- Srivastava, R.K., and Huang, S.S., 1997, Laboratory investigation of Weyburn CO₂ miscible flooding, presented at Technical Meeting/Petroleum Conference of The South Saskatchewan Section, Regina, Saskatchewan, Canada.
- Srivastava, R.K., Huang, S.S., and Dong, M., 1999, Asphaltene deposition during CO₂ flooding, *SPE Prod. Facil.* **14** (04): 235-245. SPE-59092-PA.
- Subramanian, S., Simon, S., and Sjöblom, J., 2016, Asphaltene precipitation models: a review, *J. Dispers. Sci. Technol.* **37** (7): 1027-1049.
- Tang, Y., and Saha, S., 2003, An efficient method to calculate three-phase free-water flash for water-hydrocarbon systems, *Ind. Eng. Chem. Res.* **42**: 189-197.
- Utvik, O.H., Rinde, T., and Valle, A., 2001, An experimental comparison between a recombined hydrocarbon-water fluid and a model fluid system in three-phase pipe flow, *J. Energy Resour. Technol.* **123** (4): 253-259.

- Wang, Y., and Orr Jr., F.M., 1997, Analytical calculation of minimum miscibility pressure, *Fluid Phase Equilib.* **139** (1-2): 101-124.
- Whitson, C.H., and Michelsen, M.L., 1989, The negative flash, *Fluid Phase Equilib.* **53**: 51-71.
- Willman, B.T., Valleroy, V.V., Runberg, G.W., Cornelius, A.J., and Powers, L.W., 1961, Laboratory studies of oil recovery by steam injection, *J. Pet. Tech.* **13** (7): 681-690.
- Wilson, G.M., 1968, A modified Redlich-Kwong equation of state, application to general physical data calculations, presented at the 65th National AIChE Meeting, Cleveland, Ohio.
- Yellig, W.F., and Metcalfe, R.S., 1980, Determination and prediction of CO₂ minimum miscibility pressures, *J. Pet. Technol.* **32** (01): 160-168. SPE-7477-PA.
- Young, L.C., and Stephenson, R.E., 1983, A generalized compositional approach for reservoir simulation. *SPE J.* **23** (05): 727-742. SPE-10516-PA.
- Yuan, H., and Johns, R.T., 2005, Simplified method for calculation of minimum miscibility pressure or enrichment, *SPE J.* **10** (04): 416-425. SPE-77381-PA.
- Zaghoul J., Adewumi, M., and Ityokumbul, M.T., 2008, Hydrodynamic modeling of three-phase flow in production and gathering Pipelines, *J. Energy Resour. Technol.* **130** (4): 043004.
- Zhao, G.B., Adidharma, H., Towler, B., and Radosz, M., 2006, Using a multiple-mixing-cell model to study minimum miscibility pressure controlled by thermodynamic equilibrium tie lines, *Ind. Eng. Chem. Res.* **45** (23): 7913-7923.
- Zheng, S., and Yang, D., 2017, Experimental and theoretical determination of diffusion coefficients of CO₂-heavy oil systems by coupling heat and mass transfer, *J. Energy Resour.*

- Technol.* **139** (2): 022901.
- Zhu, D., and Okuno, R., 2014, A robust algorithm for isenthalpic flash of narrow-boiling fluids, *Fluid Phase Equilibr.* **379**: 26-51.
- Zhu, D., and Okuno, R., 2015, Analysis of narrow-boiling behavior for thermal compositional simulation, presented at SPE Reservoir Simulation Symposium, Houston, Texas. SPE-173234-MS.
- Zhu, D., and Okuno, R., 2015, Robust isenthalpic flash for multiphase water/hydrocarbon mixtures, *SPE J.* **20** (6): 1350-1365. SPE-170092-PA.
- Zhu, D., and Okuno, R., 2016, Multiphase isenthalpic flash integrated with stability analysis, *Fluid Phase Equilibr.* **423**: 203-219.
- Zick, A.A., 1986, A combined condensing/vaporizing mechanism in the displacement of oil by enriched gases, presented at SPE annual technical conference and exhibition, New Orleans, Louisiana. SPE-15493-MS.
- Zirrahi, M., Hassanzadeh, H., and Abedi, J., 2015, Prediction of water solubility in petroleum fractions and heavy crudes using cubic-plus-association equation of state (CPA-EoS), *Fuel* **159**: 894-899.
- Zirrahi, M., Hassanzadeh, H., and Abedi, J., 2017, Water content of light n-alkanes: New measurements and cub-plus-association equation of state modeling, *AIChE J.* **63** (4): 1384-1389.
- Zirrahi, M., Hassanzadeh, H., and Abedi, J., 2017, Experimental and modeling studies of MacKay

River bitumen and water, *J. Petrol. Sci. Eng.* **151**: 305-310.

Zirrahi, M., Hassanzadeh, H., and Abedi, J., 2017, Experimental and modeling studies of water, light n-alkanes and MacKay River bitumen ternary systems, *Fuel* **196**: 1-12.